Reverse Electrodialysis with Bipolar Membranes (REDBP) as an Energy Storage System

von der Fakultät Energie-, Verfahrens- und Biotechnik der Universität Stuttgart
zur Erlangung der Würde eines Doktors der Ingenieurwissenschaften (Dr.-Ing.)
genehmigte Abhandlung

vorgelegt von
Jiabing Xia
aus Jilin, China

Hauptberichter:	Prof. Dr.-Ing. U. Nieken
Mitberichter:	Prof. Dr.rer.nat. K. A. Friedrich
Tag der mündlichen Prüfung:	23.02.2018

Institut für Chemische Verfahrenstechnik der Universität Stuttgart
2018

Vorwort

Die vorliegend Arbeit entstand während meiner Zeit als wissenschaftlicher Mitarbeiter am Institut für Chemische Verfahrenstechnik (ICVT) der Universität Stuttgart. Für die wohlwollende finanzielle Förderung des Forschungsprojekts bin ich der Graduierten- und Forschungschule ‚Effiziente Energienutzung' Stuttgart (GREES) sehr dankbar.

Mein besonderer Dank gilt Herrn Prof. Dr.-Ing. U. Nieken für seine langjährige, jederzeit wohlwollende Unterstützung meiner Arbeit.

Herr Prof. Dr.-Ing. G. Eigenberger und Herr Prof. Dr.-Ing. H. Strathmann danke ich für die fachliche Unterstützung und die vielen unentbehrlichen Anregungen.

Herr Prof. Dr.rer.nat. K. A. Friedrich danke ich für die Übernahme des Mitberichtes und das entgegengebrachte Interesse.

Herr Dr. S. Starnes danke ich für die Korrektur meiner Sprache.

Zum Gelingen der Arbeit hat auch die Unterstützung zahlreicher Mitarbeiter des ICVT beigetragen. Dafür bedanke ich mich beim Herrn Dr.rer.nat. Kerres, Herrn Aschenbrenner, Herrn Lorenz, Herrn Binder und Herrn Häring.

Zur guten Atmosphäre am ICVT haben zahlreiche weitere Kollegen beigetragen, die ich während meiner Zeit am Institut kennen und schätzen gelernt habe. An dieser Stelle möchte ich stellvertretend Andreas, Vladimir, Katrin, Karin, Ute, Robert und Philip nennen.

Zum Abschluß danke ich auch meinen Eltern für die Unterstützung während der gesamten Ausbildung.

Stuttgart, im Juli 2016

Schluss auf die beste Erklärung

Contents

Notation

Latin Symbols

a_j	activity of ion *j*	
A	area	[m^2]
c_j	concentration of ion *j*	[mol/m^3]
D_j	diffusivity of ion *j*	[m^2/s]
e_0	elemental charge	$1.60217657 \times 10^{-19}$ [coulombs]
E	electrode potential	[V]
E^0	standard electric potential	[V]
F	Faraday´s constant	96485 [Coulomb/mol]
$f_{l/w}$	pseudo length width ratio of transition	
f_v	void factor of spacers	80%
g	molar free energy	[J/mol]
Δg_e	changing of molar free energy of electron	[J/mol]
Δg	molar free energy of reaction	[J/mol]
i	electric current density	[A/m^2]
I	current	[A]
J_j	ionic transport of ion *j*	[mol/m^2s]
k	reaction rate constant	[$m^3/(mol \cdot s)$]
k_B	Bolzmann constant	$1.38 \cdot 10^{-23}$ [J /K]
n_e	number of mole of electrons	[mol]
n_j	number of mole of ion *j*	[mol]
N_A	Avogadro number	6.02×10^{23} [/mol]
N_{cell}	cell number in stack	
P	pressure	[Pa]
P^0	standard pressure	[Pa]
R	molar gas constant	8.3145 [J/(mol·K)]
r_j^V	the net rate of formation or extinction of ion *j* per unit volume by chemical reaction	[$mol/(m^3 \cdot s)$]
T	absolute temperature	[K]
u_j	mobility of ion *j*	[$m^2/(V \cdot s)$]
v_j	stoichiometric number	

V_{m_j}	partial molar volume	[m^3/mol]
V_T	thermal voltage	[V]
X_m	fest-ion concentration	[mol/m^3]
z_j	charge number of ion *j*	
z_{mf}	charge number of fest-ion in IEM	

Greek Symbols

γ_j	activity coefficient of ion j in solution	
δ	thickness	[m]
ε	permittivity	[F/m]
η	efficiency	
η_{BP}^{D}	efficiency of bipolar membrane by discharging	
η_{SC}^{D}	efficiency of single cell by discharging	
η_{Stack}^{D}	efficiency of stack by discharging	
η_{System}^{D}	efficiency of system by discharging	
κ	electrical conductivity	[S·m^{-1}]
λ	Debye length	[m]
μ_e	chemical potential of electron	[J/mol]
μ_j	chemical potential of ion *j*	[J/mol]
$\widetilde{\mu_e}$	electrochemical potential of electron	[J/mol]
$\widetilde{\mu_j}$	electrochemical potential of ion *j*	[J/mol]
$\tilde{\mu}_{ox}$	electrochemical potential of oxidized components	[J/mol]
$\tilde{\mu}_{red}$	electrochemical potential of reduced components	[J/mol]
ρ	resistivity	[Ω·m]
ρ_e	volumetric charge density	[C/m^3]
φ	electric potential.	[V]
Ø	diameter	[m]

Abbreviations

AEM	Anion Exchange Membrane
BMS	Battery Management System
BPAEM	Bipolar Membrane Anion Exchange Membrane side
BPCEM	Bipolar Membrane Cation Exchange Membrane side
BP	Bipolar Membrane
CAES	Compressed Air Energy Storage
CEM	Cation Exchange Membrane
Ch	Charging Process
Ch/DisCh	Charging or Discharging Process
DC	Direct Current
DisCh	DisCharging Process
DL	Diffusion Layer
EDBP	Electrodialysis with Bipolar Membranes
EMF	ElectroMotive Force
I	Current
IEM	Ion Exchange Membrane
IR-drop	Voltage Drop due to Current times Resistance of Electrolyte
OCV	Open Circuit Voltage
P2G	Power to Gas
PD	Power Density
SC	Single Cell
StackM	Stack Middle
RED	Reverse Electrodialysis
REDBP	Reverse Electrodialysis with Bipolar Membranes
SHE	Standard Hydrogen Electrode
V	Voltage

Superscripts

IEM	In IEM
solution	In solution
Donnan	Donnan distribution

Subscripts

AllSCs	sum of All Single Cells
Ch	Charging Process
DisCh	Discharging Process
mem.	IEM
s	solution
SC	single cells
simu.	by simulation
tans.	transition
meas.	by measurement
theor.max	theoretical maximum

Abstract

Traditional application field of bipolar membrane (BP) is for the conversion of a salt into its corresponding acid and base in the process of electrodialysis with bipolar membranes.

The first people introduced BP for energy storage was Alexander Mauro [1] in 1962 when he applied Poisson-Boltzmann equation which was derived by Shockley [2] in his treatment of the p-n semiconductor junction at equilibrium to fixed charge ionic membranes. He stated:

It is shown further that when a positive and negative membrane are juxtaposed, the space charge region in the 'junction' so formed provides a mechanism for the storage of electrical energy.

But he also quoted:

…the presence of transition regions of fixed charge give(s) rise to the additional property of capacitance.

Maybe because of his quotation, the followers E. K. Zholkovskij, M. C. Müller, E. Staude and J. Pretz were treating BP more like capacitance [3] [4]. Especially in the work of [3] in 1998, the authors J. Pretz and E. Staude conducted the experiment by mounting up 20 cells together and stated:

…the OCV (Open Circuit Voltage, 20 cells around 6V) approaches a limiting value. A possible explanation for this behavior is that the bipolar membrane acts in a manner similar to a capacitor.

And they concluded:

…The (capacitive) counter-voltage which is contrary to the theoretical OCV leads to a higher fuel consumption and lower energy efficiency.

Since then, no literatures about utilizing BP for energy storage are being found.

The present work is trying to clarify the behavior of BP is not a capacitor, but a real reactor where neutralization reaction takes place for production of electric energy in the process of reverse electrodialysis with bipolar membranes (REDBP) by theoretical analysis, modeling and simulation, and experiment.

Introduction and theoretical analysis as Chapter 1

Important concepts and REDBP process have been introduced. Theoretical analysis of REDBP as energy storage system has been performed as follows:

(1) Energy density of REDBP depends on concentration of acid and base. Due to the high solubility and stability of HCl and NaOH in water solution, the theoretical maximum energy density of REDBP could be as high as 181.3 kWh/m^3 or 235.6 kWh/ton. Energy density can be further increased by storage of HCl in pure liquid form and NaOH in pure solid form.

(2) The definitions of discharging efficiency have been given. One of the main tasks of this thesis is to investigate these discharging efficiencies. They are a) the discharging efficiency of BP η_{BP}^{D}, b) the discharging efficiency of single cell η_{SC}^{D}, and c) the discharging efficiency of stack η_{Stack}^{D}.

(3) Power density of REDBP is supposed to be high since its driving force is neutralization reaction. Investigation of power densities of BP, single cell and stack is also one of the main tasks of this thesis.

(4) Charging/Discharging time is considered as important which will be investigated in the thesis.

Other factors such as lifetime, environmental impact and life cycle are not included in this thesis due to the limitation of the content.

Experiments of single cell as Chapter 2

Single membrane test facility has been constructed using saturated calomel electrodes combined with Luggin capillaries to measure the voltage between membrane with various conditions such as changing temperature, current density, ionic concentration and charging/discharging time.

(1) REDBP has a good open circuit voltage which is always higher than 0.7V with solution concentration higher than 0.25M. Further increasing concentration of electrolyte and temperature will benefit OCV very little.

(2) The biggest efficiency loss of BP is product water permeability by discharging.

(3) The higher the concentration of acid and base, the higher the conductivity of electrolyte solution as well as Cation Exchange Membrane (CEM) and Anion Exchange Membrane

(AEM) will be, but also a higher crossover of acid and base which causes increasing resistance of BP.

(4) The maximum overall power density of single cell is 112mW/cm^3 with 1M solution concentration and 0.5mm thick solution chambers at -50mA/cm^2.

(5) There is always a compromise between power density and efficiency. At -10mA/cm^2 discharging efficiency is above 85% with a power density of 34mW/cm^3.

Modeling and simulation of single cell as Chapter 3

Single membrane mathematical model has been set up and simulated to investigate phenomenon inside of IEM, such as ionic distribution, ionic transport, and electric potential distribution, which are of great interest but cannot be measured at the moment. The simulated results have been displayed as profiles in diagram to illustrate what is happening inside of IEM.

One of the most important assumptions is that BP has a fixed reaction zone treated as double-layer model inside of BP interface. The simulation results compared with experiments are quite logical and interesting:

(1) Simulation results show the function of BP in the application of REDBP is rather a reactor, a place where neutralization reaction takes place, not a traditional IEM mainly for separating two chambers or electrodes.

(2) The main decrease of electric potential inside of BP is the decreasing Donnan potentials inside of BP interface due to either salt accumulation inside of BP interface, or higher reagent concentration with higher current density, or both.

(3) Salt accumulation near or in BP interface is significant. In the case of 1M solution, Na^+ or Cl^- near BP interface is the main counter-ion.

(4) Crossover depends only on concentration of Cl^- in HCl solution and concentration of Na^+ in NaOH solution.

(5) If transport of OH^- in Bipolar Membrane Aion Exchange Membrane side (BPAEM) is well handled, the quality of acid or base solution can be dramatically reduced.

(6) Due to relatively poor mobility of OH^- in BPAEM, OH^- starts to deplete earlier than H^+ with elevated current density.

Experiments of stack as Chapter 4

Stack test facility has been constructed using Pt wires to measure the voltage distribution throughout the stack with various conditions such as changing current density, ionic concentration and charging/discharging time.

(1) There are additional losses during stack mounting-up process. Besides leakages or side reactions, bad mixing and shunt current are considered the most important losses.

(2) The existence of shunt current has been proven by self-discharging tests. Fully understanding and seriously considering shunt current are the prerequisites for designing and mounting-up a stack.

(3) REDBP stack has been mounted up to 20 cells with non-ideal cell frames. With 1M solution, the maximum discharging power output of sum of all 20 cells is up to 9W, 26mW/cm^3 and 50% discharging efficiency.

(4) Performances of single cell inside of stack are not identical. By introducing Pt wires inside of a stack, inhomogeneous distribution of voltage throughout the stack has been found, mainly due to shunt current and bad mixing.

(5) The important influential parameters determining the overall performance of REDBP stack are electrode chambers, flow patterns (parallel/series flow), cell frame design (flow patterns inside of solution chamber, as well as shunt currents) and those factors affecting performance of single cell including concentration of solution, flowrate, temperature, active surface, current density and permselectivity of IEMs.

Modeling and simulation of stack as Chapter 5

The purpose of modeling and simulation of REDBP stack is for a) design of experiment, b) explanation of experimental results, c) investigation the phenomena inside of stack which are impossible to measure at moment, and d) improvement of stack.

(1) Due to the bypass connections, three different types of electric currents exit inside of stack, they are a) the electric current through active surface, b) the electric current flowing through solution chamber and transition, and c) the electric current flowing through solution channel outside of active surface .

(2) Because of the existence of the above three types of currents, the electric potential in electrolyte solution inside of stack is not homogeneously distributed. That is one of the main reasons why the unknown measuring positions of Pt wires causes huge oscillation of experimental results.

(3) Not only the magnitude of shunt current, but also its affecting number of BPs plays very important role.

(4) Voltage between each BP inside of stack is not equal. Even between the same piece of BP the voltage varies at different position.

(5) By charging, part of electric current will flow through bypass connection which elevates the current density at certain position, which ultimately causes safety concerns. By discharging, shunt current decreases with increasing discharging current density.

(6) Because of shunt current, stack voltage is lower than the sum of all single cell voltages obtained from single cell experiment. Many influential parameters have been investigated. Some strategies are suggested for improvement of stack, such as increasing active surface (especially increasing the distance between the center of active surface and inlet/outlet of solution chamber), decreasing thickness of solution chambers, increasing pseudo length width ratio $f_{l/w}$ of transition and installation of breakpoints in solution channels.

Zusammenfassung

Ein traditionelles Anwendungsgebiet der bipolaren Membran (BP) ist die Umwandlung eines Salzes in die entsprechende Säure und Base bei der Elektrodialyse mit bipolaren Membranen.

Die erste Einführung von BP für die Energiespeicherung war Alexander Mauro [1] im Jahr 1962 , als er die von Shockley [2] hergeleitete Poisson-Boltzmann-Gleichung in seiner Behandlung des p-n-Halbleiterübergangs im Gleichgewicht auf Ionenmembranen mit fester Ladung anwendete. Er erklärte:

Es wird weiter gezeigt, dass, wenn eine positive und eine negative Membran nebeneinander liegen, der Raumladungsbereich in der so gebildeten "Verbindung" einen Mechanismus zur Speicherung elektrischer Energie bereitstellt.

(It is shown further that when a positive and negative membrane are juxtaposed, the space charge region in the 'junction' so formed provides a mechanism for the storage of electrical energy.)

Er zitierte aber auch:

... Das Vorhandensein von Übergangsregionen fester Ladung führt zu der zusätzlichen Eigenschaft der Kapazität

(*…the presence of transition regions of fixed charge give(s) rise to the additional property of capacitance.)*

Vielleicht aufgrund seines Zitats behandelten die Anhänger E.K. Zholkovskij, M.C. Müller, E. Staude und J. Pretz BP eher wie Kapazität [3] [4]. Besonders in der Arbeit von [3] im Jahr 1998 führten die Autoren J. Pretz und E. Staude das Experiment durch, indem sie 20 Zellen zusammen aufbauten und sagten:

...Die OCV (Leerlaufspannung, 20 Zellen ca.6V) einen Grenzwert erreicht. Eine mögliche Erklärung für dieses Verhalten ist, dass die bipolare Membran ähnlich wie ein Kondensator wirkt.

（...the OCV (Open Circuit Voltage, 20 cells around 6V) approaches a limiting value. A possible explanation for this behavior is that the bipolar membrane acts in a manner similar to a capacitor.）

Und sie schlussfolgerten:

…Die (kapazitive) Gegenspannung, die der theoretischen OCV entgegensteht, führt zu einem höheren Kraftstoffverbrauch und einer niedrigeren Energieeffizienz.

(…The (capacitive) counter-voltage which is contrary to the theoretical OCV leads to a higher fuel consumption and lower energy efficiency.)

Seitdem wurden keine Literatur über die Verwendung von BP zur Energiespeicherung gefunden.

Die vorliegende Arbeit versucht, das Verhalten von BP zu klären, ist kein Kondensator, sondern ein echter Reaktor, in dem eine Neutralisationsreaktion zur Erzeugung elektrischer Energie bei der umgekehrten Elektrodialyse mit bipolaren Membranen (REDBP) durch theoretische Analyse, Modellierung, Simulation und experimentieren stattfindet.

Einführung und theoretische Analyse als Kapitel 1

Wichtige Konzepte und REDBP-Prozesse wurden eingeführt. Die theoretische Analyse von REDBP als Energiespeichersystem wurde wie folgt durchgeführt:

Important concepts and REDBP process have been introduced. Theoretical analysis of REDBP as energy storage system has been performed as follows:

(1) Die Energiedichte von REDBP hängt von der Konzentration von Säure und Base ab. Aufgrund der hohen Löslichkeit und Stabilität von HCl und NaOH in Wasserlösung könnte die theoretische maximale Energiedichte von REDBP 181,3 kWh/m^3 oder 235,6 kWh/ton betragen. Die Energiedichte kann durch die Lagerung von HCl in reiner flüssiger Form und von NaOH in reiner fester Form weiter erhöht werden.

(2) Die Definitionen der Entladungseffizienz wurden angegeben. Eine der Hauptaufgaben dieser Arbeit ist die Untersuchung dieser Entladungseffizienzen. Sie sind a) die Entladungseffizienz von BP η_{BP}^{D}, b) die Entladungseffizienz der Einzelzelle η_{SC}^{D} und c) die Entladungseffizienz des Stapels η_{Stack}^{D}.

(3) Die Leistungsdichte von REDBP soll hoch sein, da seine Triebkraft die Neutralisationsreaktion ist. Die Untersuchung der Leistungsdichten von BP, Einzelzellen und Stacks ist ebenfalls eine der Hauptaufgaben dieser Arbeit.

(4) Die Lade-/Entladezeit wird als wichtig angesehen.

Andere Faktoren wie Lebensdauer, Umweltauswirkungen und Lebenszyklus werden aufgrund der inhaltlichen Einschränkung nicht in diese Arbeit einbezogen.

Einzelzellenversuche als Kapitel 2

Eine Membrantestanlage wurde mit gesättigten Calomel-Elektroden in Kombination mit Luggin-Kapillaren zur Messung der Spannung zwischen den Membranen unter verschiedenen Bedingungen wie sich ändernde Temperatur, Stromdichte, Ionenkonzentration und Lade- / Entladezeit aufgebaut.

(1) REDBP hat eine gute Leerlaufspannung, die bei einer Lösungskonzentration von mehr als 0,25M immer höher als 0,7V ist. Eine weitere Erhöhung der Elektrolyt-und Temperaturkonzentration wird für OCV nur wenig von Nutzen sein.

(2) Der größte Wirkungsgradverlust von BP ist die Wasserdurchlässigkeit des Produkts durch Ableitung.

(3) Je höher die Konzentration von Säure und Base ist, desto höher ist die Leitfähigkeit der Elektrolytlösung sowie der Kationenaustauschmembran (CEM) und der Anionenaustauschmembran (AEM), aber auch eine höhere Überkreuzung von Säure und Base, die eine Zunahme bewirkt Widerstand von BP.

(4) Die maximale Gesamtleistungsdichte einer Einzelzelle beträgt 112mW/cm^3 bei einer Lösungskonzentration von 1M und 0,5 mm dicke Lösungskammern bei -50mA/cm^2.

(5) Es gibt immer einen Kompromiss zwischen Leistungsdichte und Effizienz. Bei -10mA/cm^2 liegt der Entladewirkungsgrad über 85% bei einer Leistungsdichte von 34mW/cm^3

Modellierung und Simulation einer einzelnen Zelle als Kapitel 3

Ein mathematisches Einzelmembranmodell wurde erstellt und simuliert, um das Phänomen innerhalb von IEM zu untersuchen, wie Ionenverteilung, Ionentransport und Verteilung des elektrischen Potentials, die von großem Interesse sind, aber derzeit nicht gemessen werden können. Die simulierten Ergebnisse wurden als Profile im Diagramm angezeigt, um zu veranschaulichen, was in IEM passiert.

Eine der wichtigsten Annahmen ist, dass BP eine feste Reaktionszone als Doppelschichtmodell innerhalb der BP-Schnittstelle hat. Die Simulationsergebnisse im Vergleich zu Experimenten sind ziemlich logisch und interessant:

(1) Simulationsergebnisse zeigen, dass die Funktion von BP bei der Anwendung von REDBP eher ein Reaktor ist, ein Ort, an dem eine Neutralisationsreaktion stattfindet.

(2) Die Hauptabnahme des elektrischen Potentials innerhalb von BP ist die Abnahme der Donnan-Potentiale innerhalb der BP-Grenzfläche, die entweder auf Salzansammlung in der

BP-Grenzfläche oder auf eine höhere Reagenskonzentration mit höherer Stromdichte oder auf beide zurückzuführen ist.

(3) Salzansammlung nahe oder in der BP-Grenzfläche ist signifikant. Bei 1M-Lösung ist die Na^+ - oder Cl^- nahe BP-Schnittstelle das Hauptgegenion

(4) Die Kreuzung hängt nur von der Konzentration der Cl^- in HCl-Lösung und der Konzentration von Na^+ in der NaOH-Lösung ab.

(5) Wenn der Transport von OH^- in bipolarer Membran Aion Austauschmembranseite (BPAEM) gut gehandhabt wird, kann die Qualität der Säure- oder Basenlösung drastisch gemindert werden.

(6) Aufgrund der relativ schlechten Mobilität von OH^- in BPAEM beginnt der Schwund von OH^- mit erhöhter Stromdichte früher als bei H^+.

Stapelversuche wie in Kapitel 4

Eine Stapeltestanlage wurde unter Verwendung von Pt-Drähten aufgebaut, um die Spannungsverteilung über den Stapel unter verschiedenen Bedingungen, wie etwa Änderung der Stromdichte, Ionenkonzentration und Lade- / Entladezeit, zu messen.

(1) Beim Stapelmontageprozess treten zusätzliche Verluste auf. Neben Leckagen oder Nebenreaktionen gelten schlechte Misch- und Nebenschlussströme als die wichtigsten Verluste.

(2) Das Vorhandensein eines Nebenschlussstroms wurde durch Selbstentladungstests nachgewiesen. Vollständiges Verständnis und ernsthafte Berücksichtigung des Nebenschlussstroms sind die Voraussetzungen für das Entwerfen und Montieren eines Stapels.

(3) Der REDBP Stapel wurde mit bis zu 20 Zellen mit nicht idealen Zellenrahmen bestückt. Bei einer 1M-Lösung beträgt die maximale Entladeleistung der Summe aller 20 Zellen bis zu 9W, 26mW/cm^3 und eine Entladungseffizienz von 50%.

(4) Die Leistung einer einzelnen Zelle innerhalb eines Stapels ist nicht identisch. Durch das Einführen von Pt-Drähten innerhalb eines Stapels wurde eine inhomogene Spannungsverteilung im Stapel festgestellt, hauptsächlich aufgrund von Nebenstrom und schlechtem Mischen.

(5) Die wichtigsten Einflussfaktoren für die Gesamtleistung des REDBP Stapel sind Elektrodenkammern, Flussmuster (Parallel- / Serienfluss), Zellrahmen-Design (Flussmuster

in der Lösungskammer sowie Nebenströme) und Faktoren, die die Leistung beeinflussen Einzelzelle einschließlich Konzentration der Lösung, Flussrate, Temperatur, aktive Oberfläche, Stromdichte und Permselektivität von IEMs.

Modellierung und Simulation von Stapel als Kapitel 5

Der Zweck des Modellierens und der Simulation des REDBP Stapel ist für a) Versuchsaufbau, b) Erklärung der experimentellen Ergebnisse, c) Untersuchung der Phänomene innerhalb des Stapels, die momentan nicht messbar sind, und d) Verbesserung des Stapels.

(1) Aufgrund der Bypass-Verbindungen treten drei verschiedene Arten elektrischer Ströme innerhalb des Stapels aus. Sie sind a) der elektrische Strom durch die aktive Oberfläche, b) der durch die Lösungskammer und den Übergang fließende elektrische Strom und c) der durch den Lösungskanal fließende elektrische Strom außerhalb der aktiven Oberfläche.

(2) Aufgrund der drei oben genannten Arten von Strömen ist das elektrische Potential in der Elektrolytlösung im Stapel nicht homogen verteilt. Dies ist einer der Hauptgründe, warum die unbekannten Messpositionen von Pt-Drähten zu starken Schwankungen der experimentellen Ergebnisse führen.

(3) Nicht nur die Stärke des Nebenschlussstroms, sondern auch die Anzahl der BPs spielt eine sehr wichtige Rolle.

(4) Die Spannung zwischen jedem BP innerhalb des Stapels ist nicht gleich. Selbst zwischen demselben Stück BP variiert die Spannung an verschiedenen Positionen.

(5) Beim Laden fließt ein Teil des elektrischen Stroms durch eine Bypass-Verbindung, wodurch die Stromdichte an bestimmten Positionen erhöht wird, was letztendlich Sicherheitsbedenken hervorruft. Beim Entladen nimmt der Nebenschlussstrom mit zunehmender Entladestromdichte ab.

(6) Aufgrund des Nebenschlussstroms ist die Stapelspannung niedriger als die Summe aller Einzelzellenspannungen, die aus einem Einzelzellenversuch erhalten wurden. Viele einflussreiche Parameter wurden untersucht. Es werden einige Strategien zur Verbesserung des Stapels vorgeschlagen, wie zum Beispiel die Vergrößerung der aktiven Oberfläche (insbesondere die Vergrößerung des Abstands zwischen der Mitte der aktiven Oberfläche und dem Einlass / Auslass der Lösungskammer), das Verringern der Dicke der Lösungskammern, das Pseudolängenbreitenverhältnis $f_{l/w}$) des Übergangs und der Installation von Haltepunkten in Lösungskanälen.

Chapter 1

Introduction

In this section, the idea of utilizing reverse electrodialysis with bipolar membranes (REDBP) as an energy storage system will be introduced step by step. At first a short introduction of an energy storage system will be presented followed by a detailed introduction of flow battery. Then REDBP will be explained more thoroughly, as well as the objectives of this thesis.

1.1 Energy Storage System

Large-scale integration of unsteady and intermittent renewables into the electrical grid poses critical challenges that may be overcome through the use of energy storage systems.

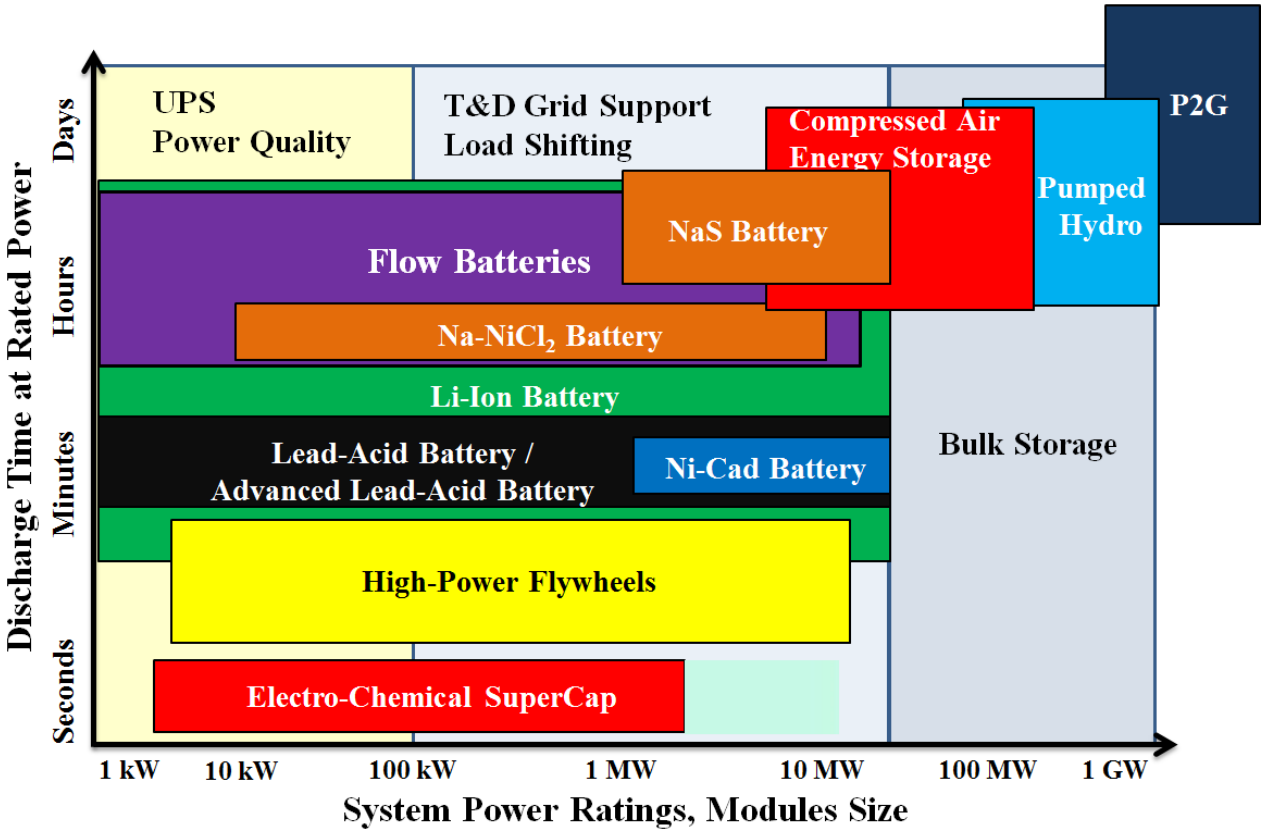

Figure 1.1: Energy storage technology comparison considering rated power, discharge time and suitable applications.

Energy storage system is the capture of energy produced at one time for use at a later time. Energy can be in multiple forms including radiation, chemical, gravitational potential, electrical potential, electricity, elevated temperature, latent heat and kinetic. Energy storage involves converting energy from forms that are difficult to store to more conveniently or economically storable forms. In the case of integration of renewables, electricity is the energy form that needs to be stored.

There are many kinds of energy storage system which are characterized from many aspects. After reviewing the existing projects from all over the world [5], figure 1.1 shows the most commonly known energy storage systems considering two most important properties: system power and discharge time. For integration of renewables the following energy storage systems are considered to be the suitable candidates.

Power to Gas

Power to Gas (often abbreviated P2G) is a chemical process which converts electrical power (often referring to renewables) to a gas fuel. It often involves splitting water into hydrogen and oxygen by electrolysis.

Pumped-Storage Hydroelectricity

The most widely used form of bulk-energy storage is currently pumped-storage hydropower, which is built around two reservoirs at different heights. Off-peak electricity is used to pump water from the lower to the higher reservoir, turning electrical energy into gravitational potential energy. When power is needed, water is released back down to the lower reservoir, spinning a turbine and generating electricity along the way.

Compressed Air Energy Storage

Compressed Air Energy Storage (CAES) is always compared with pumped-storage hydropower in terms of their applications, output and storage capacity. But, instead of pumping water from a lower to an upper pond during periods of excess power, in a CAES plant, ambient air is compressed and stored under pressure in an underground cavern. When electricity is required, the pressurized air is heated and expanded in an expansion turbine driving a generator for power production.

Sodium Sulfur Battery

A sodium sulfur battery (NaS) is a type of molten-salt battery constructed from liquid sodium (Na) and sulfur (S). It has many advantages such as inexpensive materials, high energy, high power density, high efficiency and long lifetime.

Lithium-ion battery

In a lithium-ion battery (often abbreviated LIB) lithium ions move from the negative electrode to positive electrode when discharging and back when charging. LIB is common in home electronics, and is one of the most popular types of rechargeable batteries for portable electronics. Its stationary application is under rapid development.

Flow Battery

A flow battery is a rechargeable system that stores its electrolyte—the material that provides energy—as a liquid in external tanks. Unlike typical batteries that are packaged as fixed cells or modules, a flow battery allows the battery's power to be decoupled from the battery's energy. As a result, users are free to tune the battery's specifications to their specific needs.

In short, each energy storage system has its own pros and cons. Since REDBP can be classified as flow battery, in the following section flow battery will be introduced in more detail.

1.2 Flow Battery

Flow battery is a type of rechargeable battery where chemical components are dissolved in liquids contained within the system and are separated by an Ion Exchange Membrane (IEM, section 1.3.1). IEM provides a pathway for ionic transport, while both liquids circulate in their own respective space as shown in the figure 1.2. In short a flow battery can be divided into (energy storage) tanks, (power producing) stack, tubes and pumps, and other electronic components identical to traditional batteries.

Flow batteries are very similar to fuel cell and have many unique characteristics which make them especially attractive when compared with conventional batteries, such as their ability to decouple rated power from rated capacity, as well as their greater design flexibility and nearly unlimited life of electrolyte solution. Moreover, their liquid nature allows their installation inside deactivated underground gas tanks located at gas stations, enabling a smooth transition of gas stations' business model towards the emerging electric mobility paradigm.

The fundamental difference between conventional batteries and flow batteries is that energy is stored not as the electrode material in conventional batteries but as the electrolyte solution in flow batteries.

There are many classifications of flow batteries; here are four main classifications as well as examples:

1) Based on the active species in the electrolytes
    a) Vanadium Flow Battery.
    b) Zn-Br Flow Battery.

c) Fe-Cr Flow Battery.

d) Acid-Base Flow Battery.

2) Based on the battery structure

a) Liquid-liquid: Vanadium Flow Battery.

b) Liquid-solid: Zn-Nicked Flow Battery.

c) Liquid-gas: Vanadium-Air Flow Battery.

3) Based on the supporting electrolyte

a) Aqueous Electrolyte Flow Battery.

b) Non-Aqueous Based Flow Battery.

4) Based on the number of supporting electrolytes

a) Single electrolyte: Vanadium-Air Flow Battery.

b) Two electrolytes: Vanadium Flow Battery.

e) Three electrolytes: Acid-Base Flow Battery.

The use of flow battery and most of its development was carried out by NASA for long-term space flight projects, which initially considered iron and chromium as solutions [6]. Right now the most commonly known and well developed flow battery is vanadium redox flow battery [7], which employs vanadium ions in different oxidation states to store chemical potential energy. VFB exploits the ability of vanadium to exist in solution in four different oxidation states, and uses this property to make a battery that has just one electroactive element instead of two as shown in the figure 1.2.

REDBP can be further classified as acid-base all aqueous three electrolytes flow battery, since the working electrolytes are acid, base and salt solution. In the next section, the idea of REDBP as energy storage system will be introduced more thoroughly.

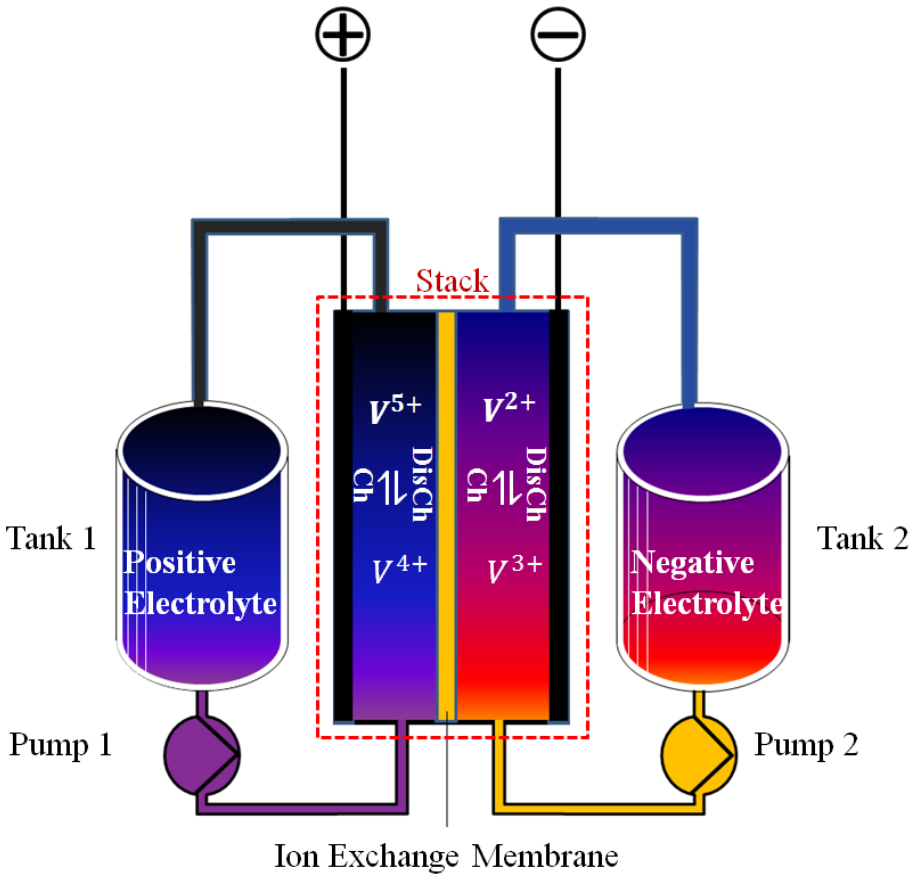

Figure 1.2: A vanadium flow battery consists of two tanks of liquids which are pumped past a membrane held between two electrodes [8]. Please note, that the color here does not correspond the really color of electrolyte solution.

1.3 Reverse Electrodialysis with Bipolar Membranes

In this section, REDBP as energy storage system will be introduced. At first, a basic knowledge of Ion Exchange Membrane (IEM) will be presented, followed by an introduction of EDBP which is a well-developed and also a reversed process of REDBP. In the end are the properties of REDBP as energy storage system, as well as the objectives of this thesis.

1.3.1 Ion Exchange Membrane

Ion Exchange Membrane (IEM) is polymeric material with charged ion groups. Cation Exchange Membrane (CEM) contains fixed anionic groups which allow the passage of mobile cations and block anions. Anion Exchange Membranes (AEM) contains fixed cationic groups with mobile anions which allow the passage of anions and block cations. Bipolar Membrane (BP) has two IEM layers with different types of fixed groups [9] [10] [11]. Theoretically, no charged particles are allowed to pass through BP. Unlike other membranes for only separation purpose, BP is mainly designate to split water into hydroxide ions (OH^-) and protons (H^+) by exposing in an electric field.

1.3.2 Electrodialysis with Bipolar Membranes

Electrodialysis with Bipolar Membranes (EDBP) is a process to produce acid and base from a neutral salt solution [12] [13] [11]. Each single cell consists of three IEMs (one CEM, one AEM and one BP) and three electrolyte solution chambers (acid, base and salt chambers). Many single cells connecting each other enhance the overall acid and base production rate. By putting two electrodes at the end, the stack of EDBP is mounted.

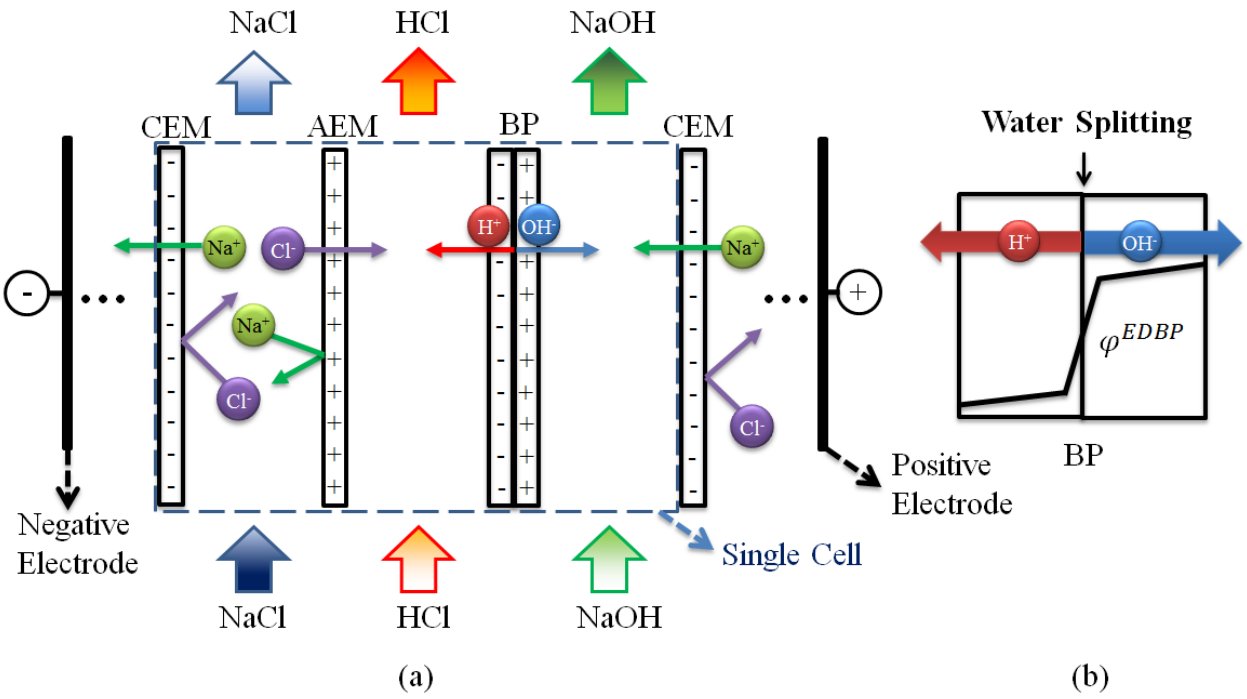

Figure 1.3: Schematic description of EDBP process. (a) EDBP single cell consists of three IEMs and three solution chambers. (b) Water splitting reaction and the profile of electric potential at the interface of BP.

If the applied electric field is high enough, at the interface of BP exists a huge electric potential gradient in the range of $10^8 - 10^9 \frac{V}{m}$ [14], which shifts chemical reaction more favor to the water dissociation side, meaning producing acid and base. A detailed discussion can be found in [15].

Figure 1.4 is a typical current-voltage characteristic curve of a single BP with an acid and a base on the two sides of the BP. Electric potential needs to cross a minimum voltage, in this case, U_{diss}, to produce current. This minimum voltage is what water dissociation needs, and it is normally around 0.8V per single BP [16].

For short, applied electric field enhances the reaction speed of water dissociation at the interface of BP, therefore, EDBP is a process of turning electric energy into chemical products (acid and base).

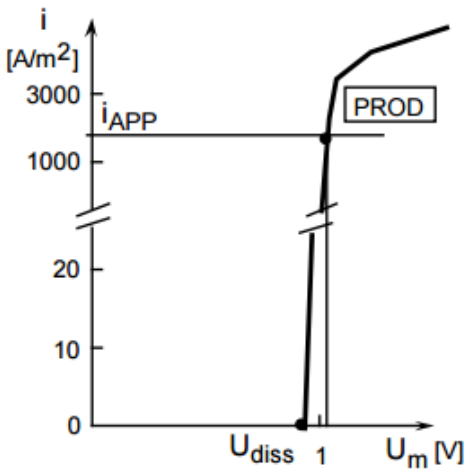

Figure 1.4: Schematic current voltage curve of a BP with an acid and a base on the cation and the anion permeable side, respectively. At the operation point "PROD" the current density i_{APP} is applied [16].

1.3.3 Reverse Electrodialysis with Bipolar Membranes

Reverse Electrodialysis with Bipolar Membranes (REDBP) is a reverse process of EDBP. The system is the same to EDBP, each single cell consists of three IEMs (one CEM, one AEM and one BP) and three electrolyte solution chambers (acid, base and salt chamber). Many single cells connecting each other enhance overall electric potential and power. By putting two electrodes at the end, the stack of REDBP is mounted.

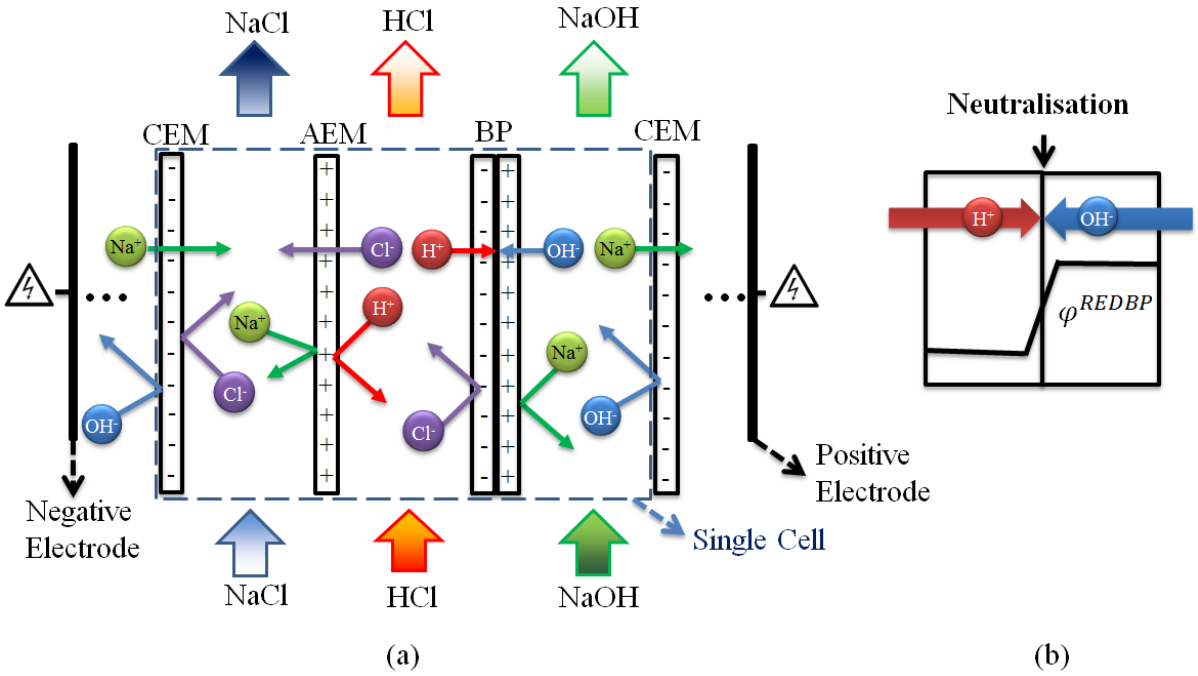

Figure 1.5: Schematic description of REDBP process. (a) REDBP single cell consists of three IEMs and three solution chambers. (b) Neutralization reaction and profile of electric potential at the interface of bipolar membrane.

The driving force of REDBP is neutralization reaction at interface of BP. Since H^+ and OH^- are very active and neutralization reaction is very aggressive, the annihilation of H^+ and OH^- in acid and base chambers respectively drives other ions in REDBP through IEMs to balance electroneutrality (section 3.1.1), which creates electric current (section 3.1.6) through REDBP. During EDBP process a huge electric potential gradient exists at the interface of BP. Therefore, theoretically during REDBP process, a similar huge electric potential should exist at the interface of BP which serves as electric potential. Thus REDBP could be utilized to transfer chemical energy into electric energy, in other words, discharging battery.

The first people introduced BP for energy storage was Alexander Mauro [1] in 1962 when he applied Poisson-Boltzmann equation which was derived by Shockley [2] in his treatment of the p-n semiconductor junction at equilibrium to fixed charge ionic membranes. 19 years ago E. K. Zholkovskij, M. C. Müller, E. Staude and J. Pretz made the first experimental, but they were treating BP more like capacitance [3] [4].

1.4 REDBP as Energy Storage System

REDBP combined with EDBP is the concept of energy storage system. EDBP is charging process: the electric energy is turning salt water into acid and base which are stored in huge tanks. Meanwhile REDBP is discharging process, the acid and base are pumped from tanks into the ‘reaction chamber’ (stack) to produce electricity.

This system consists of following components:

1) Tanks: to store acid, base and (if necessary) salt solution.

2) Stack: the ‘reaction chamber’ which consists of IEMs, solution chambers and electrodes. The detail description of stack is in Chapter 4.

3) Tubes: for connecting tanks and stack.

4) Pumps: for connecting electrolyte between tank and stack.

5) Battery Management System (BMS): electronic system that manages REDBP as energy storage system, such as by controlling its environment, monitoring its state, etc.

Like all the other batteries, many properties are critical for REDBP as energy storage system. In the following section, energy density, efficiency, power density, charge/discharge time, lifetime and other parameters will be analyzed.

Since the most essential part is discharging process, therefore, in this thesis, REDBP represents not only discharging process, but also the whole system as energy storage system.

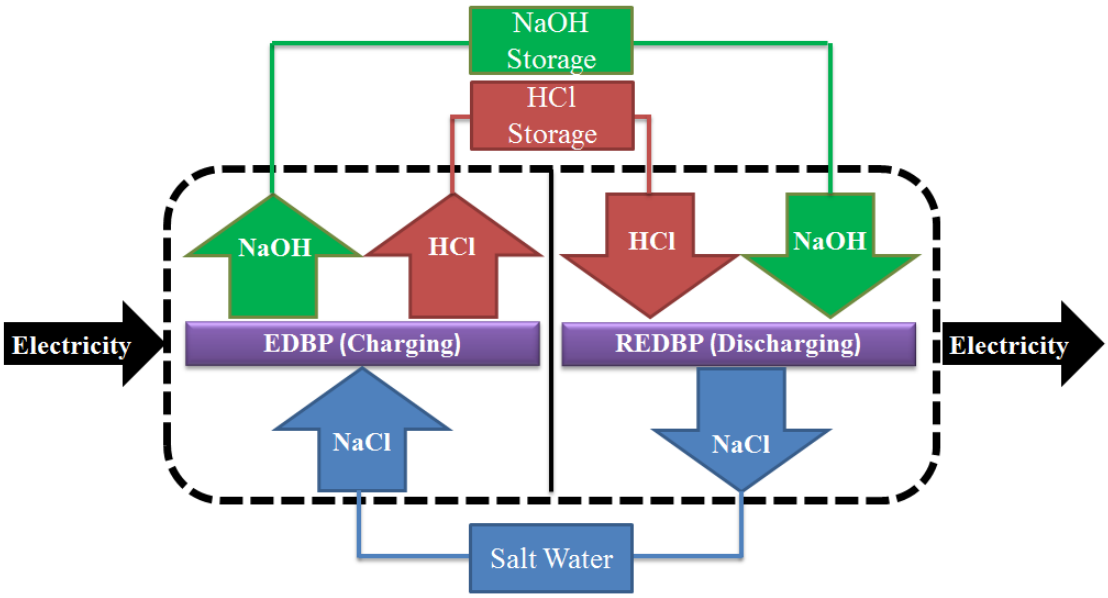

Figure 1.6: Schematic description of REDBP as energy storage system.

1.4.1 Energy Density

Energy density is the amount of energy stored per unit volume or mass, though the latter is more accurately termed specific energy density. Since almost all flow batteries are not suitable for mobile applications, energy density in this thesis specifically addresses the amount of energy per volume $(\frac{Wh}{m3})$.

The driving force of REDBP is neutralization reaction at the interface of BP, so energy density of REDBP relates primarily to concentration of acid and base. The Gibbs free energy of neutralization reaction of H^+ and OH^- per mol is -80kJ/mol at 25°C and 0.1MPa. If efficiency of transferring chemical energy to electric energy is 100%, that will equal to 22.2Wh/mol. Table 1.1 shows the relation of theoretical maximal energy density of REDBP and concentration of acid and base. Please note, that the concentration of acid and base is always the same, and concentration of salt water is always 0.5M which is identical to sea water.

It is obvious that the higher the concentration, the higher the energy density of REDBP will be. Neutralization of 1M acid and base theoretically provides 11kWh/m^3, which is comparable with vanadium redox flow battery whose energy density[1] is typically around 25kWh/m^3 [17].

Combined with concentration process (Figure 1.7) the energy density of REDBP will increase dramatically. At room temperature and pressure, maximal concentration of HCl in water is 13.75M,

[1] Vanadium redox flow battery has relatively low energy density due to poor solubility and stability of the vanadium species.

and NaOH 20.06M. The theoretical maximal energy density of REDBP is 181.3kWh/m^3, which is much better than that of vanadium redox flow battery. If necessary, HCl can be stored in liquid[1] form and NaOH in solid form. This will further increase energy density of REDBP, and this property allows REDBP a suitable candidate even for application of bulk energy storage, such as power to gas.

Concentration	Theoretical Energy Density	Theoretical Energy Density
0.25 M	5.5 Wh/2L	2.8 kWh/m3
0.5 M	11 Wh/2L	5.5 kWh/m3
0.75 M	16.5 Wh/2L	8.3 kWh/m3
1 M	22 Wh/2L	11 kWh/m3
2M	44 Wh/2L	22 kWh/m3

Table 1.1: Theoretical maximum energy density of REDBP. The first column is the concentration of acid and base. The second column is the energy per 2 liters (1 liter of acid and 1 liter of base). The third column is the energy per cubic meter for estimating the total tank size of REDBP.

	HCl in water	NaOH in water
Solubility	720 g/L	1110 g/L
Density	1198 g/L	1525.3 g/L
Molarity	13.75 M	20.06 M
Energy Density of REDBP[2]		181.3 kWh/m^3
Specific Energy Density of REDBP		235.6 kWh/ton

Table 1.2: Properties of HCl and NaOH in water at 20°C and 1bar [18], and theoretical maximal energy density and specific energy density of REDBP with maximal concentration of HCl and NaOH in water.

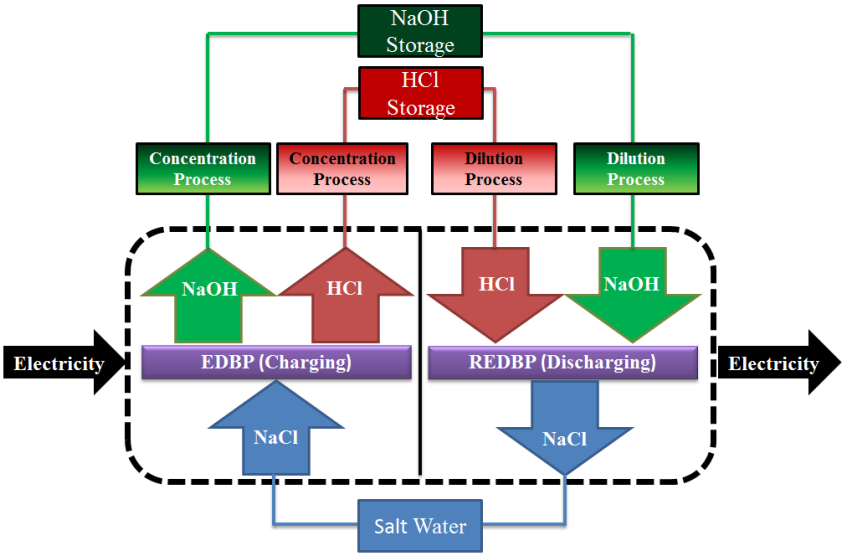

Figure 1.7: Schematic description of REDBP combined with concentration and dilute processes.

[1] Boiling point of HCl is -85.05°C
[2] 22.2Wh/mol. It is calculated by 13.75 M HCl solution and 20.06 M NaOH solution.

1.4.2 Efficiency

As previously introduced, if efficiency of transferring neutralization reaction into electric energy could be 100%, energy density of 1mol/L REDBP would be comparable with vanadium redox flow battery. So the question is what the efficiency of REDBP in reality is.

Figure 1.8 shows the energy flow of REDBP during discharge. Chemical energy will be a) transformed into electric potential and movement of H^+ and OH^- (electric current) in BP, b) further transformed into movement of Na^+ and Cl^- in single cell, c) accumulated and converted into electric energy in stack, and d) managed and provided to end users as usable electric energy in system. Each step will lose some energy due to either unnecessary lost (black processes in figure 1.8) or necessary cost for maintaining REDBP as energy storage system (blue processes in figure 1.8)[1]. Both unnecessary lost and necessary cost need to be as low as possible in order to achieve high overall efficiency. In the following section four efficiencies which represent four steps will be discussed. Please note that in order to simplify the situation, efficiency in this thesis is mainly concerning with discharging process, which means when talking about efficiency REDBP is only discussed as a primary cell.

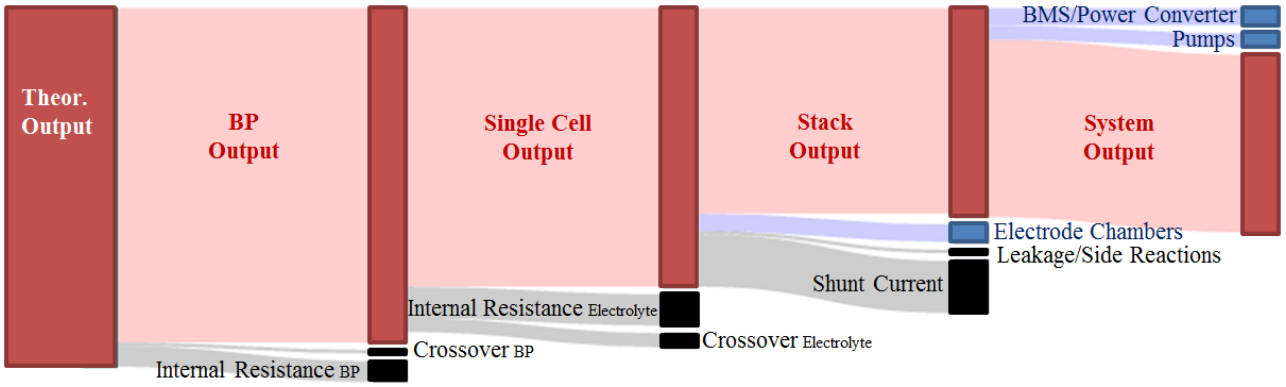

Figure 1.8: Schematic energy flow of REDBP as discharging process.

Step 1: Efficiency of BP by Discharge (η_{BP}^{D})

Due to the non-ideal permselectivity, BP has crossover effect and internal resistance. Crossover effect in BP is undesired mixing process between acid and base [16] whose influence on the performance of single cell will be discussed more thoroughly in section 2.5.3. Internal resistance of BP is a

[1] Strictly speaking there is no clear boundary between unnecessary lost and necessary cost.

macroscopic description of resistance of ionic and mass transport (mainly water molecules) through BP. Thus η_{BP}^{D} can be defined as:

$$\eta_{BP}^{D} = \frac{BP\ Output}{Theor.Maximum\ BP\ Output} \tag{1.1}$$

Output here is confined to electric energy. The usage of coupling heat and electric energy[1] to enhance overall efficiency is not the concern of this thesis. There are many definitions of efficiency[2], however, efficiency in this thesis is only limited to measured voltage divided by theoretical maximum voltage[3]. An example of BP efficiency by discharging is:

$$\eta_{BP}^{D} = \frac{BP\ Voltage}{Theor.Maximum\ BP\ Voltage} \tag{1.2}$$

There are two ways to calculate theoretical maximum BP voltage.

Boltzmann Distribution

In statistical mechanics and mathematics, a Boltzmann distribution (also called Gibbs distribution) [19] is a probability distribution, probability measure, or frequency distribution of particles in a system over various possible states. The Boltzmann distribution is expressed in the form [20]:

$$F(state) \propto e^{-\frac{E}{k_B \cdot T}} \tag{1.3}$$

where E is state energy (which varies from state to state), and $k_B \cdot T$ is the product of Boltzmann's constant and thermodynamic temperature. The ratio of a Boltzmann distribution computed for two states is known as the Boltzmann factor and characteristically only depends on the states' energy difference:

$$\frac{F(state2)}{F(state1)} = e^{\frac{E_1 - E_2}{k_B \cdot T}} \tag{1.4}$$

[1] Also known as cogeneration or combined heat and power (CHP).

[2] Most frequently used in electrochemical cell are voltage efficiency, coulombic efficiency and energy efficiency. Voltage efficiency considers the losses such as activation overpotentials (mainly electrode chambers´ loss in REDBP) and mass transports (internal resistances and water transport in BP). Coulombic efficiency relates losses such as side reactions (in electrode chambers in REDBP), crossovers and leakage currents (due to bad sealings and shunt currents). Energy efficiency equals voltage efficiency times coulombic efficiency.

[3] The main advantage is easy-to-read efficiency on current-voltage characteristic curve. Its disadvantage is neglecting many coulombic losses, such as leakage currents and side reactions.

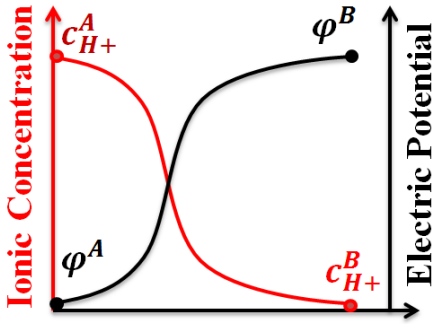

Figure 1.9: Schematic diagram of ionic distribution for calculating electric potential distribution.

As an example, figure 1.9 shows the ionic distribution of H^+. Assuming concentration can represent quantity of H^+, and according to the Boltzmann distribution:

$$\frac{c_{H+}^{B}}{c_{H+}^{A}} = e^{\frac{E_{H+}^{A} - E_{H+}^{B}}{k_B \cdot T}} \tag{1.5}$$

assuming only electric work exists:

$$E_j = W_j = e_0 \cdot z_j \cdot \varphi \tag{1.6}$$

where z_j is charge number[1] of ion j and e_0 is elemental charge, thus:

$$\varphi^A - \varphi^B = \frac{k_B \cdot T}{e_0 \cdot z_j} \ln\left(\frac{c_{H+}^{B}}{c_{H+}^{A}}\right) \tag{1.7}$$

$$\text{Since } \frac{k_B}{e_0} = \frac{R}{F} \tag{1.8}$$

where F is Faraday´s constant and R is gas constant, Equation 1.7 can be rewritten as:

$$\varphi^A - \varphi^B = \frac{R \cdot T}{F \cdot z_j} \ln\left(\frac{c_{H+}^{B}}{c_{H+}^{A}}\right) \tag{1.9}$$

If position A is 1M HCl solution and B is 1M NaOH, the electric potential difference between A and B at 25°C and 0.1MPa is:

$$\varphi^B - \varphi^A = V_T \cdot \ln\left(\frac{c_{H+}^{A} \cdot c_{OH-}^{B}}{K_W}\right) = 0.828\ [V] \tag{1.10}$$

where K_W is self-ionization constant of water, which equals $10^{-13.99}$ at 25°C and 0.1MPa, and V_T is thermal voltage which is equal to $\frac{R \cdot T}{F}$. Table 1.3 shows the change of K_W and V_T with temperature and pressure.

[1] Charge number of H^+ is +1.

Table 1.3: K_W and V_T values for liquid water [21].

Temperature (°C)	Pressure (MPa)	K_W	V_T [mV]
0	0.1	$10^{-14.95}$	23.54
25	0.1	$10^{-13.99}$	25.69
50	0.1	$10^{-13.26}$	27.85
75	0.1	$10^{-12.7}$	30.00
100	0.1	$10^{-12.25}$	32.16
150	0.47	$10^{-11.64}$	36.46
200	1.5	$10^{-11.31}$	40.77
250	4	$10^{-11.20}$	45.08
300	8.7	$10^{-11.34}$	49.39
350	17	$10^{-11.92}$	53.70

If this ionic distribution is due to BP, then this electric potential difference is the electric potential created by BP between acid and base solution, which depends on concentration of solution as well as temperature and pressure as shown in figure 1.10. This electric potential is also known as Electromotive Force (EMF).

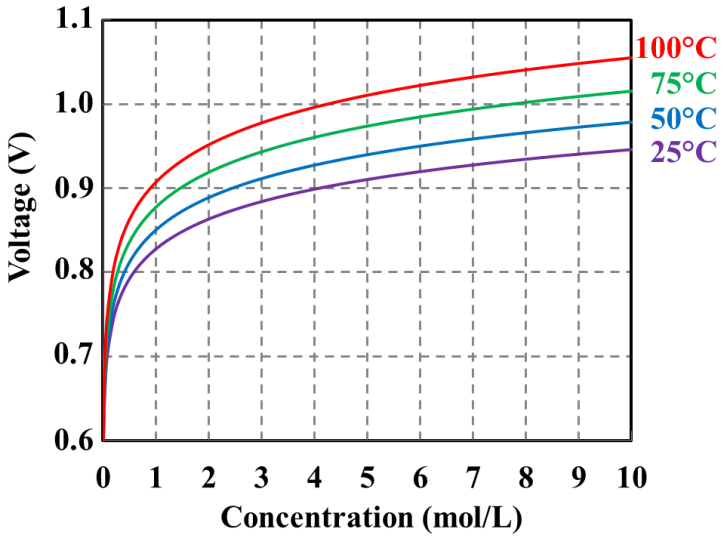

Figure 1.10: Electromotive force of neutralization reaction of H^+ and OH^- with different solution concentration and temperature at 0.1MPa.

Thermodynamics

The driving force of REDBP is neutralization reaction. The maximum or reversible work per mole at constant temperature and pressure can be expressed as molar Gibbs free energy:

$$H_3^+O + OH^- \rightarrow 2H_2O \qquad \textbf{(1.11)}$$

Assuming all the work can be converted into electric work, and move electrons to an infinite far distance:

$$\Delta g = z_{e-} \cdot F \cdot E \quad \textbf{(1.12)}$$

where E is EMF, and z_{e-} is the charge number of electron, which equals -1.

According to Nernst equation:

$$EMF_{theor.max} = EMF^0 - \frac{R \cdot T}{F} \ln\left(\frac{a^2_{H_2O}}{a_{H_3^+O} \cdot a_{OH^-}}\right) \quad \textbf{(1.13)}$$

where EMF^0 is standard[1] EMF and equals $-\frac{\Delta g^0}{F}$.

By assuming activity (section 3.1.2) of water molecule is constant by changing ionic concentration and temperature, and activity coefficient of H_3^+O and OH^- equals 1, equation 1.13 can be written as:

$$EMF_{theor.max} = EMF^0 - V_T \cdot \ln\left(\frac{c^0_{H_3^+O} \cdot c^0_{OH^-}}{c_{H_3^+O} \cdot c_{OH^-}}\right) \quad \textbf{(1.14)}$$

where $c^0_{H_3^+O}$ and $c^0_{OH^-}$ are the standard concentration of H_3^+O and OH^- in water solution, Δg^0 is standard molar Gibbs free energy of neutralization reaction in water solution.

Put different temperatures and changing concentration into equation 1.14, the results are the same as shown in figure 1.10, which is calculated by Boltzmann distribution.

The results of calculating EMF using both methods are the same. Both methods require the same assumptions of reversible electric work and neglecting inter-molecular forces (unchanged activity of water molecules and activity coefficient of ion is one). EMF sets the theoretical limitation of the highest voltage by discharging of neutralization reaction of H^+ and OH^-. Thus η^D_{BP} can be calculated by dividing measured voltage by EMF:

$$\eta^D_{BP} = \frac{BP\ Voltage}{EMF} \quad \textbf{(1.15)}$$

Step 2: Efficiency of Single Cell by Discharge (η^D_{SC})

CEM and AEM have crossover effect and internal resistance, too. Combined with internal resistance of electrolyte solutions, the single cell efficiency is lower than BP efficiency. η^D_{SC} can be defined as:

$$\eta^D_{SC} = \frac{Single\ Cell\ Output}{Theor.\ Maximum\ Single\ Cell\ Output} \quad \textbf{(1.16)}$$

In this case, theoretical maximum single cell output is theoretical maximum BP output. Thus:

$$\eta^D_{SC} = \frac{Single\ Cell\ Voltage}{EMF} \quad \textbf{(1.17)}$$

[1] 1mol/l (section 3.1.2)

Step 3: Efficiency of Stack by Discharge (η^{D}_{Stack})

A stack consists of many single cells in a series, thus the definition of η^{D}_{Stack} is clear:

$$\eta^{D}_{Stack} = \frac{Stack\ Output}{Theor.max.Stack\ Output} = \frac{Stack\ Voltage}{Stack\ Size \cdot EMF} \quad \textbf{(1.18)}$$

where stack size is how many single cells are in one stack. Calculating and measuring η^{D}_{Stack} answers the question-whether additional losses exist by build-up of the stack except the necessary energy cost in electrode chambers? The details of stack will be illustrated in Chapter 4 and 5. In short, stack efficiency is affected by properties of electrolytes, power density, self-discharge, leakage, etc.

Step 4: Efficiency of System by Discharge (η^{D}_{System})

Pumps and battery management system are the necessary energy costs for REDBP systems. BMS consumes additional energy to maintain the whole system in its safe operating area. In the case of REDBP, temperature maintenance and off-gas (H_2/O_2) treatment are considered to be the biggest consumptions. About the energy consumptions of pumps and BMS will not appear in this thesis.

In short, there are many factors influencing efficiency. Figure 1.8 does not fully illustrate the real situation. In reality, many losses and costs are correlated with each other; reducing one loss will not necessarily enhance the performance of the whole system. There are strong evidences showing the correlation between crossover and internal resistance of electrolyte (section 2.5.3), internal resistance of electrolyte and shunt current (section 5.4.2 and section 5.4.9), shunt current and power consumption of pumps (section 5.4.6-5.4.8).

1.4.3 Power Density

Power density (PD) is one of the main characters defining the application field of one energy storage technology. Like efficiency, power density has many definitions as well mainly due to the complexity of BP system.

Power Density of Bipolar Membrane

Power (W=J/s) is related to reaction rate directly. Considering the driving force of REDBP is neutralization reaction (which is very aggressive), the Power Density (PD) of BP should not be low.

Power density of BP is defined as the amount of power (time rate of energy transfer) per active surface as shown in equation 1.19. The active surface of BP is the area where the neutralization reaction is

supposed to happen. The electric potential should be homogeneously and equally distributed on this surface, and electric current should be vertically passing through it.

$$PD_{BP} = Voltage \cdot Current\ Density\ [\frac{W}{cm^2}] \quad \textbf{(1.19)}$$

Therefore, the investigation of power density can be seen as investigating voltage and current density.

Power Density of Single Cell

Each single cell has three IEMs and three solution chambers. It is confusing when active surface is being used to describe power density in a 3-dimensional way. Thus power density of single cell is defined as the amount of power per unit volume of single cell.

$$PD_{SC} = \frac{Power\ of\ Single\ Cell}{Volume\ of\ Single\ Cell}\ [\frac{W}{cm^3}] \quad \textbf{(1.20)}$$

The volume of a single cell is calculated by multiplying the active surface and total thickness of a single cell.

Power Density of Sum of All Single Cells

Power density of sum of All Single Cells (AllSCs) is therefore the amount of power per unit volume of AllSCs.

$$PD_{AllSCs} = \frac{Power\ of\ AllSCs}{Number\ of\ Single\ cells \cdot Volume\ of\ Single\ cell}\ [\frac{W}{cm^3}] \quad \textbf{(1.21)}$$

Power Density of Stack

Considering energy consumption in electrode chambers:

$$PD_{Stack} = \frac{Power\ of\ Stack}{Volume\ of\ Stack}\ [\frac{W}{cm^3}] \quad \textbf{(1.22)}$$

1.4.4 Charging/Discharging Time

If charge/discharge (Ch/DisCh) time is too short, even with very high power density, the energy density would be very low. In addition, Ch/DisCh time of energy storage system is one of the key parameters for helping large-scale integration of unsteady and intermittent renewables into the electrical grid. Therefore, it requires attention.

1.4.5 Lifetime

Lifetime of energy storage system refers to the number of Ch/DisCh cycles. Each charging or discharging process will shorten the lifetime of REDBP system by side reactions, material degradation, etc.

In the case of flow battery system, the lifetime of following components is important:

a) Lifetime of Stack

Lifetime of stack is primarily limited by the sustainability of IEMs. The life time of AEM will be shortened by exposure to strong alkaline (2M) conditions resulting from the transformation of polymeric binder of AEM [22]. This will restrain the concentration of base solution in REDBP system which affects the energy density of REDBP in practice directly, and is considered as one of the main obstacles to utilizing REDBP as energy storage system.

b) Lifetime of Electrolyte

Because of side reactions and material degradation, the composition of electrolyte will change. This will affect stack performance which harms energy density, efficiency, power density, Ch/DisCh time and lifetime of other components. In the case of REDBP, the main change of electrolyte is concentration of acid and base, which is due to crossover (section 2.5.3), self-discharge (section 4.2.3), etc.

c) Lifetime of Pumps and Pipes:

Sustainability of pumps and pipes of flow battery depends on the composition of electrolyte. Considering HCl and NaOH solutions are common materials in chemical industry, the quality and lifetime of pumps and pipes can be guaranteed for sure.

For short, the main concern of lifetime of REDBP lies in sustainability of AEM.

1.4.6 Other Factors

Environmental Impact

One of the main purposes of energy storage system is for large-scale integration of renewables into the electrical grid. Therefore, energy storage system itself must be environmental friendly. It is indeed one the most amazing aspects of REDBP: It is in principle using the most common material on earth - salt water (for instance, seawater) - to storage electric energy. Even when great leakage of tanks happens, HCl or NaOH solution will not have tremendous environmental impact compared with other forms of flow batteries.

Life Cycle Cost

Life cycle cost typically includes initial costs, installation and commissioning costs, energy costs, operation costs, maintenance and repair costs, down time costs, environmental costs, and decommissioning and disposal costs.

Currently the cost of electrolyte is the lion´s share of vanadium redox flow battery [23], which hinders its fully commercialization. However, the electrolytes of REDBP are either very cheap materials (acid and base) or free of charge material (seawater as salt solution), which makes REDBP a great candidate as energy storage system in large scale application. This is another amazing aspect of REDBP as energy storage system.

1.5 Objectives

Considering the limitation of work load and content length, there are only 3 aspects being investigated in this thesis: power densities, efficiencies and charging/discharging time. And the following part of this thesis is divided into:

Chapter 2: Experiments of Single Cell

Chapter 3: Modeling and Simulation of Single Cell

Chapter 4: Experiments of Stack

Chapter 5: Modeling and Simulation of Stack

All in all, this thesis is trying to investigate REDBP as discharging process of energy storage system as thoroughly as possible, as well as trying to be a guideline for the future on this topic.

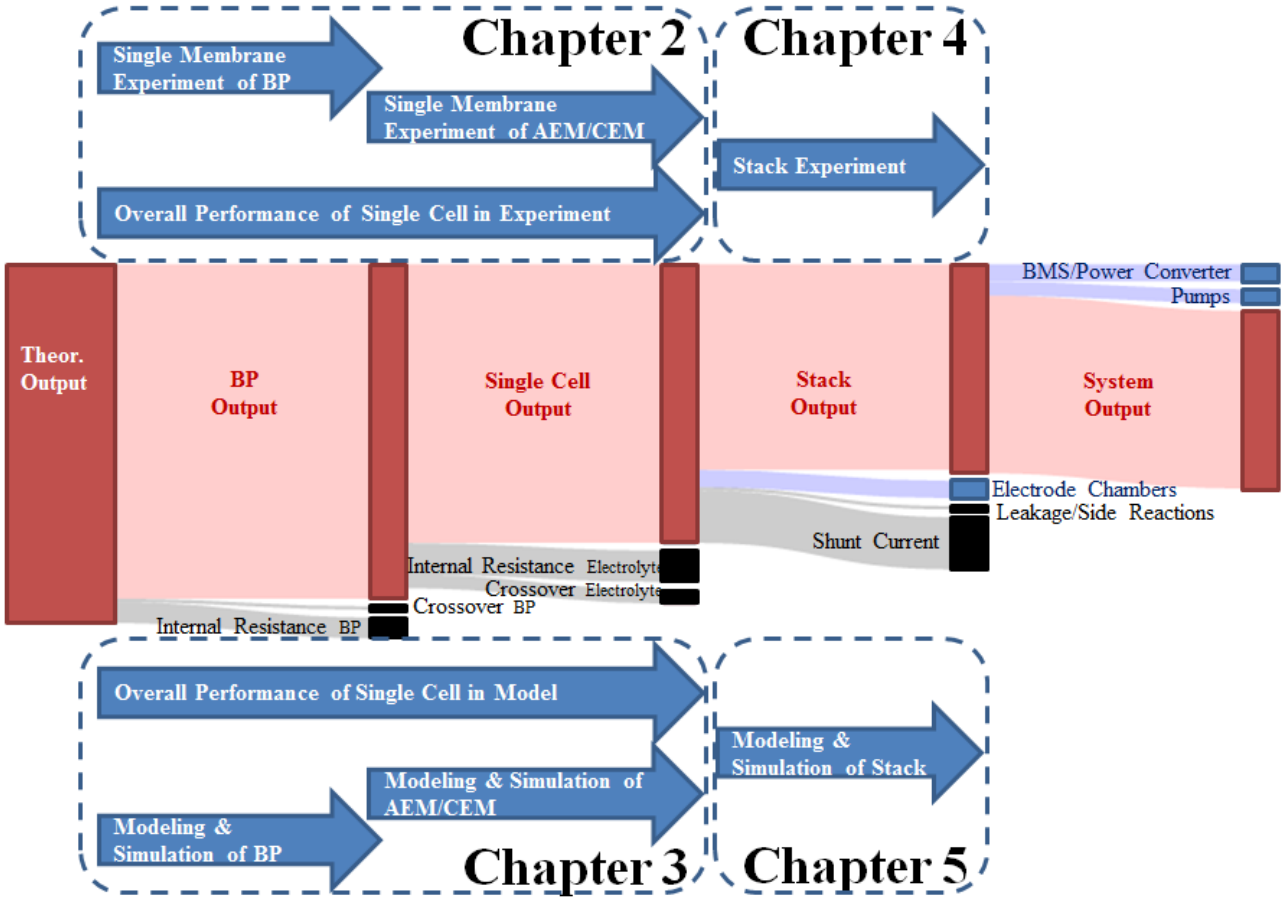

Figure 1.11: Task procedure of this thesis.

Chapter 2

Experiments of Single Cell

REDBP stack itself is a very complicated system, which consists of several single cells and two electrode chambers. Each single cell has three IEMs (one CEM, one AEM and one BP) and three electrolyte solution chambers (acid, base and salt chambers).

In this chapter, the single cell performance will be investigated. Three IEMs will be characterized separately. The overall performance of the single cell will be evaluated at last.

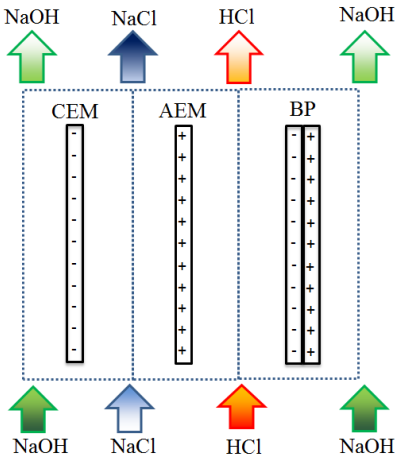

Figure 2.1: Schematic description of REDBP single cell, which consists of three IEMs and three solution chambers.

2.1 Characterization Methods

In section 1.4 many aspects have been introduced for characterization of REDBP as energy storage system, such as energy density, power density, efficiency, Charging/Discharging (Ch/DisCh) time, lifetime, cost, etc. In this thesis only power density, efficiency and Ch/DisCh time will be investigated.

2.1.1 Open Circuit Voltage

The potential difference mentioned in the batteries and cells is usually the open circuit voltage (OCV). The OCV of batteries is often quoted under particular conditions, such as temperature and state-of-charge (concentration of acid and base in the case of REDBP), which are the main influential

parameters of OCV. Theoretically OCV equals Electro Motive Force (EMF). However, due to crossover effect and other losses, OCV is always lower than EMF.

2.1.2 Current-Voltage Curve

Current-voltage characteristic curve (I-V Curve), also known as efficiency curve, is one of the main characterization methods of all electrochemical cell and solar cells. It is a relationship, typically represented as a chart or graph, between the electric current through a circuit, device, or material, and the corresponding voltage, or potential difference across it, as in the example shown below:

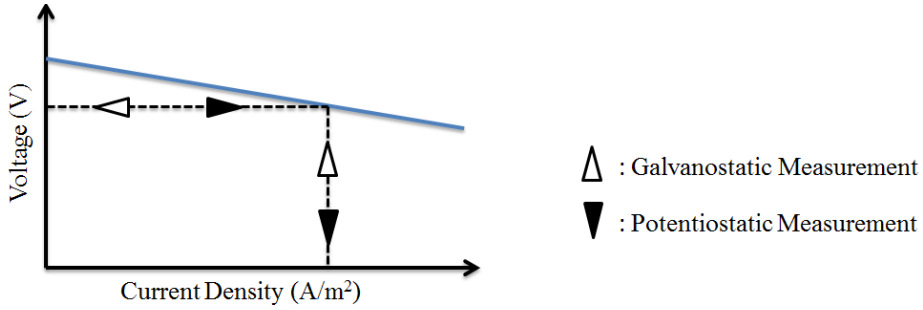

Figure 2.2: Schematic diagram of I-V curve of discharging process.

There are two ways to obtain I-V curve. One is by galvanostatic measurement, the other is by potentiostatic measurement. Both are widely employed to electrochemical process [24]. Galvanostatic measurement refers to an experimental technique in which an electrode is maintained at a constant current in an electrolyte. Potentiostatic measurement refers to an experimental technique in which a constant potential is applied and the current is recorded as a function of time. Since this thesis is mainly focusing on ionic transport, galvanostatic measurement is used to maintain a constant electric current throughout electrolyte while measuring the changes of voltage.

As previously introduced in section 1.4.2, efficiency of BP by discharging is:

$$\eta_{BP}^{D} = \frac{BP\ Voltage}{EMF} \tag{2.1}$$

The discharging efficiency can be directly calculated from I-V curve as shown in figure 2.3. η_{BP}^{D} has direct relation with current density, with increasing current density η_{BP}^{D} decreases.

The distance between charge curve and discharge curve is pure loss which should be as small as possible. Two curves converge at zero current density ($i = 0$), therefore, OCV is the maximal voltage of discharging process and the minimal voltage of charging process.

Current density times voltage equals Power Density (PD). Thus the PD curves can also be obtained on I-V curves.

At OCV, efficiency reaches its maximum but the power density is zero. Therefore, there is always a compromise between efficiency and power density.

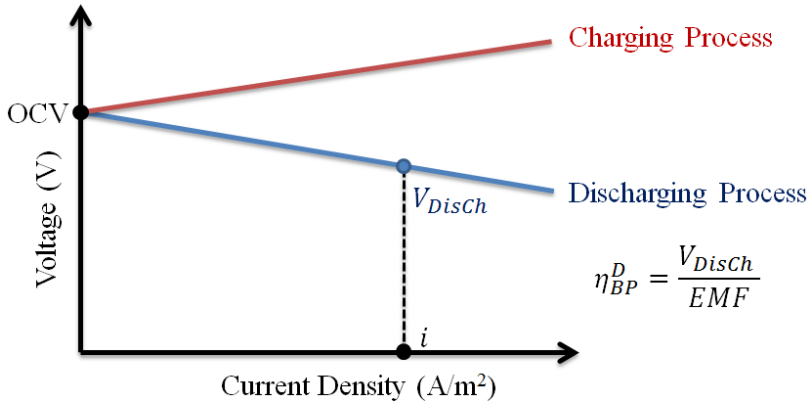

Figure 2.3: I-V curves of charging process and discharging process, as well as calculation of efficiency of bipolar membrane by discharging.

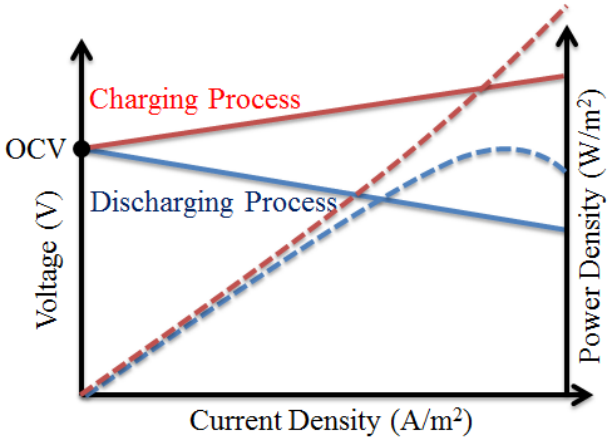

Figure 2.4: I-V curves of charging process and discharging process with power density curves.

2.1.3 Chronopotentiometry

Factor of Ch/DisCh time will be investigated using chronopotentiometry (CPM), in which a constant current is switched on and off while the time evolution of the electric potential will be recorded. A typical CPM looks like the figure 2.5:

Compared with I-V curve, CPM is mainly focusing on the change of voltage by constant current density over time. CPM curves are influenced by temperature, concentration, current density, etc. An ideal battery reflected on CPM curve should have following aspects.

1) High OCV.
2) High current density with small gap between voltage of charge (V_{Ch}) and discharge (V_{DisCh}).
3) No change of voltage of charge (V_{Ch}) or discharge (V_{DisCh}) throughout the time.
4) No change of OCV after many cycles.

Using CPM the best working condition of battery will be found.

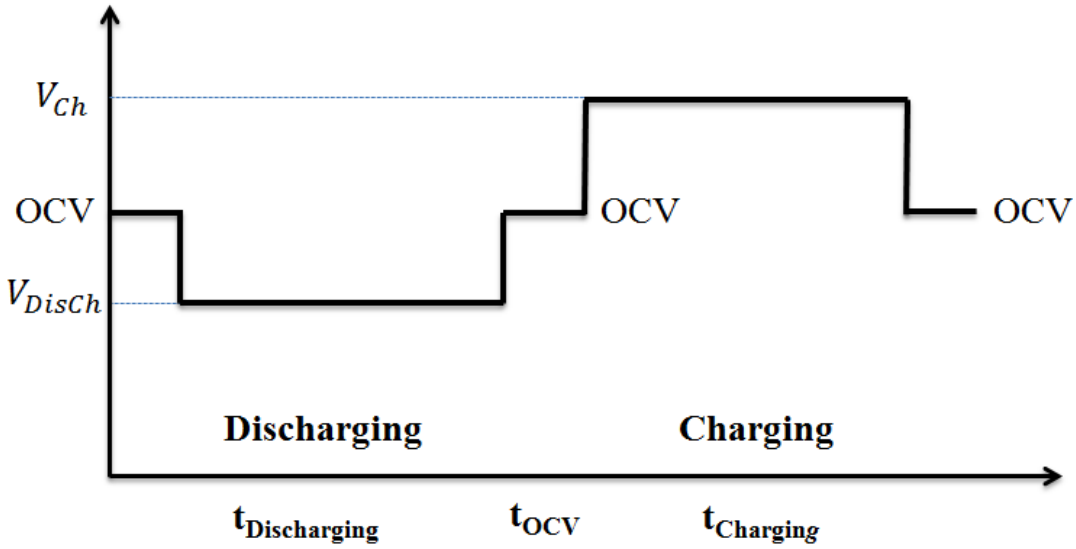

Figure 2.5: Chronopotentiometry of discharging and charging process.

2.1.4 Cycle Test

Lifetime of energy storage system refers to the number of Ch/DisCh cycles before an energy storage system starts to reduce its performance. Each charging or discharging process will shorten the lifetime of REDBP system by side reactions, material degradation, etc. In the case of single cell, assumed there is no side reaction, the main degradation is due to the changes of electrolyte solution and the aging of IEMs. And this degradation process presumably is affected by current density and concentration of solution [22].

In this thesis, cycle test will be performed by several CPM in sequence with constant current density.

2.2 Test Facility

In order to fulfill the requirement of characterization of REDBP single cell, two difficulties need to overcome:

1) How to measure electric potential between IEM with enough accuracy without introducing significant additional errors.
2) Since all experiments will be conducted galvanostatically, how to ensure the electric current flowing through electrodes equal to the electric current through testing IEM.

The first one is overcome by saturated calomel electrodes combined with Haber-Luggin capillaries. The second is resolved by careful design of single test cell.

2.2.1 Voltage Measurements in Electrolyte Solution.

Normally by connecting a voltmeter - or other voltage measurement instrument - to the circuit at proper points, the desired voltage difference will be measured. However, in the case of electrolyte solution, a metal into an aqueous solution will bring additional error, since almost any surface in contact with an aqueous salt solution will have a net charge [25] [26].

Without considering any adsorption of ions, dipoles and neutral molecules (through van der Waals or coulombic interactions with the charged surface, or even through forming stronger bonds, as in the case of chemisorption [26, p. 120]), this net charge at the interface between metal (noble or non-noble metal) and electrolyte solution is due to electrochemical reaction. The following table shows the standard potentials for gas (in contact with Pt electrode and an aqueous electrolyte) vs standard hydrogen electrode at 20°C [26, p. 96].

Half Cell	Electrode Process	Potential (V)
$\boldsymbol{Pt \mid H_2 \mid H_3O^+}$	$2H_3O^+ + 2e^- \rightleftharpoons H_2 + 2H_2O$	0.0000
$\boldsymbol{Pt \mid H_2 \mid OH^-}$	$2H_2O + 2e^- \rightleftharpoons H_2 + 2OH^-$	-0.8277
$\boldsymbol{Pt \mid Cl_2 \mid Cl^-}$	$Cl_2 + 2e^- \rightleftharpoons 2Cl^-$	+1.3700
$\boldsymbol{Pt \mid O_2 \mid H_3O^+}$	$1/2O_2 + 2H_3O^+ + 2e^- \rightleftharpoons 3H_2O$	+1.2290
$\boldsymbol{Pt \mid O_2 \mid OH^-}$	$1/2O_2 + H_2O + 2e^- \rightleftharpoons 2OH^-$	+0.4010

Table 2.1: Standard potentials for gas (in contact with Pt electrode and an aqueous electrolyte) vs standard hydrogen electrode at 20°C [26, p. 96].

At equilibrium, once a double layer is formed and a potential difference sets up:

$$\tilde{\mu}_{ox}(S) + n\tilde{\mu}_{e-}(M) = \tilde{\mu}_{red}(M) \quad \textbf{(2.2)}$$

Electric potential at the interface between metal (M) and solution (S) can be calculated:

$$\tilde{\mu}^0_{ox} + RTln(a_{ox}) + nF\varphi_S - nF\varphi_M = \tilde{\mu}^0_{red} + RTln(a_{red}) \quad \textbf{(2.3)}$$

hence

$$\Delta\varphi = \varphi_M - \varphi_S = \frac{\tilde{\mu}^0_{ox} - \tilde{\mu}^0_{red}}{nF} + \frac{RT}{nF}\ln\left(\frac{a_{ox}}{a_{red}}\right) = \Delta\varphi^0 + \frac{RT}{nF}\ln\left(\frac{a_{ox}}{a_{red}}\right) \quad \textbf{(2.4)}$$

From the above equation, it is obvious that the electric potential at the interface between metal and electrolyte solution has a direct relation with activity of oxidized and reduced components. In the case of Table 2.1 is the pressure of gas, activity of ions and type of gas and ions in solution.

As illustrated in the figure 2.6, by using two Pt wires (albeit inert metal), the measured voltage is a mixing of the electric potential of two interface potentials, two solution potentials and membrane potential (which is the desired one):

$$\varphi_{Pt2} - \varphi_{Pt1} = \Delta\varphi_{\,Pt1|Solution1} + \Delta\varphi_{\,Solution\,1} + \Delta\varphi_{\,IEM} + \Delta\varphi_{\,Solution\,2} + \Delta\varphi_{\,Solution2|Pt2} \quad \textbf{(2.5)}$$

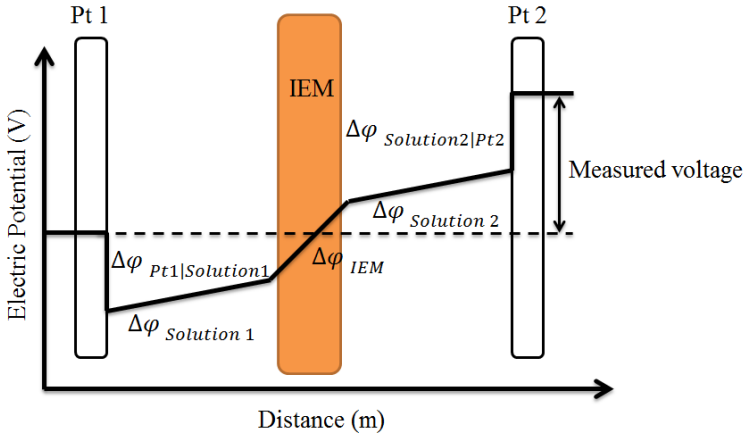

Figure 2.6: Electric potential profile between Pt1 and Pt2.

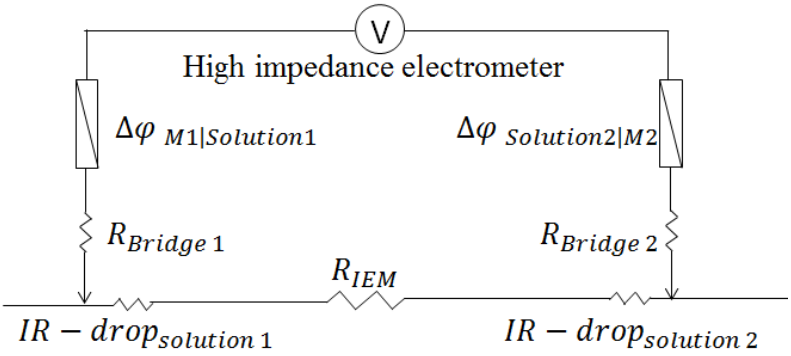

Figure 2.7: Equivalent circuit of measuring electric potential between IEM.

Please note that $\Delta\varphi_{IEM}$ is consisting two diffusional layers both of which have 50μm in order to compare with simulation result in section 3.2.1.

If the sum of two interface potentials ($\Delta\varphi_{Pt1|Solution1}$ and $\Delta\varphi_{Solution2|Pt2}$) is unknown due to unequal conditions, the electric potential between two Pt wires will be meaningless. In addition, using Pt wires cannot exactly pinpoint the measuring points, which leads to unknown and changing electric potential ($\Delta\varphi_{Solution}$) between measuring points and IEM, this electric potential is known as IR-drop (voltage drop due to current (I) times resistance (R)). Therefore, measuring electric potential in electrolyte can be presented as equivalent circuit in figure 2.7.

The physical meaning of each element will be introduced:

(1) R_{IEM}: the electric resistance of IEM (with two diffusional layers both of which have 50μm in order to compare with simulation result), the electric potential across R_{IEM} is desired potential.

(2) $IR-drop$: the electric resistance of electrolyte solution between measuring point and the surface of IEM. Since by ideal mixing the resistance of electrolyte solution is considered constant (section 5.1.1), therefore, the voltage drop in this area can be treated as current times resistance (IR).

(3) R_{Bridge}: the electric resistance of measuring probe itself. In the case of Pt wire, R_{Bridge} represents the resistance of Pt, which is proportional to its length and inversely proportional to its diameter.

(4) $\Delta\varphi_{M1|Solution1}$ or $\Delta\varphi_{Solution2|M2}$ represents the electric potential at the interface between metal and electrolyte solution due to the electrochemical reaction.

(5) High impedance electrometer is the normal voltage measuring device.

In order to eliminate or reduce the additional error due to the electrochemical reaction at the interface between metal and electrolyte solution, either these two potentials at interfaces are known[1], or these two potentials are reversely the same (under same conditions). Moreover, two IR-drops need to be eliminated as well. Therefore, saturated calomel electrodes combined with Luggin capillaries will be introduced in the following.

2.2.2 SCE with Luggin Capillaries

The saturated calomel electrode (SCE) is a reference electrode where the reaction happens between mercury chloride and elemental mercury. The aqueous phase in contact with the mercury and the mercury chloride (Hg_2Cl_2, "calomel") is a saturated solution of KCl in water. The electrode is linked via a porous frit (as a salt bridge) to the solution in which the other electrode is immersed.

A Luggin capillary (also Luggin probe, Luggin tip, or Haber-Luggin capillary) is a small tube that is used in electrochemistry which defines a clear sensing point for the reference electrode near the working electrode or IEM. The detailed structure of SCEs and Luggin capillaries is illustrated in the figure 2.8. Measuring electric potential with SCE and Luggin capillary can be presented as an equivalent circuit as shown in figure 2.9.

There are several advantages using SCE and Luggin capillary to measure electric potential:

1) $\Delta\varphi_{SCE1}$ and $\Delta\varphi_{SCE2}$ are reversely the same.
2) If ionic concentration between IEM and measuring point is known, then IR-drops will be constant and known.
3) By using intermediate KCl solution (2M), there is no additional diffusional potential[2] across R_{Bridge}.
4) By excluding two IR-drops from measuring electric potential, the required voltage between IEM will be obtained.

[1] By connecting with standard hydrogen electrode for example.
[2] K^+ and Cl^- have similar mobility in water.

But enough attention needs to be paid when using SCE and Luggin capillary to measure electric potential:

1) IR-drop should not be eliminated, because a distance should be maintained between IEM and measuring point to avoid shadow effect and concentration polarization phenomena [27]. This distance is always equal to the diameter of the tip of Luggin capillary.
2) Intermediate KCl solution in Luggin capillary is to maintain a constant electric potential between the tip of SCE and measuring point, as well as to prevent the pollution of saturated KCl solution inside of SCE. Therefore, the pollution of intermediate KCl solution itself cannot be avoided and the pollution of measuring solution by diffusion of KCl from Luggin capillary should be reduced. Therefore, the intermediate KCl solution should be fresh all the time[1], and the measuring process should not be too long. Detailed experiment protocol is in table 2.2.

Figure 2.10 is the design of Luggin capillaries in this thesis, which are made in glass by Hilgenberg GmbH[2] (see Appendix A).

All the above discussions about measuring techniques are for designing a suitable test cell in order to obtain reliable experiment results.

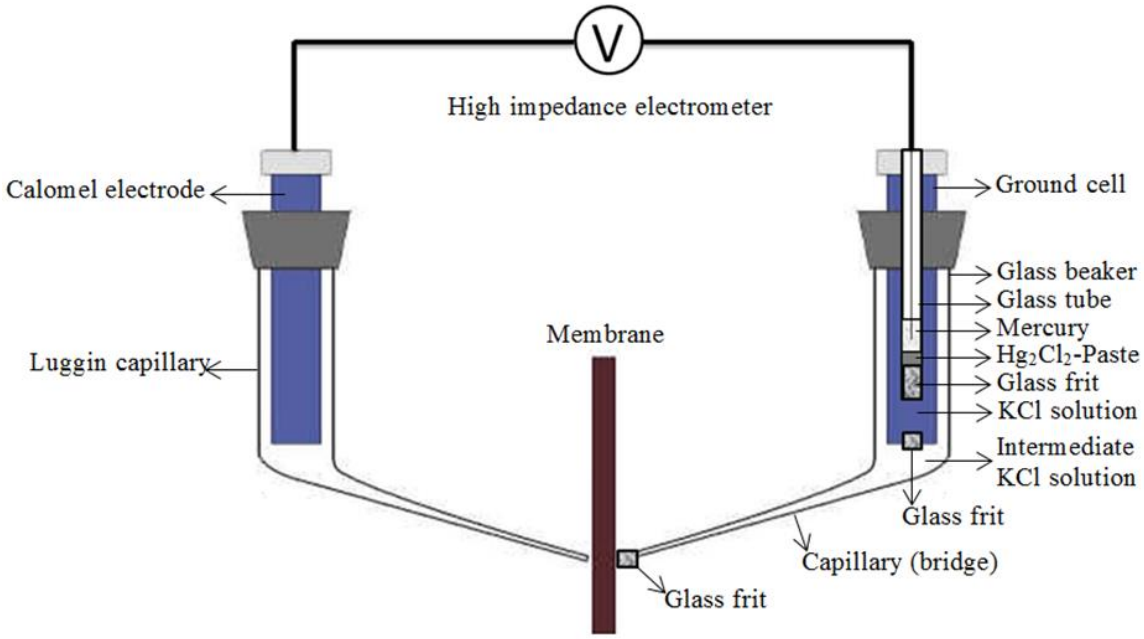

Figure 2.8: Measuring electric potential with SCE and Luggin capillaries.

[1] In this thesis, changing frequency of intermediate KCl solution and KCl solution in SCE is every 4 hours and every week respectively.
[2] http://www.hilgenberg-gmbh.de/innovative-glasprodukte/

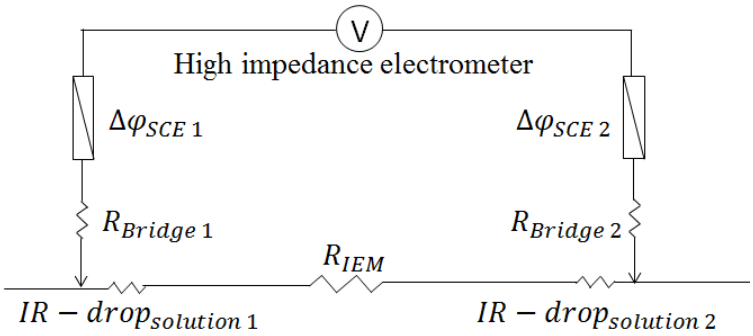

Figure 2.9: Equivalent circuit of measuring electric potential between IEM using standard calomel electrode and Luggin capillaries. IR-drop means voltage drop due to electrolyte resistance and current flowing through it.

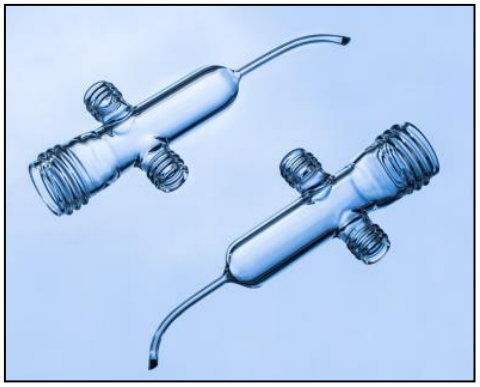

Figure 2.10: Design of Luggin capillaries.

2.2.3 Single IEM Test Stack

Test stack for single membrane in this thesis has been designed as in figure 2.11, and the real test stack is shown in figure 2.12. It has 6 compartments. Inside of stack there are one single cell of REDBP (three types of IEMs), one additional salt solution chamber and two electrode chambers. Each electrode chamber has an additional CEM to prevent transport of other ions except Na^+. The detailed descriptions of single membrane test stack are listed below:

1) The thickness of chamber 3 and 4 is 30mm. The thickness of chamber1, 2, 5 and 6 is 5mm.
2) Electrolyte solution is pumped through the test stack from bottom to top to avoid gas accumulation.
3) Electrolyte solution in chamber 2 and 5 is from the same tank. In order to avoid shunt current (section 4.2.3 or Chapter 5), the connection tubes between the chambers (both inlet and outlet) should be long enough[1].
4) As 3), the connection tubes between chamber 1 and 6 are long enough[2].

[1] In this thesis, 0.5m.
[2] In this thesis, 5m.

5) All chambers are filled up with spacers for better mixing. The void factor is 80%.
6) The measuring point of Luggin capillary is pointing at the center of active surface of IEM.
7) The distance between IEM and the tip of Luggin capillary is maintained at 1mm.
8) An additional resistor (2Ω) is connected on the outer cable to calculate electric current throughout the stack. Please note that the resistance of resistor will change by changing temperature, thus a cooling process with a small fan is necessary.
9) Direct current power supply is for delivering constant current by charging and discharging process[1].

With careful design of test stack and proper operation during experiment as listed in table 2.2, the measurement is reliable and the deviation[2] is controlled within $\pm$5mV.

Table 2.2: Single membrane experiment protocol in this thesis.

	Process	**Time**	**Reasons**
1st	Opening the valves		Valves are protecting solution in the tanks from crossover effect.
2nd	Turning on the pumps (linear velocity of 2cm/s in chamber)	5min	Checking leakage.
3rd	Rolling over the cell	2min	Degassing[a)]
4th	Filling up KCl in capillaries		Degassing and changing KCl[b)]
5th	2 Disch/Ch cycles	60min	Increasing temperature. Activating IEM[c)].
6th	Chronopotentiometry	43min /each	From 10mA/cm^2 to 90mA/cm^2
7th	Disch/Ch curves	38min /each	
8th	Taking samples from each solution		For coulombic analysis.
9th	Turning off the pumps and valves		

a) There is evidence showing that the gas bubbles attached on the surface of the tip of Luggin capillary have influence on measurement.

b) Gas bubbles inside of Luggin capillaries should be avoided.

c) During charging and discharging process, temperature of electrolyte will increase, and temperature is one of the main influence parameters of the performance of IEM, therefore, an activation process is very necessary.

[1] By discharging, the produced power of single cell is not enough for driving electrochemical reaction in electrode chambers; therefore, direct current power supply will be used to 'assist' discharging process.
[2] Deviation is defined as the difference between the observed value of a variable and the variable's mean.

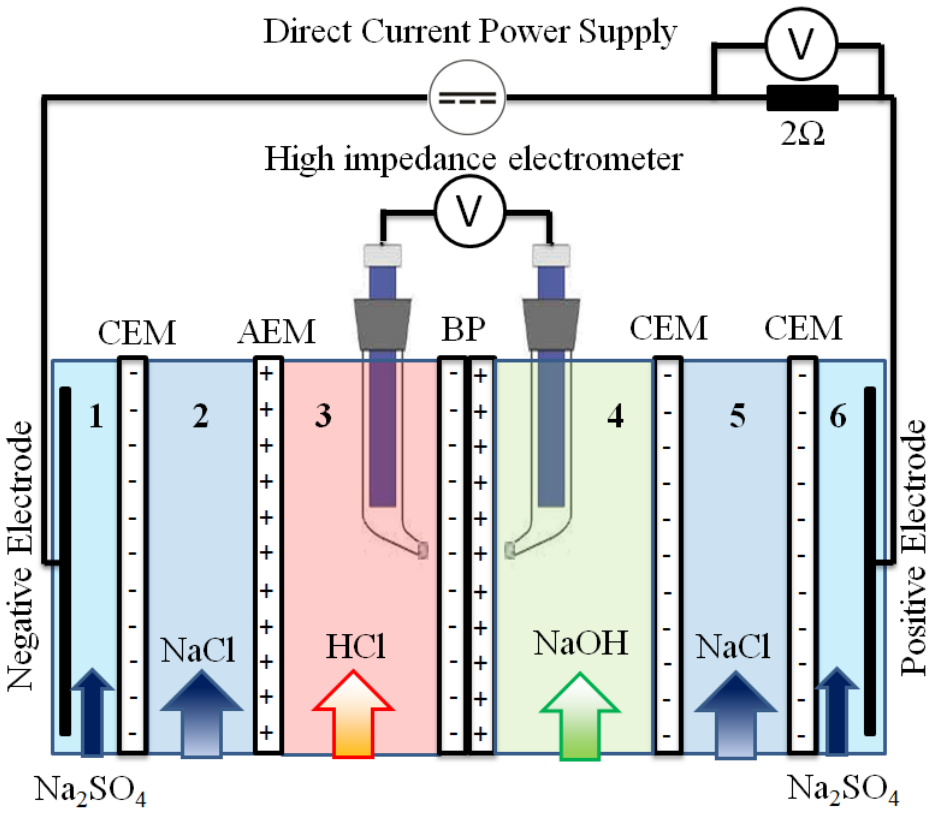

Figure 2.11: Scheme of stack for single membrane experiment for characterization of BP.

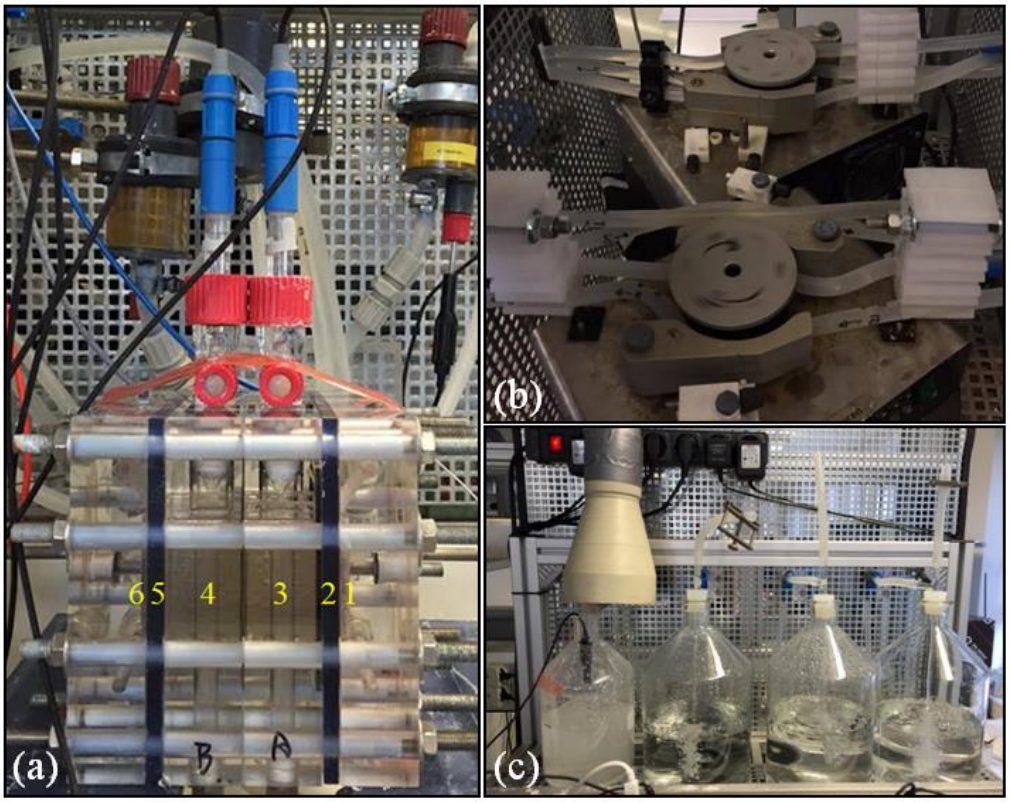

Figure 2.12: Single membrane test facility. (a) Test stack for single membrane with active surface of 5cm x 5cm. (b) Peristaltic pumps, flowrate of all electrolyte solutions is 2cm/s in chambers. (c) Tanks for 4 electrolyte solutions, from left to right, they are for Na_2SO_4 (1.5L), HCl (2L), NaCl (2L) and NaOH (2L).

2.3 Characterization of Bipolar Membrane

In this section, performance of BP in REDBP will be characterized. Since it is very difficult to isolate each parameter (such as temperature, concentration, current density, Ch/DisCh duration time and cycle number) which influences the performance of BP (such as voltage, power density and efficiency), characterization of BP is organized by characterization method. All measurements are taken on fumasep® FBM.

2.3.1 Open Circuit Voltage

OCV is the maximum potential difference between BP without current. Figure 2.13 (a) shows OCV of BP with changing concentration[1] of HCl and NaOH at 25°C under atmospheric pressure. Please refer to section 1.4.2 for calculation of theoretical maximum OCV.

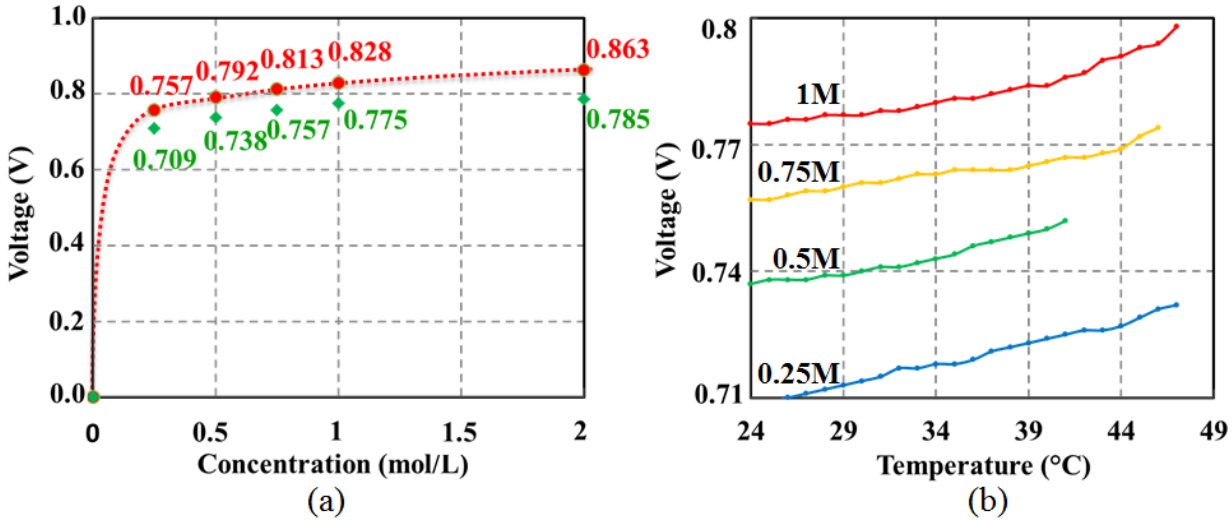

Figure 2.13: OCV of BP (a) with changing concentration of HCl and NaOH at 25°C, red round dots are electromotive force as theoretical maximum OCV, green diamond dots are measurements; (b) with changing of temperature.

With increasing concentration of acid and base, the OCV will increase as well, but it follows the property of natural logarithm. Higher concentration of acid and base, especially higher than 0.25M, will not benefit OCV too much. The green points are the OCV measurements. They are all a bit lower than EMF due to crossover effect (section 2.5.3), but their trend is similar to EMF. At 1M, OCV of BP is 0.775V, which is high considering the OCV of fuel cell is around 1V by measurement. Such high OCV indicates a very aggressive neutralization reaction at interface of BP: System needs to adjust electric potential to compensate the annihilation of H^+ and OH^- due to the poor mobility of Na^+

[1] Concentration of NaCl is always 0.5M, which is identical to NaCl concentration in sea water. Concentration of Na_2SO_4 is always 0.25M.

and Cl^- at BP interface. OCV is also influenced by temperature. Figure 2.13. (b) shows this relation, in which the OCV increases with increasing temperature.

Stated simply, BP delivers quite high OCV, which is, to the bottom, a basic parameter determining the power density by both charge and discharge process. However, increasing concentration of electrolyte and temperature will benefit OCV only minimally.

2.3.2 Discharging/Charging Curve

OCV is only an electric potential without electric current. Without current there is no power, thus DisCh/Ch curve is very necessary. Figure 2.14 shows the DisCh/Ch curve of BP in 0.25M HCl and NaOH solution at 25°C 0.1MPa. The first 19 minutes is discharging process while the second 19 minutes is charging process. By discharging process, current density is defined as negative, while by charging process as positive. Table 2.3 shows the change of current density over time during the first 19 minutes. Please note that with electric current there will be chemical reaction inside of BP, either water-splitting reaction by charging process or neutralization reaction by discharging process. Therefore, the ionic concentration between two measuring points of Luggin capillaries will be changing, meaning changing R_{BP} and IR-drops in figure 2.9. For this reason, the voltage measurement here will not exclude IR-drops.

In figure 2.14, at beginning the OCV of BP is 0.71V, and electric potential will decrease with increasing electric current density by discharging process due to resistance of electrolyte solution and BP. Voltage measurement will maintain at -50mA/cm^2 for 7 minutes to examine the performance of BP at high current density. Voltage decreases gradually at -50mA/cm^2 due to neutralization reaction which produces water molecules causing reducing conductivity of BP and concentration polarization phenomena at the interface of BP and electrolyte solution. This effect is reversible by decreasing discharging current density. Voltage will gradually return to its original OCV. By charging process, potential will increase with increasing current density. At 50mA/cm^2 measurement will be maintained for 7 minutes, then return to OCV.

DisCh/Ch curve can be utilized to find out the best working condition of BP by considering 4 aspects:

1) High OCV.
2) Small gap between discharge and charge voltage with same current density.
3) Small or even no change of DisCh/Ch voltage by high current density.
4) No change of OCV after many cycles.

Therefore, the following figures 2.15-2.17 of DisCh/Ch curves of 0.5M, 0.75M and 1M can be compared, and the following points can be summaries:

1) The OCV is higher with higher concentration of HCl and NaOH.
2) With higher concentration of HCl and NaOH, the gap between discharging and charging voltage is smaller, meaning less internal resistance.
3) Higher concentration of HCl and NaOH has higher DisCh/Ch power density. Figure 2.16 shows the power density of BP of 0.75M at -50mA/cm^2 is -27.6mW/cm^2, and gradually drops to -26.1mW/cm^2.
4) Decrease of voltage at -50mA/cm^2 is more significant with higher concentration than with lower concentration. At 1M this decrease of voltage is so dramatic that voltage will drop to almost zero within 8 minutes. This phenomenon is due to concentration polarization effect (increase of IR-drop) as well as accumulation of water molecules at the interface of BP which leads to a rapid increase of internal resistance of PB (increase of R_{BP}). The reason for this is water production both from neutralization reaction and from cross over effect dilutes the electrolyte solution and increases internal resistance of BP. Especially with higher concentration of HCl and NaOH, the crossover effect is more significant than with lower concentration. Therefore, power density of higher concentration is not stable at higher current density. This phenomenon is reversible, but not in short time.

From DisCh/Ch curve alone, the best performance of BP is concentration of 0.75M with higher current density, and 1M with lower current density. The poor performance of 1M at higher current density is due to concentration polarization effect as well as accumulation of water molecules at the interface of BP. A better mixing or shorter discharging time could overcome these.

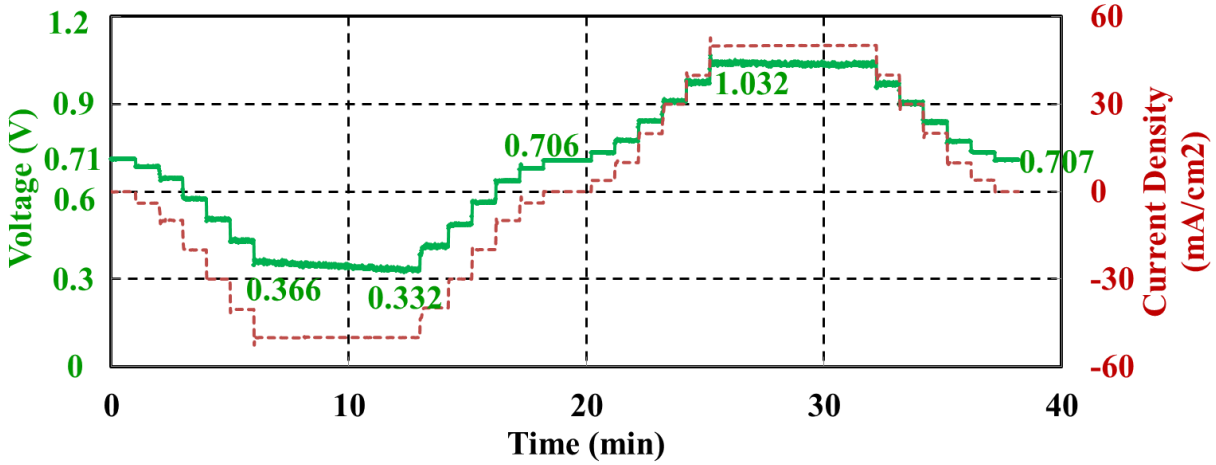

Figure 2.14: DisCh/Ch curve of BP in 0.25M HCl and NaOH at 25°C 0.1MPa.

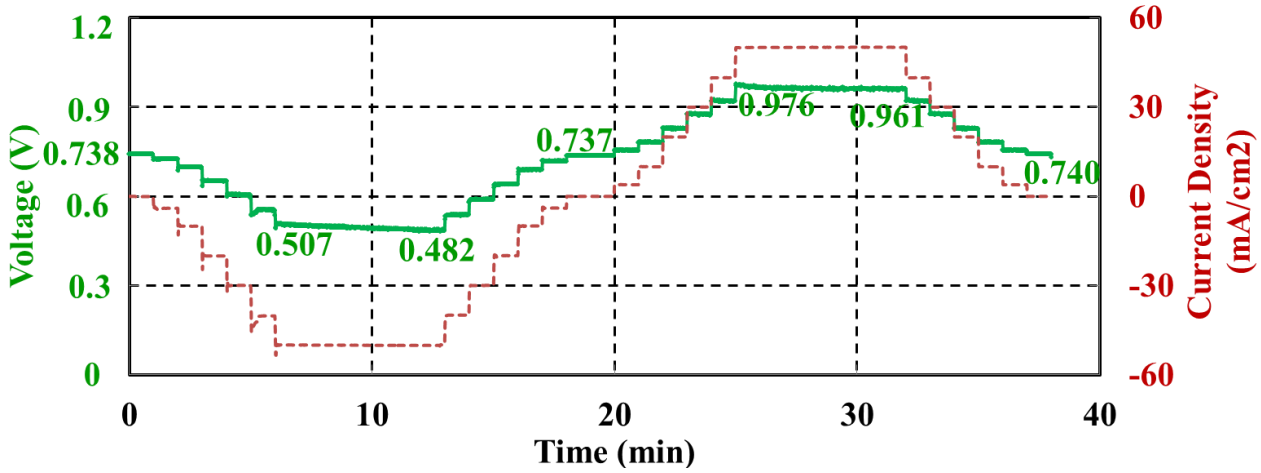

Figure 2.15: DisCh/Ch curve of BP in 0.5M HCl and NaOH at 25°C 0.1MPa.

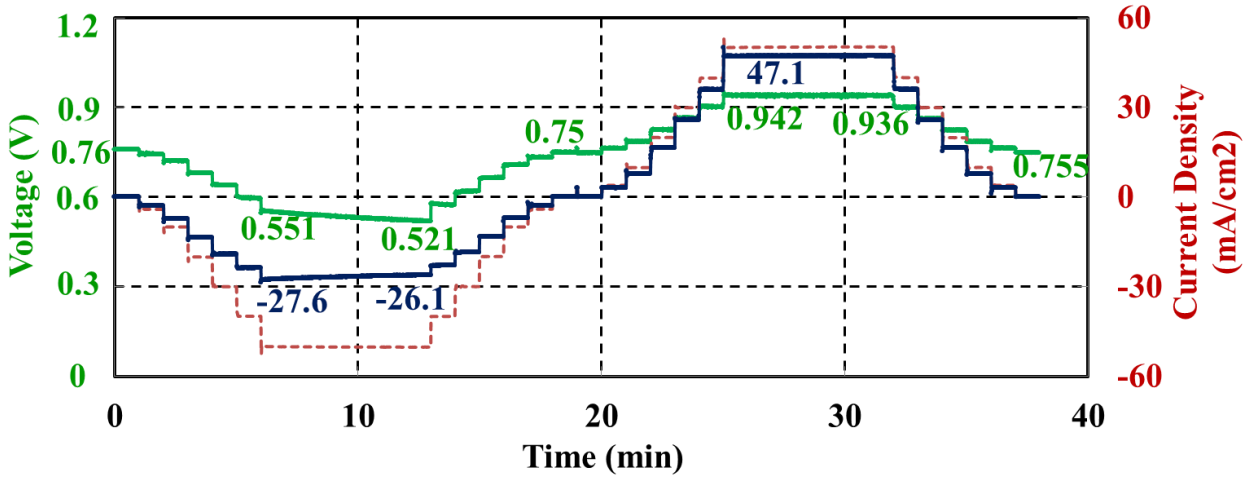

Figure 2.16: DisCh/Ch curve of BP in 0.75M HCl and NaOH at 25°C 0.1MPa with power density (mW/cm^2).

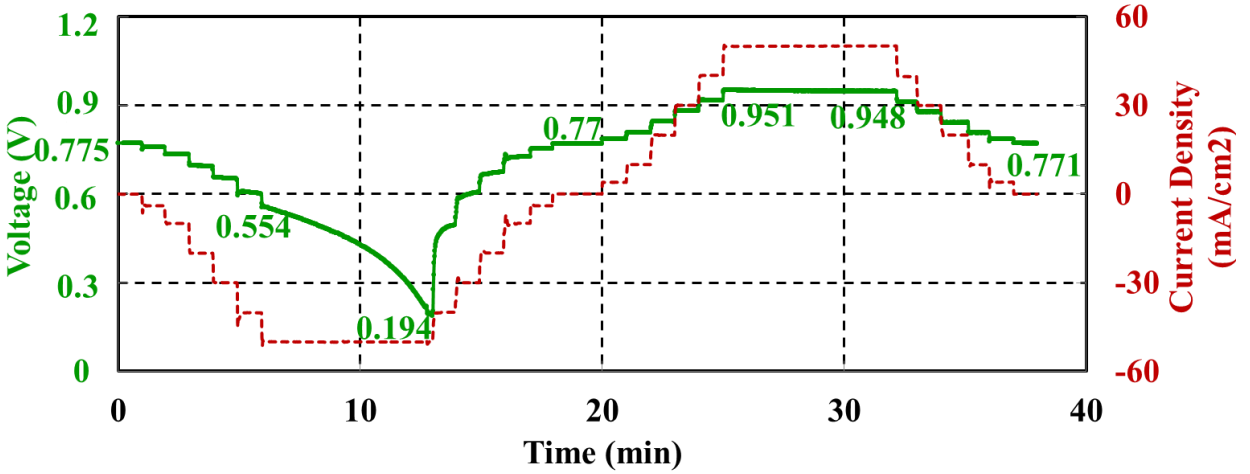

Figure 2.17: DisCh/Ch curve of BP in 1M HCl and NaOH at 25°C 0.1MPa.

Table 2.3: Change of current density over time by discharging process.

Time (min)	Measuring Duration[1] (min)	Current Density (mA/cm^2)
0-1	**1**	**0**
1-2	**1**	**-4**
2-3	**1**	**-10**
3-4	**1**	**-20**
4-5	**1**	**-30**
5-6	**1**	**-40**
6-13	**7**	**-50**
13-14	**1**	**-40**
14-15	**1**	**-30**
15-16	**1**	**-20**
16-17	**1**	**-10**
17-18	**1**	**-4**
18-19	**1**	**0**

2.3.3 Current-Voltage Curve

For obtaining I-V curves of both charging and discharging process, the measuring duration for each point is crucial due to the concentration polarization effect as well as accumulation of water molecules at the interface of BP. For example, figure 2.18 shows 4 BP I-V curves of concentration of 1M. They are all measurement of the same BP under same conditions including same measuring duration.

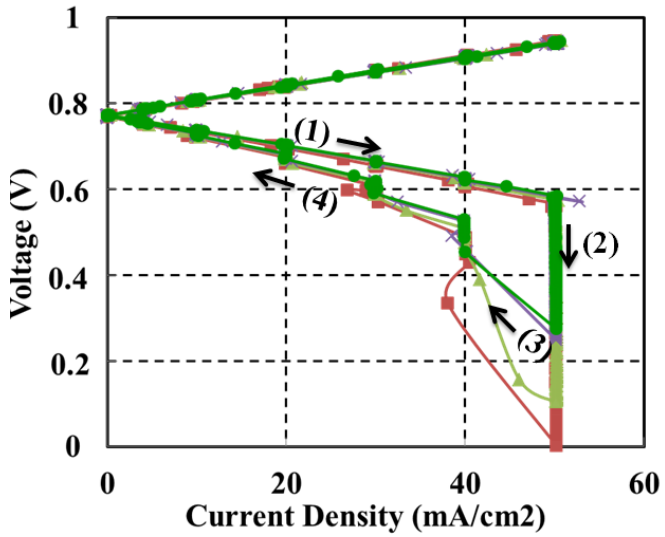

Figure 2.18: 4 BP I-V curves of concentration of 1M at 25°C 0.1MPa. Stage (1) is discharging process with increasing current density; Stage (2) is discharging process at -50mA/cm^2 current density for 7 minutes. Stage (3) is discharging process with decreasing current density in high current density range. Stage (4) is discharging process with decreasing current density in low current density range.

[1] Measuring duration in this thesis represents the time of voltage measurement under constant current density.

By charging process, all the 4 curves are identical. However, by discharging process at -50mA/cm^2 for 7 minutes, 4 I-V curves begin to deviate from each other due to the concentration polarization effect and accumulation of water molecules at the interface of BP. This makes the experimental results not reliable at stage (2), (3) and stage (4).

Therefore, in this section, I-V curve is measured by taking each point within a very short time (1s), and switching between charging and discharging process, as shown in figure 2.19. One of the advantages of this method is that, there is no significant change of ionic concentration between two measuring points of Luggin capillaries because the measuring duration (duration of chemical reaction) is very short, thus no change of IR-drops as well as no change of R_{IEM}, if crossover effect is neglected.

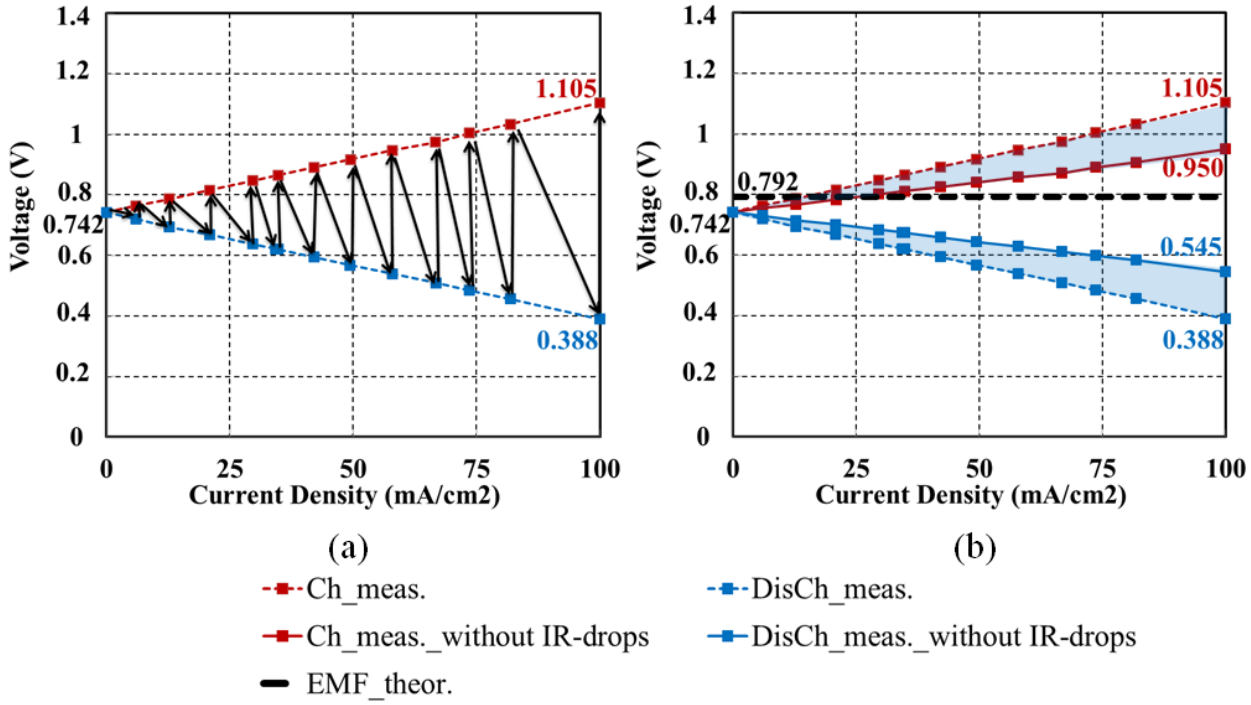

Figure 2.19: (a) I-V curve measurement of BP 0.5M by taking voltage of charge and discharge alternatively. Blue points are voltage measurement during discharging process while red points are during charging process. (b) By excluding IR-drops of both acid and base chamber, the solid lines are the voltages of charge and discharge between BP. The blue area is the IR-drop between BP and measuring point of Luggin capillary. The EMF is labeled as black dashed line.

Figure 2.19 (b) is the I-V curve of BP with 0.5M concentration of electrolyte solution by excluding the IR-drops of both acid and base chamber (the blue area in the figure). This is considered as the real voltage between BP. Please note that in experiment the distance between measuring point and BP is 1mm, however, BP is considered having two diffusional layers both of which have 50µm, thus each IR-drop is calculated in the length of 0.95mm. In reality it is impossible to identify the exact ionic conductivity of IR-drop, its conductivity is calculated by measuring the conductivity of bulk solution. For this reason, the linear flowrate of electrolyte solution needs to be high enough to maintain a

constant diffusional layer between IEM and bulk solution as well as eliminate concentration polarization effect to the greatest extend. The theoretical EMF has labeled as black dashed line. With 0.5M solution, EMF should be 0.792V, and can be treated as the maximum discharging voltage and minimum charging voltage. By charging when the current density is lower than 25mA/cm^2, voltage between BP is not high enough to trigger water-splitting process. In other words, the electric current in BP is not carried by produced H^+ and OH^- from BP interface, but rather by diffused H^+ and OH^- (and salt ions) from acid and base chamber.

Figure 2.20 shows the I-V curves of different concentration of HCl and NaOH solution from 0.25M to 1M. With increasing concentration, the gap between charging curve and discharging curve is presumably getting smaller due to the decreasing internal resistance of electrolyte. It indeed follows the prediction from 0.25M to 0.75M according to experiments (dotted lines in the figure). However, if the IR-drops of both acid and base chamber are excluded, the voltage between BP (solid lines) will not follow the trend with concentration higher than 0.5M. The reason for that is the crossover effect which is more significant with higher concentration. This undesired mixing process of acid and base causes neutralization reaction, which dilutes ionic concentration of HCl and NaOH inside and near BP. Neutralization reaction inside of BP leads to higher R_{BP}, and near BP causes change of conductivity of diffusional layers. By 1M, the crossover effect is so significant, that even the measurement (dotted lines) is not better than 0.75M. In table 2.5 the area resistance of BP with different solution concentration is calculated according to experimental results.

$$Area\ Resistance = \frac{V_{BP}}{Current\ Density}\ [\Omega \cdot m^2] \qquad \textbf{(2.6)}$$

With the same solution concentration, the BP area resistance of charging process is similar to that of discharging process. However, with increasing solution concentration, the area resistance of BP is not getting smaller. This indicates that the conductivity of BP is not only determined by solution concentration, but also transport of water molecular. Moreover, by charging when voltage is lower than EMF (the black dashed line in the figure) which is considered as the minimum charging voltage, electric current is carried out only by diffused ions.

Table 2.4: Resistivity of different solution at 20°C [28].

Concentration (mol/l)	**Resistivity of HCl Solution (Ω·m)**	**Resistivity of NaOH Solution (Ω·m)**	**Resistivity of Na_2SO_4 Solution (Ω·m)**	**Resistivity of NaCl Solution (Ω·m)**
0.25	0.1050	0.2058	0.316	
0.5	0.0554	0.1074		0.2355
0.75	0.0385	0.0765		
1	0.0301	0.0594		

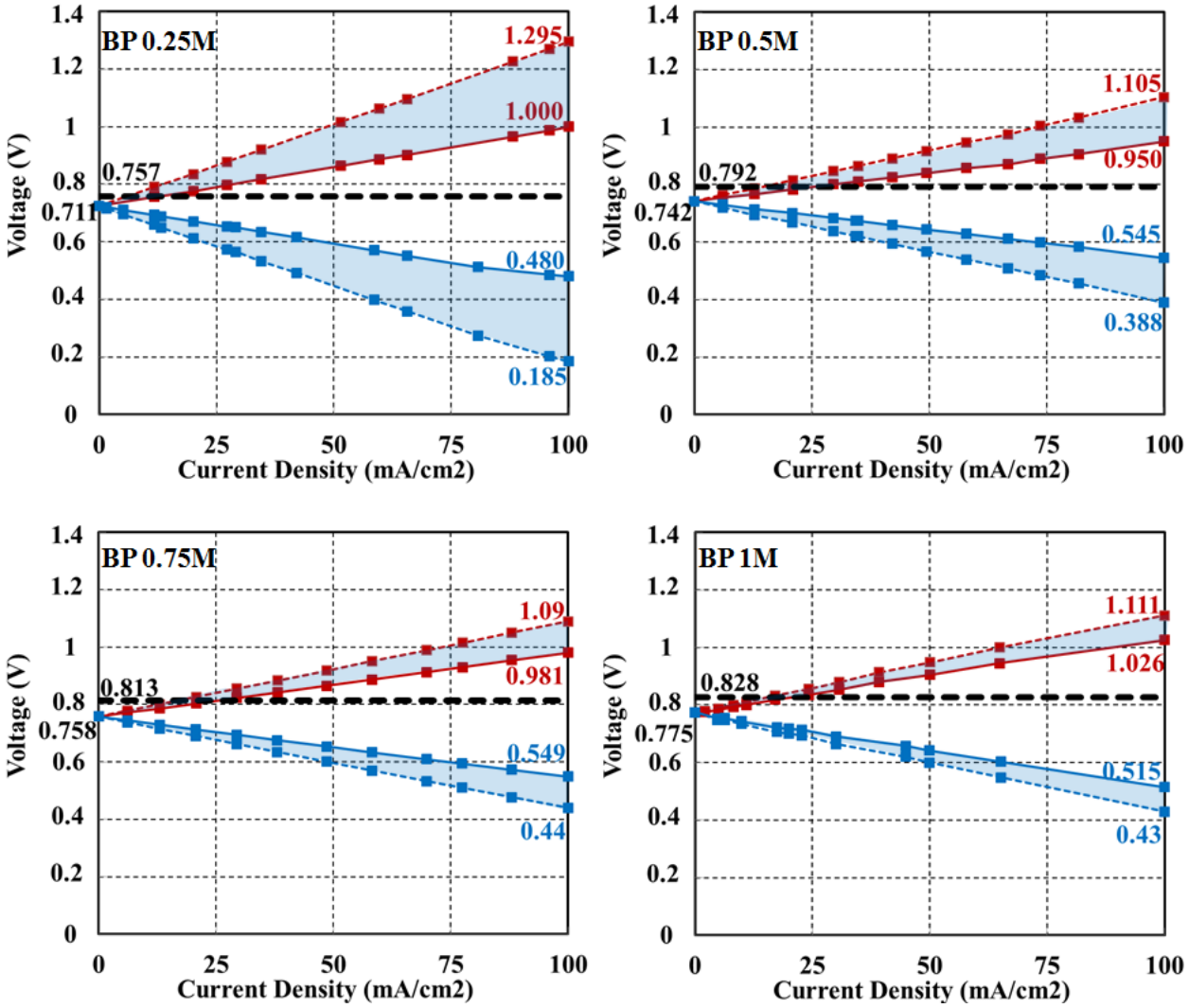

Figure 2.20: I-V curves of different concentration of HCl and NaOH at 25°C 0.1MPa. Red curve which has positive slope is charging process, while the blue curve which has negative slope is discharging process. Dotted lines are voltage measurements while solid lines are voltage measurements excluding IR-drops of both electrolyte solutions (the blue area). The EMF is labeled as black dashed line.

	0.25M	0.5M	0.75M	1M
Ch	2.89×10^{-4} Ω·m^2	2.08×10^{-4} Ω·m^2	2.23×10^{-4} Ω·m^2	2.51×10^{-4} Ω·m^2
DisCh	2.31×10^{-4} Ω·m^2	1.97×10^{-4} Ω·m^2	2.09×10^{-4} Ω·m^2	2.60×10^{-4} Ω·m^2

Table 2.5: The area resistance of BP with 50μm diffusional layers in different solution concentration calculated according to single membrane experiments.

Current density times voltage equals power density (PD). Thus the PD curves can be obtained on I-V curves. Figure 2.21 shows the I-V curves as well as PD curves of BP with concentration of 0.75M. With increasing current density, the PD of both charging and discharging process will increase. At 100mA/cm^2 PD of discharging process reaches to 56mW/cm^2. Increasing current density leads to increasing losses due to decreasing conductivity of BP (more produced water inside of BP), therefore, the efficiency will decrease with increasing current density. EMF of 0.75M is 0.813V, so the

efficiency of BP by discharging process with certain current density is calculated and labeled in figure 2.21. It is obvious, that there is a compromise between PD and efficiency.

For short, PD of BP with 0.75M is quite high, and efficiency is good enough considering REDBP for bulk energy storage application in which efficiency is not that important compared to cost.

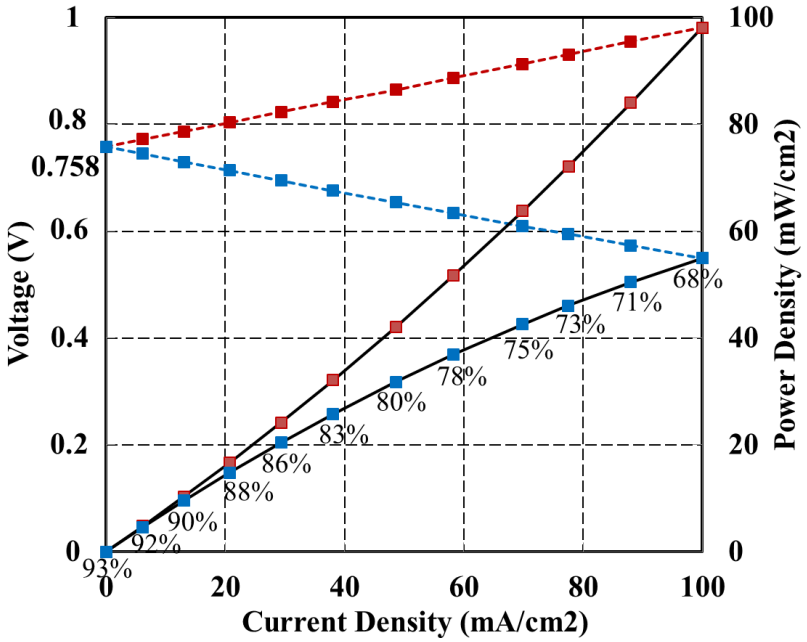

Figure 2.21: I-V curve of BP of 0.75M with power density curves at 25°C. Dotted lines are Ch/DisCh voltage measurements. Solid lines are Ch/DisCh power density. Percentage represents the efficiency of BP by discharging with certain current density.

2.3.4 Chronopotentiometry

In the previous section, the voltage measurements are taken within very short time (1s), and BP shows very good power density and efficiency. In this section, factor of Ch/DisCh time will be investigated using chronopotentiometry (CPM), in which a constant current is switched on and off while the time evolution of the electric potential will be recorded.

Figures 2.22 - 2.24 are the CPM curves of 0.25M, 0.5M and 0.75M concentration of HCl and NaOH solution. The measurements are all started with 1 minute OCV, followed by 20 minutes discharging process, back to OCV for 1 minute, and then begin charging process with the same current density, after 20 minutes back to OCV. Please note that with electric current there will be chemical reaction inside of BP, either water-splitting reaction by charging process, or neutralization reaction by discharging process. Therefore, the ionic concentration between two measuring points will be changing, meaning changing R_{BP} and IR-drops in both acid and base chamber. For this reason, the voltage measurement here will not exclude IR-drops.

The following points summarize comparisons with each figure:

(1) With lower current density (20mA/cm^2 or 40mA/cm^2), the gap between discharging and charging voltage decreases with increasing concentration of HCl and NaOH solution due to increasing conductivity of both IEM and electrolyte solution between two measuring points.

(2) With higher current density (60mA/cm^2 or 80mA/cm^2), at the first 4 minutes, the gap between discharging and charging voltage follows the same pattern as in (1). However, after that, the voltage of 0.75M deteriorates further and further. With 60mA/cm^2 the voltage drops to zero within 18 minutes and with 80mA/cm^2 within less than 8 minutes. The reason for this is concentration polarization effect as well as accumulation of water molecules at the interface of BP which leads to a rapid increase of internal resistance of PB.

As a summary of CPM, higher concentration increases conductivity of electrolyte solution and BP, but it also enhances concentration polarization effect and accumulation of water molecules at the interface of BP. If discharging duration is short, higher concentration is better. If discharging duration is long, then higher concentration is not suitable compared with lower concentration.

2.3.5 Cycles

Each charging or discharging process will shorten the lifetime of BP by side reactions, material degradation, etc. In this experiment, cycle test will be performed by 20 CPM tests in sequence with constant current density of 40mA/cm^2 such as in figure 2.25 which is a 20 cycles test of a fresh BP (without activation procedure see table 2.2) with solution concentration of 0.75M. There are many interesting findings in it which are listed below:

(1) The orange dots (●) are the temperature measurement by attaching the measuring sensor of a very thin[1] thermal couple on the surface of BP near voltage measuring points. According to the temperature measurement, in the first 1 hour (the first 1-2 cycles), normally the temperature on the surface of BP will rise 1-2°C. The heat is from neutralization reaction due to crossover effect, ionic transport through electrolyte solution and BP, electrochemical reactions in electrode chambers and pumps. Temperature stays constant between the 2nd cycle and 6th cycle, since the test stack is stabilized. However, due to the rise of ambient temperature[2], the electrolyte solution is heated up around 2°C. This rise of temperature does not have much influence on the performance of BP such as OCV (the black dotted line ●-) or Ch/DisCh curves.

(2) The blue square dot (■) is the first voltage measurement during discharging process (V_{Disch_start}). It can be seen as the voltage measurement in I-V curve. In the first 1-2 cycles,

[1] In order to avoid shadow effect, thermal couple must be very thin. Cross section is 0.05mm.
[2] This test facility is not thermally insulated from ambient environment.

BP is activated and V_{Disch_start} is getting a little higher. Throughout the entire experiments V_{Disch_start} does not change much.

(3) The blue diamond dot (◆) is the last voltage measurement of each 20 minutes discharging process (V_{Disch_end}). It is lower than V_{Disch_start} due to concentration polarization effect as well as accumulation of water molecules at the interface of BP. It remains constant in the first 10 cycles, but drops gradually afterwards, indicating either worse mixing or leakage (holes in BP) of electrolyte solution passing from one chamber to the other. Using scanning electron microscope several holes are found on the anode side of BP (AEM). The thing which bulges out from BP is the net for reinforced membrane. These holes are due to frictions between BP and spacers. It is one of the main disadvantages of single membrane measurement. In order to acquire reliable result (constant and known IR-drops), the electrolyte chambers are filled with spacers, which are not elastic. Normally after 8 hours (10 cycles), the membrane surface begins to be worn out by these spacers. That is the main reason why after 10 cycles, the performance of BP has deteriorated.

(4) The red square dot (■) is the first voltage measurement during charging process (V_{Ch_start}). It cannot be seen as the voltage measurement in I-V curve during charging process, because it has direct influence from the previous discharging process. For example, until the 10th cycle due to the activation process V_{Ch_start} is getting smaller and becoming more stable. But after 10th cycle due to the worn out process of BP, concentration polarization effect is getting more significant by discharging process, thus the initial (by charging process) conductivity of BP is becoming worse. That is the reason for the increase of V_{Ch_start} from 0.884V to 0.893V.

(5) The red diamond dot (◆) is the last voltage measurement during charging process (V_{Ch_end}). It can be treated as the voltage measurement in I-V curve during charging process. It remains almost constant (raise from 0.88V to 0.884V) throughout the entire experiment, indicating a quite constant conductivity of BP and electrolyte solution, and very small leakage of electrolyte by charging process.

(6) The black dotted line (-●-) is OCV. Before and after 20 cycles test it remains almost constant (drops from 0.769V to 0.766V), indicating a very small leakage of electrolyte and quite constant capacity (concentration of HCl and NaOH solution).

It is certain that fresh BP needs 1 hour activation procedure to stabilize temperature and its conductivity. Due to the flaws of single membrane test stack, there is worn out process after 10th cycle (8 hours), but the concentration of electrolyte solution has no significant change according to OCV.

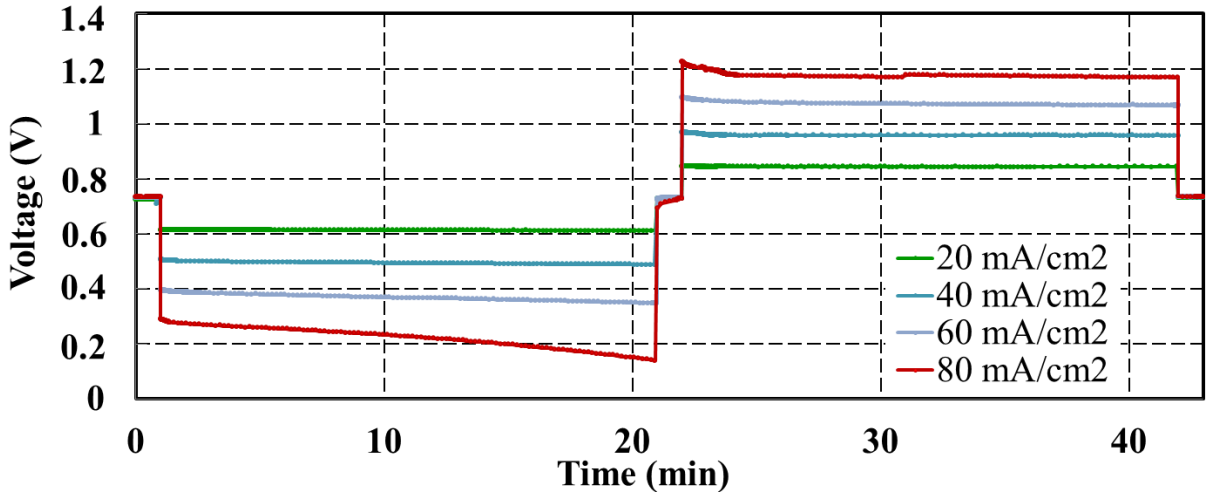

Figure 2.22: CPMs of BP of 0.25M concentration of HCl and NaOH at 25°C 0.1MPa.

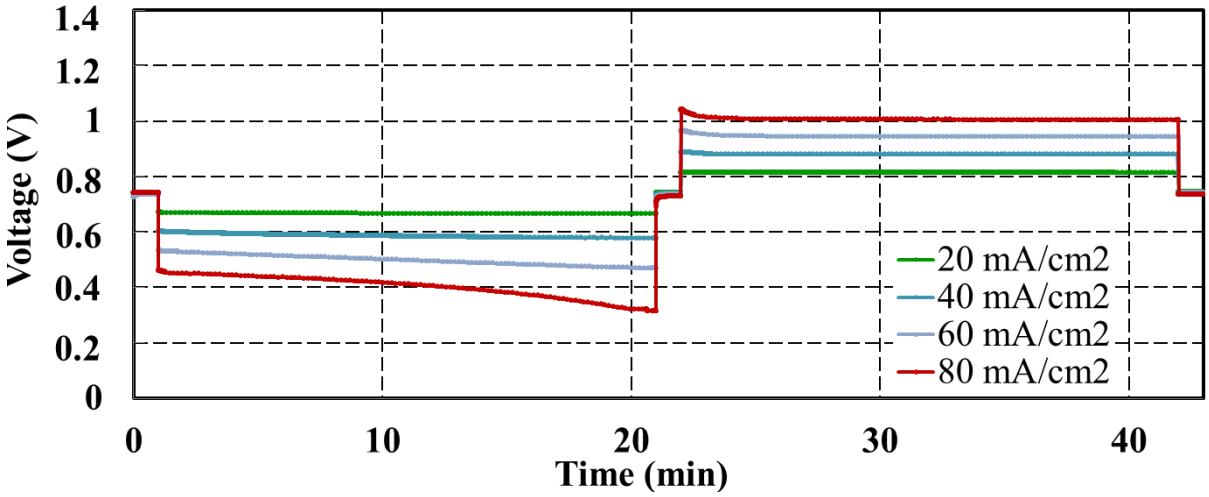

Figure 2.23: CPMs of BP of 0.5M concentration of HCl and NaOH at 25°C 0.1MPa.

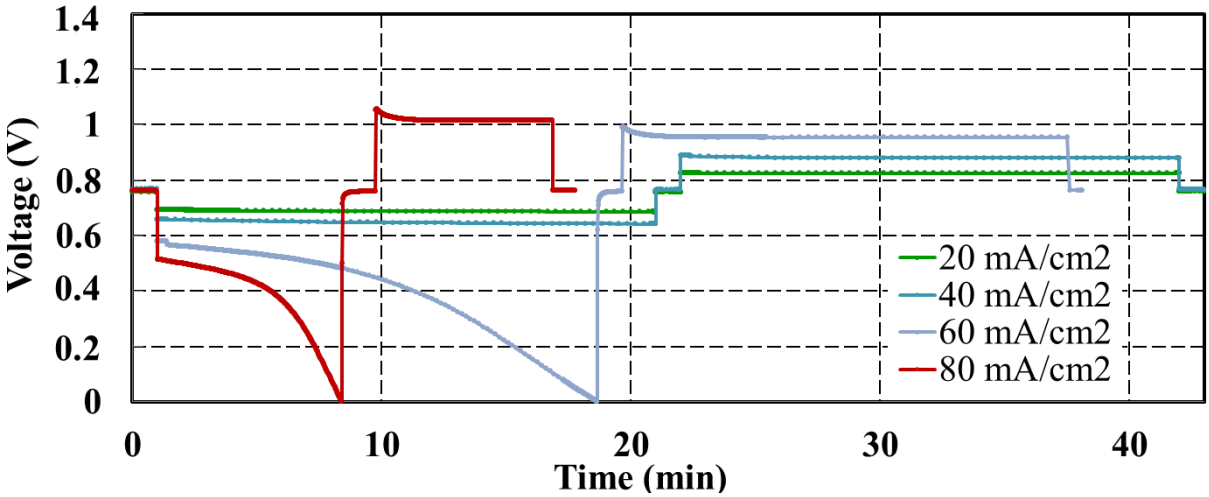

Figure 2.24: CPMs of BP of 0.75M concentration of HCl and NaOH at 25°C 0.1MPa.

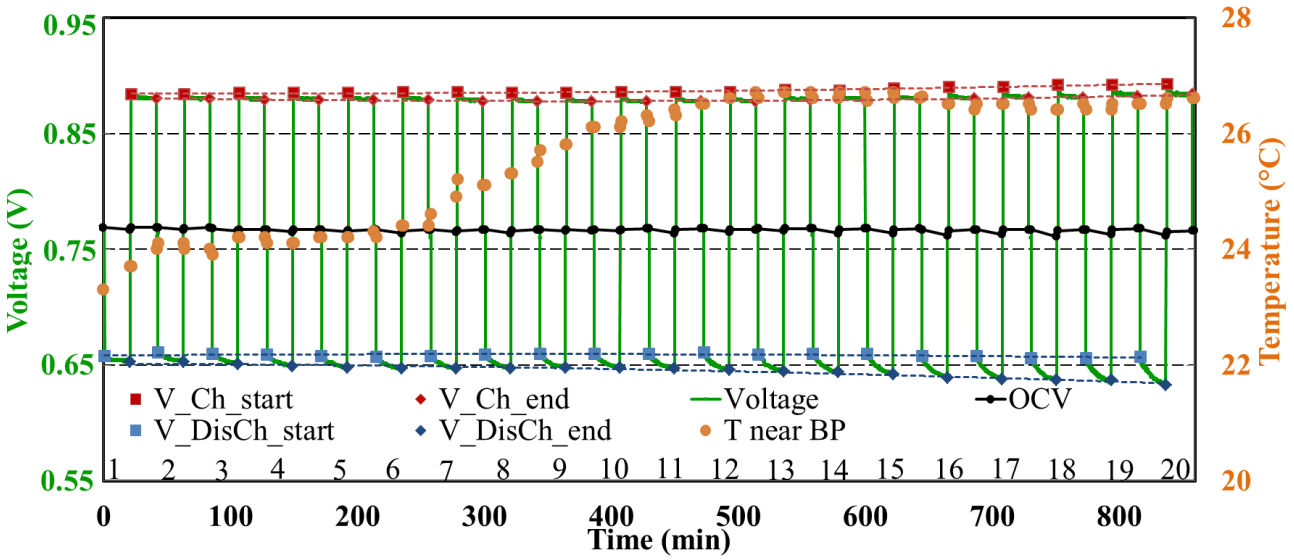

Figure 2.25: 20 Cycles of Chronopotentiometry of 0.75M with 40mA/cm^2. The green line is voltage measurement. The orange dots ( ) are the temperature measurement near BP. The black dotted line ( ) is OCV; The blue diamond dot ( ) is the last voltage measurement during discharging process (V_{Disch_end}). The blue diamond dot ( ) is the last voltage measurement during discharging process (V_{Disch_end}). The red square dot ( ) is the first voltage measurement during charging process (V_{Ch_start}). The red diamond dot ( ) is the last voltage measurement during charging process (V_{Ch_end}).

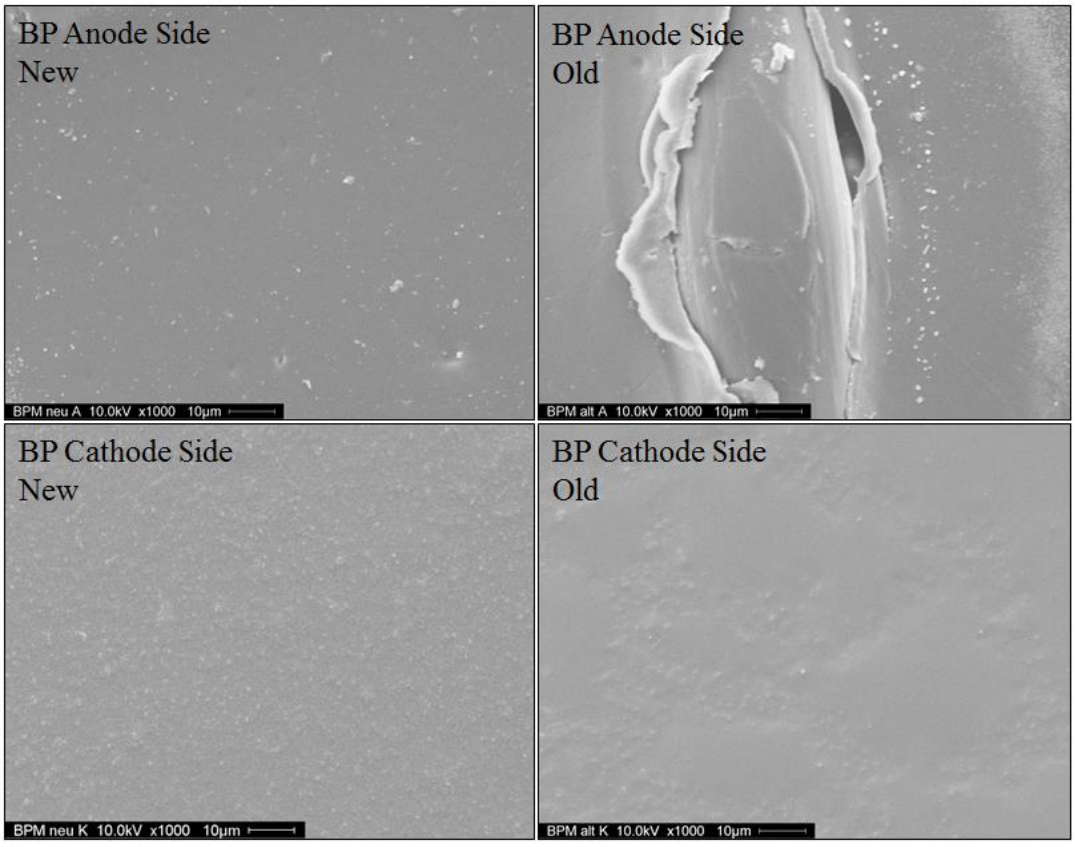

Figure 2.26: Scanning electron microscope before (new membrane) and after 20 cycles test (old membrane) on the surface of BP.

2.4 Characterization of CEM and AEM

In the previous sections the performance of BP has been characterized. In this section the other two IEMs, which build up one single cell of REDBP combined with BP, will be investigated.

All measurements are taken on fumasep® FAB and fumasep® FKB. The properties of each testing membrane are listed in the table 2.6.

Table 2.6: Properties of Testing Membrane.

	fumasep® FAB	**fumasep® FKB**
Reinforcement	PK	PEEK
Thickness (dry)	100 - 120 µm	110 - 130 µm
Ion exchange capacity	1.1 - 1.2 meq·g^{-1}	1.2 - 1.3 meq·g^{-1}
Selectivity[a)]	> 98%	> 98%
Uptake in H_2O at 25°C[b)]	14 – 15 wt%	25 – 30 wt%
Conductivity	In Cl- Form[c)] 1.2-1.5 mS·cm^{-1}	In H^+ form[d)] 15 mS·cm^{-1} / In Na^+ from[e)] >2 mS·cm^{-1}

a) Determined from membrane potential measurement in a concentration cell 0.1 / 0.5M KCl at 25 °C
b) Reference membrane dried over P_2O_5 in vacuo
c) In Cl^- form in 0.5 M NaCl at 25 °C, measured in standard measuring cell (through-plane)
d) In H^+ form at 25 °C in H_2O, measured in four-electrode cell (in-plane) by AC-impedance
e) In Na^+ form in 0.5 M NaCl at 25 °C

2.4.1 Cation Exchange Membrane

CEM separates base chamber and salt chamber, theoretically allows only Na^+ passing through it as figure 2.27 (a) and (b) show. The measuring techniques are the same as measuring BP. Figure 2.27 (c) is a schematic diagram of stack for characterization of CEM. The testing stack has 5 chambers, the two chambers with Luggin capillary is 30mm thick, and the rests are 5mm. Chamber 2 is to prevent leakage of OH^- into the electrode chamber. There is no additional salt chamber between testing salt chamber (chamber 4) and positive electrode chamber (chamber 5) for reducing the total internal resistance of testing stack[1]. The distance between CEM and measuring point of Luggin capillary is maintained at 1mm, which creates too much resistance mainly due to low conductivity of salt solution. Therefore, the testing result has to exclude these voltage drops by constantly measuring the conductivity of salt solution and removing the IR-drop in salt chamber from it.

Figure 2.28 shows the I-V curves of CEM between NaOH and salt chamber with different concentration of NaOH solution. The OCV of different concentration is around 0V. The gap between charging and discharging voltage with constant current density decreases with increasing

[1] The contamination of electrode chamber to testing chamber is very limited.

concentration of NaOH solution due to increasing conductivity of CEM. Table 2.7 is area resistance of CEM calculated according to figure 2.28. Theoretically, the area resistance of charging and discharging process should be the same, but the resistance by charging process is a little bit smaller than discharging process. This is due to the crossover of OH^- from base chamber into salt chamber. As in figure 2.27, the diffusion direction of OH^- is from left to right which can be treated as an electric current from right to left according to Faraday´s law (section 3.1.6). In single membrane experiment, the electric current from right to left is called charging process. Therefore, the conductivity of CEM is higher by charging process than by discharging process. Moreover, discharging process can be considered as a depleting process of OH^- in salt chamber and in CEM, which decreases conductivity of electrolyte solution and CEM, and charging process as an accumulation process of OH^- in salt chamber and in CEM. Because of the above two reasons, the area resistance by charging process is lower than that of discharging process. This is also an evidence of OH^- leakage from base chamber to salt chamber.

Unlike BP, there is no chemical reaction involved in this experiment[1]; which means the ionic concentration stays constant throughout the time, although there is small leakage of OH^- from base chamber to salt chamber[2]. For this reason, CPM measurement of CEM will not be presented here.

Table 2.7: The area resistance of CEM with different solution concentration calculated according to single membrane experiments at 25°C 0.1MPa.

	0.25M	**0.5M**	**0.75M**	**1M**
Ch	$4.16\times10^{-4}\ \Omega\cdot m^2$	$2.32\times10^{-4}\ \Omega\cdot m^2$	$1.26\times10^{-4}\ \Omega\cdot m^2$	$1.06\times10^{-4}\ \Omega\cdot m^2$
DisCh	$5.20\times10^{-4}\ \Omega\cdot m^2$	$2.36\times10^{-4}\ \Omega\cdot m^2$	$1.36\times10^{-4}\ \Omega\cdot m^2$	$1.06\times10^{-4}\ \Omega\cdot m^2$

2.4.2 Anion Exchange Membrane

Characterization of AEM between salt chamber (to the left) and acid chamber (to the right) is the same as that of CEM. Figure 2.29 (c) is a scheme of stack for characterization of AEM. The testing stack has 5 chambers. The two chambers with Luggin capillary is 30mm thick, the rests are 5mm. Chamber 4 is to prevent leakage of H^+ into the positive electrode chamber (chamber 5). There is no additional salt chamber between testing salt chamber (chamber 2) and negative electrode chamber (chamber 1). The reason is to reduce total internal resistance of stack[3]. The distance between AEM and measuring point of Luggin capillary is maintained at 1mm, for the same reason as when

[1] Except in electrode chambers where electrochemical reactions take place. But these reactions have almost no effect on testing chambers.
[2] Tanks for base and salt solution are both 2 litters, the small leakage of OH^- does not have much influences.
[3] The contamination of electrode chamber to testing chamber is very limited.

characterization of CEM. The testing result has to exclude these voltage drops by constantly measuring the conductivity of salt solution and removing the IR-drop in salt chamber from it.

Figure 2.30 shows the I-V curves of AEM between salt and acid chamber with different concentration of HCl solution. The area resistance of each situation has been calculated in table 2.8. Like CEM between base and salt chamber, there is also a crossover effect of H^+ from acid chamber to salt chamber (in figure 2.29 from right to left) through AEM. This ionic transport of H^+ can be seen as an electric current from right to left according to Faraday´s law. Thus area resistance by charging process is lower than that of discharging process. In addition, the charging process can be considered as an accumulation process of H^+ in salt chamber and in AEM, which increases conductivity of electrolyte solution and AEM, while by discharging process the concentration of H^+ in salt chamber and in AEM is depleting. Therefore, the area resistance by charging process is lower than that of discharging process. CPM measurement of AEM is also neglected for the same reason like CEM.

Table 2.8: The area resistance of AEM with different solution concentration calculated according to single membrane experiments at 25°C 0.1MPa.

	0.25M	**0.5M**	**0.75M**	**1M**
Ch	$6.14\times10^{-4}\ \Omega\cdot m^2$	$3.52\times10^{-4}\ \Omega\cdot m^2$	$2.16\times10^{-4}\ \Omega\cdot m^2$	$1.34\times10^{-4}\ \Omega\cdot m^2$
DisCh	$6.14\times10^{-4}\ \Omega\cdot m^2$	$3.76\times10^{-4}\ \Omega\cdot m^2$	$2.26\times10^{-4}\ \Omega\cdot m^2$	$1.44\times10^{-4}\ \Omega\cdot m^2$

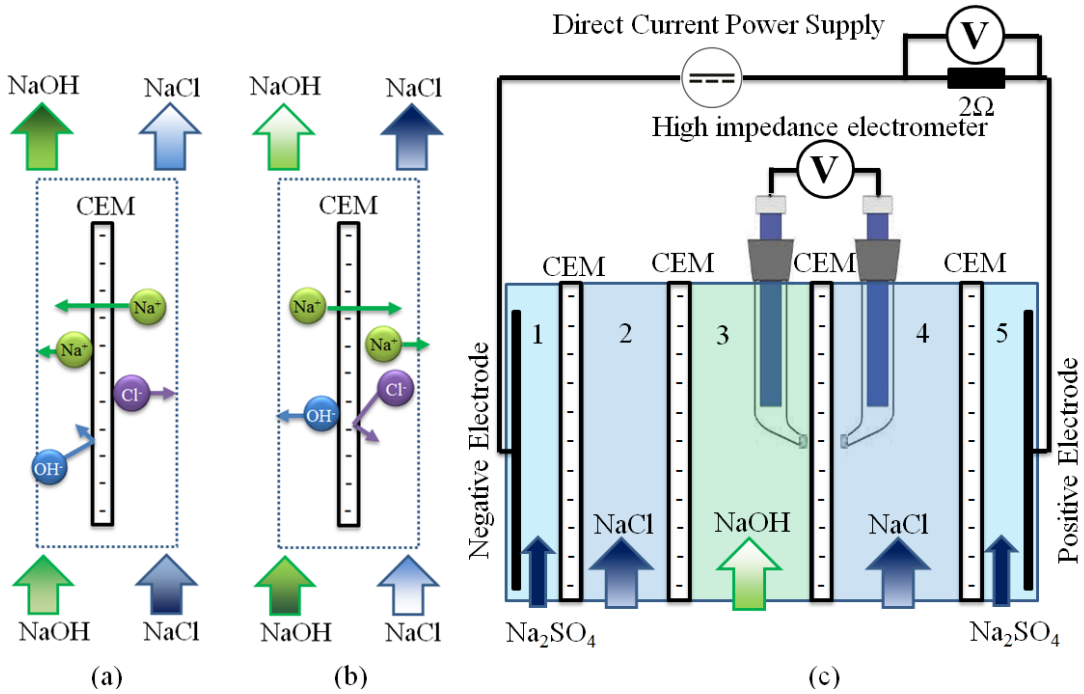

Figure 2.27: CEM between base and salt solution by (a) charging process, and (b) discharging process. (c) Scheme of stack for single membrane experiment for characterization of CEM.

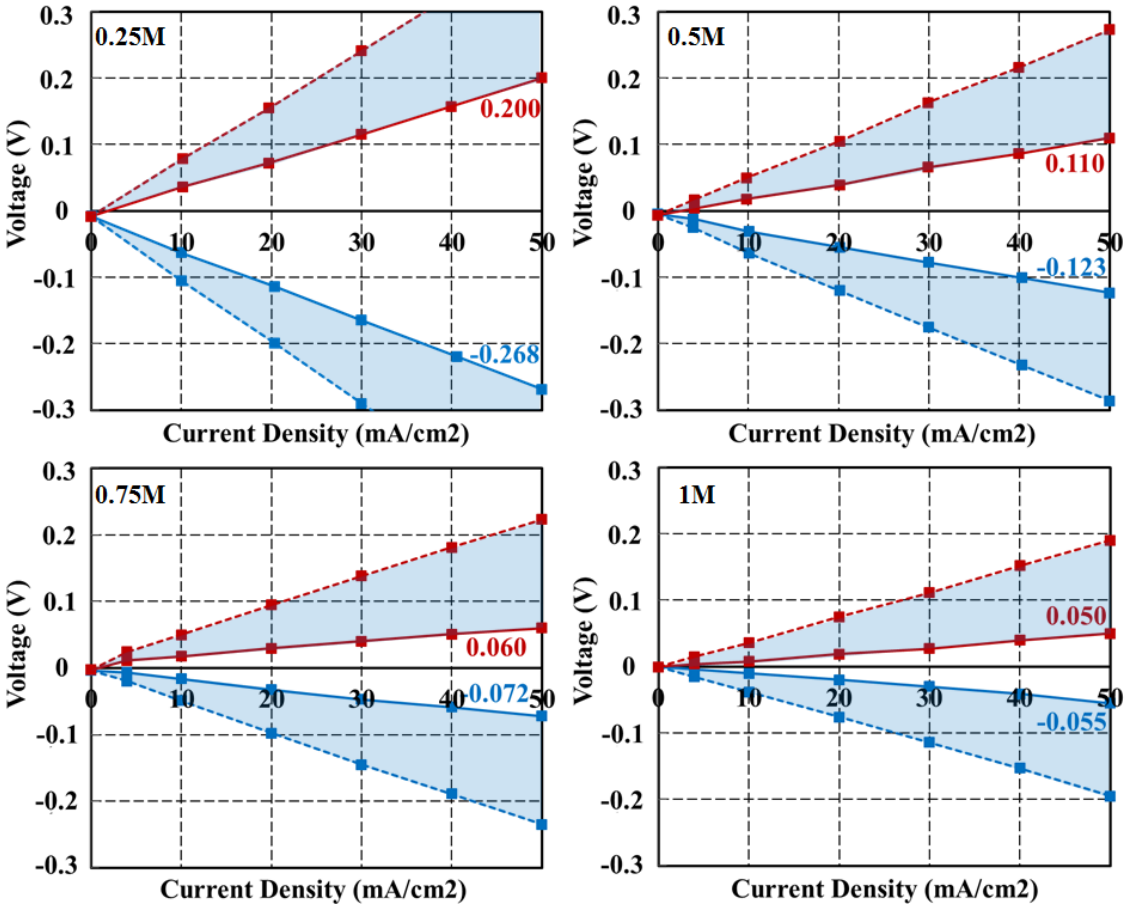

Figure 2.28: I-V curves of CEM between NaOH and NaCl chamber with different concentration of NaOH solution at 25°C 0.1MPa. Dotted lines are voltage measurements which solid lines are voltage measurements excluding IR-drops of both electrolyte solutions (the blue area). The area resistance of each situation has been labeled.

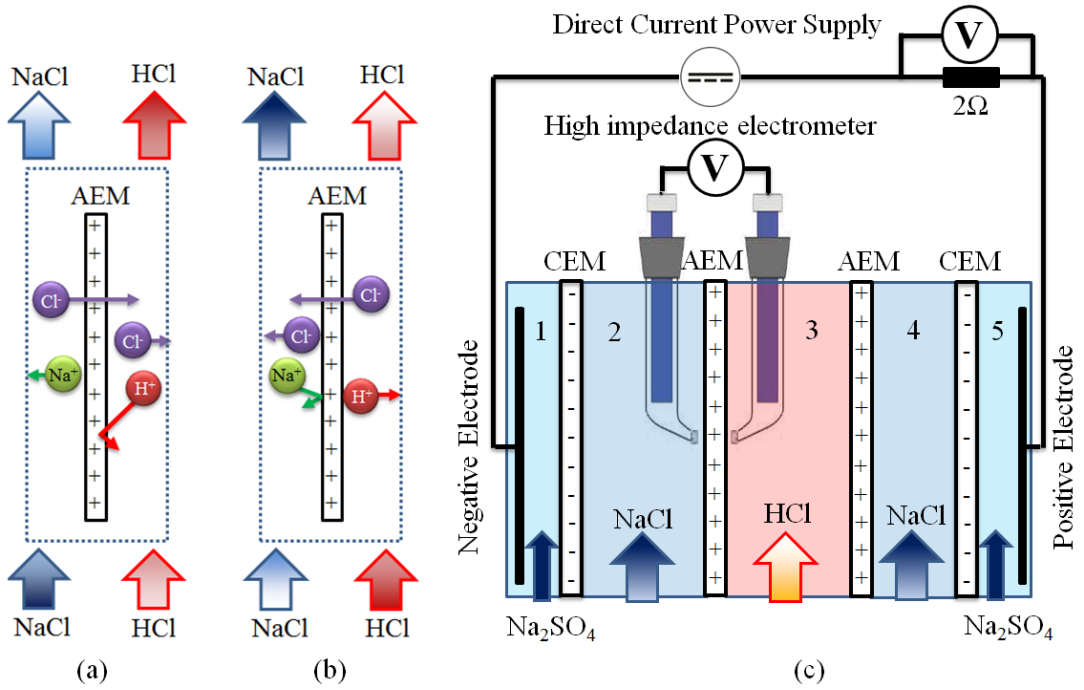

Figure 2.29: AEM between salt and acid solution by (a) charging process, and (b) discharging process. (c) Scheme of stack for single membrane experiment for characterization of AEM.

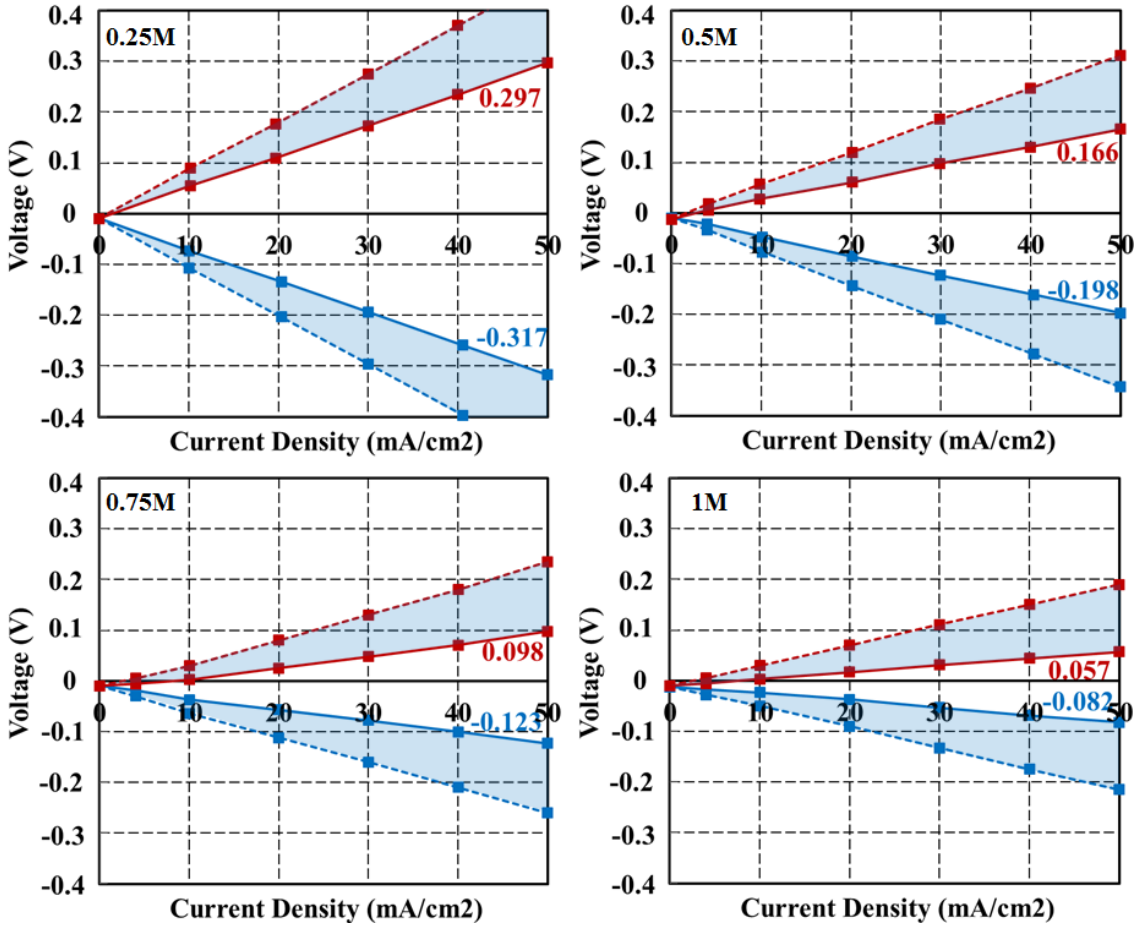

Figure 2.30: I-V curves of AEM between NaCl and HCl chamber with different concentration of HCl solution at 25°C 0.1MPa. Dotted lines are voltage measurements which solid lines are voltage measurements excluding IR-drops of both electrolyte solutions (the blue area). The area resistance of each situation has been labeled.

2.5 Overall Performance of Single Cell

Single cell performance can be evaluated by considering three IEMs and three solution chambers as a whole.

2.5.1 Current-Voltage Curve

Figure 2.31 shows I-V curves of single cell with 0.5mm thick solution chambers at 25°C 0.1MPa. The red lines are charging curves while the blue lines are discharging curves. The solid lines with square points are Ch/DisCh voltage measurements between BP alone (section 2.3.3). The dashed lines are voltage measurements of all IEMs without considering electrolyte solution. The solid lines with round points are voltage of REDBP single cell with electrolyte solution in 0.5mm thick chamber. There are several interesting points by comparing each curve:

(1) The difference between solid line with round points and dashed line (the blue area) is voltage drop due to resistance of electrolyte solution. It does not change much with increasing solution concentration, since the main resistance is due to the poor conductivity of salt solution (always 0.5M).
(2) The difference between dashed line and solid lines with square points (the yellow area) is voltage drop due to AEM and CEM, which is getting smaller with increasing solution concentration, indicating the conductivity of AEM or CEM depends on acid or base greatly. It is one of the main losses, especially with low concentration of acid and base.
(3) Performance of BP (solid lines with square points, the brown area) with 0.75M is better than with 1M. This is due to significant crossover effect by 1M solution, which increases resistivity of BP by producing too much water. This indicates the conductivity of BP is determined by water transport greatly.
(4) Although the performance of BP is not optimal with higher concentration, the overall performance of REDBP single cell improves with increasing concentration of acid and base due to increasing conductivity of CEM and AEM.
(5) Due to the high internal resistance of single cell (mainly high resistance of CEM and AEM) at low concentration of acid and base, in order to maintain a proper efficiency, the depth of discharge of REDBP should not be deeper than 0.5M with high current density.
(6) Table 2.9 is area resistance of REDBP single cell. Resistance by charging is smaller than by discharging. This is due to crossover of acid/base through AEM/CEM, as well as produced acid and base enhancing conductivity of electrolyte solution.

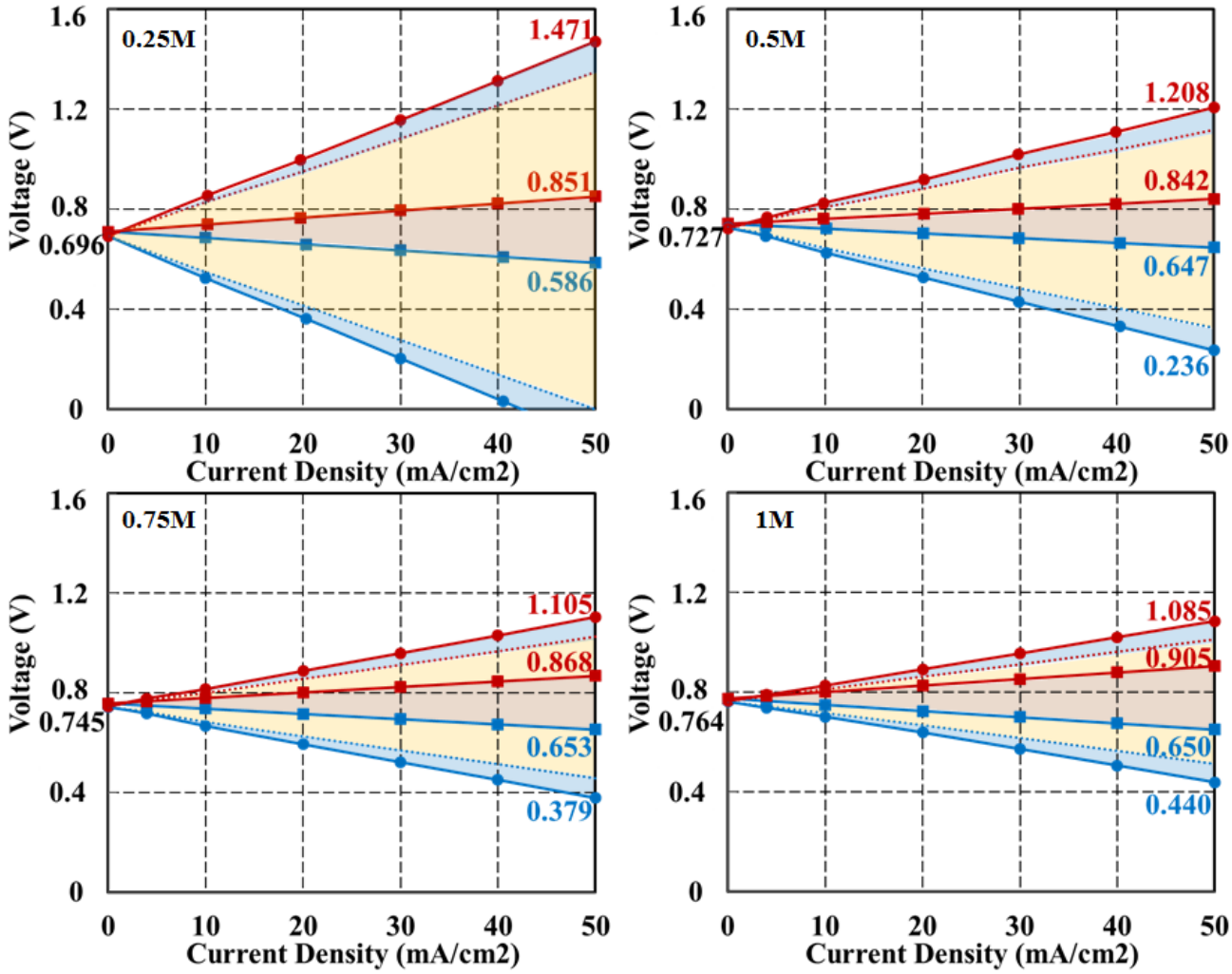

Figure 2.31: I-V curves of REDBP single cell with different solution concentration at 25°C. The red lines with positive slop are charging processes. The blue lines with negative slop are discharging processes. The solid line with square points is voltage between BP only. The dashed line is voltage of all IEMs without consideration of electrolyte solutions. The solid line with round points is voltage of REDBP single cell with electrolyte solutions with cellframe of 0.5mm thickness.

	25M	0.5M	0.75M	1M
Ch	15.5×10^{-4} Ω·m^2	9.62×10^{-4} Ω·m^2	7.20×10^{-4} Ω·m^2	6.42×10^{-4} Ω·m^2
DisCh	16.1×10^{-4} Ω·m^2	9.82×10^{-4} Ω·m^2	7.32×10^{-4} Ω·m^2	6.48×10^{-4} Ω·m^2

Table 2.9: The area resistance of REDBP single cell with different solution concentration calculated according to single membrane experiments at 25°C 0.1MPa. The solution chamber is 0.5mm thick.

2.5.2 Power Density

Figure 2.32 shows the I-V curves of REDBP single cell with 0.5mm thick chambers at 25°C. The maximum Power Density (PD)[1] by discharging has been marked. It is obvious, that with increasing

[1] The definition of PD, please check section 1.4.3.

concentration of solution the maximum PD is increasing. With 1M solution at -50mA/cm2, the maximum PD by discharging reaches 112mW/cm^3 and has potential to increase further with higher current density (not mentioning increasing PD by utilizing thinner IEM and solution chambers). The efficiency increases with increasing concentration due to decreasing resistance of solution chambers, CEM and AEM, although higher concentration causes increasing resistance of BP. The efficiency of 1M solution is over 77% with current density lower than 20mA/cm^2. This is very high considering each REDBP single cell having 3 IEMs and 3 solution chambers (too much internal resistance). There is always a trade-off between PD and efficiency depending on different applications.

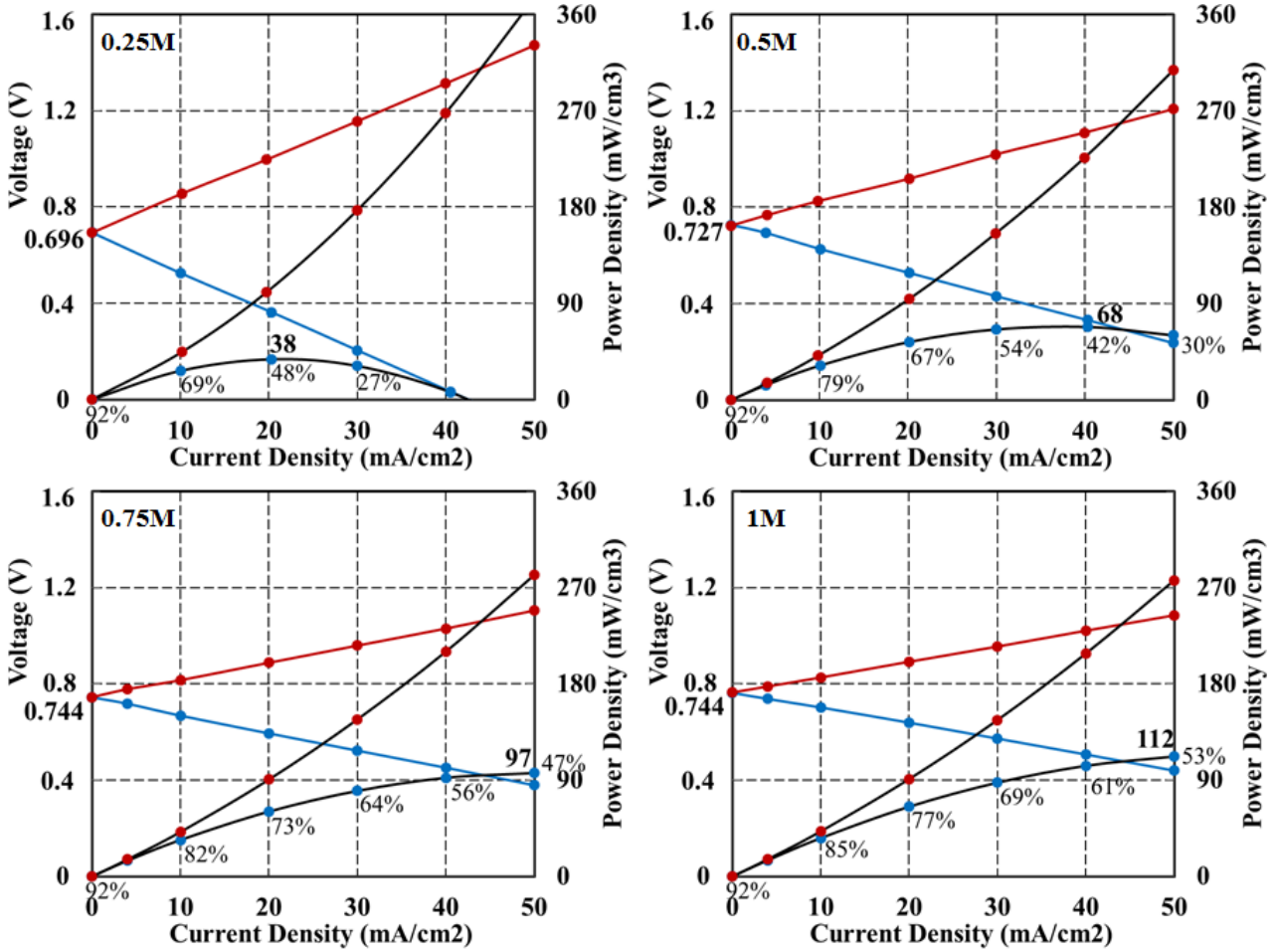

Figure 2.32: I-V curves and power density curves of REDBP single cell with 0.5mm solution chambers with different solution concentration at 25°C 0.1MPa The thickness of AEM, BP and CEM is 0.12mm, 0.22mm and 0.12mm, respectively. Red lines are charging curves, blue are discharging curves. Black lines with red dots are power density curves by charging, black lines with blue dots are power density by discharging. The maximum discharging power density has been marked. The efficiency of each situation has been calculated and labeled.

2.5.3 Crossover, Scaling and Fouling

REDBP single cell has three IEMs; each IEM separates two different solution chambers. Theoretically IEM allows only specific ions passing through it (for example, only cations can pass

through CEM), but in reality no IEM has 100% selectivity, especially when solution concentration difference between IEM is high. According to Faraday´s law (section 3.1.5- 3.1.6), ionic transport does not necessarily form electric current.

In figure 2.33, all possible ionic transports are illustrated. The solid arrows are ionic transport forming electric current while dashed arrows are not forming electric current. These ionic transports, illustrated in dashed arrows, are crossovers.

Crossover can be seen as an intra-cell leakage. Leakage here is not defined as gradual material losses due to non-ideal design of cell frame or sealing inside of REDBP single cell, although it is quite a challenge for the complexity of REDBP single cell. Rather intra-cell leakage is limited to ionic transports which do not form electric current, cause unwanted chemical reactions, and ultimately lead to change of ionic concentration inside of single cell.

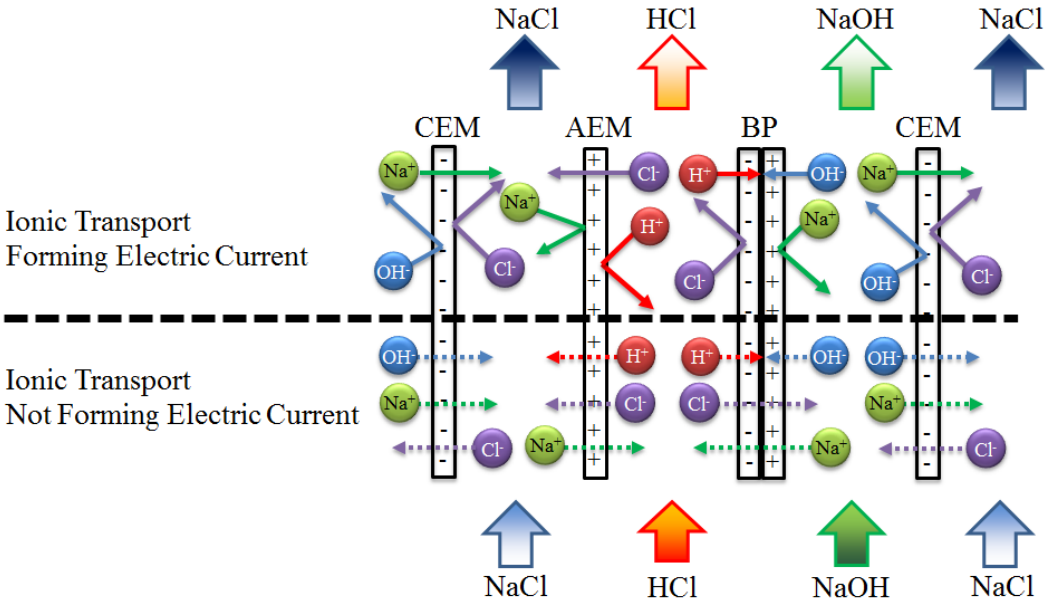

Figure 2.33: All possible ionic transports inside of REDBP single cell. Solid arrows are ionic transport forming electric current. Dashed arrows are ionic transport not forming electric current.

Everything has its pros and cons even for the crossovers. In the following section the disadvantages as well as advantages of crossover will be discussed.

Disadvantages of Crossover:

(1) One of the main disadvantages of crossover is loss of fuel. In the case of REDBP, the loss is of both acid and base. This leakage will directly influence the capacity change of REDBP as an energy storage system. But due to the limitation of content, this part - serious investigation of coulomb efficiency - is not investigated.

(2) Second disadvantage is neutralization reaction inside of BP causing production of water molecules which increases resistance of BP as well as resistance of diffusional layers both in acid and base chambers.

(3) Moreover, it causes the change of properties of electrolyte solution. For example, a) salt chamber will not be neutral, and b) salt concentration in acid and base chamber will be changing. The former will be discussed later and is not considered as bad. The latter does not have much influence on the performance of BP according to the experiment[1]. But nonetheless, it indeed requires additional monitoring procedures by battery management system which complicates the entire system, and anti-corrosive pipes for salt solution which raises the overall costs.

Advantages of Crossover:

Before experiment, no one has ever considered the advantages of crossover. But it indeed enhances the performance of REDBP single cell:

(1) Leakage of acid and base due to the non-ideal selectivity of BP causes neutralization reaction which elevates temperature of BP and enhances its voltage (section 2.3.1).

(2) Leakage of acid through AEM enhances the conductivity of AEM and the diffusional layer between AEM and bulk salt solution. The area resistance of a typical[2] AEM is 7-8 $\Omega \cdot cm^2$. But according to single membrane experiment of AEM (section 3.4.1), AEM between salt solution and acid solution has much smaller area resistance. For example with 1M acid solution, area resistance is around 1.4 $\Omega \cdot cm^2$.

(3) Leakage of base through CEM enhances the conductivity of CEM and the diffusional layer between CEM and bulk salt solution for the same reason as (2).

(4) No scaling in salt solution chamber if sea water is directly used due to the excess leakage of acid from acid chamber. One of the main problems of electrodialysis process (ED) is scaling of Mg^{2+} and Ca^{2+} on/in IEM which occurs when salts present in the water precipitate out and settle on the membrane surface and/or within membrane channels [29]. A very important factor affecting scaling formation is pH of treated solution. It was reported that the membrane scaling formed by minerals of Ca^{2+} and Mg^{2+} on IEM surface mostly takes place at basic pH values [30]. In REDBP due to the high permeability of H^+, the pH value of salt chamber is always in the range of 2 to 4 depending on the working condition[3]. In this condition scaling is

[1] Experiments are performed as comparison of 0.5M acid and base with or without additional 0.1M NaCl in single membrane test stack. The results are identical.
[2] In Cl^- form in 0.5 M NaCl at 25 °C, measured in standard measuring cell (through-plane).
[3] Conditions like flowrate of electrolyte solutions, temperature, current density, etc.

almost impossible near AEM. In the diffusional layer between CEM and bulk salt solution where OH^- exists, scaling can be easily recovered by flushing electrolyte chambers with acid.

(5) No fouling in salt solution chamber if sea water is directly used due to low pH value in salt chamber. It appeared from the results of [31] that the membrane fouling had mainly affected the ED efficiency in basic conditions. For the same reason as (4), the pH value of salt chamber of REDBP is lower enough to prevent fouling.

(6) For the reasons of (4) and (5), sea water can be used almost directly without sophisticated pretreatment, which significantly reduces the system cost.

Although there are several advantages due to the crossovers of acid and base, it is still very difficult to determine whether it is good or bad without thoroughly investigation of capacity change over time. But considering of lower resistance of IEM and directly usage of sea water, leakage can be tolerated. At least it can be immediately prevented by switching off the pumps.

2.6 Conclusion

Due to its complexity, investigation of REDBP single cell has been divided into measurement of BP, CEM and AEM separately. There are many influencing parameters like temperature, flowrate, current density, concentration and properties of IEMs on the performance of REDBP as an energy storage system. Due to the limitation of content in this dissertation, only a few parameters have been investigated, especially concentration and current density.

It has been found that OCV has direct influence from temperature and concentration. OCV is always higher than 0.7V with solution concentration higher than 0.25M. Further increasing concentration of electrolyte and temperature will benefit OCV very little.

The higher concentration of acid and base, the higher conductivity of electrolyte solution as well as CEM and AEM will be. But leads to higher crossover of acid and base which causes increasing resistance of BP.

The maximum overall power density is $112mW/cm^3$ with 1M solution concentration and 0.5mm thick solution chambers at $-50mA/cm^2$. There is always a compromise between power density and efficiency. At $-10mA/cm^2$ efficiency is above 85% with a power density of $34mW/cm^3$ by discharging.

Crossover effect has been discussed, too. It is the reason for gradual capacity loss of REDBP and increasing resistance of BP. At the same time it allows direct usage of sea water in salt chamber as well as reduces the overall resistance of REDBP single cell.

Chapter 3

Modeling and Simulation of Single Cell

In the previous section, the single cell experiments have been performed by measuring electric potential using Luggin capillaries combined with saturated calomel electrodes with changing current density at various conditions. However, what is happening inside of IEMs is still unclear. At moment it is impossible to measure the real-time temperature, electric current (ionic transports), ionic activities, water molecule activity, electric potential at different positions inside of IEMs and the neutralization reaction at BP interface without introducing significant additional errors. Therefore, this section is an attempt to use mathematical methods for describing and understanding microscopic phenomena inside of IEMs, which are the key components of REDBP single cell. First some fundamental concepts and basic assumptions have to be introduced before constructing mathematical model of IEMs. Then, discussions of simulation results will be presented mainly as ionic distribution and profile of electric potential throughout the IEM as well as validation with single cell experiments.

3.1 Fundamentals and Assumptions

In this section the basic concepts which are crucial for understanding modeling methods mainly concerning electrochemistry are introduced.

3.1.1 Charge Density and Electroneutrality

The volumetric charge density in an electrolyte solution is defined as:

$$\rho_e = \sum_{j=1}^{J}(N_A \cdot e_0 \cdot z_j \cdot c_j) \quad \textbf{(3.1)}$$

where ρ_e is volumetric charge density [C/m^3], N_A is Avogadro constant, e_0 is elementary charge, z_j is charge number of the ion j, c_j is concentration of the ion j. The value of the product $N_A \cdot e_0$ is numerically equal to 96485 [C/mol], and this quantity is termed as the Faraday constant, and denoted by the symbol F. Therefore, equation (3.1) can be rewritten as:

$$\rho_e = \sum_{j=1}^{J}(F \cdot z_j \cdot c_j) \quad \textbf{(3.2)}$$

The principle of electroneutrality dictates that any charge (dissolved ion or surface) must have an equal and opposite quantity of charges nearby, which means charge density is always equal to zero. Strictly speaking, electroneutrality is only an approximation which was first introduced by Walther Nernst in 1889 [32], but it has been proven that for most systems it fails only at very short timescales (nanosecond) where the finite mobility of ions prevents the instantaneous passage of charge, or at very short space scales (nanometers) where the approximation of screening of charge separation over an infinitesimal distance is no longer accurate [33]. Therefore, in this thesis electroneutrality is assumed to be valid, which means there is no charge separation anywhere in electrolyte and so neutrality is maintained everywhere. In electrolyte solution it holds:

$$\sum_{j=1}^{J} z_j \cdot c_j = 0 \tag{3.3}$$

where c_j is concentration of ion j, z_j is charge number of ion j.

In IEM:

$$\sum_{j=1}^{J} z_j \cdot c_j + z_{mf} \cdot X_m = 0 \tag{3.4}$$

where z_{mf} is number of charge of fixed ions in IEM, and X_m is fixed ion concentration in IEM.

In double-layer model electroneutrality also holds as shown in figure 3.1 of metal surface contacting electrolyte solution. Within the double layer according to electroneutrality approximation, charge density equals zero. About the detail description of double-layer model, please see section 3.4.2.

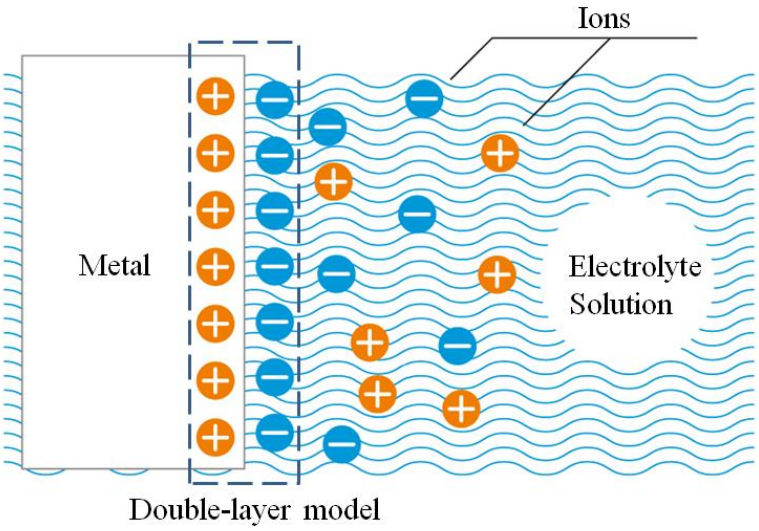

Figure 3.1: Double-layer model of metal surface contacting electrolyte solution.

3.1.2 Activity Coefficient and Ideal Mixture

Activity is the 'effective' concentration in chemical thermodynamics. An activity coefficient is a factor to account for deviations from ideal behavior in a mixture of chemical substances. In solution, ionic activity is defined as:

$$a_j = \gamma_j \frac{c_j}{c_j^0} \tag{3.5}$$

where γ_j is activity coefficient of ion j in solution, c_j is ionic concentration of ion j in solution, and c_j^0 is standard concentration which is defined as 1mol/l in this thesis[1].

In order to simplify computational procedures, ions in electrolyte solution as well as IEMs are treated as ideal mixture, γ equals 1.

3.1.3 Electrochemical Potential and Electrochemical Equilibrium

The chemical potential of a species can be regarded as the change in free energy when one mole of j is added to an infinite amount of the mixture, so that the mole fractions of all other components are unaltered:

$$\mu_j = \left(\frac{\partial G}{\partial n_j}\right)_{n_j \neq n_i, p, T} \tag{3.6}$$

where μ_j is chemical potential of species j [J/mol], G is free energy [J], n_j is the total number of moles of species j.

The chemical potential is more specifically called total chemical potential [34]. If two locations have different total chemical potentials for a species, some may be due to potentials associated with 'external' force fields (electric potential energy differences, gravitational potential energy differences, etc.), while the rest would be due to 'internal' factors (density, temperature, etc.) Therefore, the total chemical potential can be split into internal chemical potential and external chemical potential:

$$\mu_{tot} = \mu_{internal} + \mu_{external} \tag{3.7}$$

[1] In many literatures according to the application, definition of a_j can be expressed using molality or mass concentration. The reasons why 1mol/l is being used as standard concentration are: Firstly [mol/l] is often used as standard solution in analytical chemistry which is suitable for future coulombic analysis of REDBP electrolyte solution; Secondly 1M solution of acid and base is considered as one of the standard working conditions for analyzing the performance of REDBP in this thesis; Thirdly molality or mass concentration is useless by describing ionic activity in dilute solution since water molecules are too abundant.

The chemical potential is often being referred as total chemical potential. However, in the field of electrochemistry, it will create misunderstandings.

Here, like all the previous work relating to electrochemistry, all the other external potentials (like gravitational potential) are being neglected. Therefore, electrochemical potential is used to describe total chemical potential, and chemical potential means internal chemical potential:

$$\widetilde{\mu_j} = \mu_j + z_j \cdot F \cdot \varphi \tag{3.8}$$

where $\widetilde{\mu_j}$ is electrochemical potential (as defined as total chemical potential), μ_j is chemical potential (as defined as internal chemical potential), and φ is the electric potential. If defined by conditions of pressure, temperature, activity and electric potential, electrochemical potential $\widetilde{\mu_j}$ can be rewritten as:

$$\widetilde{\mu_j} = \mu_j^0 + \mathrm{P} \cdot V_{m_j} + R \cdot T \cdot ln\left(a_j\right) + z_j \cdot F \cdot \varphi \tag{3.9}$$

where μ_j^0 is standard chemical potential, P is pressure, V_{m_j} is partial molar volume, a_j is activity and φ is the electric potential.

As previously introduced in section 1.4.2, in REDBP efficiency of 100% means all the Gibbs free energy produced by neutralization reaction will transform into electric work moving electron to an infinite far distance:

$$\Delta g = z_{e-} \cdot F \cdot E \tag{3.10}$$

where E is electromotive force (EMF)[1]. However, neutralization reaction can only drive the movement of ions in electrolyte. There is no electron exchange during this process simply because there is no free electron. Therefore, systems like REDBP require electrode chambers to transform the former to the latter in the form of electrochemical reactions or vice versa. In electrode chambers electrochemical reactions take place:

$$\sum_{red} v_{red} \cdot a_{red} \leftrightarrow \sum_{ox} v_{ox} \cdot a_{ox} + n_e \cdot e^- \tag{3.11}$$

where a_{ox} and a_{red} are termed the oxidized and reduced components activity, respectively, n_e is number of electrons and v_j is stoichiometric number. At electrochemical equilibrium:

$$\Delta\tilde{\mu} = \sum_j v_j \cdot \widetilde{\mu_j} = 0 \tag{3.12}$$

[1] About calculation of EMF of REDBP, please check section 1.4.2.

a generalized Nernst equation can be established:

$$\Delta\varphi = \Delta\varphi^0 + \frac{R\cdot T}{n_e \cdot F}\ln\left(\frac{\prod_{ox} a_{ox}^{v_{ox}}}{\prod_{red} a_{red}^{v_{red}}}\right) \quad \textbf{(3.13)}$$

where $\Delta\varphi$ is electric potential between electrode and electrolyte solution.

Or, more generally, described as electrode potential:

$$E = E^0 + \frac{R\cdot T}{n_e \cdot F}\ln\left(\frac{\prod_{ox} a_{ox}^{v_{ox}}}{\prod_{red} a_{red}^{v_{red}}}\right) \quad \textbf{(3.14)}$$

It is very possible the following reactions[1] take place in electrode chambers.

Oxidation reaction at anode side:

$$H_2O \rightarrow 2H^+ + \frac{1}{2}O_2 + 2e^- \qquad E^0_{anode} = -1.229V \quad \textbf{(3.15)}$$

While reduction at cathode side:

$$2H_2O + 2e^- \rightarrow 2OH^- + H_2 \qquad E^0_{cathode} = -0.828V \quad \textbf{(3.16)}$$

And with an overall reaction:

$$3H_2O \rightarrow 2H^+ + \frac{1}{2}O_2 + 2OH^- + H_2 \qquad E^0_{electrode} = -2.057V \quad \textbf{(3.17)}$$

According to Nernst equation (3.14):

$$E_{electrode} = E_{anode} + E_{cathode} \quad \textbf{(3.18)}$$

$$= E^0_{anode} + \frac{R\cdot T}{-2\cdot F}\ln\left(\frac{{a_{H^+}}^2 \cdot \left({P_{O_2}}/{P^0}\right)^{1/2}}{a_{H_2O}}\right) + E^0_{cathode} + \frac{R\cdot T}{2\cdot F}\ln\left(\frac{{a_{H_2O}}^2}{{a_{OH^-}}^2 \cdot \left({P_{H_2}}/{P^0}\right)}\right)$$

$$= E^0_{electrode} + \frac{R\cdot T}{2\cdot F}\ln\left(\frac{{a_{H_2O}}^3}{{a_{OH^-}}^2 \cdot \left({P_{H_2}}/{P^0}\right)\cdot {a_{H^+}}^2 \cdot \left({P_{O_2}}/{P^0}\right)^{1/2}}\right)$$

Where P_{O_2} is partial pressure of oxygen, P_{H_2} is partial pressure of hydrogen, P^0 is the standard pressure of 1 atmosphere ($\equiv 101325\ Pa$).

As equation (3.18) shows, an increase of gases´ partial pressure and acid/base activity will further decrease electrode potential, meaning consume more energy.

[1] More detail description of possible electrochemical reactions in electrode chambers, please check section 4.1.3.

Here, if an additional electrical field E_{add} is being applied, electrochemical equilibrium would be shifted. In the case of electrodialysis, if $E_{add} + E_{electrode} < 0$, external electric current could not be produced. If $E_{add} + E_{electrode} > 0$, external electric current could be produced. E_{add} could be either a DC potential difference applied between two electrodes, or electric potential in electrolyte due to electrochemical equilibrium. REDBP is an example of the latter.

3.1.4 Donnan Potential

At the interface between an IEM and adjacent electrolyte solution (for example, salt solution, as shown in figure 3.2), once electrochemical equilibrium is established, the following relations could be expected:

For Na^+: $$\mu_{Na^+}^{solution} + F \cdot \varphi^{solution} = \mu_{Na^+}^{CEM} + F \cdot \varphi^{CEM} \quad \textbf{(3.19)}$$

For Cl^-: $$\mu_{Cl^-}^{solution} - F \cdot \varphi^{solution} = \mu_{Cl^-}^{CEM} - F \cdot \varphi^{CEM} \quad \textbf{(3.20)}$$

where $\mu_j^{solution}$ is chemical potential of species j in solution, μ_j^{CEM} is chemical potential of species j in CEM and φ is electrical potential.

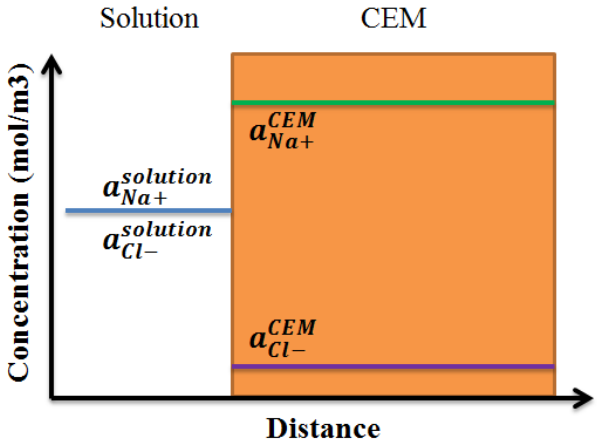

Figure 3.2: Schematic diagram of ionic distribution at the interface between CEM and its adjacent salt solution.

From equation (3.9), if neglecting pressure term, Donnan distribution can be generalized as:

$$a_{Na^+}^{solution} \cdot a_{Cl^-}^{solution} = a_{Na^+}^{CEM} \cdot a_{Cl^-}^{CEM} \quad \textbf{(3.21)}$$

and the overall potential drop across the interface between an IEM and adjacent electrolyte solution $\Delta\varphi$ can be calculated as:

$$\Delta\varphi^{Donnan} = \varphi^{CEM} - \varphi^{solution} = \frac{R \cdot T}{F} \ln\left(\frac{a_{Na^+}^{solution}}{a_{Na^+}^{CEM}}\right) = \frac{R \cdot T}{F} \ln\left(\frac{a_{Cl^-}^{CEM}}{a_{Cl^-}^{solution}}\right) \quad \textbf{(3.22)}$$

$\Delta\varphi^{Donnan}$ is the so-called Donnan potential locating at the interface between IEM and electrolyte solution.

Please note, once electrochemical equilibrium has been reached, electric potential of all ions in the same phase must be equal, as illustrated in equation (3.19) or equation (3.20), and Donnan distribution should be applied to all kinds of ion as equation (3.22).

In short, Donnan potential and Donnan distribution are the consequences of electrochemical equilibrium, and both of them can be deducted from Boltzmann distribution.

3.1.5 Ionic Transport in Ideal Mixture

There are three kinds of ionic transport process in electrolyte solution: convection, diffusion and migration.

$$\vec{J}_j^{total} = \vec{J}_j^{convection} + \vec{J}_j^{diffusion} + \vec{J}_j^{migration} \tag{3.23}$$

The driving force for each transport process is movement of electrolyte solution itself, concentration gradient of component j, and electric potential gradient, respectively. In an ideal mixture (normally at infinite dilution), it is believed there is a direct relation between ionic mobility[1] and its diffusion coefficient:

$$u_j = \frac{|z_j|\cdot F}{R\cdot T} D_j \tag{3.24}$$

The above equation is known as Nernst-Einstein equation, where u_j is mobility of ion j, and D_j is its diffusion coefficient. Thus equation (3.23) can be expressed as:

$$\vec{J}_j^{total} = c_j \cdot \vec{v} + D_j\left(-\nabla c_j\right) + z_j \frac{F}{R\cdot T} D_j \cdot c_j(-\nabla\varphi) \tag{3.25}$$

This is the Nernst-Planck equation. It is not suitable for concentrated solution due to the definition of mobility and diffusion coefficient. However, due to its simplicity, it will be used throughout this thesis.

[1] About the physical meaning of mobility, please check [26, pp. 13-14]

3.1.6 Electric Current in Electrolyte and Faraday´s Law

According to Faraday´s law, electric current in electrolyte is carried by ionic transport of dissolved ions, as describe as following:

$$i = \frac{I}{A} = \sum_{j=1}^{J}(F \cdot z_j \cdot \vec{J}_j^{total}) \quad \textbf{(3.26)}$$

Where i is electric current density [A/m^2]. Electric current density has direction: in this thesis, positive is charging process while negative is discharging process.

3.1.7 Conservation Equation of Ion

The conservation equation of ion j in electrolyte solution can be expressed as:

$$\frac{\partial c_j}{\partial t} = -\nabla \cdot \vec{J}_j^{total} + r_j^V \quad \textbf{(3.27)}$$

where r_j^V represents the net rate of formation or extinction of ion j per unit volume by chemical reaction.

3.1.8 Steady State

Steady state describes a system or a process that has no time changes of its variables defining its behavior. Combined with conservation equation of ion, at any given point the sum of currents flowing into it equals to the sum of currents flowing out of it:

$$\nabla \cdot i = 0 \quad \textbf{(3.28)}$$

It is also known as Kirchhoff's current law.

Applying steady state to IEMs dictates that all properties of IEM are unchanged in time. This also implies neither accumulation nor depletion of water molecules in the process, since production or consumption of water molecules will change the ionic activity, osmotic pressure, reaction speed, etc. In order to simplify the whole system, influences of water molecules are neglected.

Those are the basic simplified equations and assumptions that are the building blocks for constructing mathematical model for REDBP single cell.

3.1.9 Summary of Equations

This section is to summarize all the above mentioned equations according to their application conditions.

Condition 1: At the interface between solution and IEM:

a) Electroneutrality:

$$\sum_{j=1}^{J} z_j \cdot c_j + z_{mf} \cdot X_m = 0 \quad \textbf{(3.4)}$$

where in solution $z_{mf} = 0$ and in IEM $z_{mf} \neq 0$.

b) Electrochemical equilibrium (Donnan potential/distribution) across interface, take CEM as an example:

$$\Delta\varphi^{Donnan} = \frac{R\cdot T}{F}\ln\left(\frac{a_{Na^+}^{solution}}{a_{Na^+}^{CEM}}\right) = \frac{R\cdot T}{F}\ln\left(\frac{a_{Cl^-}^{CEM}}{a_{Cl^-}^{solution}}\right) = \frac{R\cdot T}{F}\ln\left(\frac{a_{H^+}^{solution}}{a_{H^+}^{CEM}}\right) = \frac{R\cdot T}{F}\ln\left(\frac{a_{OH^-}^{CEM}}{a_{OH^-}^{solution}}\right) \quad \textbf{(3.22)}$$

Condition 2: Inside of solution or IEM:

a) Electroneutrality:

$$\sum_{j=1}^{J} z_j \cdot c_j + z_{mf} \cdot X_m = 0 \quad \textbf{(3.4)}$$

where in solution $z_{mf} = 0$ and in IEM $z_{mf} \neq 0$.

b) Nernst-Planck equation:

$$\vec{J}_j^{total} = c_j \cdot \vec{v} + D_j\left(-\nabla c_j\right) + z_j \frac{F}{R\cdot T} D_j \cdot c_j(-\nabla\varphi) \quad \textbf{(3.25)}$$

c) Faraday´s law:

$$i = \frac{I}{A} = \sum_{j=1}^{J}(F \cdot z_j \cdot \vec{J}_j^{total}) \quad \textbf{(3.26)}$$

d) Conservation equation:

$$\frac{\partial c_j}{\partial t} = -\nabla \cdot \vec{J}_j^{total} + r_j^V \quad \textbf{(3.27)}$$

where $r_j^V = 0$, and due to steady state:

$$\nabla \cdot \vec{J}_j^{total} = 0 \quad \textbf{(3.29)}$$

Condition 3: At reaction double-layer:

In order to achieve integrity of summary of equations, this part, which will be explained in details in section 3.4.2, will be included as well.

a) Electroneutrality on both layers:

$$\sum_{j=1}^{J} z_j \cdot c_j = 0 \tag{3.3}$$

b) Electrochemical equilibrium (Nernst equation) across double-layer:

$$EMF = EMF^0 - \frac{R \cdot T}{F} \ln\left(\frac{c^0_{H_3^+O} \cdot c^0_{OH^-}}{c_{H_3^+O} \cdot c_{OH^-}}\right) \tag{3.30}$$

c) Conservation equation:

$$\frac{\partial c_j}{\partial t} = -\nabla \cdot \vec{J}_j^{total} + r_j^V \tag{3.27}$$

where $r_j^V \neq 0$, and due to steady state:

$$\nabla \cdot \vec{J}_j^{total} = r_j^V \tag{3.30}$$

for H^+:

$$\nabla \cdot \vec{J}_{H+}^{total} = r_{H+}^V = -k_{NR} c_{H+} c_{OH-} \tag{3.37}$$

for OH^-:

$$\nabla \cdot \vec{J}_{OH-}^{total} = r_{OH-}^V = -k_{NR} c_{H+} c_{OH-} \tag{3.38}$$

where k_{NR} is reaction speed constant of neutralization reaction.

3.2 Cation Exchange Membrane

In order to further simplify computational procedure, an IEM model with fixed diffusional layers will be introduced.

3.2.1 Ion Exchange Membrane with Fixed Diffusional Layers

Assuming ideal mixing, according to equation (3.25) there is no diffusion nor convection term (solution transport direction perpendicular to the surface of IEM is zero) in bulk solution. However, on the no-slip boundary condition, there always exists a diffusional layer between IEM and bulk solution. In this thesis, the thickness of diffusional layer is considered as constant, equals 50μm, as illustrated in figure 3.3.

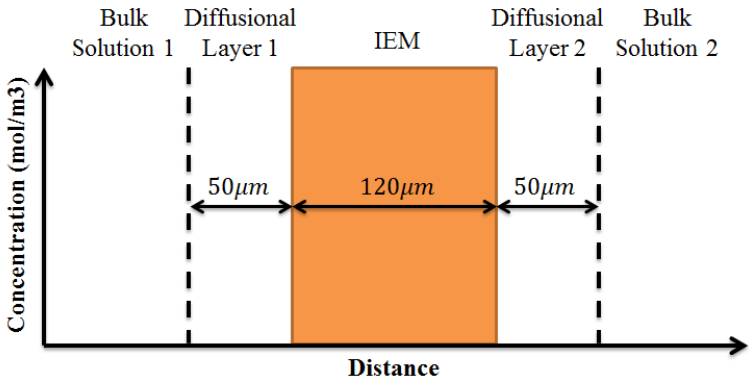

Figure 3.3: Schematic diagram of modelling of IEM with diffusional layers which have fixed thickness of 50μm.

The most important input parameter is mobility of ions in solutions and IEM. Table 3.1 shows the ionic mobility according to the work of [35]. Unfortunately there is no literature about the mobility of OH^- in CEM. Therefore, it is assumed to be 1/10 of its value in water solution. Moreover, H^+ is not included in this model due to negligence of water dissociation.

Table 3.1: Mobility of different ions in CEM and electrolyte solution [35].

	In CEM	In Solution	
u_{Na+}	$0.25 \cdot 10^{-8}$	$5.19 \cdot 10^{-8}$	$[m^2/(V \cdot s)]$
u_{Cl-}	$0.15 \cdot 10^{-8}$	$7.91 \cdot 10^{-8}$	$[m^2/(V \cdot s)]$
u_{OH-}	$2.04 \cdot 10^{-8}$	$20.4 \cdot 10^{-8}$	$[m^2/(V \cdot s)]$

With these further simplifications and treatment bulk solutions as boundary conditions, the mathematical model has been set up and simulated by MATLAB using Newton methods for nonlinear problems.

3.2.2 Concentration and Electric Potential Profiles of CEM

Figure 3.4 shows the typical ionic concentration and electric potential profiles of CEM between 1M NaOH solution and sea water by open circuit at 25°C 0.1MPa. Theoretically, CEM allows only cations passing through it, but due to the high concentration difference of Cl^- and OH^- between base and salt solution, transport of co-ions[1] is inevitable. This is the reason for crossover. Because of such spontaneous ionic transport through IEM, electric potential needs to 'adjust itself' to adapt to this new condition. That is the reason the electric potential across CEM is not zero. According to simulation result, it shows -25mV on the right side compared with the left side. The physical meaning is that system automatically creates a negative electric potential on its right side to counter the ionic transport of OH^-. The sudden changes of electric potential at the interface between electrolyte solution and CEM are two Donnan potentials.

Figure 3.5 is a series of discharging profiles. According to Faraday´s law (section 3.1.6), electric current is carried by transport of dissolved ions. By discharging the direction of electric current is from left to right. It is the same as the direction of transport of positive ions like Na^+, and opposite to that of negative ions like Cl^- and OH^-. That is the reason why ionic transport of OH^- is getting smaller with increasing discharge current. In other words, discharging is like a depletion process of OH^- both in CEM and in salt chamber. And due to this depletion process, the electric conductivity of CEM deteriorates. Although permeability of Cl^- through CEM is very poor, however with very high current density, the accumulation of Cl^- in base chamber is becoming significant, which will change the property of base solution.

Unlike discharging, the direction of electric current by charging is from right to left, meaning positive ions should be moving from right to left, or/and negative ions from left to right, as shown in figure 3.6. That is the reason why transport of Na^+ is getting smaller (or even shift the transport direction) with increasing current density by charging. As well as accumulation of OH^- in CEM and in salt solution chamber, because of crossover effect, the electric conductivity of CEM improves with increasing charging current density, which lowers the overall internal resistance of single cell by charging at the cost of leakage of the fuel. About the pros and cons of crossover effect in CEM please check section 2.5.3.

[1] Co-ion is any ion having the same charge as the fixed ion of IEM.

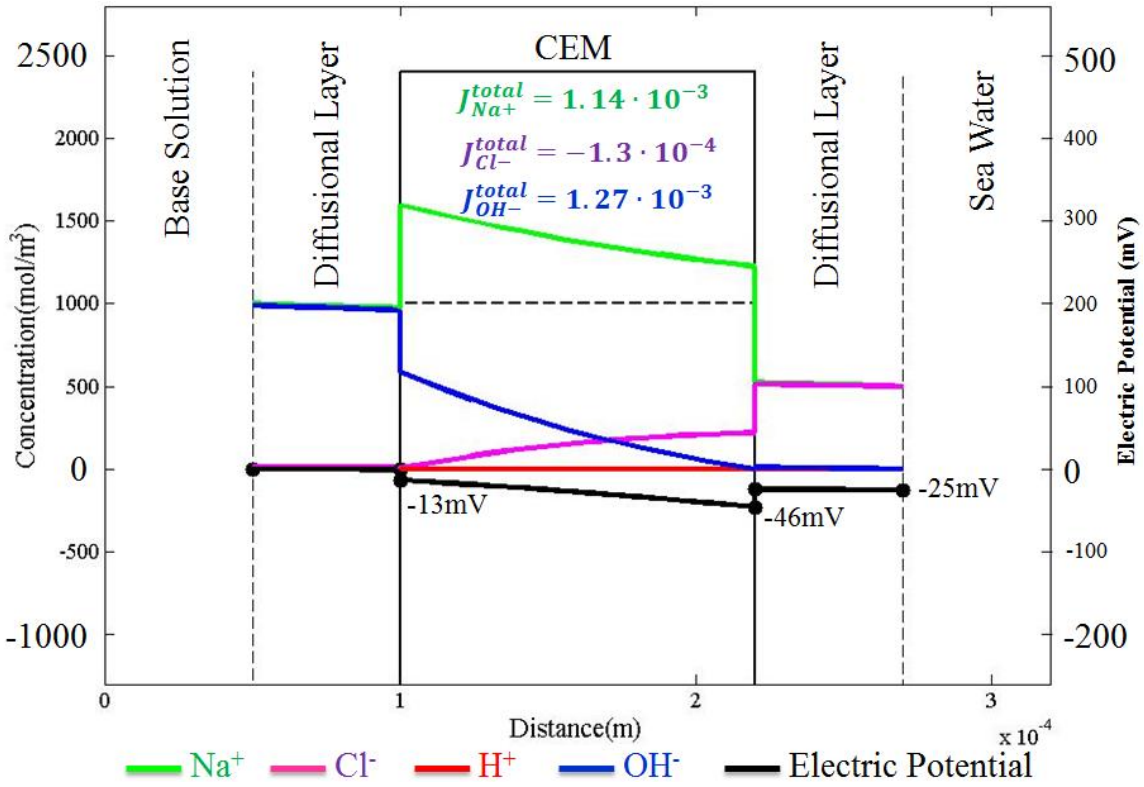

Figure 3.4: Concentration and electric potential profiles of CEM between 1M NaOH solution and sea water by open circuit at 25°C 0.1MPa. Each ionic transport is labelled on the diagram with the unit of [mol/(m^{2}s)].

3.2.3 Comparison with Experiment

Figure 3.7 shows comparison between measurement and simulation result of CEM between 1M base and sea water chamber.

(1) The measured OCV is indeed negative, but around -4mV. This maybe because the difference between chosen values of mobility of OH^- and Na^+ (for simulation) is not big enough. Therefore, the transport of Na^+ alone (or combined with transport of Cl^-) could counter the crossover of OH^- to balance electroneutrality on the right side.

(2) By discharging, the measurement and simulation result separate from each other significantly. The reason why the simulated electric conductivity of CEM between base and salt solution by discharging deteriorates is the depletion of OH^- in CEM and in salt chamber. In other words, electric current is mainly carried by transport of Na^+ and Cl^- through CEM. However, in reality, it seems that the concentration of OH^- in CEM or/and in salt chamber is high enough to lower the electric resistivity of CEM, which means the crossover effect of OH^- is higher in reality than in modelling.

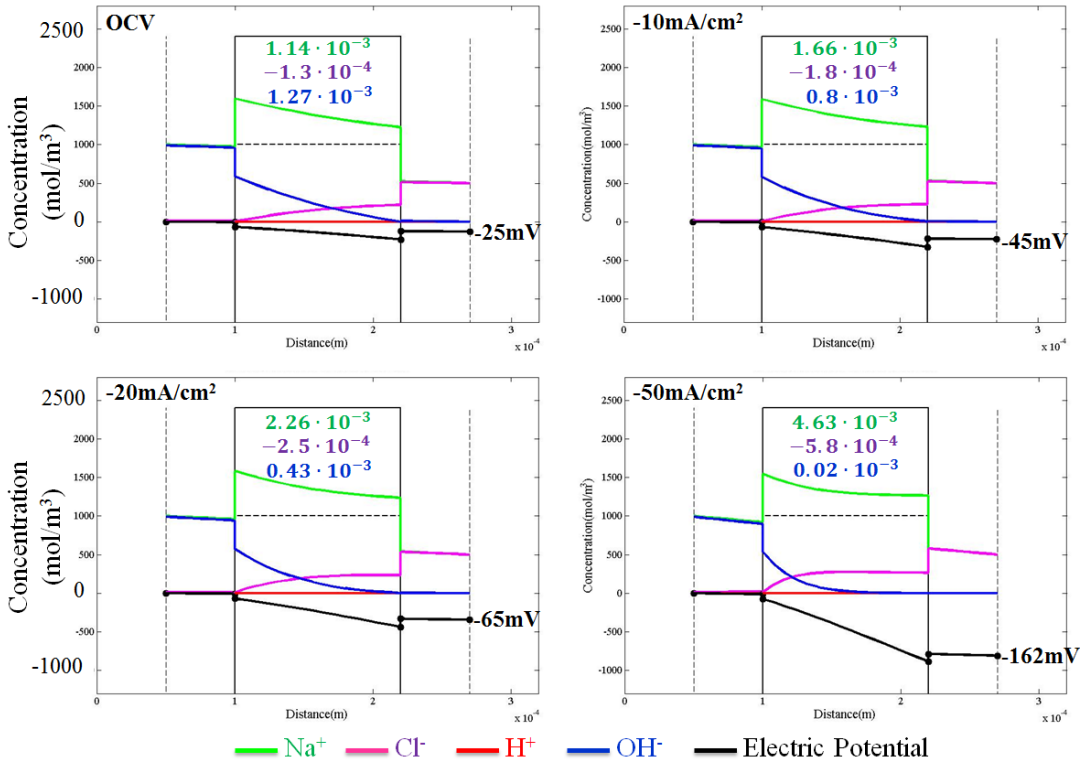

Figure 3.5: Concentration and electric potential profiles of CEM between 1M NaOH solution and sea water by discharging at 25°C 0.1MPa. Each ionic transport is labelled on the diagram with the unit of [mol/(m^{2}s)]. The direction of discharging current density is from left to right.

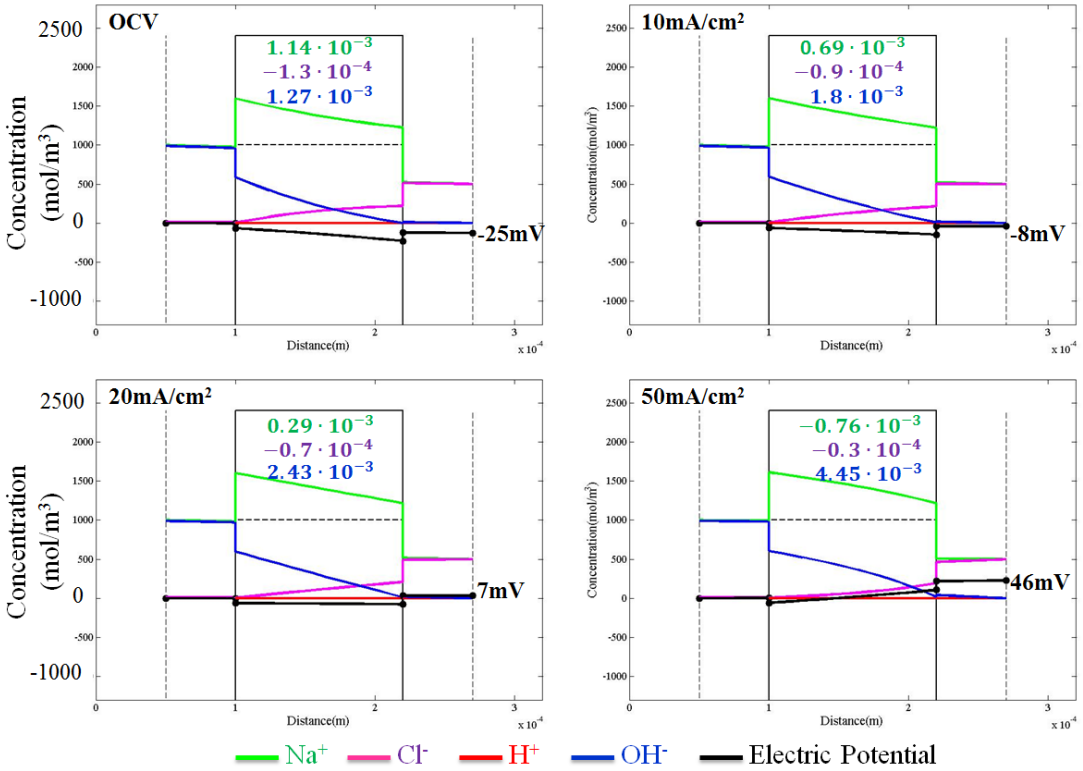

Figure 3.6: Concentration and electric potential profiles of CEM between 1M NaOH solution and sea water by charging at 25°C 0.1MPa. Each ionic transport is labelled on the diagram with the unit of [mol/(m^{2}s)]. The direction of charging current density is from right to left.

That is one of the drawbacks using ideal mixing and steady state as assumption, since ionic mobility and ionic activity are not constant in reality, and both relate to molecular interaction which has direct influence from ionic concentration. Moreover, the boundary condition by simulation is 'fresh solution'; this contradicts the experimental condition in which IEM will be activated by Ch/DisCh for 1 hour before experiment, which changes the properties of testing solution, especially in the case of discharging.

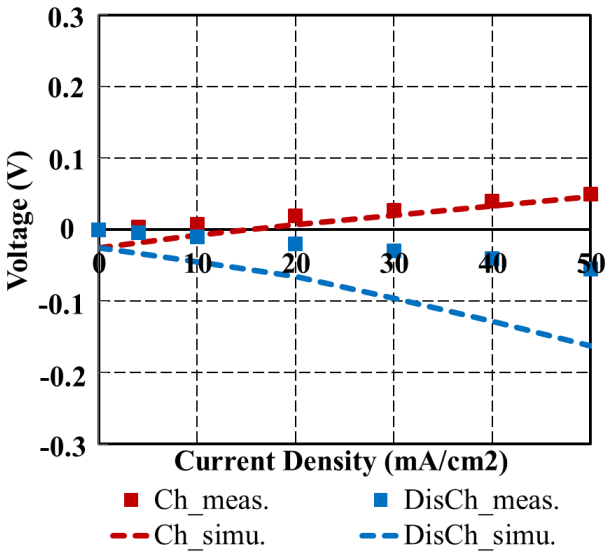

Figure 3.7: Comparison between measurement and simulation result of CEM between1M base and sea water chamber at 25°C 0.1MPa.

3.3 Anion Exchange Membrane

The chosen ionic mobilities are listed in table 3.2. Unfortunately there is no literature about the mobility of H^+ in AEM. Therefore, it is assumed to be 1/10 of its value in water solution. Moreover, OH^- is not included in this model due to negligence of water dissociation.

Table 3.2: Mobility of different ions in AEM and electrolyte solution [35].

	AEM	Solution	
u_{Na+}	$0.25 \cdot 10^{-8}$	$5.19 \cdot 10^{-8}$	$[m^2/(V \cdot s)]$
u_{Cl-}	$0.15 \cdot 10^{-8}$	$7.91 \cdot 10^{-8}$	$[m^2/(V \cdot s)]$
u_{H+}	$3.63 \cdot 10^{-8}$	$36.3 \cdot 10^{-8}$	$[m^2/(V \cdot s)]$

3.3.1 Concentration and Electric Potential Profiles of AEM

Figure 3.8 shows concentration and electric potential profiles of AEM between sea water and 1M HCl solution by open circuit at 25°C 0.1MPa. Due to the high ionic concentration difference

and high mobility of H^+, there exists crossover effect of acid into salt chamber, and because of that, electric potential on the right is relative lower than on the left. Figure 3.9 is a series of discharging profiles. As with CEM between base and salt chamber (section 3.2), discharging can be seen as depletion process of H^+ in AEM and in salt chamber. Therefore, electric conductivity of AEM declines with increasing discharging current density. When current density is high enough, there is a significant accumulation process of Na^+ in acid chamber which changes the properties of acid solution. Figure 3.10 is series of profiles while charging. Although by charging electric current can be carried by transport of H^+, due to the high crossover effect of acid, the electric potential between AEM is negative most of the time. This low value of electric potential may benefit the overall charging voltage between single cell (meaning better voltage efficiency), but at the cost of leakage of acid into the salt chamber (meaning poor coulombic efficiency). About the discussion of pros and cons of such leakage, please check section 2.5.3.

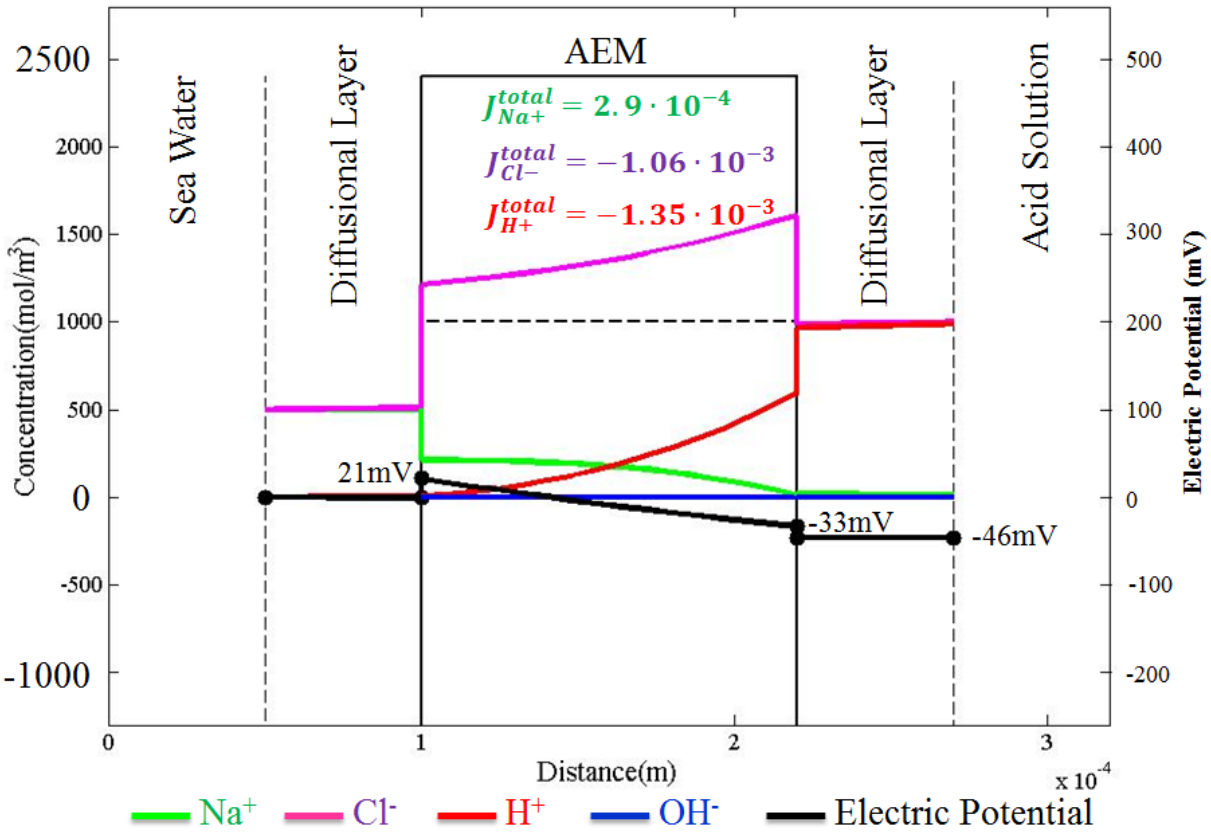

Figure 3.8: Concentration and electric potential profiles of AEM between sea water and 1M HCl solution by open circuit at 25°C 0.1MPa. Each ionic transport is labelled on the diagram with the unit of [mol/(m^2s)].

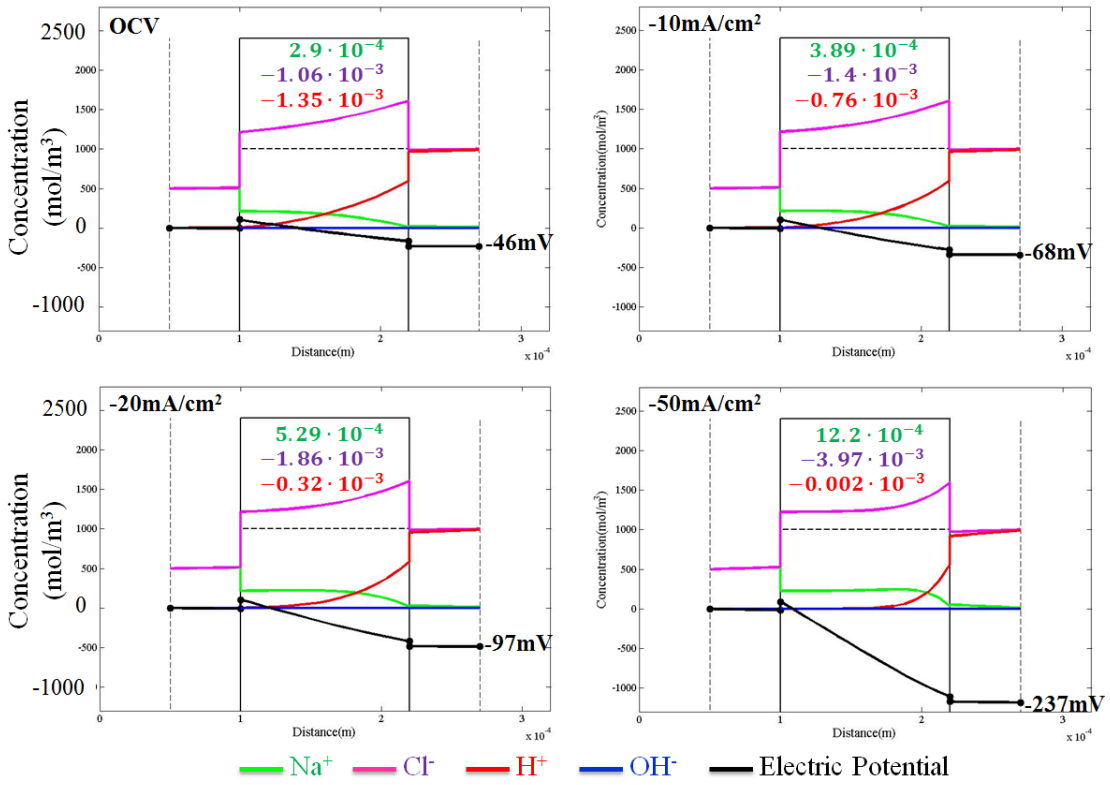

Figure 3.9: Concentration and electric potential profiles of AEM between sea water and 1M HCl solution by discharging at 25°C 0.1MPa. Each ionic transport is labelled on the diagram with the unit of [mol/(m^{2}s)]. The direction of discharging current density is from left to right.

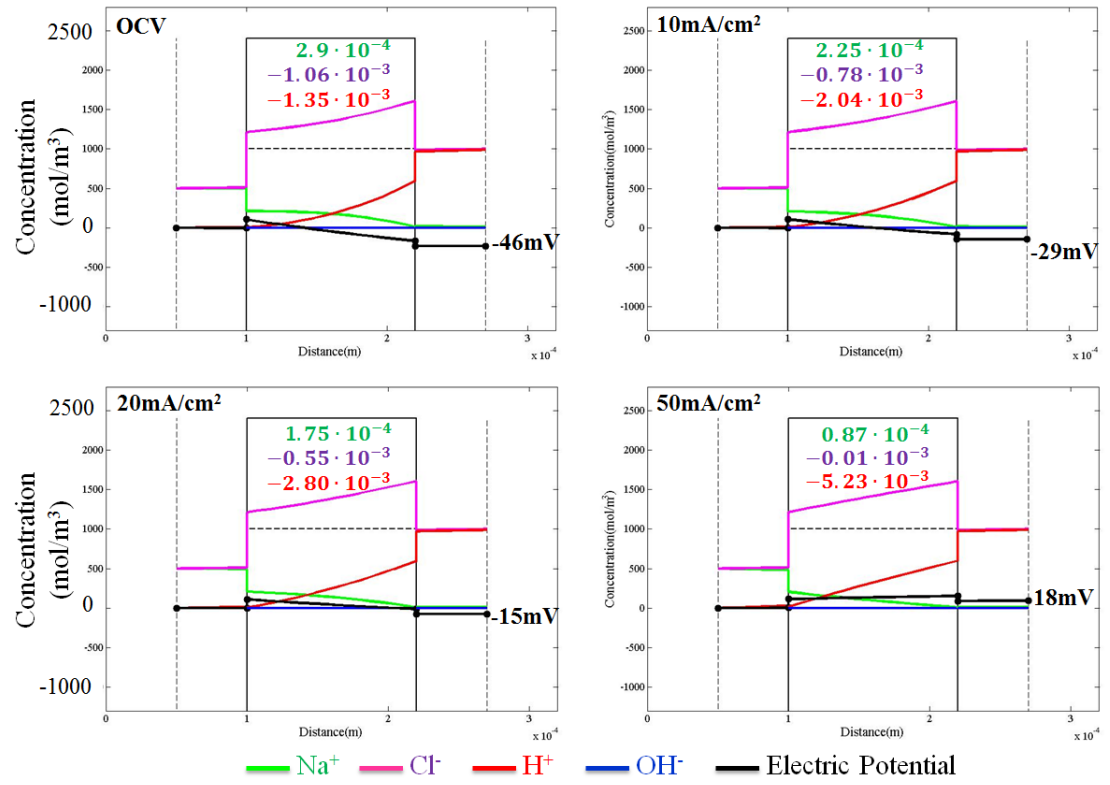

Figure 3.10: Concentration and electric potential profiles of AEM between sea water and 1M HCl solution by charging at 25°C 0.1MPa. Each ionic transport is labelled on the diagram with the unit of [mol/(m^{2}s)]. The direction of charging current density is from right to left.

3.3.2 Comparison with Experiment

Compared with experiment as shown in figure 3.11, simulation of AEM shows the same problem as CEM due to the assumption of ideal mixture, steady state and chosen boundary condition. Nonetheless, as a qualitative analysis, this model shows how the electric current is carried by ionic transports, and how it will affect the ionic concentration of solution chambers.

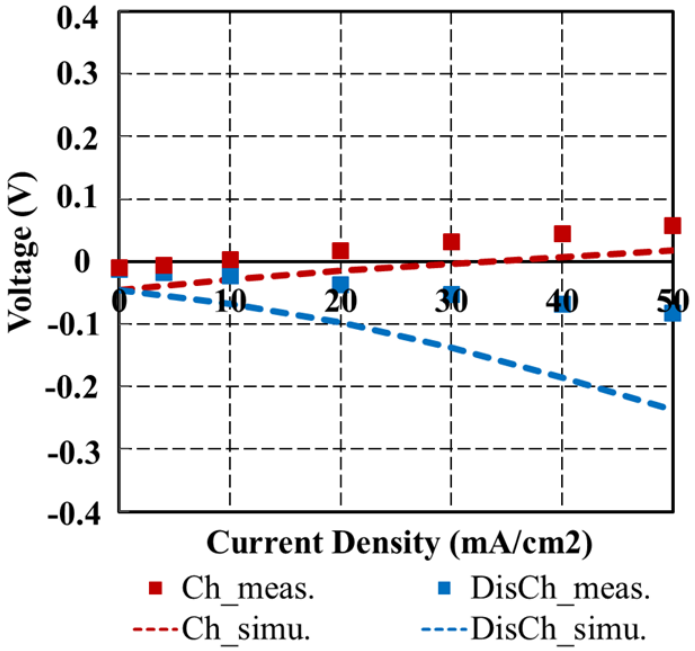

Figure 3.11: Comparison between measurement and simulation result of AEM with sea water and 1M HCl acid chamber at 25°C 0.1MPa.

3.4 Bipolar Membrane by Discharging

Modeling of BP follows the same principles as modeling of CEM/AEM. The main difference to the former is that chemical reaction is involved. In this section, only discharging process will be investigated. Details about modeling of charging process, please see [11] [36].

3.4.1 Bipolar Membrane with Fixed Reaction Zone

BP is relatively complicated due to its complex structure. Figure 3.12 is a schematic diagram of modelling of BP, which has two IEM layers (BPCEM shortened for Bipolar Membrane Cation Exchange Membrane side and BPAEM shortened for Bipolar Membrane Anion Exchange Membrane side) and one interface (shortened as BP interface) in the bipolar junction of the membrane where the anion and the cation permeable layers are in direct contact. In this thesis BP interface is treated like a water film which is 3nm thick and considered having no

fixed ions of any IEM. Due to the existence of water (either as product from neutralization reaction or permeated from bulk solution), BP interface is believed consisting of three parts.

- one reaction zone, which is 1nm thick.
- two diffusional layers between reaction zone and IEM, each has 1nm thick.

In addition, it is assumed that this structure and the position of reaction[1] remain unchanged as well as neglecting of water molecules.

3.4.2 Reaction Zone as Double-Layer Model

Double-layer model, which was introduced by H. von Helmholtz in the mid-1800s, dictates that there is a single layer of oppositely charged ions adjacent to a surface. Its main assumptions are point-charge model for ions, electroneutrality and neglecting of electrostatic attraction of counter-ions[2] and repulsion of co-ions [25, pp. 588-592]. This model has been significantly refined by M. Gouy [37] and D. L. Chapman [38], respectively, and was further improved by O. Stern [39] for the correction of finite ion size, which is known as Gouy-Chapman-Stern model. In the Gouy-Chapman-Stern model, the region between surface and the Stern layer in electrolyte solution is treated as Helmholtz double-layer (uncharged $\rho_e = 0$), while the region between Stern layer and a few Debye lengths is charged ($\rho_e \neq 0$) where $|\rho_e|$ decays gradually to zero as well as gradually changing of electric potential. Using Poisson-Boltzmann equation, the Debye length is calculated as:

$$\lambda = \left(\frac{F^2}{\varepsilon \cdot R \cdot T} \sum z_j^2 c_{j\infty}\right)^{-0.5} \tag{3.31}$$

where ε is permittivity of medium which is exposed to electric field, and $c_{j\infty}$ is concentration of ion j far away from the surface. For a univalent-univalent salt in water at 25°C, $\lambda = 0.3 {c_{j\infty}}^{-0.5}$, where λ is in nm and the salt concentration is in mol/l. For instance, $\lambda = 3$nm for salt solution of 0.01M. For higher concentration, Debye length is so small that the system can be simplified back to Helmholtz double-layer model [26, p. 120].

In this thesis reaction zone in BP interface is treated as double-layer model. Figure 3.13 illustrates the double-layer model for describing reaction zone in BP interface. Due to the

[1]There are many theories on the location of water-splitting reaction inside of BP, but the position of neutralization reaction zone is under debate. It is not logical to exclude the possibility of anywhere in or near BP except BP interface, especially in BPAEM or in diffusional layer in base chamber due to the higher mobility of H^+.

[2] Counter-ion is any ion having the opposite charge as the other ions in surrounding electrolyte solution (or fixed ion of IEM).

aggressive neutralization reaction of H^+ and OH^- and slow mobility of Na^+ and Cl^- as shown in figure 3.13 (a), double layers have been created in which system has too many negative charges (Cl^-) on the left layer and too many positive charges (Na^+) on the right layer as shown in figure 3.13 (b). Therefore, electric potential on the right is higher than electric potential on the left, and it drives reaction direction more favor to the water-splitting side according to Second Wien Effect [15] [16] or/and accelerate the movement of Na^+ (from right to left in figure 3.13 (b)) and Cl^- (from left to right in figure 3.13 (b)). In other words, if mobility of Na^+ and Cl^- is zero, electrochemical equilibrium causes the system to oscillate between situation (a) and situation (b).

The electric potential in double layers is calculated according to Nernst equation (microscopically speaking, Gibbs free energy transforms into electric work only pushing ions to infinite far distance, see section 1.4.2):

$$EMF = EMF^0 - \frac{R \cdot T}{F} \ln\left(\frac{c^0_{H_3^+O} \cdot c^0_{OH^-}}{c_{H_3^+O} \cdot c_{OH^-}}\right) \quad \textbf{(3.32)}$$

where $c_{H_3^+O}$ and c_{OH^-} are the reagents of neutralization reaction in reaction zone.

In ideal condition where Na^+ and Cl^- cannot move, electrochemical equilibrium causes the system oscillating between situation (a) and situation (b), in other words, the forward and backward reaction rates are equal. However, due to the mobility of Na^+ and Cl^- (although very poor compared with H^+ and OH^- as listed in table 3.3), produced electric potential does not only push reaction to water-splitting side, but also accelerates the crossover of Na^+ and Cl^- through the reaction zone. The latter should not be excluded since the ratio of mobility of H^+ or OH^- to that of Na^+ or Cl^- is between 3 and 7. Moreover, the typical selectivity of commercial BP is around 90%, which means the other 10% is just lost due to crossover [13]. Therefore, this thesis dictates that 10% of neutralization reaction energy is wasted due to the crossover of ions through reaction zone in BP interface.

$$EMF_{real}^{Reaction\ Zone} = 90\% \cdot EMF_{theor.}^{Reaction\ Zone} \quad \textbf{(3.33)}$$

With the above further simplifications and treating bulk solutions as boundary conditions, the mathematical model has been built and simulated by MATLAB using Newton methods for nonlinear problems. Further details about this model can be found in Appendix B.

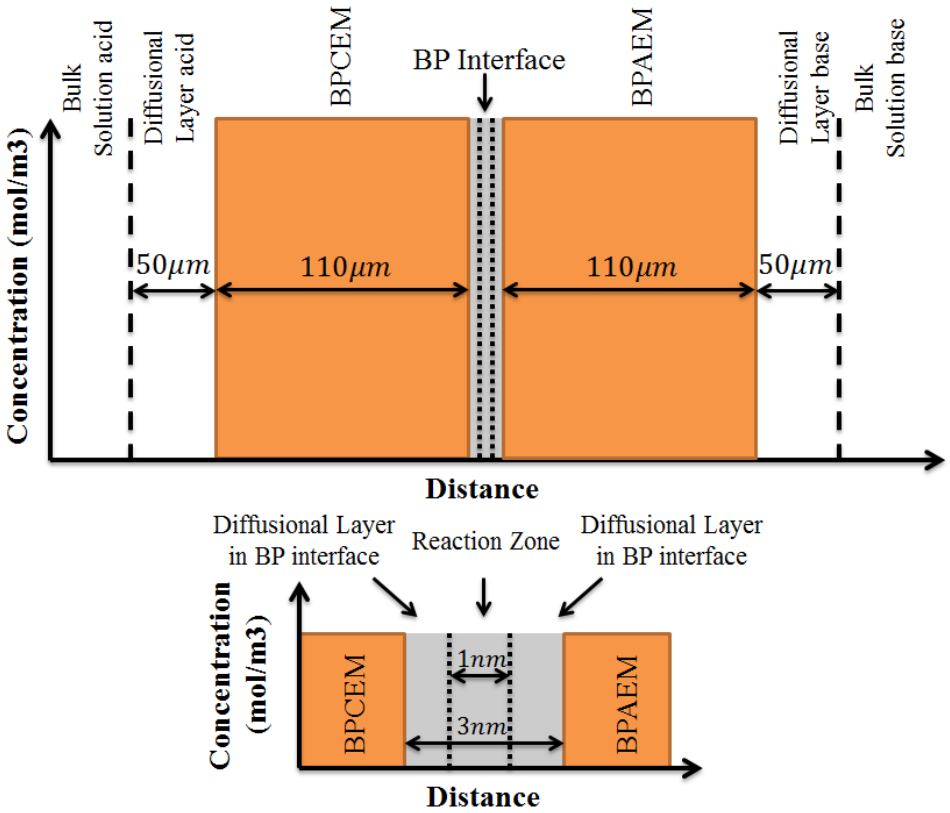

Figure 3.12: Schematic diagram of modelling of BP with two diffusional layers contacting bulk solutions, as well as one interface in the bipolar junction of the membrane where the anion and the cation permeable layers are in direct contact.

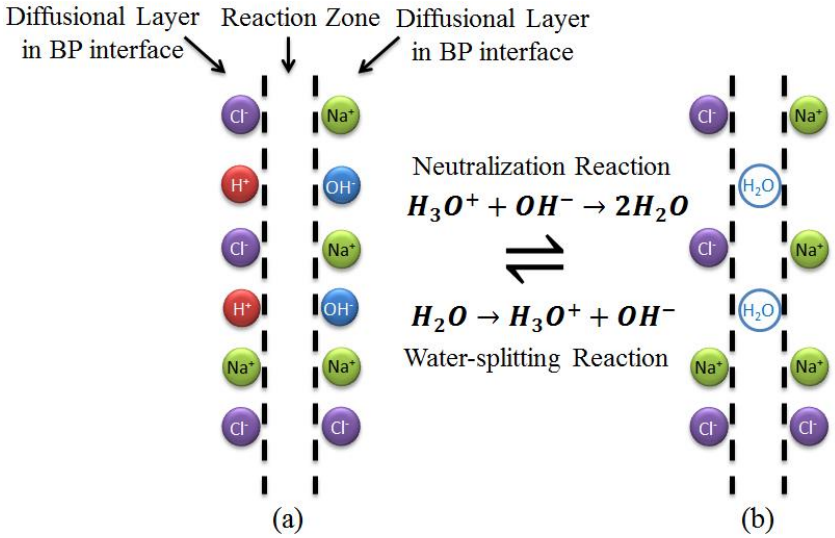

Figure 3.13: Schematic diagram of treating reaction zone as double-layer model. Due to the aggressive neutralization reaction and slow mobility of Na^+ and Cl^- as shown in (a), double layers have been created in which system has too many negative charges (Cl^-) on the left side layer and too many positive charges (Na^+) on the right side layer as shown in (b). Therefore, electric potential on the right is higher than electric potential on the left, and it drives reaction direction more favorably to the water-splitting side. If mobility of Na^+ and Cl^- is zero, electrochemical equilibrium causes the system to oscillate between situation (a) and situation (b).

Table 3.3: Mobility of different ions in AEM, CEM and electrolyte solution [35].

	In AEM	**In CEM**	**In Solution**	
u_{Na+}	$0.25\cdot10^{-8}$	$0.25\cdot10^{-8}$	$5.19\cdot10^{-8}$	$[m^2/(V\cdot s)]$
u_{Cl-}	$0.15\cdot10^{-8}$	$0.15\cdot10^{-8}$	$7.91\cdot10^{-8}$	$[m^2/(V\cdot s)]$
u_{H+}	$3.63\cdot10^{-8}$	$3.63\cdot10^{-8}$	$36.3\cdot10^{-8}$	$[m^2/(V\cdot s)]$
u_{OH-}	$2.04\cdot10^{-8}$	$2.04\cdot10^{-8}$	$20.4\cdot10^{-8}$	$[m^2/(V\cdot s)]$

3.4.3 Concentration and Electric Potential Profiles of Bipolar Membrane

Figure 3.14 shows the ionic concentration profiles and electric potential profile of BP with 1M acid and base solution by open circuit at 25°C 0.1MPa. As with CEM and AEM there is a 50μm thick diffusional layer between BP and bulk solution. In the following three main aspects are being discussed: ionic transport, ionic distribution and electric potential.

Ionic Transport

Figure 3.14 is by open circuit, but due to the non-ideal permselectivity of BP, Na^+ and Cl^- will travel across the membrane. This, although very small amount, will shift reaction equilibrium to neutralization reaction side, which ultimately causes transport and consumption of H^+ and OH^-. Because of conservation of ions and electroneutrality, there is no accumulation or annihilation of any charge anywhere, so by open circuit:

$$F\sum z_j J_j^{total} = 0 \tag{3.34}$$

On the left side of reaction zone:

$$J_{Na+}^{total} - J_{Cl-}^{total} + J_{H+}^{total} = 0 \tag{3.33}$$

On the right side of reaction zone:

$$J_{Na+}^{total} - J_{Cl-}^{total} - J_{OH-}^{total} = 0 \tag{3.35}$$

Accumulation of salt inside of BP is huge, especially near BP interface. This does not have much influence on the Donnan potential inside of BP interface, but will enhance the possibility of wasting more neutralization reaction energy to push Na^+ and Cl^- across reaction zone.

One of the interesting phenomena is that transport of Na^+ is relatively higher than that of Cl^- which is contrary to the common sense that the mobility of Na^+ is smaller than that of Cl^- in solution according to table 3.3. That phenomenon cannot be simply explained since it is the consequence of many interactions. One possible explanation is that the transport of H^+ is so

good in BPCEM (compared with OH^- in BPAEM) that electroneutrality has to be rebalanced by more Na^+ transport.

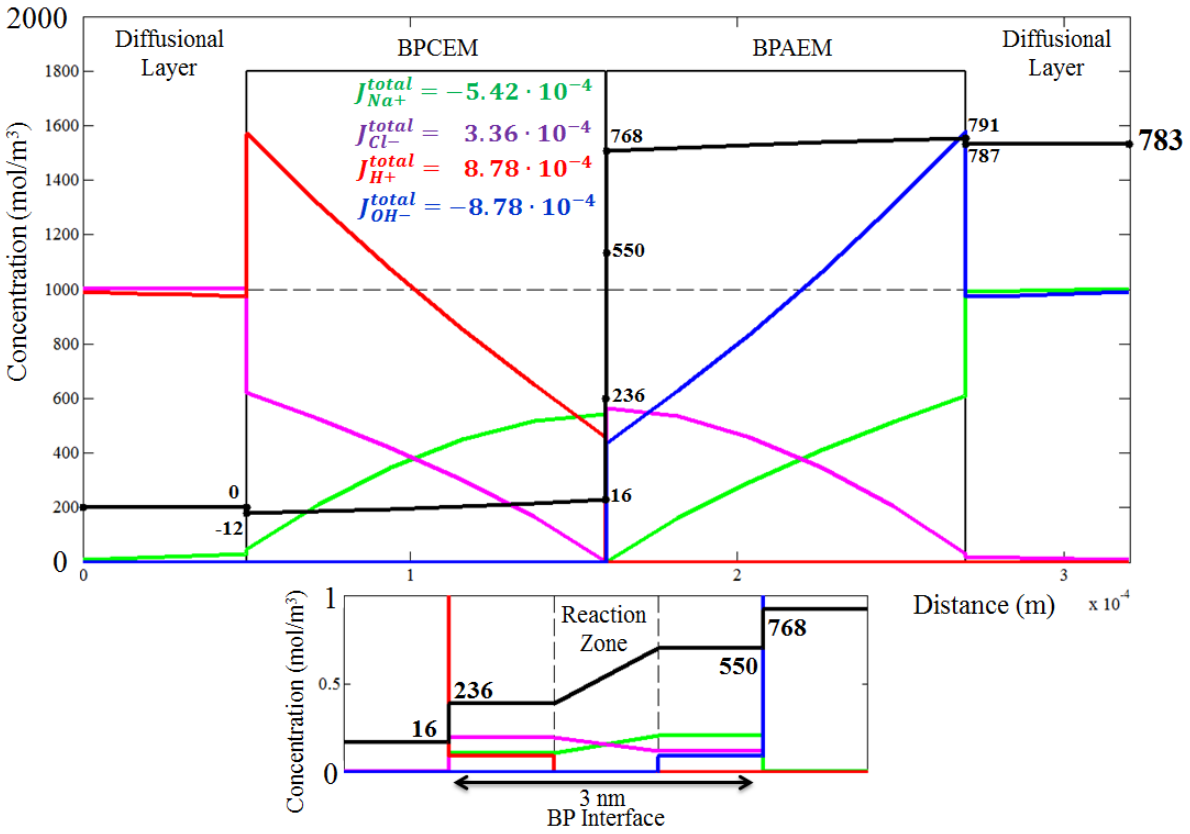

Figure 3.14: Simulated profiles of ionic concentrations and electric potential of BP with 1M acid and base solution both of which have 1% NaCl as impurities by open circuit at 25°C 0.1MPa. The lines with green, purple, red and blue colors are the profiles of Na^+, Cl^-, H^+ and OH^-, respectively. The black line is the profile of electric potential with the unit of [mV]. The dashed line is the fixed ion concentration in BPCEM and BPAEM. Each ionic transport has been labeled on the diagram with the unit of [mol/(m^2s)]. Positive direction is from left to right.

Ionic Distribution

Due to the crossover of Na^+ and Cl^-, concentration of H^+ or OH^- in IEM near BP interface is lower than that of Na^+ and Cl^-.

If conservation equation is applied to H^+:

$$\frac{\partial c_{H+}}{\partial t} = -\nabla \cdot \vec{J}_{H+}^{total} + r_{H+}^{V} = 0 \qquad \textbf{(3.36)}$$

then:

$$\nabla \cdot \vec{J}_{H+}^{total} = r_{H+}^{V} = -k_{NR} c_{H+} c_{OH-} \qquad \textbf{(3.37)}$$

where k_{NR} is reaction speed constant of neutralization reaction, which is equal to $1.1 \cdot 10^8$ [$m^3mol^{-1}s^{-1}$] [11], and water-splitting reaction is neglected since its reaction speed constant is too small ($3.63 \cdot 10^{-10}$ [$m^3mol^{-1}s^{-1}$])

and it is same to OH^-:

$$\nabla \cdot \vec{j}_{OH-}^{total} = r_{OH-}^{V} = -k_{NR} c_{H+} c_{OH-} \quad \textbf{(3.38)}$$

Electric Potential

There are three main electric potential changes inside of BP:

(1) Donnan potential, especially inside of BP interface where a sudden change of concentration of H^+ or OH^- is.

(2) Electric potential inside of reaction zone due to the electrochemical equilibrium.

(3) Diffusion potential across IEM due to higher mobility of H^+ or OH^- compared with Na^+ or Cl^-.

The electric potentials inside of BP interface determines the main changes of the overall voltage. In the following section, the most important influential parameters will be under investigation, especially on how they influence the electric potential inside of BP interface.

3.4.4 Influential Parameters

Electric Current Density

Figure 3.15 is a series of discharging profiles of BP with 1M acid/base at 25°C 0.1MPa. Please note that the direction of discharging current is from left to right, and its value is negative[1]. With increasing discharging current density, the electric potential decreases. The main decrease is due to decreasing Donnan potentials inside of BP interface. That is because the increasing current density increases the concentration of reactant (H^+ and OH^-) inside of reaction double-layer[2]. Higher current density causes the problem of OH^- transport. OH^- starts to deplete near BP interface more significantly than H^+.

[1] In this thesis, discharging current is defined as negative, while charging current is positive.
[2] Since current density is proportional to neutralization reaction speed. The higher the current density, the higher the reaction speed will be. This will increase the consumption of H^+ and OH^-, which increases their concentration inside of reaction double-layer.

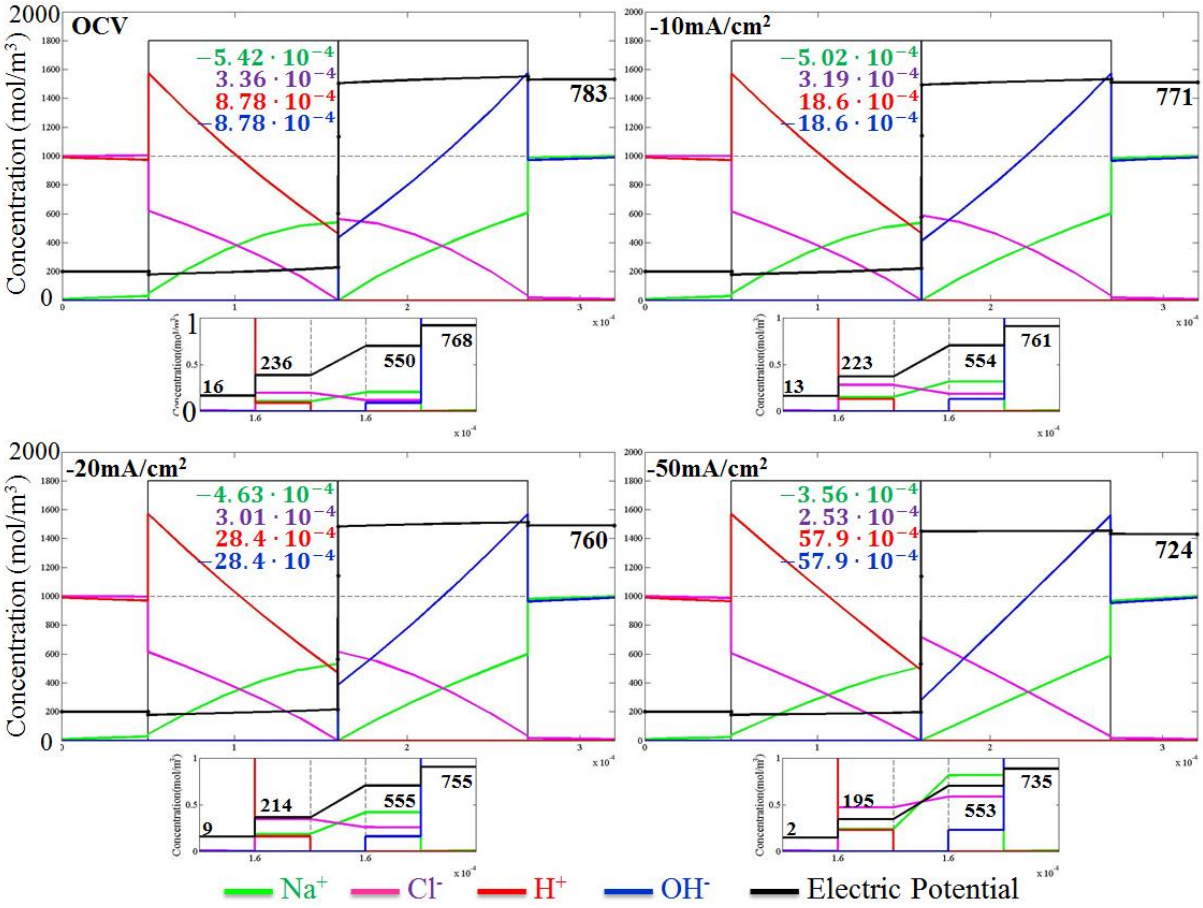

Figure 3.15: Concentration and electric potential profiles of BP with 1M HCl and NaOH solution both of which have 1% NaCl as impurities with increasing discharging current density at 25°C 0.1MPa. The lines with green, purple, red and blue colors are the profiles of Na^+, Cl^-, H^+ and OH^-, respectively. The black line is the profile of electric potential with the unit of [mV]. The dashed line is the fixed ion concentration in BPCEM and BPAEM. Each ionic transport has been labeled on the diagram with the unit of [mol/(m^2s)]. The direction of discharging current density is from left to right.

Higher current density decreases crossover effect of Na^+ or Cl^- since its transport can be treated as leakage electric current flowing in the opposite direction of discharging current. Unlike CEM/AEM whose main electric potential loss is due to its poor conductivity, BP shows a very high conductivity, which leads to very small electric potential losses across membrane, which further means the function of BP in the application of REDBP is a reactor, not for separation purpose like traditional IEMs.

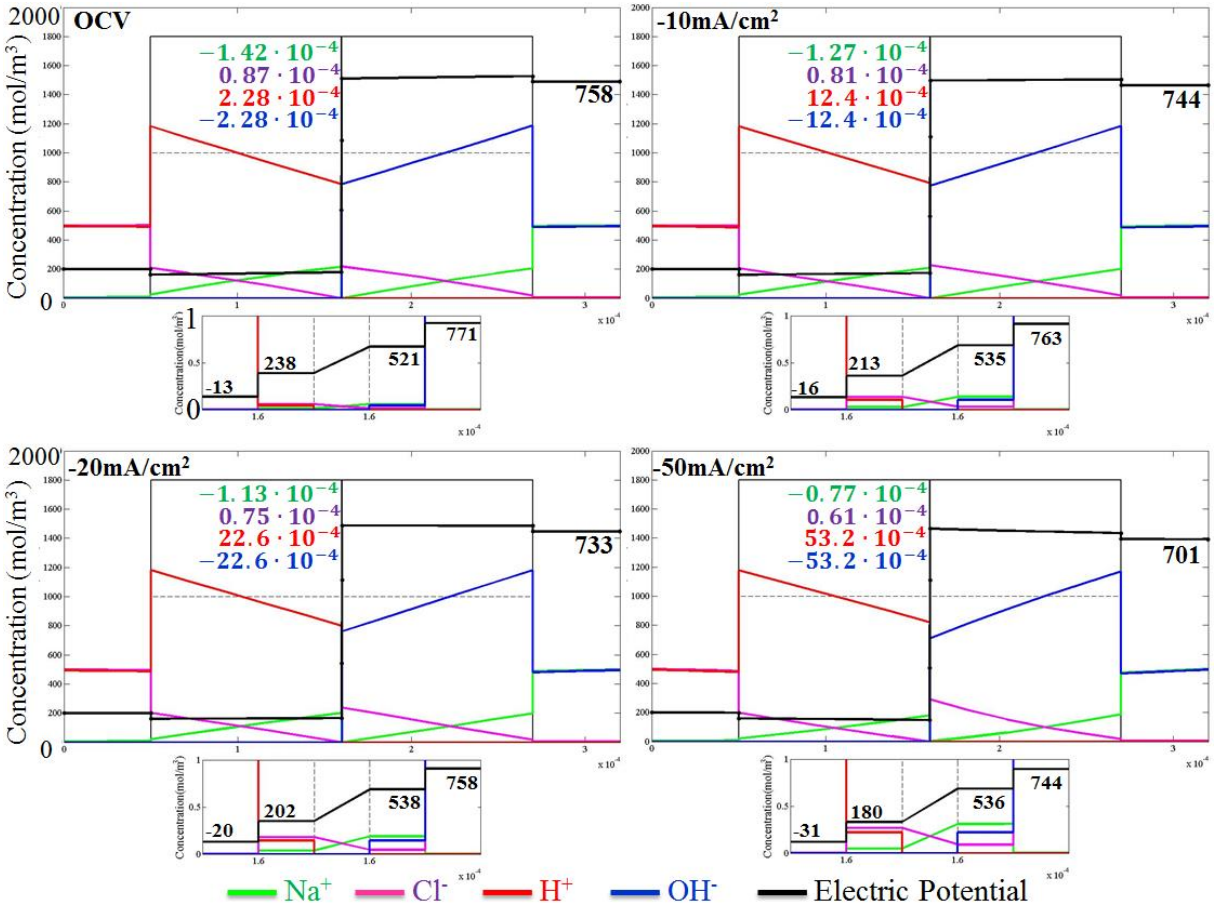

Figure 3.16: Concentration and electric potential profiles of BP with 0.5M HCl and NaOH solution both of which have 1% NaCl as impurities by discharging at 25°C 0.1MPa. The lines with green, purple, red and blue colors are the profiles of Na^+, Cl^-, H^+ and OH^-, respectively. The black line is the profile of electric potential with the unit of [mV]. The dashed line is the fixed ion concentration in BPCEM and BPAEM. Each ionic transport has been labeled on the diagram with the unit of [mol/(m^2s)]. The direction of discharging current density is from left to right.

Acid/Base Concentration

Figure 3.16 is a series of discharging profiles of BP with 0.5M acid/base at 25°C 0.1MPa. Compared with figure 3.15, 0.5M has less crossovers and less significant accumulation of salt at BP interface, indicating acid/base concentration has direct influence on the two. Especially lower concentration of salt inside of BP will consume less neutralization reaction energy for transport Na^+ and Cl^- through reaction zone. With current, 0.5M has higher ionic resistance in BPAEM compared with 1M due to the fact of lower concentration of electric current carrier.

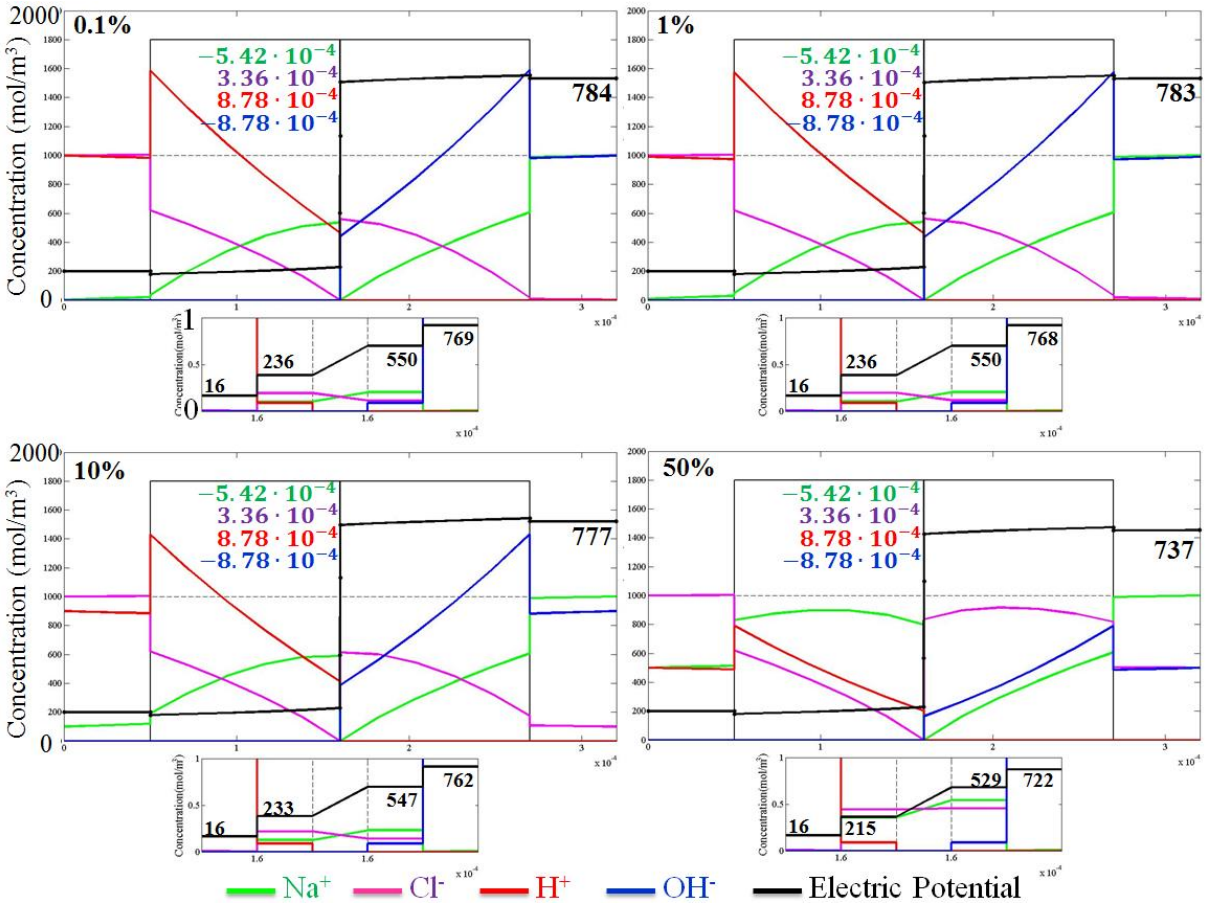

Figure 3.17: Simulated profiles of ionic concentrations and electric potential of BP with 1M acid and base solution by open circuit at 25°C 0.1MPa with increasing concentration of impurities. The lines with green, purple, red and blue colors are the profiles of Na^+, Cl^-, H^+ and OH^-, respectively. The black line is the profile of electric potential with the unit of [mV]. The dashed line is the fixed ion concentration in BPCEM and BPAEM. Each ionic transport has been labeled on the diagram with the unit of [mol/(m^2s)]. Positive direction is from left to right.

Impurity Concentration

Since the accumulation of salt inside of BP interface is so significant with 1M solution, the most immediate and obvious approach is to investigate the influence of impurities inside of solution. Impurity is defined as the salt content in acid/base solution, described as percentage, meaning how many percent of positive ion is Na^+ in HCl solution and how many percent of negative ion is Cl^- in NaOH solution. For example, Figure 3.14 shows the 1M acid and base solution with 1% impurities, which means in HCl solution there are 1mol/l Cl^-, 0.99mol/l H^+ and 0.01mol/l Na^+. And NaOH solution contains 1mol/l Na^+, 0.99mol/l OH^- and 0.01mol/l Cl^-.

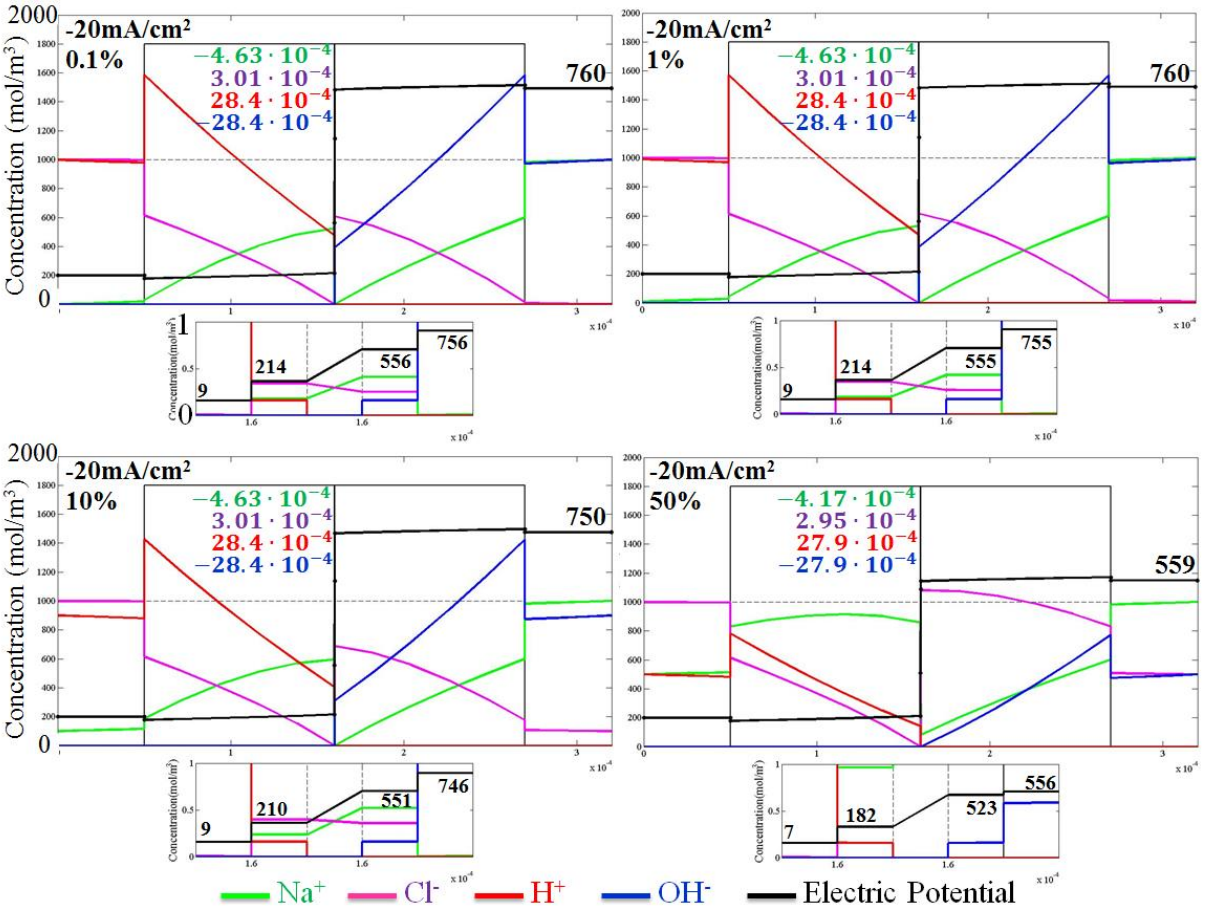

Figure 3.18: Simulated profiles of ionic concentrations and electric potential of BP with 1M acid and base solution with discharging current 20mA/cm^2 at 25°C 0.1MPa with increasing concentration of impurities. The lines with green, purple, red and blue colors are the profiles of Na^+, Cl^-, H^+ and OH^-, respectively. The black line is the profile of electric potential with the unit of [mV]. The dashed line is the fixed ion concentration in BPCEM and BPAEM. Each ionic transport has been labeled on the diagram with the unit of [mol/(m^{2}s)]. Positive direction is from left to right.

Figure 3.17 illustrates the profiles of BP by open circuit with changing impurities´ concentration. The most surprising finding is the constant crossovers with changing impurities´ concentration, indicating the crossover effect depends only on the concentration of Cl^- in HCl solution and that of Na^+ in NaOH solution. With increasing salt concentration the accumulations of salt inside of BP interface and in IEM near BP interface are more significant - especially the latter lowers the concentration of H^+ and OH^- as counter-ions in IEM which ultimately lowers the Donnan potential inside of BP interface.

Figure 3.18 illustrates profiles of BP at 20mA/cm^2 with changing impurities´ concentration. From 0.1% to 10%, the impurities´ concentration has little influence on the performance of BP, implying the quality of acid or base solution can be reduced. However, too high impurities´

concentration lowers the concentration of H^+ and OH^- too significantly inside of BP, which ultimately lowers the Donnan potential inside of BP interface, thus it needs to be avoided.

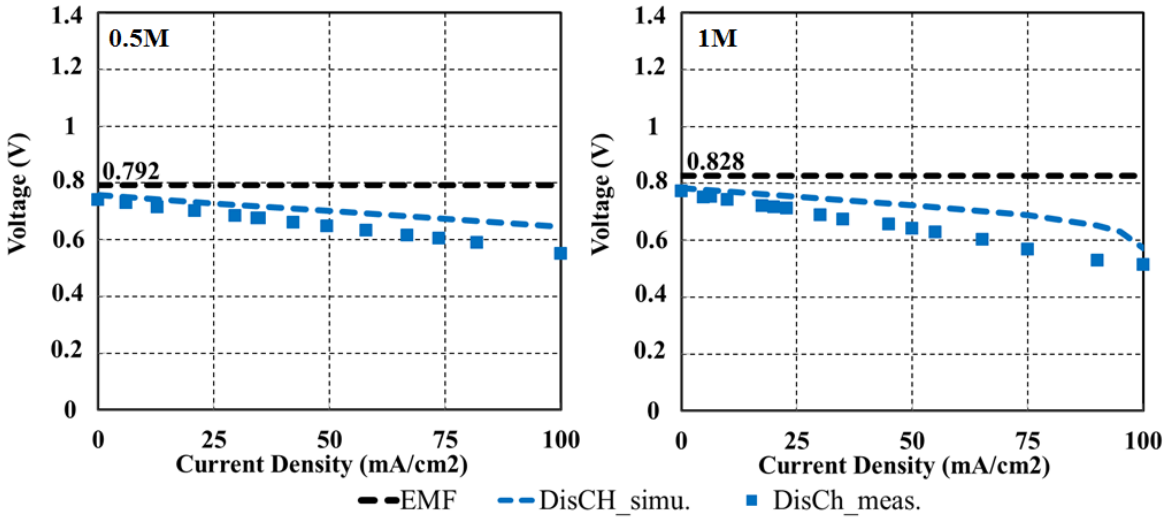

Figure 3.19: Comparison between measurement and simulation results of BP by discharging between 0.5M (left diagram) and 1M (right diagram) acid/base solution with 1% impurities at 25°C 0.1MPa.

3.4.5 Comparison with Experiment

Figure 3.19 shows the comparison between measurement and simulation results of BP between 0.5M (left diagram) and 1M (right diagram) acid and base solutions at 25°C 0.1MPa by discharging. EMF has been labeled as well. At OCV measurement and simulation results match each other, indicating the assumption of 10% neutralization reaction energy wasting on transport of Na^+ and Cl^- in section 3.4.2 is suitable. With increasing current density, the simulation results deviate from the measurement. This is mainly due to the produced water molecules influencing both activity and mobility of ions. The huge deviation between measurement and simulation in case of 1M solution is also a consequence of non-ideal measuring method[1] due to the polarization effect between measuring point and BP leading to a much higher ionic resistance in that region and accumulation of water molecule inside of BP. With 1M solution, if current density is higher than 95mA/cm^2, the simulated overall voltage will drop dramatically. That is because the concentration of OH^- near and in BP interface is so low that Donnan potential due to OH^- inside of BP interface is almost zero (similar to the problem of figure 3.18, the fourth diagram). It may be due to the limitation of fixed reaction zone model.

[1] Data is being required by voltage measurement excluding IR-drop. Due to polarization effect, the real IR-drop is higher than the resistance of bulk solution. Therefore, the real discharging voltage between BP with 1M solution should be higher than in the diagram (for details please check section 2.3.3).

3.5 Conclusion

The purpose of this chapter is to use mathematical method to investigate phenomenon inside of IEM, such as ionic distribution, ionic transport, and electric potential distribution, which are of great interest but cannot be measured at the moment. Therefore, almost all simulation results have been displayed as profiles in diagram to illustrate what is happening inside of IEM.

There are many assumptions and simplifications during the construction of mathematical model for CEM/AEM, and especially for BP, in which fixed reaction zone treated as double-layer model inside of BP interface is being dictated. Although simple and rough, the simulation results compared with experiments are quite logical, especially the results of BP modeling, some of which are very interesting and are listed below.

(1) The first impression of BP is high resistance due to its double membrane layers. However, simulation results show the function of BP in the application of REDBP is rather a reactor, a place where neutralization reaction takes place, not a traditional IEM mainly for separating two chambers or electrodes.

(2) The main decrease of electric potential inside of BP is the decreasing Donnan potentials inside of BP interface due to either salt accumulation inside of BP interface, or higher reagent concentration with higher current density, or both.

(3) Salt accumulation near or in BP interface is significant. In the case of 1M solution, Na^+ or Cl^- near BP interface is the main counter-ion.

(4) Crossover depends only on concentration of Cl^- in HCl solution and concentration of Na^+ in NaOH solution.

(5) If transport of OH^- in BPAEM is well handled, the quality of acid or base solution can be dramatically reduced (figure 3.18).

(6) Due to relatively poor mobility of OH^- in BPAEM, OH^- starts to deplete earlier than H^+.

This model has plenty of room for improvement:

i. Water transport, which is very crucial in REDBP, has not been considered in this thesis. Considering water transport will automatically introduce convection term in ionic transport (section 3.1.5), add osmotic pressure at the interface between IEM and electrolyte solution (especially between BP interface and BP), influence ionic

activity inside of BP, especially inside of BP interface, and ultimately change overall voltage between BP.

ii. Changing thickness of BP interface is one of several consequences of considering water transport.

iii. The real position of neutralization reaction zone.

iv. Improvement of double-layer model for reaction zone, adding water-splitting reaction and transport of salt for calculating the real electrochemical equilibrium.

v. Changing boundary conditions (solution properties) to achieve 2D simulation in order to investigate whether or not the performance of BP is homogeneously distributed from entrance to the exit inside of one solution chamber.

vi. Replace local electroneutrality with global electroneutrality.

vii. Eventually find a more microscopic approach to describe BP interface. After all, the size of water molecule is typically 0.26 nm, the sizes of ion with hydration shell are all bigger than 0.6 nm. It seems 3nm, as the assumed thickness of BP interface in this thesis, is not good environment for using local electroneutrality (section 3.1.1), ideal mixture (section 3.1.2) and Donnan distribution (section 3.1.4) as assumptions.

Those are the main advices for the improvement of modeling and simulation of REDBP single cell.

Chapter 4

Experiments of Stack

In section 2 the performance of single cell has been investigated. The application field for REDBP as energy storage is Megawatt (as grid support and load shifting) or even Gigawatt (as bulk storage), thus many single cells have to be mounted together as a stack. The questions are:

(1) Is there any additional loss during mounting process?
(2) What is the overall performance of stack?
(3) What is the performance of each single cell inside of stack?
(4) How significant is the loss due to electrode chambers?
(5) Which parameters influence the performance of stack significantly?

With the above concerns the stack experiments are conducted, and this section will address all the questions above. Initially, the stack layout, characterization methods as well as test facility will be introduced.

4.1 Stack Layout and Characterization Methods

4.1.1 Cell Frame

All the cell frames for stack experiment are from DEUKUM[1]. There are many different kinds of cell frames depending on applications. The chosen cell frame is the most common one in the laboratory for testing electro membranes as shown in figure 4.1. The properties of this cell frame are listed in the table 4.1. The active surface of this cell frame is not a strictly square. It loses 4 corners which 'shrinks' its real actual surface. To simplify experiment procedure, the active surface of testing cell is assumed to be 100cm^2.

Table 4.1: Properties of cell frame in stack experiment

Thickness	Material for Sealings and Frame	Material for Spacers	Active Surface	Diameters for Electrolyte Channels
0.5mm	Thermoplastic Olefin	Polyethylen	92.1425cm^2	0.85mm

[1] http://www.deukum.de/

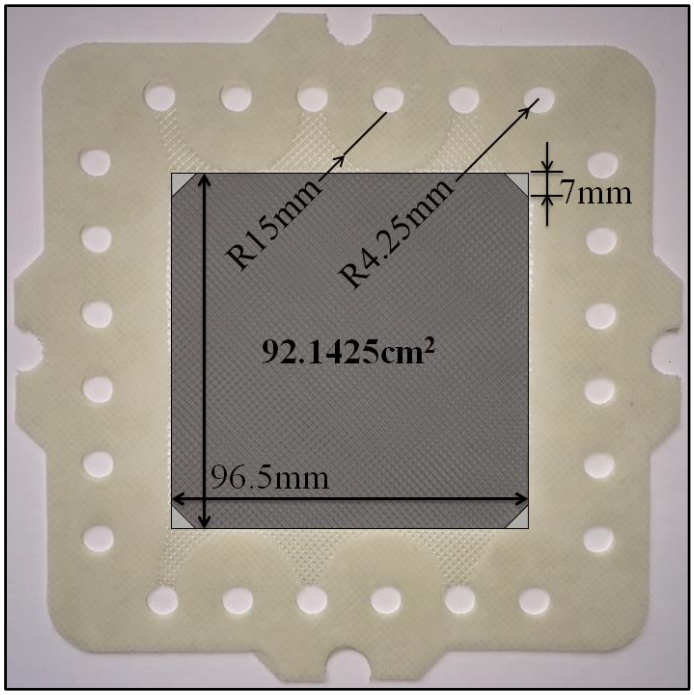

Figure 4.1: Cell frame in stack experiment.

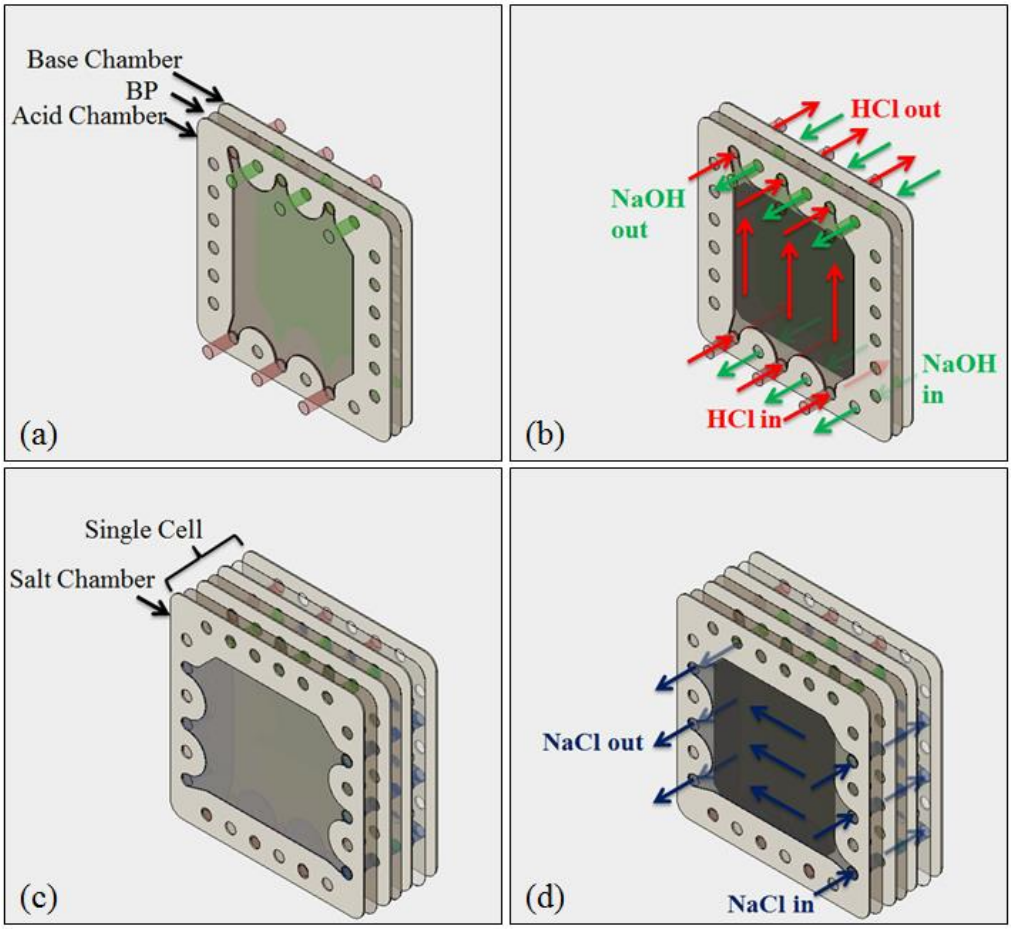

Figure 4.2: Layout of (a) bipolar membrane between acid and base chambers, (b) the flow direction of acid and base in solution chambers, (c) the single cell, and (d) the flow direction of salt solution in solution chamber. The dark area is active surface.

4.1.2 Building-Up Single Cell of REDBP

By correctly putting 3 IEMs and 3 cell frames together, the single cell of REDBP will be built up as shown in figure 4.2. The flow direction of acid and base in solution chamber is always from bottom to top. The dark area is the active surface.

4.1.3 Mounting REDBP Stack with Electrode Chambers

By correctly mounting up many single cells as well as two electrode chambers at both ends, the proper stack will be mounted. Figure 4.3 shows an example of 5 cells stack. There are two major types of electrolyte transport through the stack, parallel flow and series flow. Figure 4.4 illustrates these two flow types. It is obvious that parallel flow (figure 4.4 (a)) requires less energy to pump the electrolyte solution than with series flow (figure4.4 (b)). In this thesis for stack experiment, the flow of electrolyte solution through stack is always parallel flow.

Table 4.2: Possible necessary electrochemical reactions in electrode chambers.

Ch/ DisCH	Position of Stack in figure 4.3	Polarity for Stack	Definition in Electrochemical Cell.	Electrochemical Reaction In Electrode Chamber	Standard Potential vs SHE at 25°C
DisCh	Left Electrode	Negative Electrode	Cathode	$e^- + H_2O \rightarrow OH^- + \frac{1}{2}H_2 \uparrow$	$-0.8277V$
	Right Electrode	Positive Electrode	Anode	$\frac{1}{2}H_2O \rightarrow H^+ + \frac{1}{4}O_2 \uparrow + e^-$	$-1.229V$
Ch	Left Electrode	Negative Electrode	Anode	$\frac{1}{2}H_2O \rightarrow H^+ + \frac{1}{4}O_2 \uparrow + e^-$	$-1.229V$
	Right Electrode	Positive Electrode	Cathode	$e^- + H_2O \rightarrow OH^- + \frac{1}{2}H_2 \uparrow$	$-0.8277V$

The electrode chambers are important for transforming ionic transport to electron transport. As previously introduced (section 3.1.3), because of neutralization reaction and electroneutrality, inside of stack there exists a very good electric current formed by ionic transports. Ionic transport cannot be utilized directly by mankind as electric power which is considered as the backbone of modern industrial society. That is the reason why at both ends of REDBP stack two electrode chambers are needed, and form the negative and positive electrode of REDBP stack. Inside of electrode chamber the electrochemical reactions take place.

If side reactions are neglected, the possible electrochemical reactions in both electrode chambers by charging and discharging are listed in table 4.2 and are illustrated in figure 4.5 and 4.6.

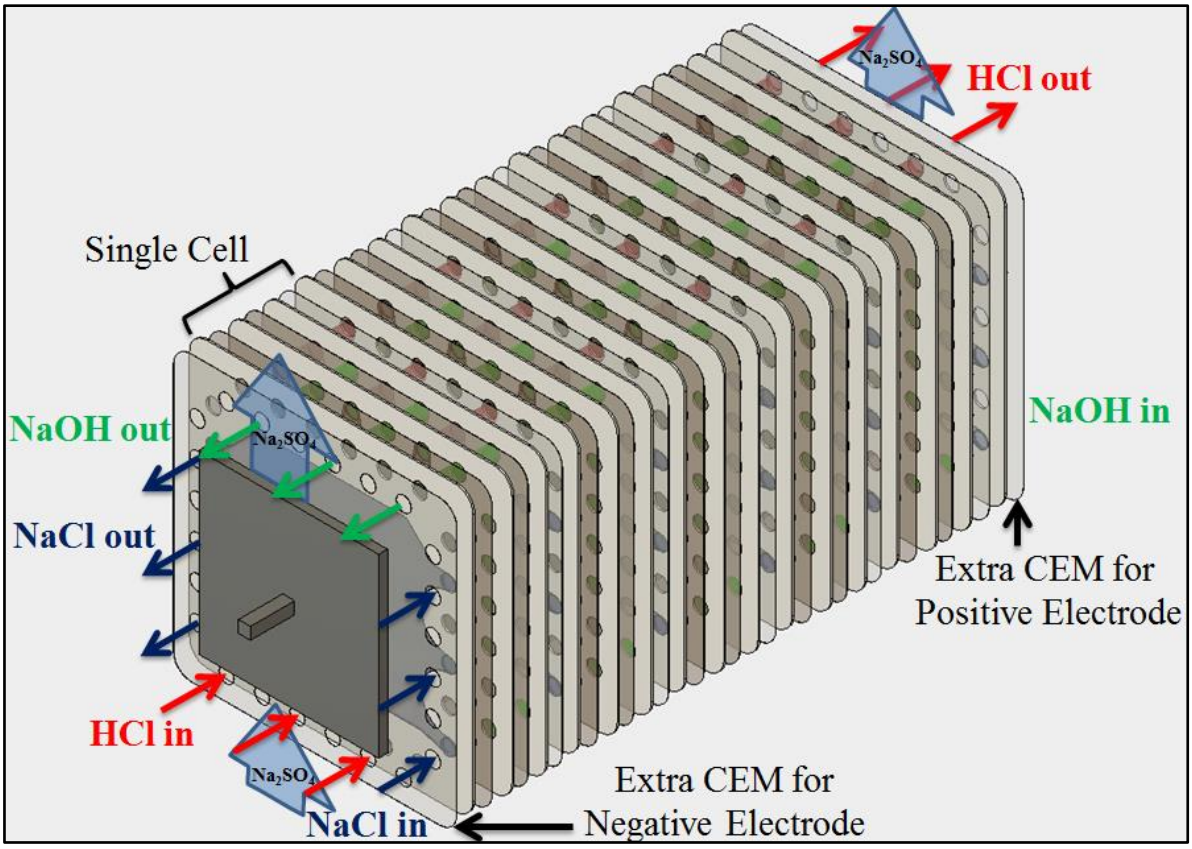

Figure 4.3: 5 cells stack.

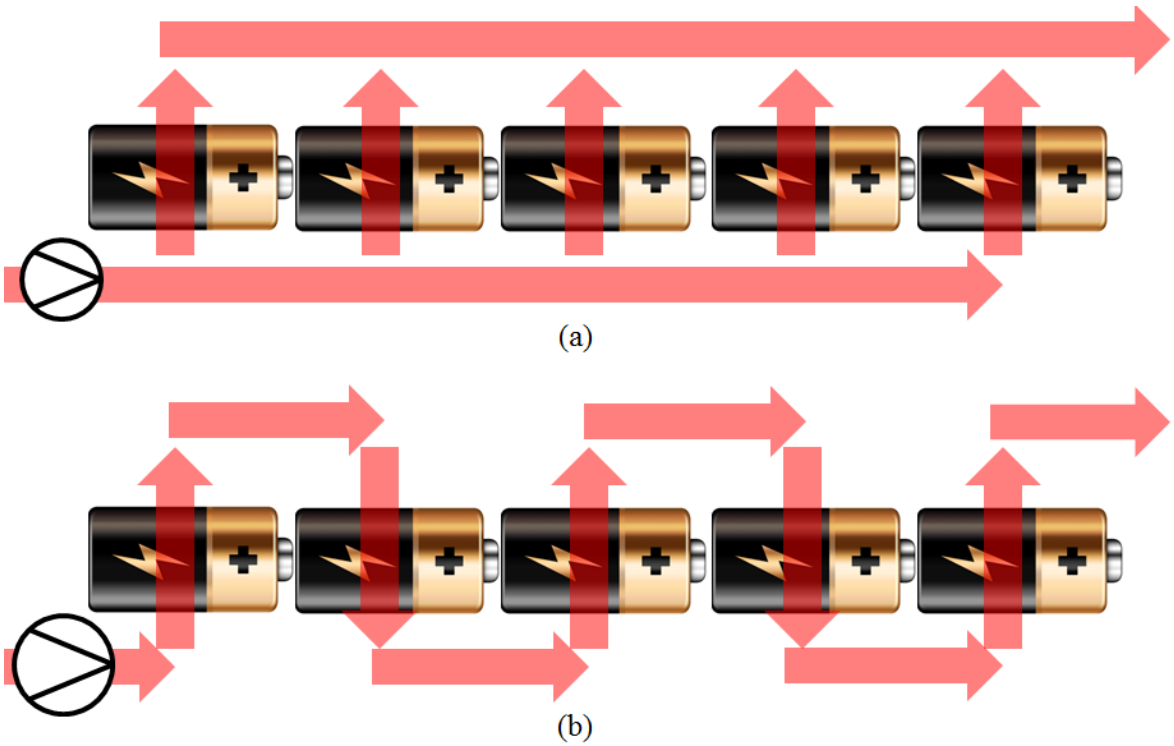

Figure 4.4: Schematic diagram of parallel flow (a) and series flow (b) of electrolyte solution.

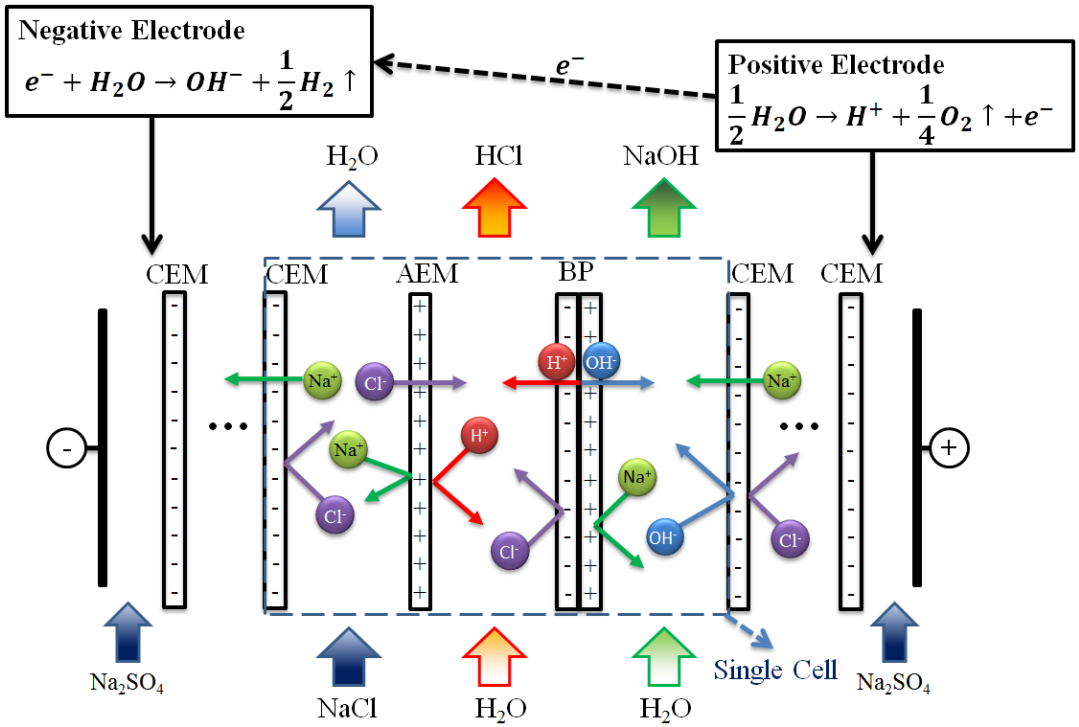

Figure 4.5: Charging (EDBP) with electrochemical reactions in electrode chambers.

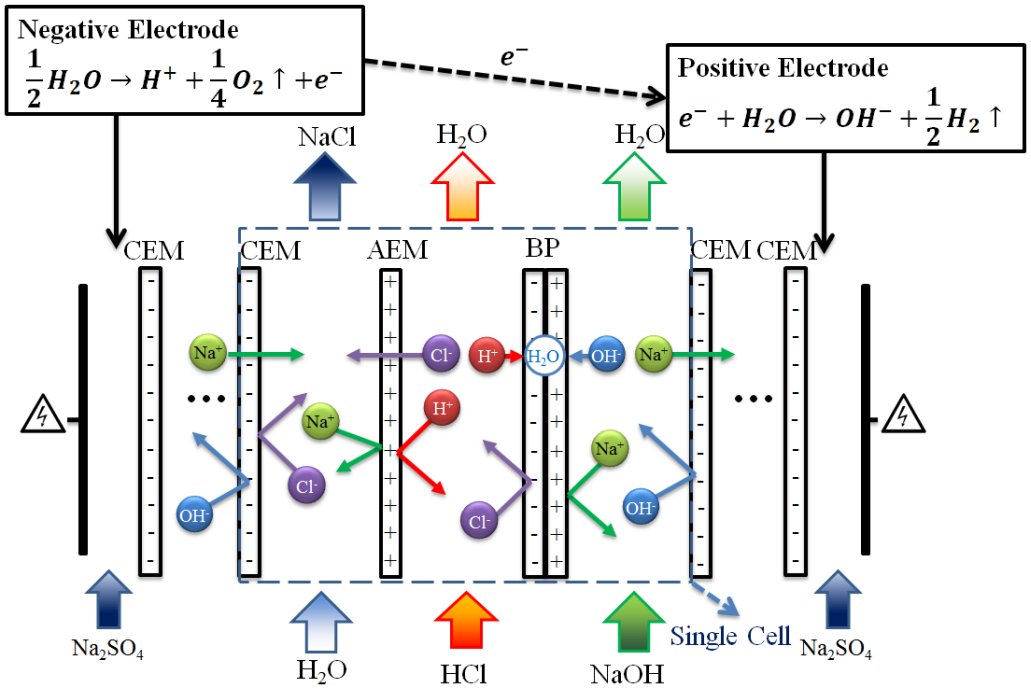

Figure 4.6: Discharging (REDBP) with electrochemical reactions in electrode chambers.

The standard potentials of all the reactions in table 4.2 are negative, meaning consume additional energy. Because of that, the electric potential between electrodes (V_{stack}) is less than the sum of all single cells (shorted for AllSCs, V_{AllSCs}) as shown in figure 4.7. The potential difference between V_{AllSCs} and V_{stack} at standard condition is 2.0567V. According to single cell experiment, OCV, the maximum electric potential by discharging process, with 1M solution is only 0.764V. This means at least three single cells are needed only to power electrode chambers

by discharging process at standard condition, not mentioning increasing current density increases loss of electrode chambers and decreases single cell voltage. Figure 4.8 shows an example of the significance of electrode chambers on the stack voltage by assuming the voltage of single cell is constant at 0.764V, and the loss of electrode chamber is always 2.0567V. If the loss of electrode chamber remains constant with increasing stack size (how many single cells are in one stack), bigger stack has less influence from electrode loss. From this perspective, REDBP makes sense only with big stack. For instance, as big as 100 cells at standard condition, the efficiency loss due to electrode chamber is only 2.7%, theoretically.

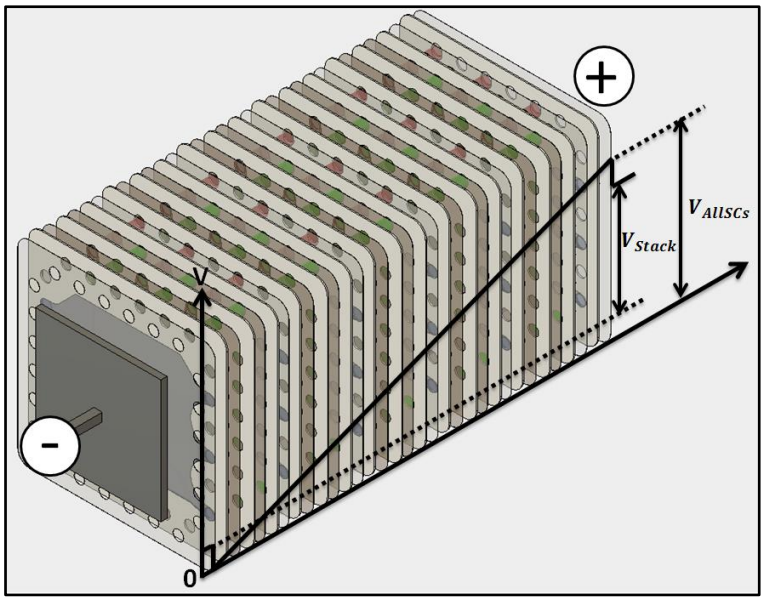

Figure 4.7: Schematic diagram of electric potential distribution throughout REDBP stack. Due to additional energy consumption in electrode chambers, the total stack electric potential V_{stack} is smaller than the sum of all single cells V_{AllSCs}

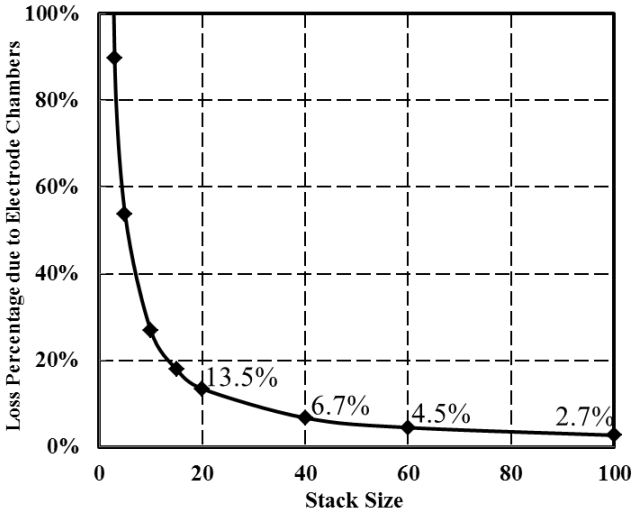

Figure 4.8: Loss percentage of stack due to electrode chambers only, by assuming the voltage of single cell is constant at 0.764V, and the loss of electrode chamber is always 2.0567V.

4.1.4 Pt Wires

Energy loss in electrode chamber is not a problem, if single cells can be mounted to build up a big stack. The question is whether additional losses exist during this mounting process. In order to answer this question, the detail performance of single cells inside of stack needs to be investigated. The most direct and effective way is to investigate voltage distribution through the stack with changing concentration of acid and base and changing electric current density.

By considering both accuracy and precision, the introduction of thin Pt wire (Ø0.2mm) with electrical and liquid insulation (in total Ø1mm) in acid chamber is used for acquiring electric potential at given position inside of stack. The following points are important for voltage measurement with Pt wires inside of stack.

(1) In order to pinpoint the desired measuring position, Pt wires must be coated with electrical insulation and leave a small tip (1mm long) attaching the measuring point.
(2) Measuring points should be at the center of active surface, especially have to avoid the active surface near inlet and outlet of solution chamber (section 4.2.3 and section 5.3.1). In order to acquire a one-dimensional analysis of voltage distribution throughout the stack (section 4.2.4), it is recommended the measuring points should be in one straight line throughout the stack.
(3) Pt wires must be sandwiched by two flat sealings to prevent leakage, and should avoid blocking electrolyte solution channels.
(4) The space between Pt wire and electrical insulation must be filled up by liquid plastic which will be further dried out to prevent electrolyte solution leakage through it.
(5) Pt wires must be very thin to limit the influences from measurement method itself. For example, introducing thick Pt wire will significantly enlarge the thickness of solution chamber which changes the internal resistance of testing single cell (section 4.2.3 and section 5.4.6).
(6) Change in the thickness of testing chamber is inevitable when introducing Pt wire. Therefore, proper spacers have to fill up the extra space.
(7) In order to acquire an accurate and reliable voltage, the electric potentials at the interface between different Pt wires and their surrounding solution must be equal (section 2.2.1), meaning $\Delta\varphi_{Pt1|Solution1} + \Delta\varphi_{Solution2|Pt2} = 0$. That can be only achieved by measuring the same electrolyte solution under the same conditions.

(8) For precise measurement, the IR-drop (section 2.2.1) must be constant and known, or can be neglected. The former is not achievable by introducing very thin Pt wire due to its softness. It must be done by measuring acid chamber because of its low resistivity.

Strict usage of Pt wires alone cannot guarantee a reliable result. In order to eliminate other influencing factors, the working condition of stack experiment must be carefully adjusted:

(1) Flowrate of electrolyte must be high enough to eliminate influences due to flow patterns of electrolyte solution alongside the solution chamber, and capacity changes (ionic concentration changes) due to neutralization reaction or water-splitting reaction.
(2) Before each experiment a warm-up process must be proceed to activate IEMs and to reach a constant temperature.

If all the above requirements are fulfilled, the actual test can be conducted.

4.1.5 Characterization Methods

Figure 4.9 shows an example of the arrangement of 4 Pt wires inside of 5 cells stack for measuring V_{SC}, V_{2SCs} and V_{4SCs}. All the measuring positions of Pt wires are pointed at the center of active surface.

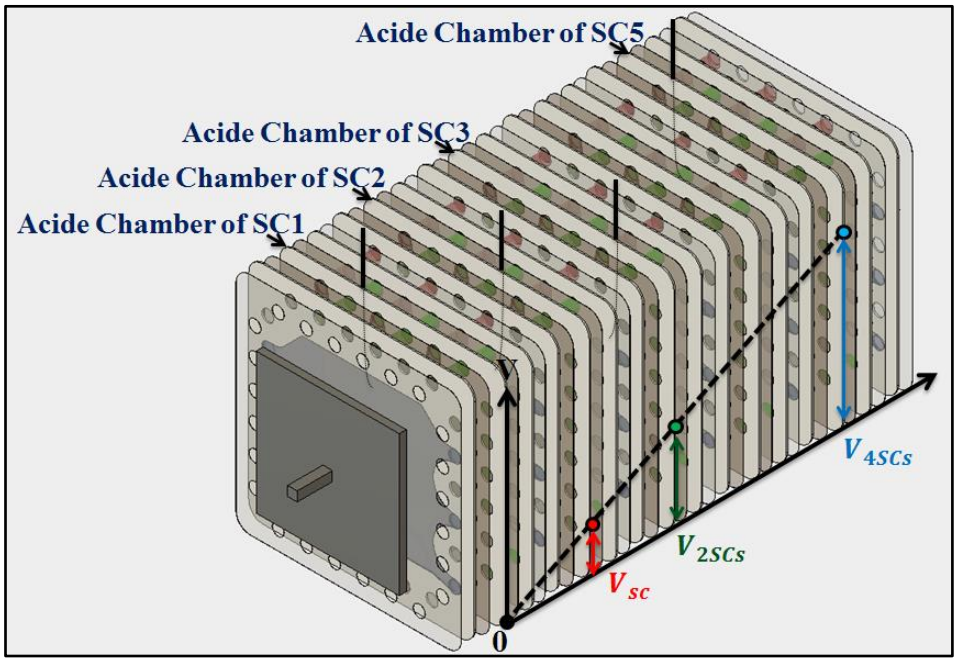

Figure 4.9: 4 Pt wires arrangement inside of 5 cells stack.

If assuming the single cell near negative electrode and single cell near positive electrode are identical (which is proven to be true by experiments and simulation), the voltage of sum of all

single cells (V_{AllSCs}) is sum of V_{SC} and V_{4SCs}. Thereby the voltage distribution through stack is known, and it is the first characterization method for REDBP stack.

Voltage Distribution

Voltage distribution is to analyze performance of single cell throughout the stack by measuring voltage at several positions inside of the stack. Figure 4.10 shows an example of 20 cells stack. If V_{SC} is 0.76V, assuming the performance of single cell at any given position of stack is constant, then the first 5 cells voltage ($V_{5cell_{1st}}$) should be 5 times V_{SC} and equal to the second 5 cells voltage ($V_{5cell_{2nd}}$), and sum of all single cells (V_{AllSCs}) should be 20 times V_{SC} .

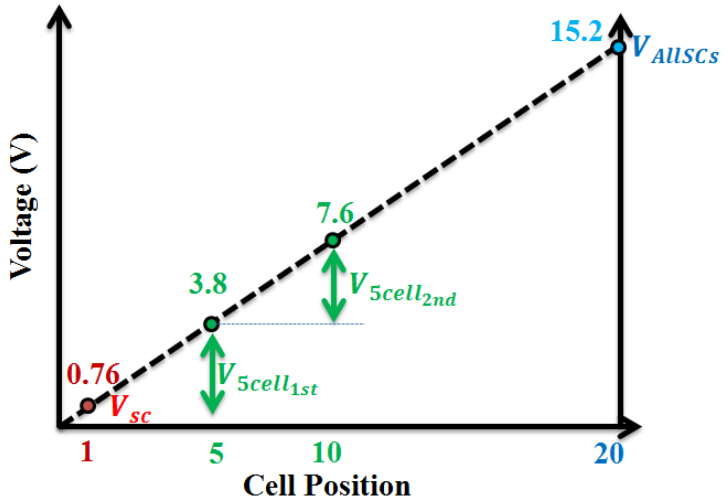

Figure 4.10: Schematic diagram of voltage distribution throughout a 20 cells stack with 1M solution concentration at 25°C 0.1MPa.

Current-Voltage Curves

By measuring several voltages simultaneously, several I-V curves can be obtained in one diagram as in figure 4.11. The lines with positive slope are charging processes while with negative slope are discharging processes. Red lines with the lowest value are single cell measurements (OCV_{SC}). Green lines above single cell measurements are the measurements in the middle of the stack (OCV_{StackM}). The blue lines are the measurements of all single cells (OCV_{AllSCs}). The black lines are voltages between two electrodes (OCV_{Stack}). Theoretically the following relations are supposed to be hold :

(1) $OCV_{Stack} = OCV_{AllSCs} = Stack\ size \times OCV_{SC}$
(2) $\eta_{Stack} < \eta_{AllSCs} = \eta_{StackM} = \eta_{SC}$

where stack size means how many single cells are inside of one stack.

Chronopotentiometry

By measuring the chronopotentiometries at different position of REDBP stack, the different changes of voltage over time throughout the stack can be examined as in figure 4.12.

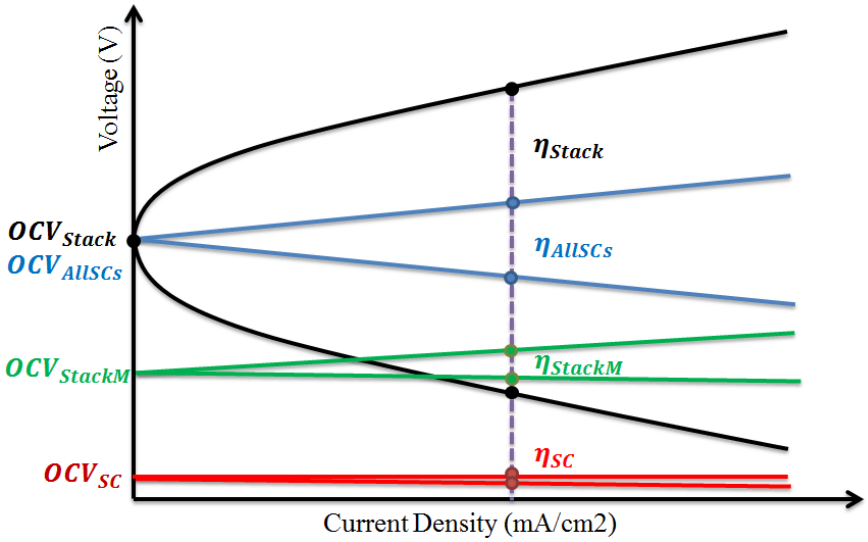

Figure 4.11: I-V curves at different positions in stack. The lines with positive slope are charging processes while with negative slope are discharging processes. Red lines with the lowest value are single cell measurements. Green lines above single cell measurements are the measurements in the middle of the stack. The blue lines are the measurements of all single cells. The black lines are voltages between two electrodes.

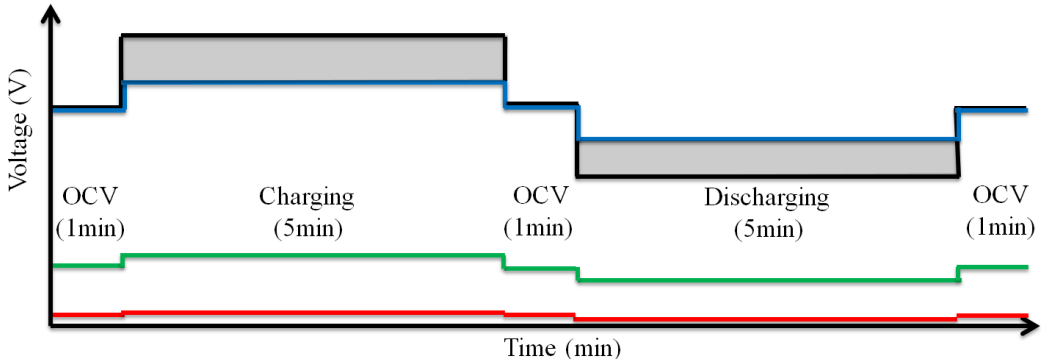

Figure 4.12: Chronopotentiometries of different position of REDBP stack. The red, green, blue and black lines are chronopotentiometries of single cell, stack middle, sum of all single cells and stack, respectively. The grey areas are the losses due to electrochemical reactions in electrode chambers.

4.1.6 Stack Test Facility

The test facility of stack experiment is shown in figure 4.13. (a)-(c) show a 20 cells REDBP stack with two end plates as well as many screw clamps. (d) Pt wires arrangement. (e) Membrane pumps. (f) Tanks for electrolyte solution. By strictly following experimental protocol as listed in table 4.3, the reliable experimental results are acquired and discussed in the following section.

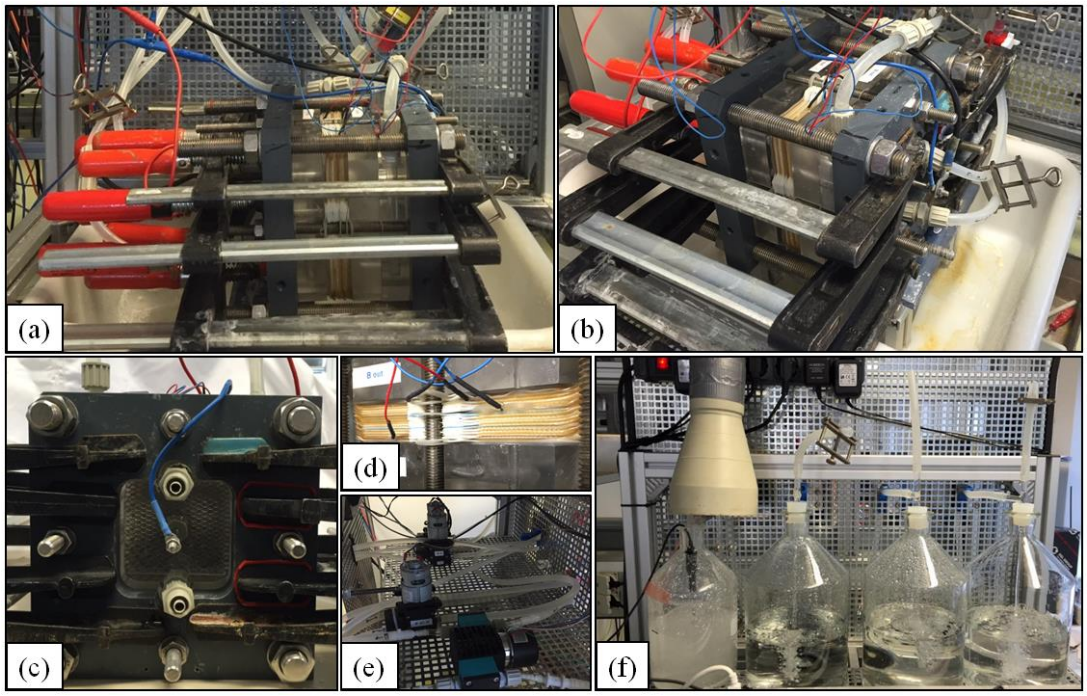

Figure 4.13: Test facility of REDBP stack. (a)-(c) REDBP stack from different views. (d) Pt wires arrangement. (e) Membrane pumps. (f) Tanks for storage of electrolyte solution. From left to right, they are 1.5l Na_2SO_4 of 0.25M, 2l HCl, 2l NaCl of 0.5M, and 2l NaOH.

Table 4.3: Stack experiment protocol in this thesis.

	Process	**Time**	**Reasons**
1st	Stack build-up	1-3h	
2nd	Over night	10h	Dry out IEMs
3rd	Tightening screws again		Dry IEMs are thinner
4th	Checking leakage		
5th	Turning on the pumps		Checking leakage
6th	1 DisCh/Ch cycle	20min	(1) Activating BPM (2) Degassing
7th	I-V curve	10min	
8th	Chronopotentiometry	60min	(1) 0.3A (3mA/cm^2) *) (2) 0.6A (6mA/cm^2) *) (3) 0.9A (9mA/cm^2) *)
9th	Turning off the pumps and valves	60min	
10th	Self-discharge test		

*) Calculated by 100cm^2 of active surface, which is larger than the actual active surface.

4.2 Characterization of REDBP Stack

In this section, performance of single cells inside of REDBP stack as well as stack performance as a whole will be investigated.

4.2.1 Open Circuit Voltage

The most immediate and effective procedure is to measure OCV of sum of all single cells (OCV_{AllSCs}) with increasing stack size. There are several interesting OCVs.

(1) EMF_{AllSCs}: Electromotive force is the theoretical maximum OCV on the premise of existing only electric work. It is the theoretical limit of the highest OCV_{AllSCs}, equals to stack size · EMF_{SC}. For instance with 1M solution, EMF_{SC} is 0.828V, then EMF_{AllSCs} of 20 cells should be 16.6V.

(2) Stack Size · $OCV_{SC\_meas.}$: This is multiplying the number of single cells (stack size) and OCV_{SC_meas} which is obtained by single cell experiment in section 2.3.1.

(3) $OCV_{AllSCs\_meas.}$: measured by stack experiment directly.

(4) $OCV_{Stack\_meas.}$: OCV between two electrodes.

Figure 4.14 shows the comparison of these OCVs. With increasing stack size, the difference between stack size · OCV_{SC_meas} and OCV_{AllSCs_meas}. increases, suggesting the existence of additional losses during mounting-up process. Very interestingly, $OCV_{Stack\_meas.}$ is always between stack size · OCV_{SC_meas} and OCV_{AllSCs_meas}. This phenomenon might be due to side reactions inside of electrode chambers and will not be discussed in this thesis. In order to understand figure 4.14, the detail performance of single cells inside of stack needs to be investigated.

Since REDBP stack has too many influencing factors (such as stack size, flowrate and flow patterns of electrolyte in solution chamber, flow types through stack, temperature, active surface, concentration of electrolyte, IEMs, and current density), the following section will focus on the measurement of 20 cells stack only and try to examine as many influencing parameters as possible.

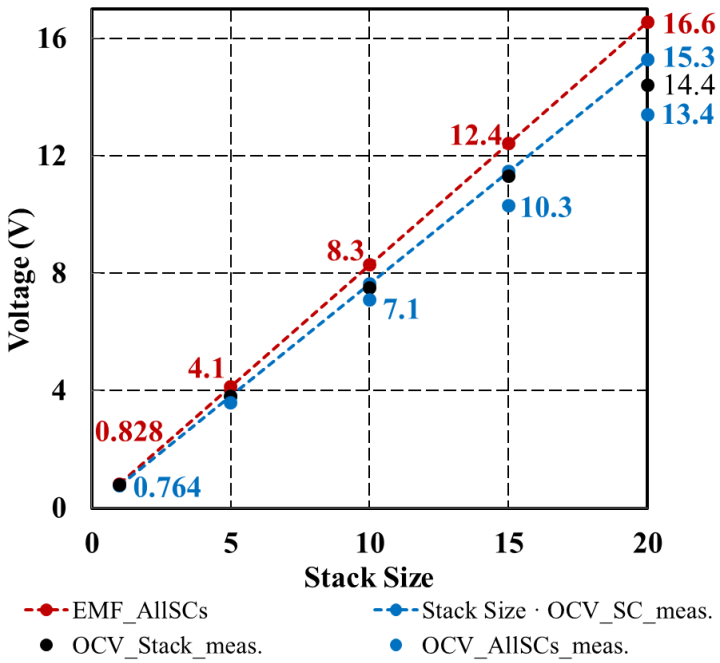

Figure 4.14: OCVs vs stack size. The red dotted dashed line is theoretical maximum OCV of sum of all single cells (EMF_{AllSCs}). The blue dotted dashed line is stack size times single cell OCV according to single cell experiment (Stack Size · $OCV_{SC\_meas.}$). The blue dots are the direct voltage measurement of OCV of AllSCs ($OCV_{AllSCs\_meas.}$). The black dots are the experiments of OCV between two electrodes ($OCV_{Stack\_meas.}$).

4.2.2 Current-Voltage Curve

Figure 4.15 shows I-V curves of 20 cells stack with 1M solution concentration at 25°C 0.1MPa.

Loss of electrode chambers

The distance between V_{Stack} (black lines in the figure 4.15) and V_{AllSCs} (blue lines in the figure 4.15) is the loss of electrode chambers, which increases with increasing current density. According to table 4.2 the electrochemical reactions by charging and by discharging are the same, so theoretically at the same current density, the distance between V_{Stack} and V_{AllSCs} by charging should be the same as by discharging. However, test results show the loss of electrode chambers is higher by charging than discharging, indicating a higher loss by charging process. Moreover, stack size does have influence on the loss of electrode chambers. Figure 4.16 shows I-V curves of Ch/DisCh of 1M 15 cells at 25°C 0.1MPa, by both charging and discharging process. Its loss of electrode chambers is relatively smaller compared to 20 cells stack with same current density. This also implies an additional loss by stacking up the single cell. More detailed discussion of electrode chambers is in section 5.4.3 and 5.4.4.

Voltage measurement of single cell in stack V_{SC}

The accuracy and precision of Pt wire measurement is far less than that of Luggin capillaries with saturated calomel electrodes. The variation of the former is larger than ±0.1V while the latter can be within ±0.005V. Therefore, it is very difficult to compare V_{SC} of stack tests with that of single cell tests, although by open circuit, these two are almost identical. V_{SC} of stack by discharging drops dramatically when the current density reaches 8-9mA/cm^2. This might be due to the shadow effect when Pt wire being introduced in the testing chamber, or non-ideal distribution of electrolyte solution in solution chamber (although the linear flowrate of electrolyte solution is as high as 2cm/s inside of solution chamber). Bad mixing is indeed one of the biggest issues of this testing stack, which will be mentioned again in discussion of power of 20 cells stack in section 4.2.4.

Nonhomogeneous distribution of voltage

$V_{5cell_{1st}}$ (the first 5 cells voltage in figure 4.10) and $V_{5cell_{2nd}}$ (the second 5 cells voltage in figure 4.10) are not the same, not only by open circuit, but also with current density. It is one of most important findings, a direct evidence of nonhomogeneous distribution of voltage throughout the stack, indicating a higher loss in the middle of the stack. In order to explain this as well as other phenomena, shunt current must be introduced in advance.

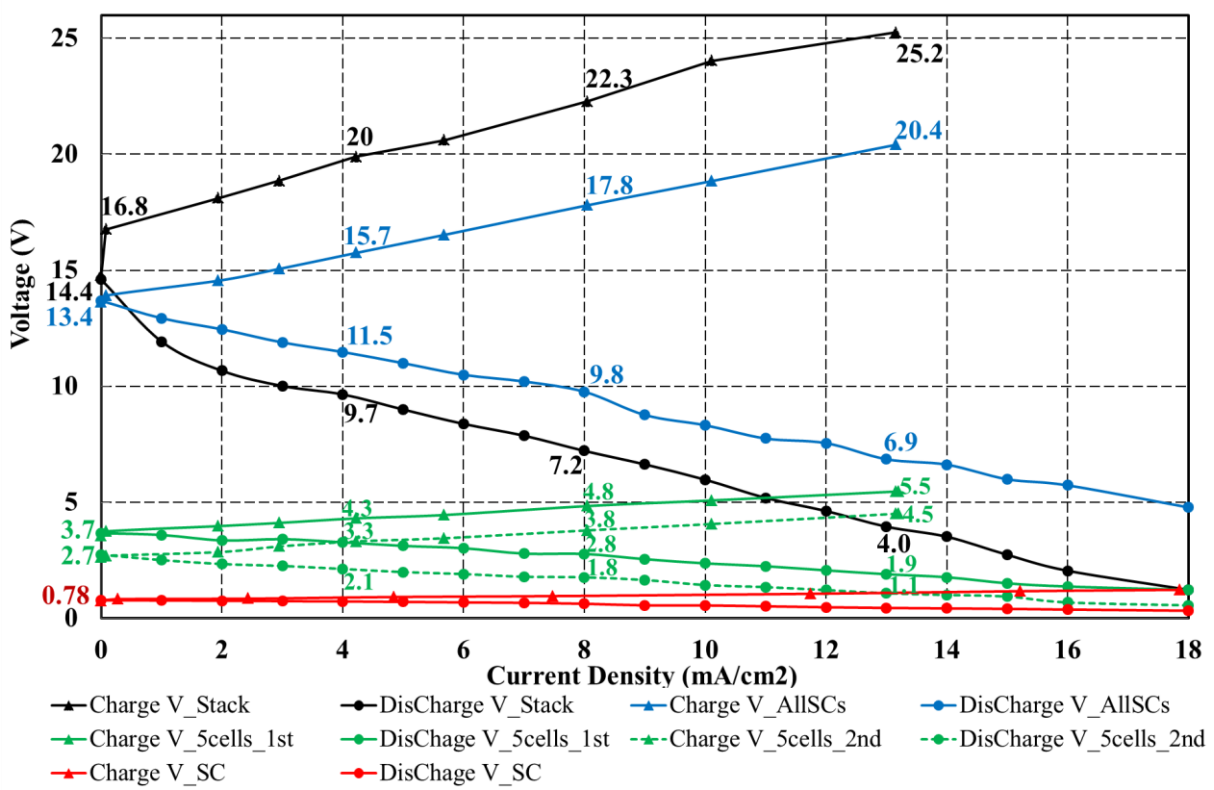

Figure 4.15: I-V curves of Ch/DisCh of 1M 20 cells stack at 25°C 0.1MPa. Curves with positive slop are charging processes, with negative slop are discharging processes. The red, dotted dashed green, green solid, blue and black lines are V_{SC}, $V_{5cell_{2nd}}$, $V_{5cell_{1st}}$, V_{AllSCs} and V_{Stack} respectively.

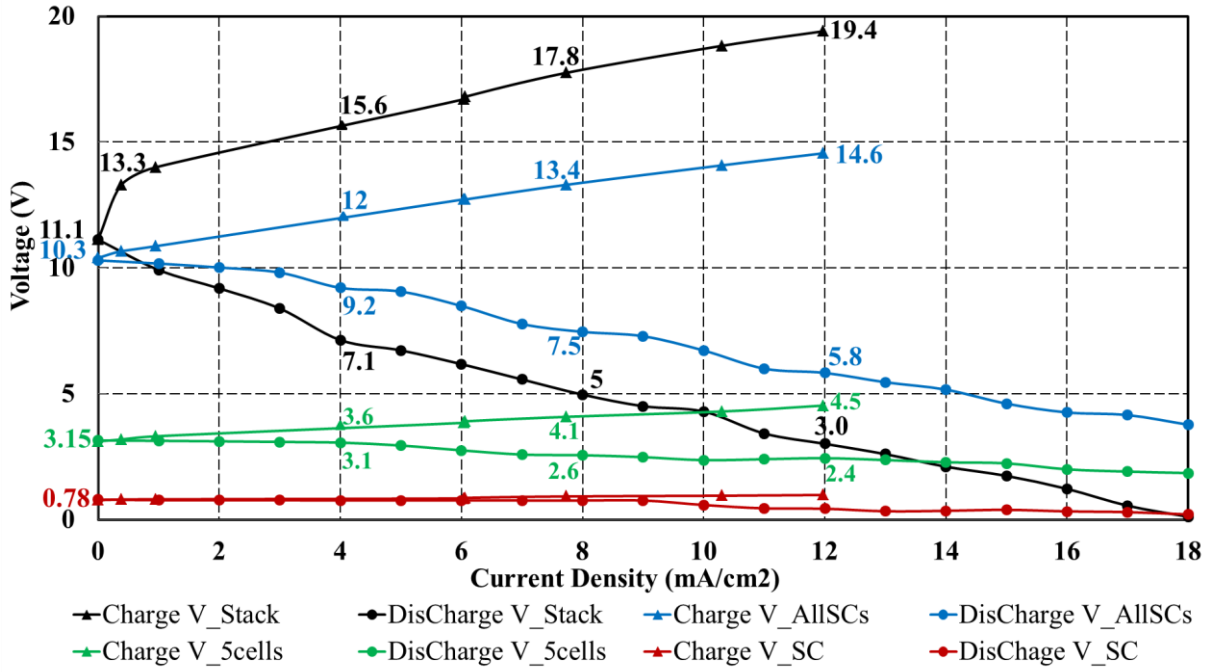

Figure 4.16: I-V curves of Ch/DisCh of 1M 15 cells stack at 25°C 0.1MPa. Curves with positive slop are charging processes, and curves with negative slop are discharging processes. The red, green solid, blue and black lines are V_{SC}, V_{5cells}, V_{AllSCs} and V_{Stack} respectively.

4.2.3 Shunt Current and Self-Discharging Tests

As a flow battery, electrolyte solution is pumped through the stack. If the electrolyte solutions are transported in parallel throughout the stack as shown in figure 4.4 (a), inside of stack the single cells are inter-connected with each other via ionically conductive pathways or so-called salt bridges (or bypass connections) through which parasitic currents can flow. These parasitic currents are so-called shunt currents. Shunt current is one of main problems needing to be avoided by designing a stacks, since it reduces the efficiency[1] of a flow battery by causing an internal self-discharge: It enables an undesirable run of the discharge reactions at simultaneous and spontaneous ion shift through the salt bridges. Many literatures relate to numerically understanding shunt current [40], implementing shunt current into certain flow battery type [41], and giving suggestions of better stack/system design [42]. The more detailed qualitative and quantitative analysis of shunt current is in Chapter 5.

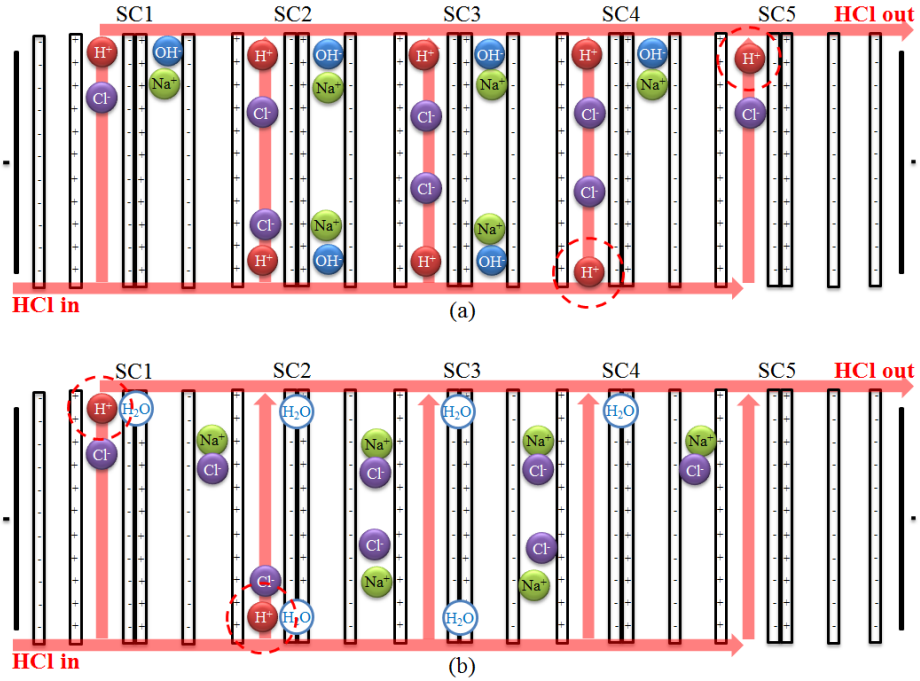

Figure 4.17: Schematic diagram of shunt current through acid bypass connections in REDBP stack by open circuit. It enables an undesirable run of the discharge reactions (neutralization reaction at BP interface) at simultaneous and spontaneous ion shift (H^+) through the acid bypass connections. Because of migration of H^+ from (a) to (b), for example, H^+ migration from SC5 to SC1 and from SC4 to SC2, electrochemical equilibrium no longer exists. System rebalancing causes neutralization reaction and ionic transport, which form electric current throughout the stack.

[1] To be more specific, shunt current reduces coulombic efficiency.

Here are some general descriptions of shunt currents for understanding the voltage distribution through stack:

(1) REDBP has 4 types of electrolyte solutions: acid, base, salt and Na_2SO_4 solution. According to simulation (section 5.4.2), with 1M concentration of acid and base by open circuit, more than 60% of shunt currents are through acid bypass connections, more than 30% are through base, and less than 10% through salt. With 5m long pipe, shunt current through Na_2SO_4 solution can be neglected.

(2) Shunt current is not crossover. It is electric current and is one of the main causes[1] of internal self-discharge as illustrated in figure 4.17. Like all electric current, its magnitude is proportional to electric potential between two electrodes of stack and electrolyte conductivity.

(3) According to charge conservation (section 3.1.7), there are three types of electric currents inside of stack as illustrated in figure 4.18.

(4) $I_{channel}$ represents the electric current through bypass connections (in electrolyte channels) in x direction. It is outside of active surface.

(5) I_{cell} is the current in x direction inside of active surface.

(6) J is the current in y direction flowing along with the solution chamber.

(7) Shunt current will be higher in the middle of stack.

(8) I_{cell} is not homogeneously distributed over active surface. Normally (exceptions are explained in section 5.3.2) the current density near the entrance and exit of solution chamber is much higher than at the center of active surface.

(9) J is higher in chambers which are near electrode sides.

(10) In one chamber, J is higher near the inlet/outlet of electrolyte channel than in the center of active surface.

If the properties of shunt current are clear, then the following phenomena can be explained:

a) Because of (2), (5) and (7), considering V_{SC} decreases with increasing discharging current density and shunt current is a type of (self-) discharging current, V_{SC} is smaller in the middle of stack than near electrodes. That explains why voltage distribution throughout the stack is not homogeneous.

b) Because of (7), increasing stack size (meaning how many single cells in one stack) will increase the number of bypass connections, and will increase I_{cell} in the middle of stack,

[1] The other causes such as crossover, leakage of IEMs and inter-cell leakage due to bad sealing.

and decrease V_{SC} in the middle of stack. That explains why the difference between stack size · $OCV_{SC\_meas.}$ and $OCV_{AllSCs\_meas.}$ is getting bigger with increasing stack size (section 4.2.1).

c) Because of (2), shunt current by charging is bigger than discharging (since charging electric potential between two electrodes is higher than discharging). That explains why the loss in electrode chambers by charging is bigger than discharging with constant current density: more electric energy has been consumed by driving shunt current through bypass connections in charging process than discharging process.

d) Because of (8), voltage measurement should avoid the active surface near the inlet/outlet of solution chamber.

e) Because of (6) and (9), introducing Pt wire in solution chamber, especially which near electrode side, will enlarge the thickness of testing chambers, and will lead to relative higher shunt current of J.

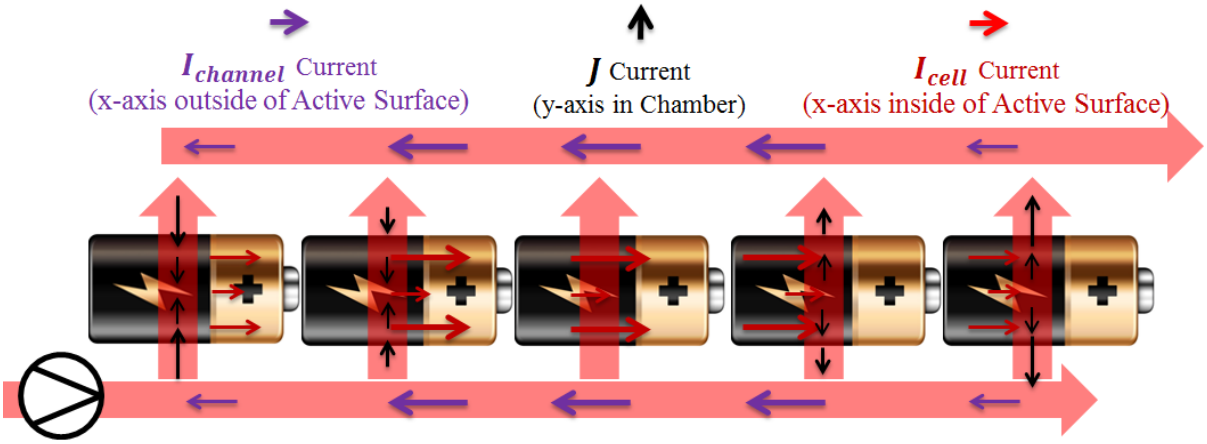

Figure 4.18: Schematic diagram of electric currents inside of stack by open circuit.

Self-discharging test is a direct way to confirm and examine shunt current. During the test, all pumps and valves are closed; voltage will be recorded over time. If only crossover effect exits, the change of measured OCV should be independent on the stack size or cell position. Figure 4.19 to 4.22 are the self-discharging tests of 5 cells, 10 cells, 15 cells and 20 cells stack respectively. After OCV is lower than 4-5V, all these curves are identical. But before that, the speed of capacity loss (concentration of acid and base) will be accelerated with increasing stack size. This is due to the shunt current which causes neutralization reaction at BP interface. With increasing stack size, the number of bypass connections increases, thus I_{cell} increases in the middle of stack, meaning enhancing self-discharging process. Figure 4.22 supports this argument in details. $OCV_{5cells_{2nd}}$ is lower than $OCV_{5cells_{1st}}$, and decreases more quickly than $OCV_{5cells_{1st}}$. Shunt current is due to ionic bypass, so the conductivity of electrolyte solution determines its magnitude. Figure 4.23 shows the self-discharging test of 20 cells stack with

0.5M solution concentration. The decreasing slope of 0.5M is flatter than that of 1M, meaning slower capacity loss[1].

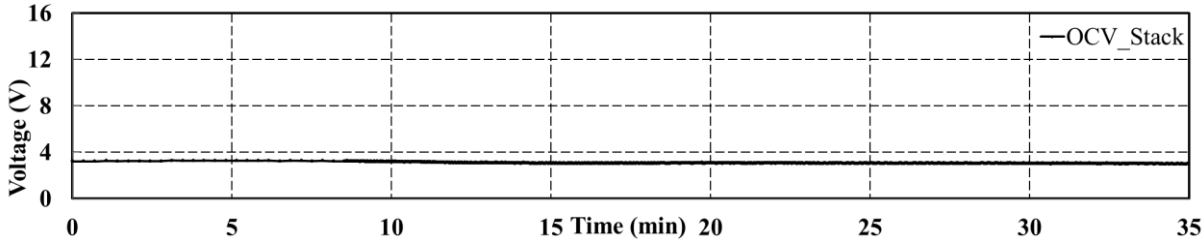

Figure 4.19: Self-discharging test of 5 cells stack with 1M solution concentration at 25°C 0.1MPa.

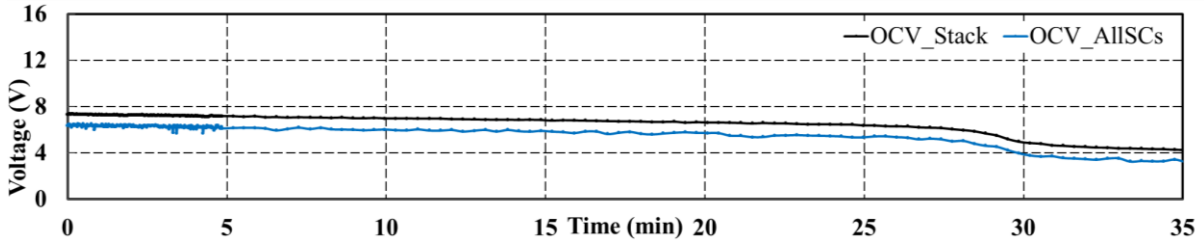

Figure 4.20: Self-discharging test of 10 cells stack with 1M solution concentration at 25°C 0.1Mpa.

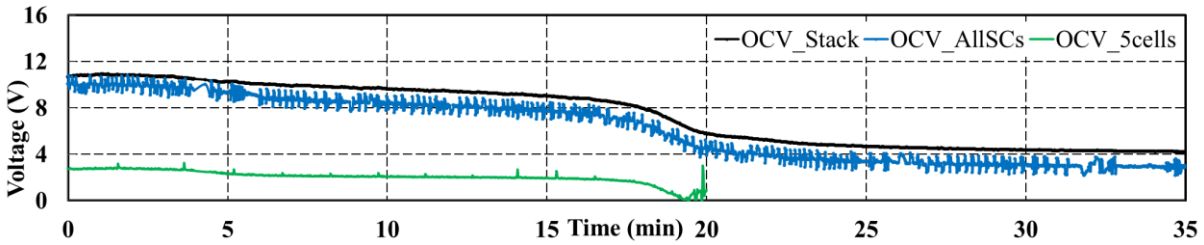

Figure 4.21: Self-discharging test of 15 cells stack with 1M solution concentration at 25°C 0.1Mpa.

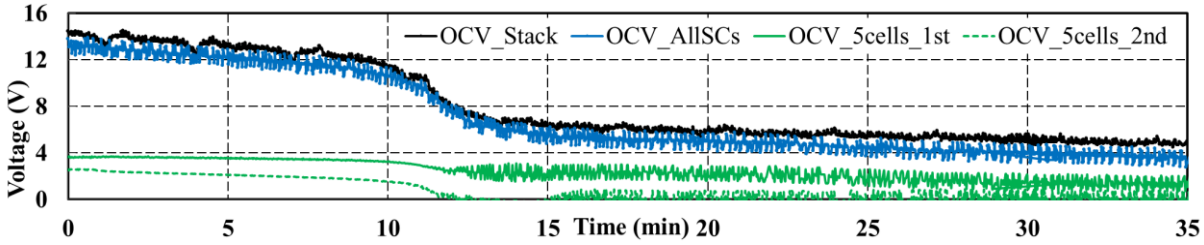

Figure 4.22: Self-discharging test of 20 cells stack with 1M solution concentration at 25°C 0.1Mpa.

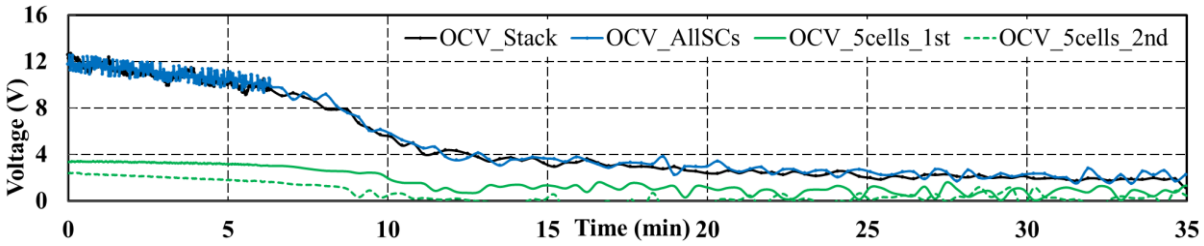

Figure 4.23[2]: Self-discharging test of 20 cells stack with 0.5M solution concentration at 25°C 0.1Mpa.

[1] 0.5M reaches 4V quicker than 1M does not mean its capacity loss is more significant. It is simply due to its own concentration being only half of 1M.

[2] The curves have fewer fluctuations because their saving interval of data acquisition program is longer (60s) than the others (1s). The same to figure 4.20.

4.2.4 Voltage Distribution Curve

By measuring the voltage at different positions throughout the stack, the voltage distribution curve can be acquired. Figure 4.24 shows the voltage distribution throughout the stack with 1M at 25°C 0.1MPa. Due to shunt current, average voltage of single cell decreases from electrode sides to the middle of stack.

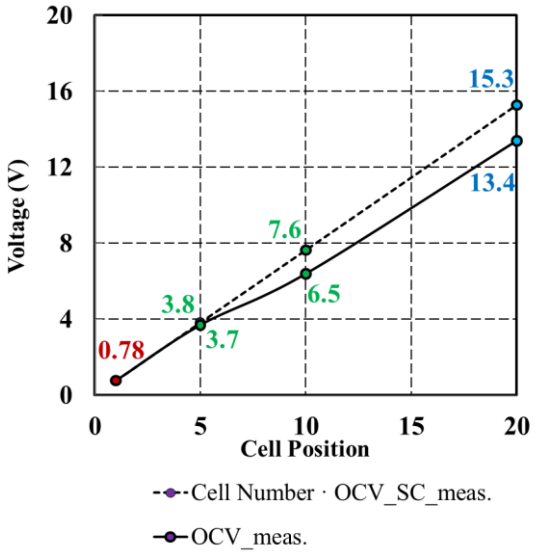

Figure 4.24: Voltage distribution throughout the stack by open circuit with 1M at 25°C 0.1MPa. Red, green and blue dot represent the first single cell, middle of stack and sum of all single cells (AllSCs), respectively. The dashed line is cell number (within the two voltage measuring points) times $OCV_{SC\_meas.}$, while the solid line is measured voltage distribution throughout the stack.

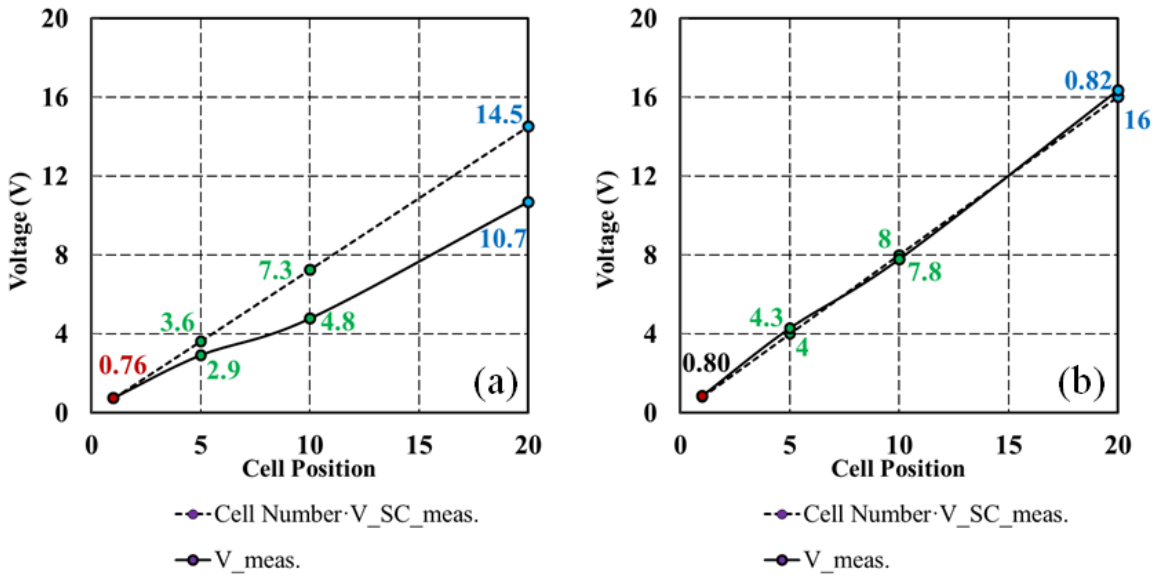

Figure 4.25: Voltage distribution throughout the stack by 6mA/cm^2 discharging (a) and 6mA/cm^2 charging (b) with 1M at 25°C 0.1MPa.

Figure 4.25 shows the voltage distribution throughout the stack by discharging (a) and charging (b) with 1M at 25°C 0.1MPa. The difference between Cell Number · $V_{SC_{meas.}}$ and $V_{meas.}$ is much

more significant by discharging process than by charging process. This does not necessarily mean the shunt current (or any other loss) by discharging is much higher than charging. This is due to the non-ideal mixing of electrolyte in the chamber, especially by discharging, water, as product, dilutes the electrolyte concentration, which leads to higher inner resistance of the stack. Therefore, discharging poses more challenges on Pt wire measurement. It is one of the drawbacks of only investigating voltage, since many coulombic losses cannot be presented in voltage curves, for example shunt current. Voltage investigations can only qualitatively analyze the existence of coulombic loss, not quantitatively analyze the extend of coulombic loss. The detailed explanations of figure 4.25 will be in section 5.3.2.

Moreover, both by discharging and charging, $V_{5cells_{1st}}$ is higher than $V_{5cells_{2nd}}$, indicating the shunt current accumulating in the middle of the stack. Section 5.4.3 will focus on this effect more in details.

4.2.5 Discharging Power Density and Efficiency

Electric power is provided between two electrodes of REDBP stack, but the power density (PD) at different positions inside of a stack is very useful for analyzing the losses inside of stack, as well as pointing out where and how REDBP stack can be improved. Figure 4.26 shows discharging voltage and discharging power density of 1M 20 cells stack at 25°C 0.1MPa with 0.196cm thickness of SC (section 2.5). The following voltages and PDs have been listed below. In order to compare each PD, the thickness of electrode chambers (as well as the two additional CEMs) is not considered when calculating PD_{Stack}.:

(1) $\boldsymbol{EMF_{20\ cells}}$**:** The theoretical EMF in 20 cells stack.
(2) $\boldsymbol{20\ cells \cdot PD_{theor.max}}$: The theoretical limitation of PD of 20 cells stack calculated by $\boldsymbol{EMF_{20\ cells}}$.
(3) $\boldsymbol{20\ cells \cdot V_{SC_{meas.}}}$: 20 cells multiplying measured voltage in single cell experiment.
(4) $\boldsymbol{20\ cells \cdot PD_{SC_{meas.}}}$: 20 cells multiplying measured PD in single cell experiment.
(5) $\boldsymbol{V_{AllSCs}}$: The measured voltage of AllSCs inside of 20 cells REDBP stack.
(6) $\boldsymbol{PD_{AllSCs}}$: The measured PD of AllSCs inside of 20 cells REDBP stack.
(7) $\boldsymbol{V_{Stack}}$: The measured voltage between two electrodes of 20 cells REDBP stack.
(8) $\boldsymbol{PD_{Stack}}$: The measured PD between two electrodes of 20 cells REDBP stack.

According to figure 4.26, the highest PD_{Stack} and PD_{ALLSCs} are 15mW/cm^3 and 24mW/cm^3, respectively. Compared with $\boldsymbol{EMF_{20\ cells}}$ this stack has many losses and a huge space for

improvement. Below, the four main losses (illustrated in figure 4.26 in different colors) are listed and discussed:

(1) The grey area in figure 4.26 is the loss in electrode chambers where the electrochemical reactions take place. Some are necessary costs, but some are shunt current and side reactions which need to be avoided.

(2) PD_{AllSCs} increases with current density, but after 8mA/cm^2 it loses its momentum of increase. One of the reasons is bad mixing inside of solution chambers due to non-ideal design of cell frame. This loss, illustrated as blue area in figure 4.26, can be overcome by better cell frame and/or more powerful pumps.

(3) Between PD_{AllSCs} and $20\ cells \cdot PD_{SC_{meas.}}$ there is a huge difference indicating a huge loss. Besides bad mixing, it is believed the cause of such loss is primarily[1] due to shunt current. Please note that there is a strong correlation between the bad mixing and shunt current.

(4) As introduced in section 2.5, the difference between $20\ cells \cdot PD_{theor.max}$ and $20\ cells \cdot PD_{SC_{meas.}}$ is due to the resistance of electrolyte (IEMs and solutions), crossover effect, and transport of water molecule[2] inside of BP. This loss only depends on the permselectivity of IEMs, the thickness of chambers, and the conductivity of electrolyte, and considered as small loss in small current density range.

Those four areas are considered the main tasks for future investigation. However, those four losses are not isolated problems: They are correlated among each other. For instance:

(1) Shunt current causes neutralization reaction which produces water molecule and enhance the problem of mixing;

(2) Internal resistance, chamber thickness and mixing have direct influence on shunt current.

(3) Shunt current affects the electrode chambers, where side reactions might take place.

[1] Leakage has been strictly checked before each experiment, including leakage among different electrolyte solutions, and leakage of electrolyte into external environment.
[2] With low current density, transport of water molecule inside of BP can be neglected.

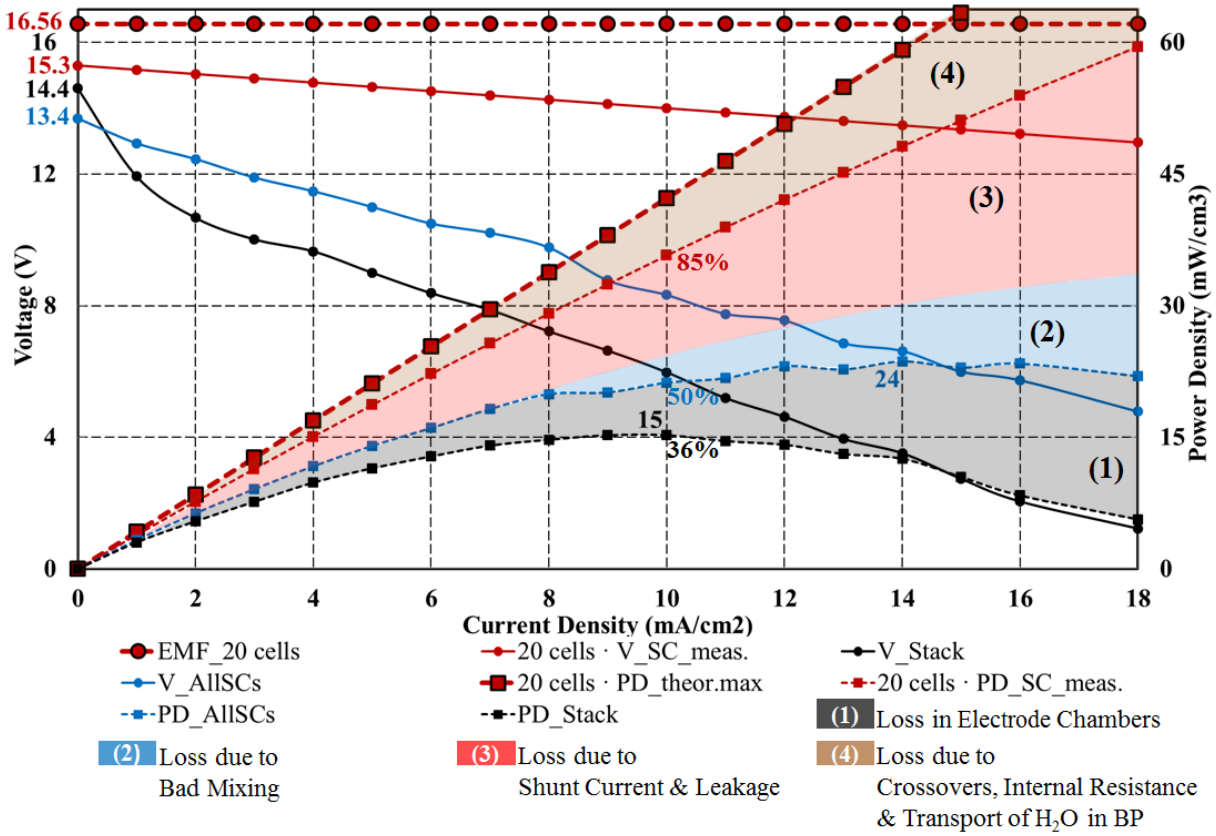

Figure 4.26: Discharging voltages and discharging power densities of 1M 20 cells stack at 25°C 0.1MPa. The thickness of SC is 0.196cm (section 2.5). The discharging efficiencies at 10mA/cm^2 have been labeled.

4.2.6 Chronopotentiometry

Chronopotentiometry (CPM) is performed under galvanostatic condition (section 2.1.2). Figure 4.27-4.29 are CPMs of 20 cells stack with 1M solution at 25°C 0.1MPa with increasing current density. By comparing each figure, the following points can be summarized:

(1) The difference between V_{Stack} and V_{AllSCs} is the loss in electrode chambers, and its magnitude is bigger by charging than by discharging, which has previously been explained. What is interesting its unstable behavior, indicating an unstable conductivity of electrolyte in electrode chambers[1] due to gases production, or side reactions in electrode chambers, or both.

(2) By turning off the electric current, all membrane voltages will change sharply such as V_{AllSCs} and V_{StackM}. But V_{Stack} will change sharply followed by a slow relaxation

[1] Electrode chamber has thickness of 10mm, and it is filled with spacers. The linear flowrate of Na_2SO solution is maintained at 2cm/s.

process, indicating either a rearranging diffusional layer between electrode plate and Na_2SO_4 solution, or side reactions, or both.

(3) V_{AllSCs} and V_{StackM} are quite constant, the tiny decrease of voltage by discharging process is mainly due to bad mixing.

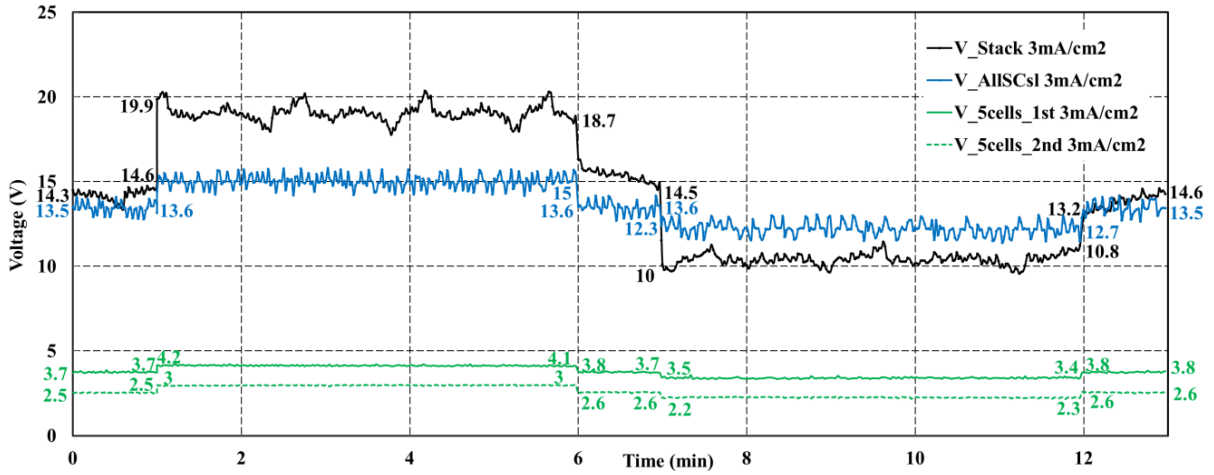

Figure 4.27: CPM of 20 cells stack with 3mA/cm^2 and 1M solution at 25°C 0.1MPa.

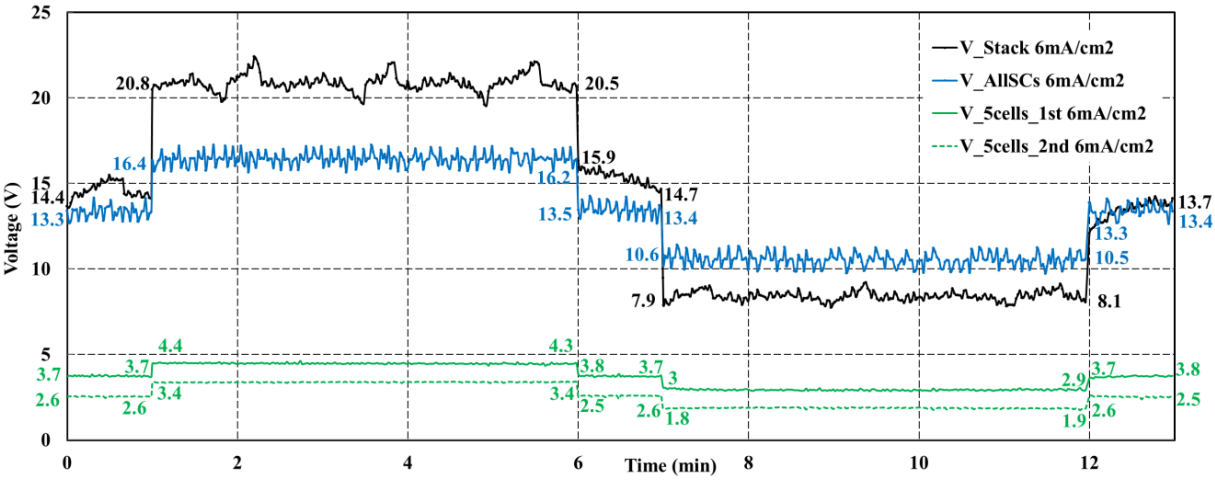

Figure 4.28: CPM of 20 cells stack with 6mA/cm^2 and 1M solution at 25°C 0.1MPa.

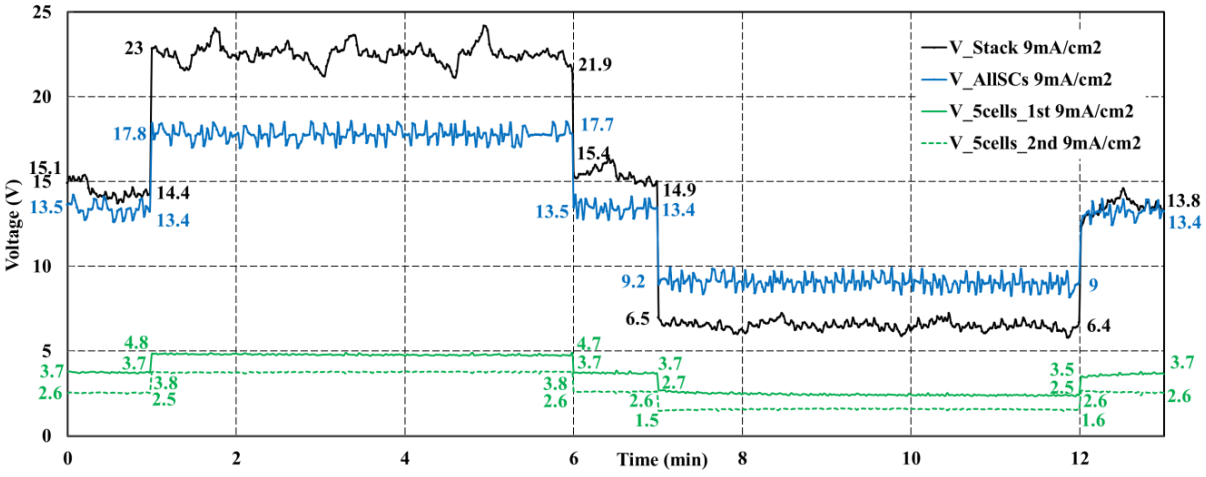

Figure 4.29: CPM of 20 cells stack with 9mA/cm^2 and 1M solution at 25°C 0.1MPa.

4.3 Conclusion

After experiments of stack, many questions on the first page of chapter 4 are answered.

(1) There are indeed additional losses during mounting up process. Besides leakages or side reactions, bad mixing and shunt current are considered the most important losses. Shunt current enables unwanted discharging process by spontaneous ionic shift through bypass connections. By mounting up the stack, the shunt currents will be enhanced and cause more losses with increasing stack side. The existence of shunt current has been proven by self-discharging tests. However, it is merely a qualitative analysis. Future researchers will need to analyze the ionic changes in electrolyte solution in order to have a quantitative view of coulombic loss due to shunt current. Briefly stated, fully understanding and seriously considering shunt current are the prerequisites for designing and mounting up a stack.

(2) The overall performance of REDBP stack could be very high. Although current cell frame in this thesis is not appropriate, with 1M solution the maximum power output between two electrodes of 20 cells stack reaches 6W, corresponding to 15mW/cm^3 with 36% discharging efficiency. Neglecting electrode chambers, those numbers go up to 9W, 24mW/cm^3 and 50%. If considering the real active surface is not 100cm^2 but rather 92.1425cm^2 (figure 4.1), the real power density is 26mW/cm^3.

(3) Performances of single cell inside of stack are not identical. By introducing Pt wires inside of a stack, inhomogeneous distribution of voltage throughout the stack has been found, mainly due to shunt current and bad mixing.

(4) By studying electrode chambers, evidences indicate additional losses due to bad mixing, shunt current, and side reactions. Due to the limitation of this thesis, a thoroughly investigation has not been conducted.

(5) The important influential parameters determining the overall performance of REDBP stack are electrode chamber, flow patterns (parallel/series flow), cell frame design (flow patterns inside of solution chamber, as well as shunt currents) and those factors affecting performance of single cell including concentration of solution, flowrate, temperature, active surface, current density and permselectivity of IEMs.

In this thesis, REDBP 20 cells stack reaches 26mW/cm^3 and 50% discharging efficiency with only neutralization reaction as driving forces. BP has been proven as a ‘reactor’ powering the whole system, not simply a capacitor with two double layers.

Chapter 5

Modeling and Simulation of Stack

In the previous section the outcomes of the stack experiments were described. The results show additional losses during mounting up process. Besides increasing pump losses, the most significant loss is stacking-up shunt currents. In section 4.2.3 shunt currents were briefly introduced in order to explain unexpected experiment results. This section uses mathematical method to investigate these phenomena, mainly on the distribution of electric potential and electric current throughout the stack. At first, necessary assumptions will be introduced, followed by simplifications for constructing mathematical model of stack, and then simulation results will be discussed and compared with stack experiments.

5.1 Assumptions and Simplifications

Many assumptions in this section are the same as modeling of single cell, such as electroneutrality (section 3.1.1), ionic transport in ideal mixture (section 3.1.5), conservation of charges (section 3.1.7) and steady state (section 3.1.8). In order to simplify the model, ideal mixing, homogeneous IEMs and no leakage are added.

5.1.1 Ideal Mixing

According to Nernst-Planck equation (section 3.1.5), the driving forces for ionic transport process are movement of electrolyte solution itself, concentration gradient of component j, and electric potential gradient, respectively.

$$\vec{J}_j^{total} = c_j \cdot \vec{v} + D_j\left(-\nabla c_j\right) + z_j \frac{|z_j| \cdot F}{R \cdot T} D_j \cdot c_j(-\nabla \varphi) \qquad \textbf{(5.1)}$$

Applied to Faraday´s law (section 3.1.6):

$$i = F \cdot \vec{v} \cdot \sum_{j=1}^{J}(z_j \cdot c_j) + F \cdot \sum_{j=1}^{J}(D_j \cdot z_j \cdot \left(-\nabla c_j\right)) + F^2 \cdot (-\nabla \varphi) \cdot \sum_{j=1}^{J}(z_j^2 \cdot \frac{|z_j|}{R \cdot T} D_j \cdot c_j) \qquad \textbf{(5.2)}$$

If electroneutrality (see section 3.1.1) holds, then the first term of equation (5.2) will be eliminated.

Ideal mixing dictates that electrolyte solution is transported throughout the stack so rapidly that the change of its properties can be neglected, such as ionic concentration, conductivity, and temperature. Therefore, the second term of equation (5.2) vanishes in bulk solution.

Thus Nernst-Planck equation according to Faraday´s law can be simplified as:

$$i = F^2 \cdot (-\nabla\varphi) \cdot \sum_{j=1}^{J} (z_j^2 \cdot \frac{|z_j|}{R \cdot T} D_j \cdot c_j) \quad \textbf{(5.3)}$$

where $F^2 \cdot \sum_{j=1}^{J} (z_j^2 \cdot \frac{|z_j|}{R \cdot T} D_j \cdot c_j)$ is a constant and known as electrical conductivity κ with unit of [S·m^{-1}]. Equation (5.3) can be written as:

$$i = \kappa \cdot (-\nabla\varphi) \quad \textbf{(5.4)}$$

Conductivity κ is reciprocal of the resistivity:

$$\kappa = \rho^{-1} \quad \textbf{(5.5)}$$

which is defined as:

$$\rho = R \frac{A}{l} \quad \textbf{(5.6)}$$

with unit of [Ω·m], where $\frac{A}{l}$ is the ratio of area and length of electric current pathway.

With the above assumptions and simplifications, density of electric current flowing through electrolyte solution can be treated as proportional to electric potential gradient and conductivity of electrolyte solution.
Applying steady state to charges (section 3.1.8) is the principle of Kirchhoff's current law:

$$\nabla \cdot i = 0 \quad \textbf{(5.7)}$$

Steady state also dictates that all properties of IEM are unchanged in time. This implies neither accumulation nor depletion of water molecules in the process.

5.1.2 Homogeneous IEMs with Diffusional Layers

Homogeneous IEM dictates that there is no positional change of any property of IEM, such as its conductivity, fixed ion concentration, thickness, etc. Also, there always exists a diffusional layer between IEM and bulk solution according to no-slip boundary condition (section 3.2.1).

5.1.3 No Leakage

Leakage is defined as gradual material losses due to non-ideal design of cell frame or sealing inside of REDBP stack. For constructing mathematical model, leakage is neglected.

Those are the assumptions and simplifications for constructing mathematical model. The main advantage is neglecting microscopic ionic transport and focusing on macroscopic current-voltage characteristics of the whole system.

5.2 Modeling of Stack

In this section, mathematical model will be constructed into equivalent circuit based on previously introduced assumptions and simplifications, and will be further simplified into 2D model.

5.2.1 Equivalent Circuit

Although mathematical model of BP is complicated (section 3.4) which consists of two IEM layers, two diffusional layers and one BP interface, the measured I-V characteristic curve (I-V curve) is simple and it is similar to an electrical circuit of a combination of one constant voltage source and one resistance[1]. Two circuits are equivalent if they have the same I-V characteristics at a specified pair of terminals. Figure 5.1 shows the comparison of measured I-V curve (dots) and equivalent I-V curve (dashed lines). The measurements are nearly perfectly matching the equivalent line. Although equivalent circuit is only valid under specific conditions, such as certain ionic activity, composition of electrolyte solution, the transport of water molecular, electric current direction (Ch/DisCh) and temperature (section 4.3), with all the previously introduced assumptions and simplifications, an equivalent circuit depends only on ionic

[1] More specifically, one area resistance with the unit of [$\Omega \cdot m^2$], since the voltage is calculated by multiplying area resistance with current density [A/m^2].

concentration which defines the constant voltage source and resistance of electrolytes. Based on this idea, modeling of stack can be dramatically simplified.

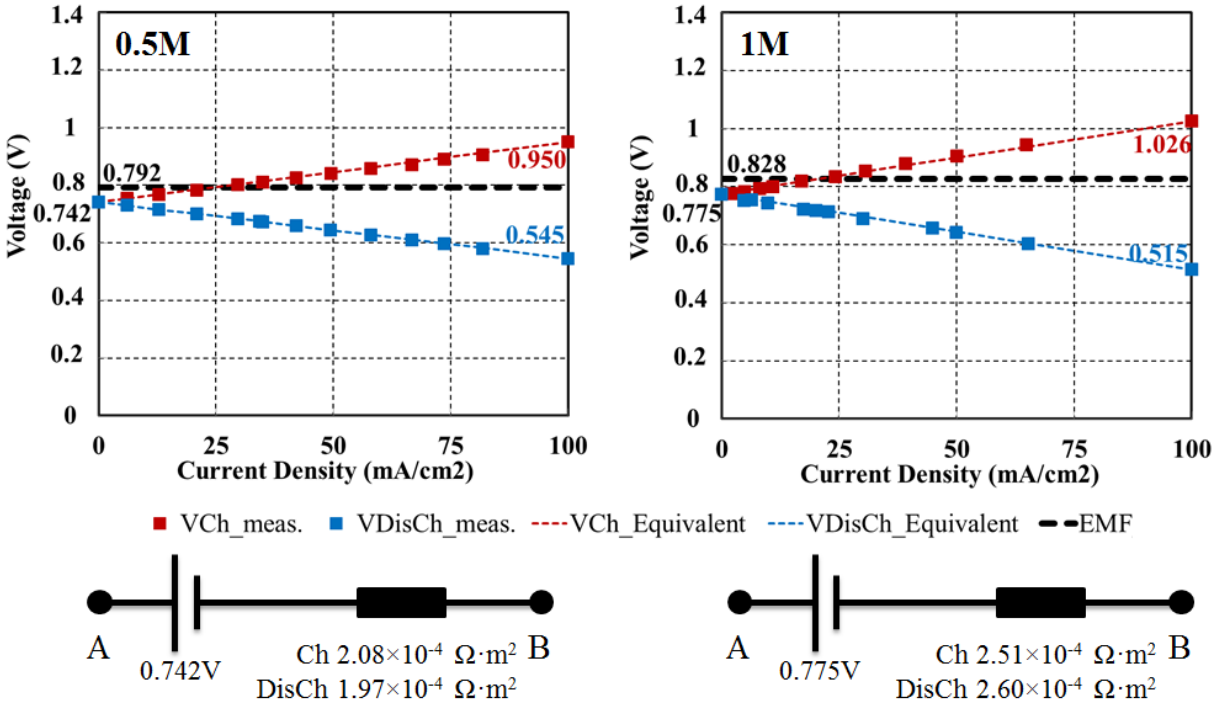

Figure 5.1: Comparison of measured I-V curve (dots) and equivalent I-V curve (dashed lines).

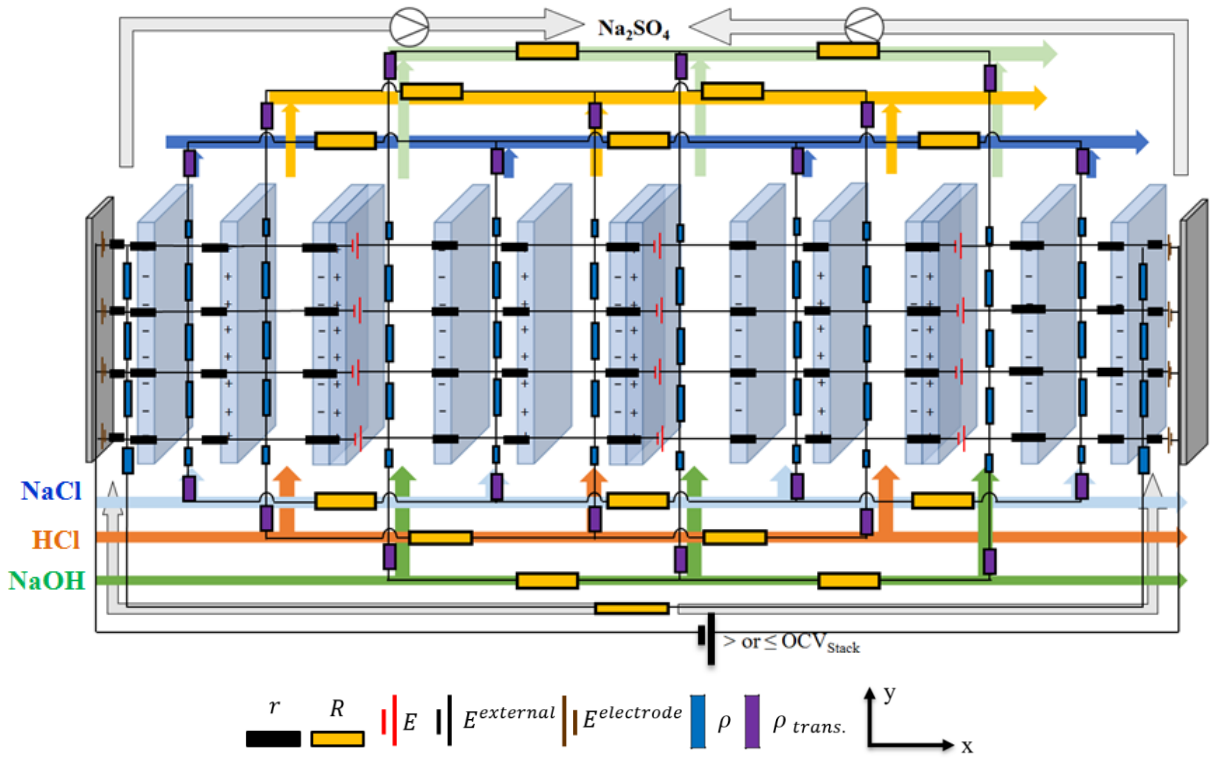

Figure 5.2: 2D equivalent circuit of REDBP stack with 3 single cells.

5.2.2 2D Model of REDBP

The model of REDBP can be simplified into 2D as in figure 5.2. The detailed description of simplification process is in Appendix C.

Here are the explanations of each component of figure 5.2:

(1) r: represents the resistance of electrolyte solution and IEM when electric current is flowing in x direction[1]. The value is calculated by multiplying area of finite element and area resistance of electrolytes, which are taken from the single cell experiment (see Chapter 2). Electric current flowing through it is called ΔI_{cell} with the unit of [A]. Its physical meaning is local electric current in x direction through finite active surface. Sum of all ΔI_{cell} is the electric current flowing throughout the entire active surface. ΔI_{cell} dividing area of finite element is local current density i_{cell} with the unit of [A/m^2].

(2) ρ: represents the resistance of electrolyte solution when electric current is flowing in y direction. Figure 5.3 shows 2D discretization of resistance of solution chamber when electric current flows in y direction, arrows are electric currents and blocks are finite elements of electrolyte solution. Discretization number in x direction is 5 while in y direction 1. The reason why discretization number in y direction is always 1 is the ratio of the thickness of solution chamber and the length of active surface is very small. Please note that this figure illustrates electric current flowing in y direction only. The resistance of solution chamber in x direction is included in r. Electric current flowing through it is called J_{cell} with the unit of [A]. Its physical meaning is local electric current in y direction. J_{cell} tends to accumulate itself from the center of active surface to the both ends (the inlet and outlet of electrolyte solution) and reaches its maximum at both ends. J_{cell} dividing the area it flows through is local current density in y direction j_{cell}. At the entrance and exit of electrolyte solution j_{cell} reaches its maximum.

(3) $\rho_{trans.}$: represents the resistance as transition between solution chamber and solution channel as shown in figure 5.4. This area is out of active surface, meaning electric current flows only in y direction. Electric current flowing through it is the maximum J_{cell} flowing its nearby solution chamber. $j_{trans.}$ represents the local current density flowing through $\rho_{trans.}$.

[1] Sometimes r represents only the resistance of electrolyte solution when electric current is flowing in x direction in electrode chambers.

(4) R: represents the resistance of solution channel. In REDBP there are 4 different solutions: sea water, acid, base and Na_2SO_4. The resistance of Na_2SO_4 depends primarily[1] on the length and diameter of its pipe, therefore, the usage of a long and small tube can also eliminate the influence of Na_2SO_4 solution. Electric current flowing through it is $I_{channel}$. With increasing stack size (meaning how many single cells inside of one stack), the number of bypass connections increase. Therefore, $I_{channel}$ tends to accumulated itself by collecting more J_{cell} from electrode chamber to the middle of stack and reaches its maximum at the middle of stack. Please note that the pumps serve as breakpoints. Thus, there is no parasitic current flowing through them.

(5) E: represents the EMF of single cell. In this thesis, $OCV_{SC\_meas.}$ (Chapter 2) is used as E in order to fulfil the simplifications requirement of equivalent circuit.

(6) $E^{electrode}$: represents the voltage drop in electrode chambers.

(7) $E^{external}$: represents the external constant voltage source for calculating charging or discharging process. By charging process $E^{external}$ is larger than OCV_{Stack}, while by discharging $E^{external}$ is smaller than OCV_{Stack}.

Table 5.1 shows the parameters for simulation REDBP stack. All parameters are chosen according to single cell experiment (Chapter 2) and structure of testing stack. Simulation (Appendix C) using MatLAB/Simulink will calculate the electric potential and electric current of all important points such as all nodes and the point between two resistances as shown in figure 5.5.

[1] Concentration of Na_2SO_4 is always 0.25M.

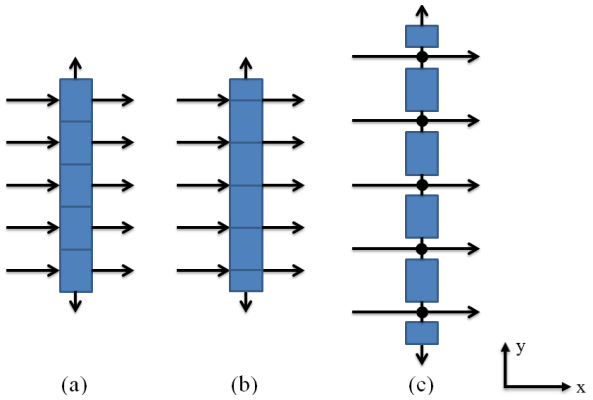

Figure 5.3: Discretization of resistance of solution chamber when electric current flows in y direction, arrows are electric currents and blocks are finite elements of electrolyte solution. Discretization number in x direction is 5 while in y direction 1. (a): Solution chamber is divided into 5 parts. (b): Discretization equivalent to (a) but with two smaller parts at the both ends. (c): Transforming (b) into electrical circuit in each point KCL easily applies. Please note that this figure illustrates electric current flowing in y direction only. The resistance of solution chamber in x direction is included in r.

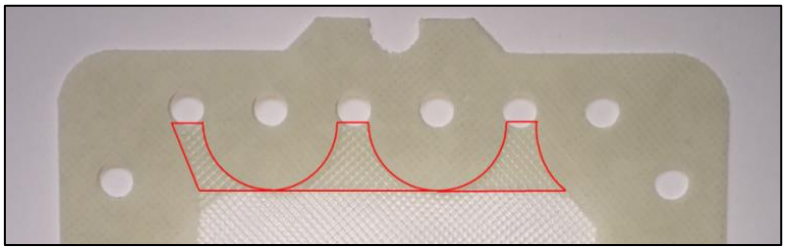

Figure 5.4: Transitions between solution chamber and solution channel.

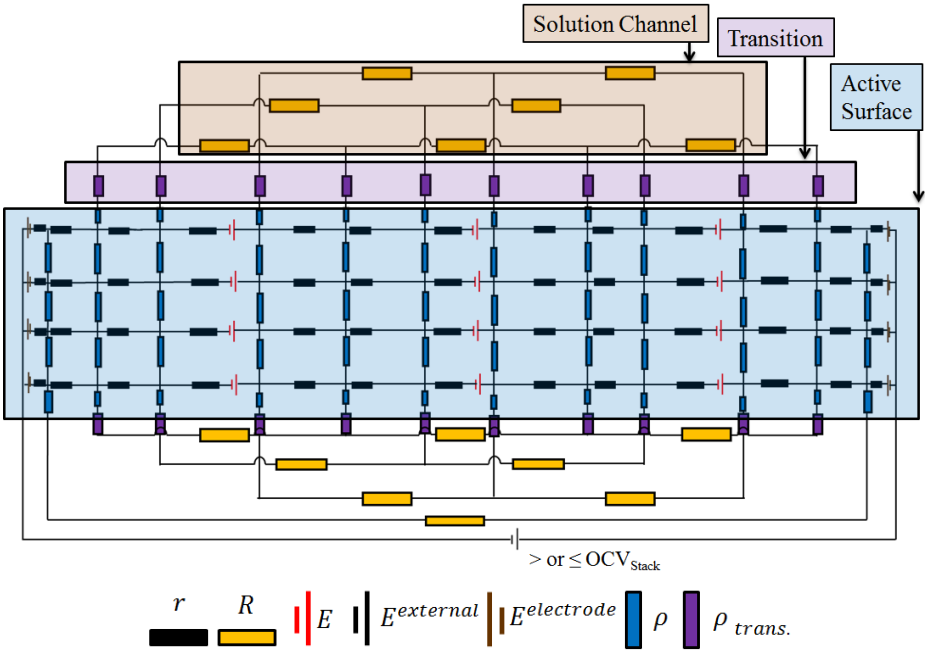

Figure 5.5: Three main blocks of 2D equivalent circuit of REDBP stack with 3 single cells. Active surface, solution channel, and transition which connects the former two.

Table 5.1: Parameters for simulation of REDBP stack.

		0.25M	**0.5M**	**0.75M**	**1M**
Area Resistance ($10^{-4}\Omega\cdot m^2$)	AEM	6.14	3.64	2.21	1.39
	BP	2.6	2.03	2.16	2.56
	CEM	4.68	2.34	1.31	1.06
Resistivity ($\Omega\cdot m$)	HCl	0.105	0.055	0.039	0.030
	NaCl		0.236		
	NaOH	0.206	0.107	0.077	0.059
	Na_2SO_4	0.306			
$\rho_{trans.}$ (Ω)	HCl	120.7	63.6	44.2	34.6
	NaCl		270.6		
	NaOH	236.4	123.4	87.9	68.2
ρ[a] (Ω)	HCl	260.5	138.5	96.3	75.3
	NaCl		588.8		
	NaOH	514.4	268.5	191.3	148.5
	Na_2SO_4[b]		39.5		
r ($m\Omega$)	Na_2SO_4/CEM/NaCl[b]		252		
	HCl/BP/NaOH[c]	34.7	24.8	24.8	28.1
	NaOH/CEM/NaCl	59.2	33.0	21.9	18.9
	NaCl/AEM/HCl	71	44.6	29.8	21.4
R[d] (Ω)	HCl	1.38	0.73	0.51	0.40
	NaCl		3.09		
	NaOH	2.70	1.41	1.00	0.78
	Na_2SO_4[e]		$3.14\cdot10^4$		
EMF (V)	Na_2SO_4/CEM/NaCl		0		
	HCl/BP/NaOH[f]	0.709	0.738	0.757	0.775
	NaOH/CEM/NaCl		0		
	NaCl/AEM/HCl		0		
Thickness (mm)	Electrode Chambers		10		
	Other Chambers		0.5		
	AEM		0.13		
	BP		0.22		
	CEM		0.13		
Diameter of solution channel (mm)	HCl		8		
	NaCl		8		
	NaOH		8		
	Na_2SO_4		8		

a) This is the resistance of the whole solution chamber before discretization.

b) Thickness of electrode chamber of testing stack is 10mm.

c) Due to the problem of water transport, the resistance of BP will not decrease with increasing concentration of HCl and NaOH.

d) R is calculated by averaging the resistances of three inlet (or outlet) channels. See Figure 5.5.

e) Na_2SO_4 is flowing in a pipe of 5m long, therefore, the calculated R is much bigger than that of other solutions.

f) From single cell OCV experiment, please check section 2.3.1. All the OCVs of other IEMs between different solutions are neglected.

5.3 Simulation Result

There are many interesting results. In order to understand the detailed performance inside of stack conveniently, all the important information are put into 4 major diagrams. They are a) distribution of voltage in electrolyte solution, b) distribution of voltage difference between BP, c) distribution of currents and current densities and d) distribution of voltage throughout stack. Since section 5.4 is based on these 4 diagrams, in the following section, these 4 diagrams will be introduced.

5.3.1 Distribution of Voltage in Solution

Figure 5.6 illustrates the distribution of voltage in solution of 1M 20 cells stack with active surface of 100 cm^2 by open circuit. Each grid is calculated voltage of each important point in figure 5.5. The discretization number in x direction is 50 and in y direction 1, so the middle 50 rows are within the active surface. The color of negative electrode is dark blue which represents 0V in the figure while the positive electrode is dark red with calculated voltage of 14V. The two rows which are adjacent but out of active surface are the edges of active surface which connect the transition. In this thesis, this area is called inlet/outlet of solution chamber. The row near the inlet/outlet but not in active surface is the electric potentials inside of solution channels. This row is a combination of all solution channels including HCl, NaOH and NaCl. That is the reason why every third grid has similar color. In order to investigate the electric potential distribution inside of each solution channel, three additional rows are added above it near outlet (below it near inlet) and their meanings are labelled in figure 5.6.

Since one of the main assumptions is ideal mixing which dictates no difference between inlet solution and outlet solution, the distribution of voltage in solution chambers in this thesis is (almost[1]) symmetric around the center of active surface. Each row inside of active surface represents the pathway in which ΔI_{cell} is flowing. The very first and very last column represent the platinum electrode plates. For the rest of the columns, each represents the voltage distribution inside of one solution chamber. Between each column is an IEM. In every three columns the color will change significantly. This is due to EMF inside of BP interface. Therefore, the location of the sharp color change is the position of BP. Assuming the descriptions of figure 5.6 are clear, the discussion will proceed:

[1] 'Almost' is due to the existence of Na_2SO_4. Since pumps are serving as breakpoints as shown in figure 5.5, the distribution of voltage in solution chambers in this thesis is almost symmetric around the center of active surface.

(1) The color difference between channel and inlet/outlet is huge. That is due to the high resistance of $\rho_{trans.}$which is the way the shunt current must pass. Normally $\rho_{trans.}$ is very high. However, due to the stacking-up voltage between two electrodes and high conductivity of solution channel, shunt current cannot be avoided. The detailed discussion about $\rho_{trans.}$ will be in section 5.4.7.

(2) Bypass connection is the main reason for the existence of shunt currents and nonhomogeneous distribution of voltage. Electric current tends to flow from the higher electric potential to the lower electric potential. Therefore, $I_{channel}$ exists with the direction from positive electrode to the negative electrode. In the case of figure 5.6, the electric potential in the solution channel near negative electrode is 5.2V while near positive electrode 8.6V. This more than 3V difference may cause electrolysis if transport of electron is possible. The detailed discussion about channels is in section 5.4.8.

(3) The voltage distribution inside of one solution chamber (each column) is not homogeneous. J_{cell} exists inside of solution chamber, and flows in the direction from the center of active surface to the inlet/outlet near positive electrode and with the opposite direction near negative electrode.

(4) The significant color change inside of active surface is due to EMF inside of BP interface, but the sharpness declines from electrode side to the middle of stack, indicating a decrease of voltage between BP from electrode side to the middle of stack. As Chapter 2 and Chapter 3 introduced, a significant decline of voltage between BP is only due to either decreasing ionic concentration of acid and base or increasing discharging current density at constant temperature. The former is excluded by the assumption of ideal mixing. The latter implies an enhanced shunt current (as discharging current) in the middle of stack inside of active surface, especially near the inlet/outlet.

Since shunt current has influence on the performance of BP, a diagram of the distribution of voltage difference between BP is of great interest.

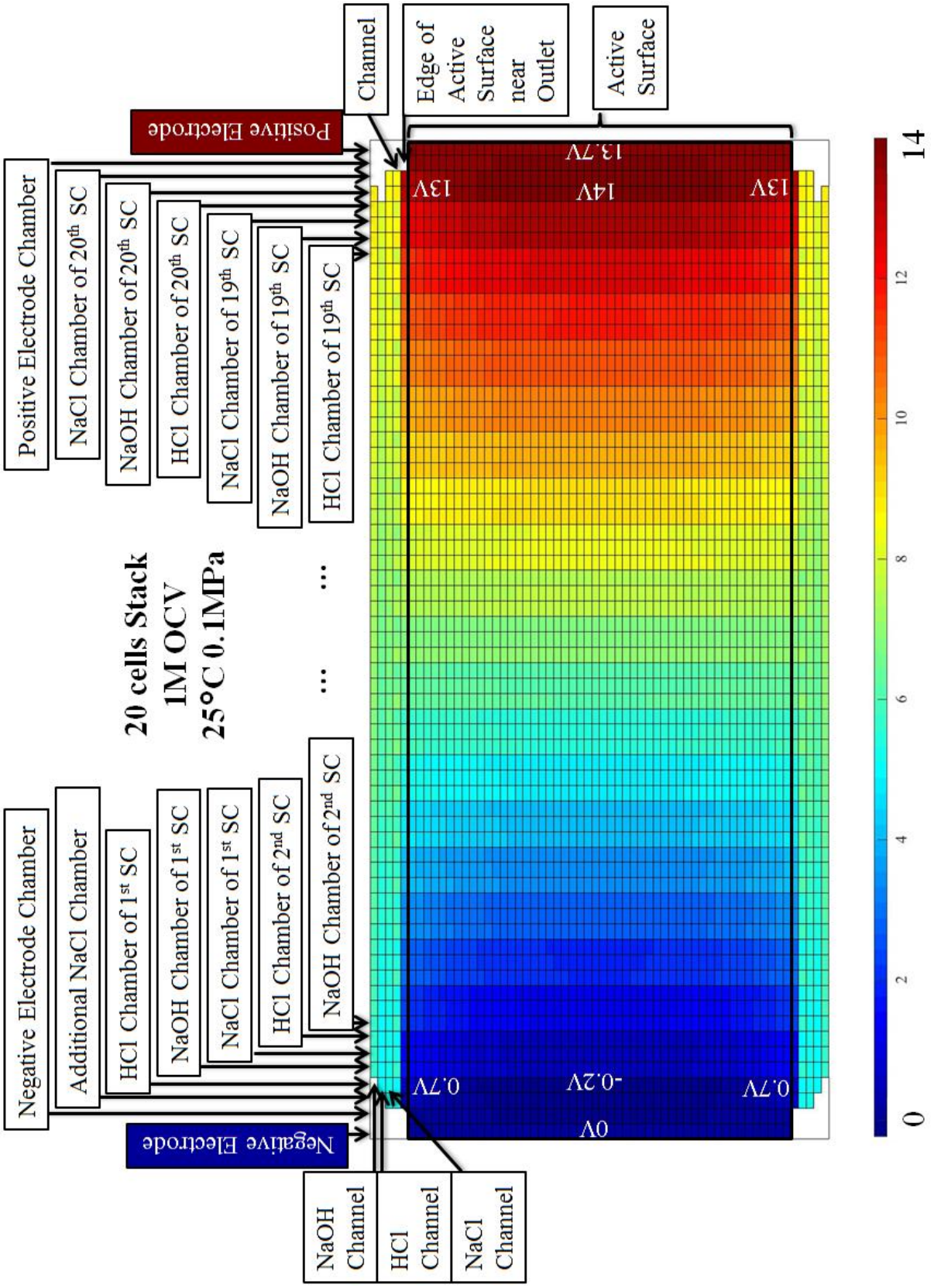

Figure 5.6: Distribution of voltage in solution of 1M 20 cells stack with active surface of 100cm^2 by open circuit. Discretization number is 50. The color of dark blue represents 0V while dark red 14V. Please note that the dimension of each small grid does not represent the real dimension of discretized stack. Each grid represents merely the electric potential at given point.

5.3.2 Distribution of Voltage Difference between BP

Due to the existence of shunt current inside of stack, the voltage difference between BP inside of stack is not homogenously distributed. Figure 5.7 illustrates the distribution of voltage difference between BP inside of REDBP stack. Each column is one piece of BP. Black color represents the highest voltage and white color the lowest. From this figure the following two points can be concluded:

(1) Inside of the same row which is the pathway ΔI_{cell} is flowing, the voltage difference between BP in the middle of stack is always the lowest due to enhanced shunt current in the middle of stack.

(2) For each BP, normally the voltage difference between it declines from the center of active surface to the inlet/outlet. The exceptions happen to the one or two BPs near electrodes. Figure 5.8 is an explanation of this phenomenon. The white arrows are electric current inside of stack. Point 'a' is a normal case, where electric currents are flowing from the top (channel) and the left (negative electrode side) to the bottom (center of active surface) and the right (middle of stack). However, at point 'b' in NaOH chamber, there is no current flowing from the left. Moreover, the electric potential of negative electrode is always 0V and there is no electrical resistance of platinum electrode plate[1]. Therefore, at point 'b' an electric current exists running towards negative electrode. This current is passing through BP and its direction is the same as the direction of charging current. Although there is no water-splitting process simply because the voltage difference is still under 0.828V, this current is raising the voltage difference between BP at point 'b' (see section 2.3.2). That is the reason the voltage difference between BP near electrode at inlet/outlet is higher than single cell OCV.

Distribution of voltage difference between BP is very important for analyzing not only the significance of shunt current at different position inside of stack, but also the Ch/DisCh condition of BP, which will be investigated more thoroughly in section 5.4.3.

[1] In this thesis, the electrical resistance of electrode plate is assumed to be zero.

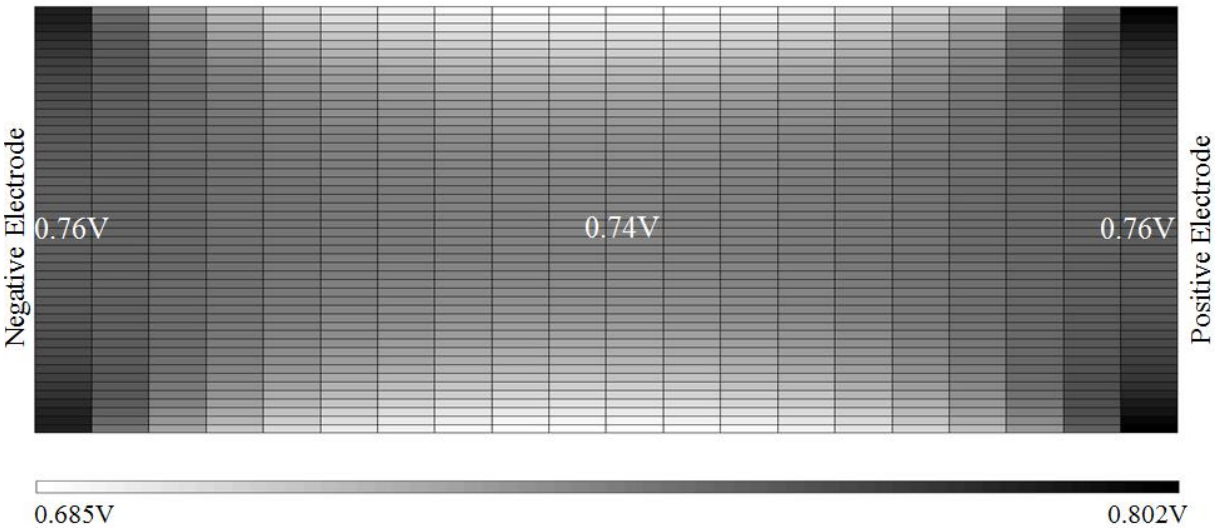

Figure 5.7: Distribution of voltage difference between BP inside of REDBP stack of 1M 20 cells with active surface of 100cm^2 by open circuit. Discretization number is 50. Black color represents the highest voltage and white color the lowest.

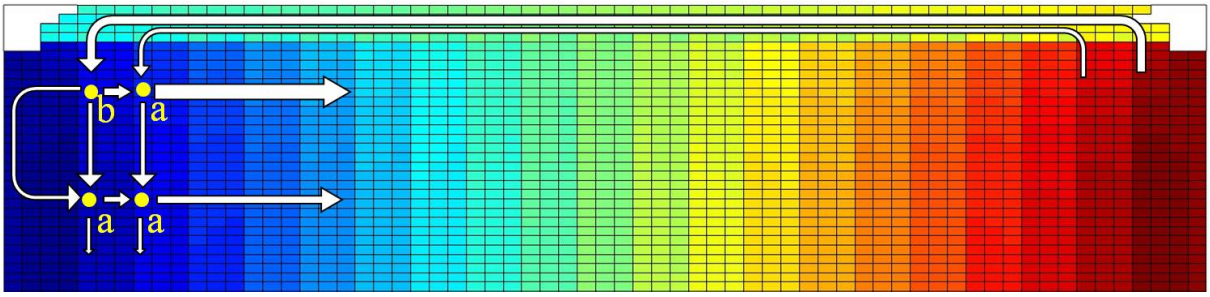

Figure 5.8: Schematic explanation of high voltage difference between BP near electrode at inlet/outlet. Point ‘a’ is normal case. Point ‘b’ is special case located near electrodes at inlet/outlet.

5.3.3 Distribution of Currents and Current Densities

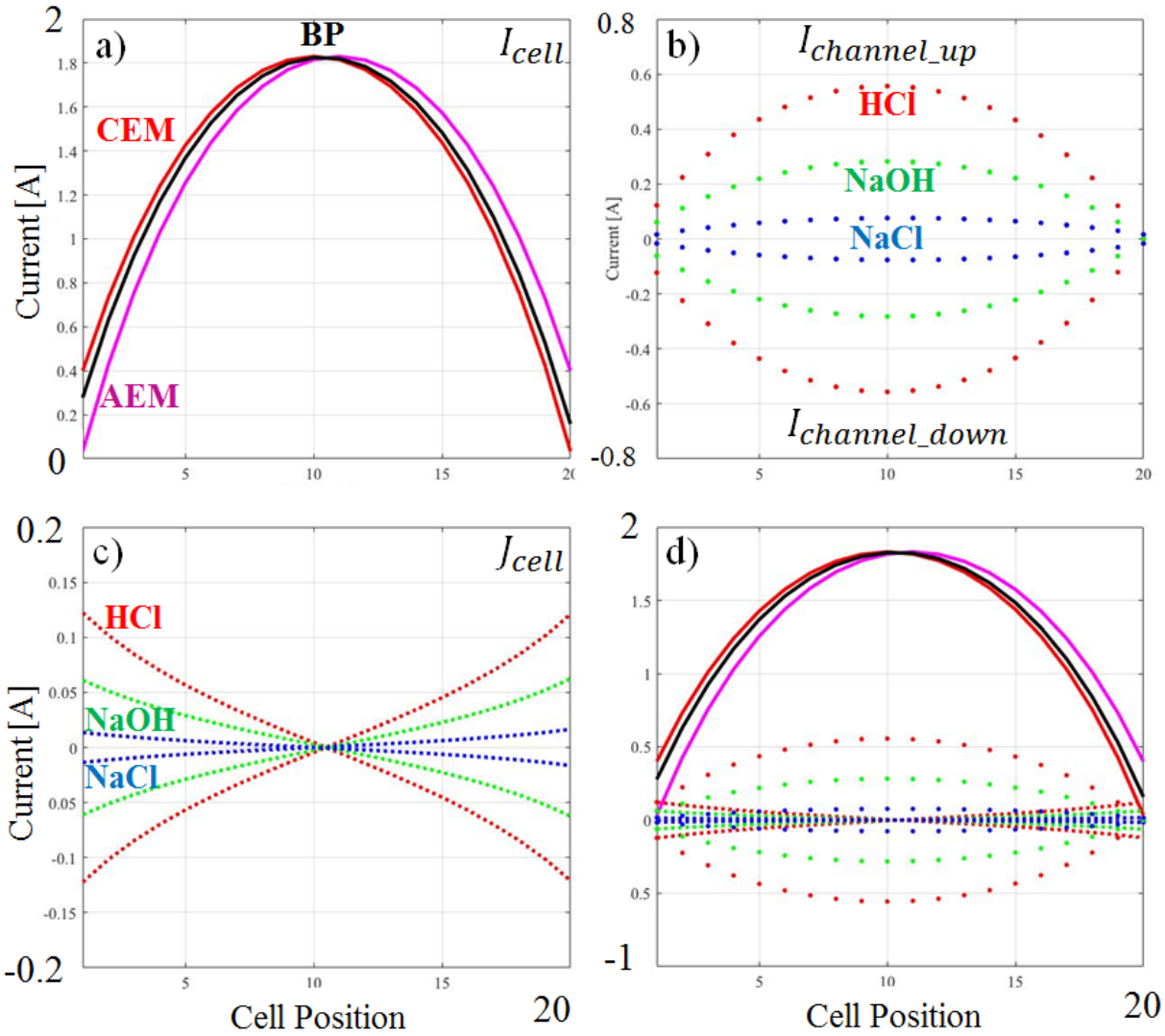

Figure 5.9: Distribution of electric currents inside of stack of 1M 20 cells with active surface of 100cm^2 by open circuit. Discretization number is 50. a), b) and c) are merely separate diagrams from d). In d) the above three solid lines which look like arch bridges, are the distribution of I_{cell} passing through three IEMs. Red, black and purple solid lines are electric currents I_{cell} passing through CEM, BP and AEM, respectively. The dots are the distributions of $I_{channel}$. The dashed lines are distributions of J_{cell}. Red, green and blue represent electric current in HCl, NaOH and NaCl solution, respectively.

As previously introduced, there are three different currents existing inside of stack. By putting them into one diagram, the distribution of currents is obtained as shown in figure 5.9. Please note that the definition of positive current is from left to right or from bottom to top inside of stack.

(1) I_{cell}: The above three solid lines which look like arch bridges, are the distribution of I_{cell} passing through three IEMs in x direction inside of active surface. Red, black and

purple solid lines are electric currents I_{cell} passing through CEM, BP and AEM, respectively. Due to the gathering of J_{cell}, each I_{cell} reaches its maximum in the middle of stack. The reason why these three curves do not overlap is because the definition of single cell is manmade to investigate the behavior of REDBP stack: That means the x-axial of figure 5.9 cannot represent the real 'geographic location' of REDBP stack. On the left side of figure 5.9, I_{cell} of CEM is higher than that of BP or AME because CEM of the first single cell is the third IEM of the first single cell and the fourth IEM of REDBP stack. Due to shunt current accumulating from electrode to the middle of stack, I_{cell} of CEM is higher than the I_{cell} flowing through the other two IEM in the same single cell near negative electrode.

(2) $I_{channel}$: The dots are the distributions of $I_{channel}$, which are the electric currents passing through solution channels in x direction outside of active surface. Red, green and blue represent electric current in HCl, NaOH and NaCl solution, respectively. The dots with positive value are $I_{channel}$ in upper channel connecting the outlet of each solution chamber, while the dots with negative value are $I_{channel}$ in lower channel connecting the inlet of each solution chamber. According to the definition of direction of current, all $I_{channel}$ should be negative. But in order to investigate the difference[1] between inlet and outlet, the $I_{channel}$ in upper channel is dictated as positive. Moreover, putting $I_{channel}$ in upper channel above 0 will give a more intuitive and obvious feeling about the significance of shunt currents: The bigger difference between $I_{channel\_up}$ and $I_{channel\_down}$, the bigger the maximum shunt current will be. $I_{channel}$ has the same problem as I_{cell}- the definition of single cell. Even worse, $I_{channel}$ is in channel which serves as a bridge between two chambers. Therefore, the number of $I_{channel}$ is one less than the number of I_{cell} or J_{cell}. Nevertheless, by open circuit, the following relation can be roughly obtained according to Kirchhoff's current law (see section 5.1.1):

$$\left|I_{channel}^{HCl}(x) + I_{channel}^{NaOH}(x) + I_{channel}^{NaCl}(x)\right| \approx \left|I_{cell}^{CEM\ or\ AEM\ or\ BP}(x)\right| \qquad \textbf{(5.8)}$$

where $I_{channel}$ is the sum of both $I_{channel\_up}$ and $I_{channel\_down}$, I_{cell} is the current flowing through the active surface of IEM, and x is the cell position.

(3) J_{cell}: The dashed lines are the maximum electric currents passing through solution chamber in y direction, which means the J_{cell} near inlet/outlet. Red, green and blue

[1] Although this thesis is neglecting the difference between inlet and outlet, it is still very important for future researchers.

represent electric currents in HCl, NaOH and NaCl solution, respectively. According to equation 5.4, electric current should be proportional to electric potential gradient. The reason why the absolute value of J_{cell} declines from electrode to the middle of stack is due to the decrease of the voltage difference between BP from the electrode to the middle of stack. $I_{channel}$ accumulate itself by collecting J_{cell} of each solution chamber, and a relation can be obtained:

$$I_{channel}^{solution}(x) = \sum_{x=1}^{x} J_{cell}^{solution}(x) \quad \textbf{(5.9)}$$

where $x <$ stack size, and solution can be either HCl, or NaOH, or NaCl. Please note that J_{cell} will gradually change its direction from negative electrode chamber to positive electrode chamber, therefore, $I_{channel}$ reaches its maximum in the middle of stack.

By dividing current with the area of finite element which this current is passing through, the local current density is obtained. Figure 5.10 illustrates the distribution of current densities both in electrolyte solution (the top three diagrams) and in IEMs (the bottom three diagrams).

In diagrams of electrolyte solution (the top three diagrams in figure 5.10), the solid lines are distributions of j_{cell} near inlet/outlet. The dots are $i_{channel_down}$and $i_{channel\_up}$. The dashed lines are the maximum $j_{trans.}$, which are near channels (section 5.4.7). By open circuit due to shunt currents, the maximum $j_{trans.}$ near electrode chamber is up to 10000A/m^2, which is very high. With increasing charging current density, the maximum $j_{trans.}$ increases as well. Consequently, attention should be paid on the safety issue. Due to the different conductivity of HCl, NaOH and NaCl, the magnitudes of shunt current flowing through each solution are not equal. By 1M acid/base solution, more than 60% of shunt current is flowing through HCl, more than 30% through NaOH, less than 10% through NaCl (section 5.4.2).

In diagrams of IEMs (the bottom three diagrams in figure 5.10), the current density is not homogeneously distributed in IEM. The distribution of current density becomes more and more non-homogeneous from the center of active surface to the inlet/outlet of solution chamber. The diagram of BP can explain the behavior of the distribution of voltage difference between BP as shown in figure 5.7.

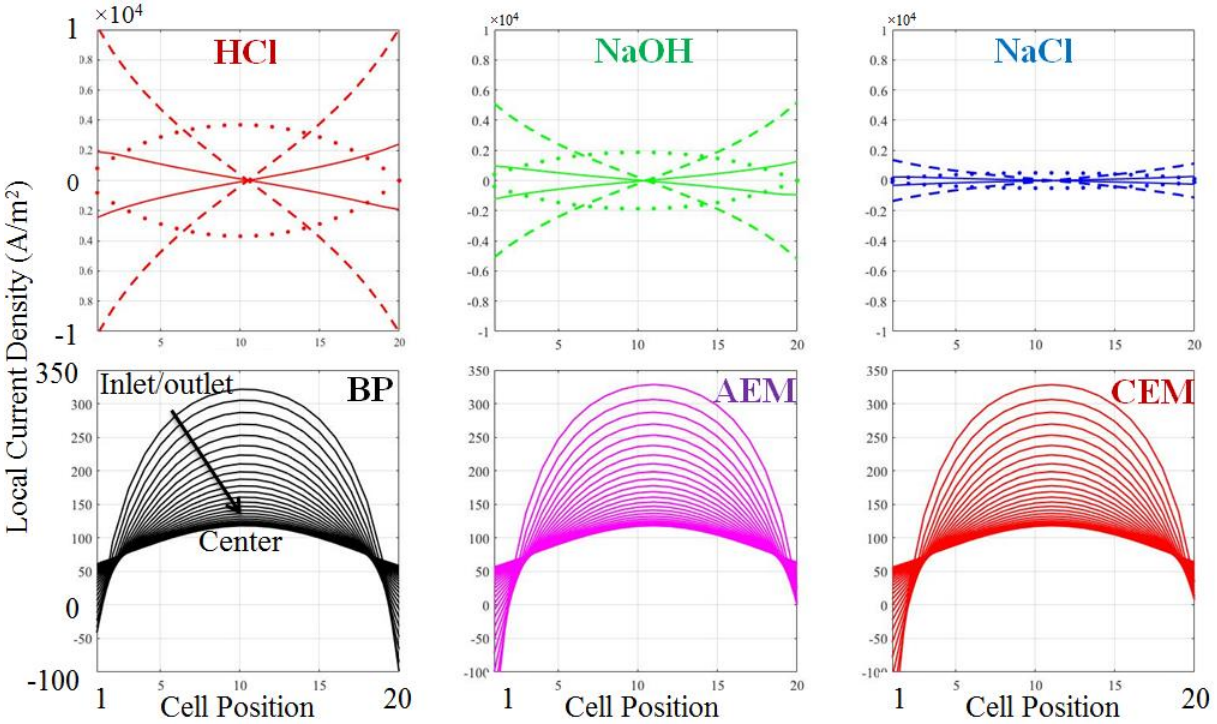

Figure 5.10: Distributions of current densities inside of stack of 1M 20 cells with active surface of 100cm^2 by open circuit. Discretization number is 50. The first three diagrams are the distributions of current densities in electrolyte solution. The solid lines are j_{cell} near inlet/outlet. The dots are $i_{channel_down}$and $i_{channel\_up}$. The dashed lines are the maximum $j_{trans.}$. Red, green and blue represent HCl, NaOH and NaCl solution, respectively. The lower three diagrams are the distributions of local current densities in IEMs. Black, purple and red represent current densities through BP, AEM and CEM, respectively. The distribution of local current densities through IEM becomes more non-homogenous from the center of active surface to the inlet/outlet of solution chamber.

5.3.4 Distribution of Voltage throughout the Stack

Figure 5.11 illustrates the distribution of local single cell voltage and the voltage of sum of all local single cells inside of 1M 20 cells stack with active surface of 100cm^2 by open circuit.

The blue lines are the distributions of local single cell voltage along the same row of figure 5.6. Each line is the pathway in which ΔI_{cell} is flowing. The distribution of local single cell voltage becomes more non-homogeneous from the center of the active surface to the inlet/outlet of solution chamber. This behavior is one of the consequences of shunt currents flowing through IEMs. Shunt currents do not only affect the performance of BP, but also the performance of single cell as a whole. The shunt currents (which can be treated as self-discharging currents) flowing through three solution chambers and the other two IEMs will create additional voltage

drop. The blue dashed line is the measured single cell voltage[1]in single membrane experiment. Almost all simulated single cell voltage is below measured single cell voltage. The exceptions happen to the first 1 or 2 BP near electrode, which has been explained previously (section 5.3.2).

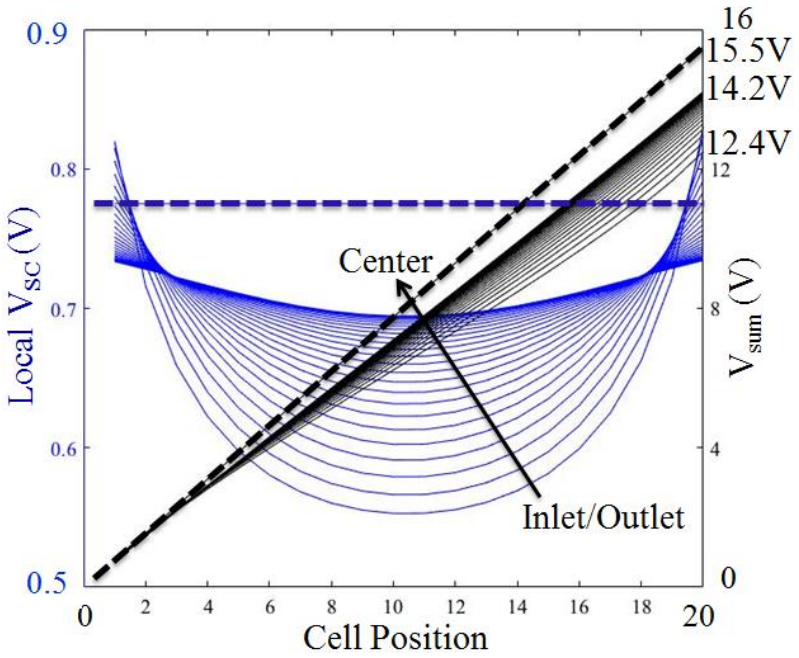

Figure 5.11: Distribution of local single cell voltage and the voltage of sum of all local single cells inside of stack of 1M 20 cells with active surface of 100cm^2 by open circuit. The blue solid lines are the distributions of local single cell voltage along the same row of figure 5.6. The blue dashed line is the measured single cell voltage from Chapter 2. The black dashed line is stack size multiplying measured single cell voltage. The black solid lines are the distributions of sum of all local single cells along the same row of figure 5.6.

The black dashed line is stack size multiplying measured single cell voltage. The black lines are the distributions of the voltage of sum of all local single cells along the same row of figure 5.6. Shunt currents cause non-homogeneous distribution of voltage inside of stack. Stack voltage varies from the center of active surface to the inlet/outlet. In the case of 1M 20 cells stack with active surface of 100cm^2 by open circuit, this variation can be up to 1.8V. This is one of the most important meanings of this diagram: Measurement of stack voltage has direct relation with measuring points. For example, if two measuring points are exactly pinpointing the center of active surface, the measured stack voltage should be 14.2V; If two measuring points are exactly pinpointing the surface of IEM near inlet/outlet of solution chamber, the measured stack voltage should be 12.4V; If the positions of measuring points are unknown, the measured stack voltage should be anywhere between 12.4V and 14.2V.

[1] In this case it is 0.775V

5.4 Discussion

In the previous section, all the important simulation results are formulated into 4 diagrams. Those are the a) distribution of voltage in solution, b) the distribution of voltage difference between BP, c) the distribution of currents and current densities, as well as d) the distribution of voltage throughout the stack. In this section, many influential parameters will be investigated and analyzed according to those 4 diagrams.

5.4.1 Discretization

The physical meaning of discretization is transferring continuous models and equations into discrete counterparts. The bigger the number of discretization, the smaller the dimension of finite element will be, and the higher accuracy of simulation results will be. Figure 5.12 illustrates three distributions of voltage difference between BP of 20 cells stack with active surface of 100cm^2 by open circuit with discretization number of 10, 50 and 200. Discretization number of 10 means the active surface of BP has been divided into 10 pieces equally, the height of each element is 10mm. Therefore, discretization number of 50 or 100 means the height of each element is 2mm or 0.5mm, respectively. According to figure 5.12, it is obvious that bigger number of discretization leads to more accurate simulation results. This can be observed also in Figure 5.13, which shows three distributions of voltage in solution of 20 cells stack with active surface of 100cm^2 by open circuit with discretization number of 10, 50 and 200.

Since currents inside of REDBP stack are not homogeneously distributed, bigger number of discretization will lead to more polarized results, meaning bigger difference between the highest and the lowest value. Figure 5.14 shows this phenomenon - the bigger number of discretization, the more non-homogeneous distribution will be, and the bigger difference between the highest and the lowest value will be.

By considering both accuracy and time consumption of simulation, the number of discretization is fixed at 50, meaning each finite element has 2mm of height.

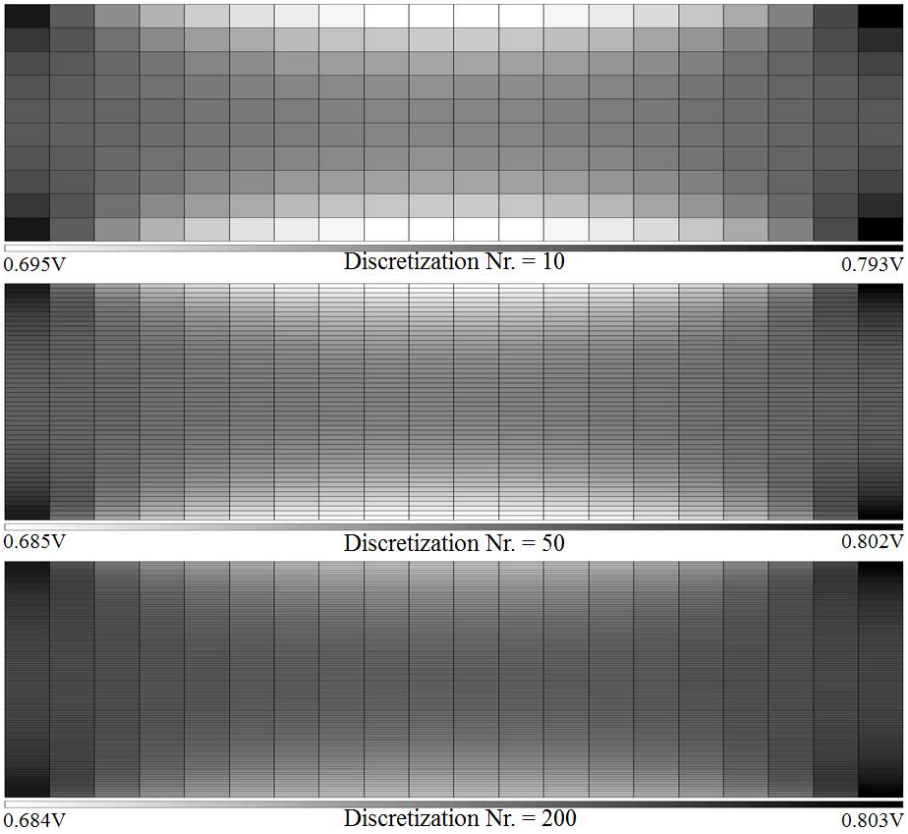

Figure 5.12: Distributions of voltage difference between BP of 20 cells stack with active surface of 100cm^2 by open circuit with discretization number of 10, 50 and 200.

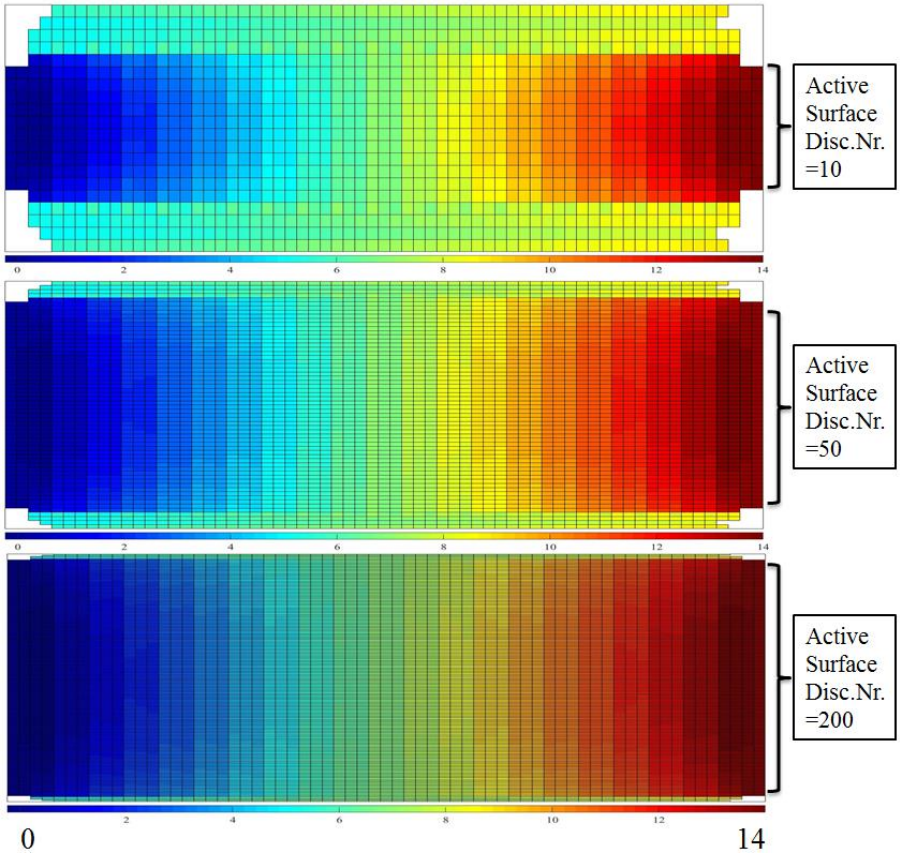

Figure 5.13: Distributions of voltage in solution of 20 cells stack with active surface of 100cm^2 by open circuit with discretization number of 10, 50 and 200.

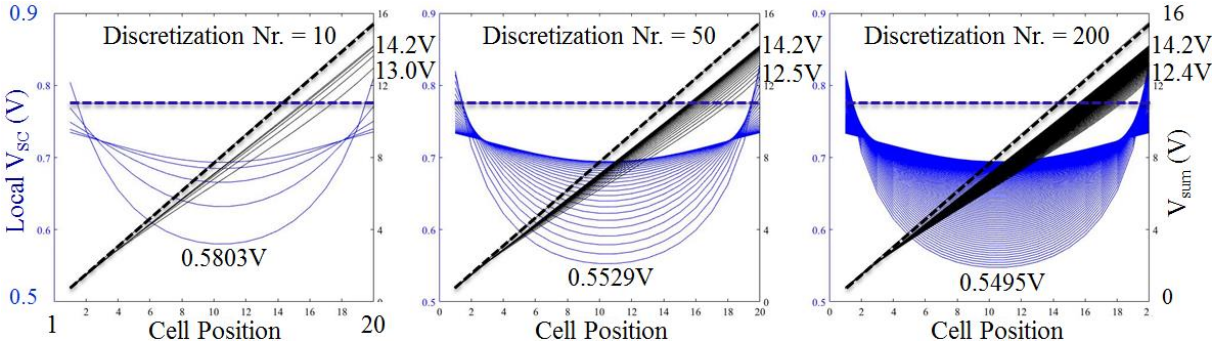

Figure 5.14: Distributions of local single cell voltage and the voltage of sum of all local single cells inside of stack of 1M 20 cells with active surface of 100cm^2 by open circuit with discretization number of 10, 50 and 200.

5.4.2 Ionic Concentration

Ionic concentration determines not only the EMF of single cell, but also the conductivity of both electrolyte solution and IEMs inside of REDBP stack. Figure 5.15 illustrates the increasing shunt current with increasing concentration of HCl and NaOH. Please note that the concentration of NaCl remains constant at 0.5M. The cake charts below illustrate the magnitude of maximum shunt current of each case as well as the share of each solution. Due to the high conductivity of HCl, more than half of the shunt currents are flowing through HCl channels. Therefore, the strategies for reducing shunt current and avoiding accident due to shunt current should be focusing on HCl channels.

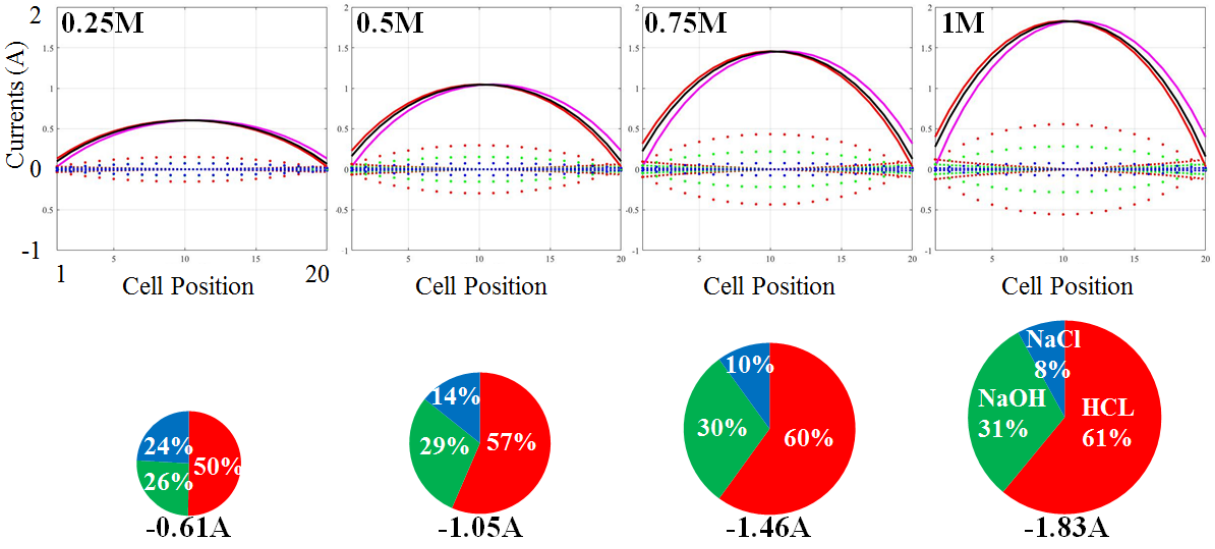

Figure 5.15: Distributions of currents inside of 20 cells stack with active surface of 100cm^2 by open circuit with discretization number of 50 with increasing ionic concentration. The four cake charts illustrate the magnitude of maximum shunt current of each case.

5.4.3 Charging/Discharging

Both by charging and discharging, the external current exists. In this thesis, positive current means charging current while negative current means discharging current. In this section, charging process and discharging process will be discussed separately.

Charging

Figure 5.16 illustrates the distributions of currents inside of 1M 20 cells stack with active surface of 100cm^2 by charging. The detailed explanations of the figures are in section 5.3.3. Please note that $V_{Electrode}$ is the voltage between two electrodes in mathematical model. In reality, electrochemical reactions in electrode chambers require additional 2V, which is not included in $V_{Electrode}$. $I_{External}$ is the electric current in external circuit, and I_{Shunt} is the maximum shunt current inside of stack.

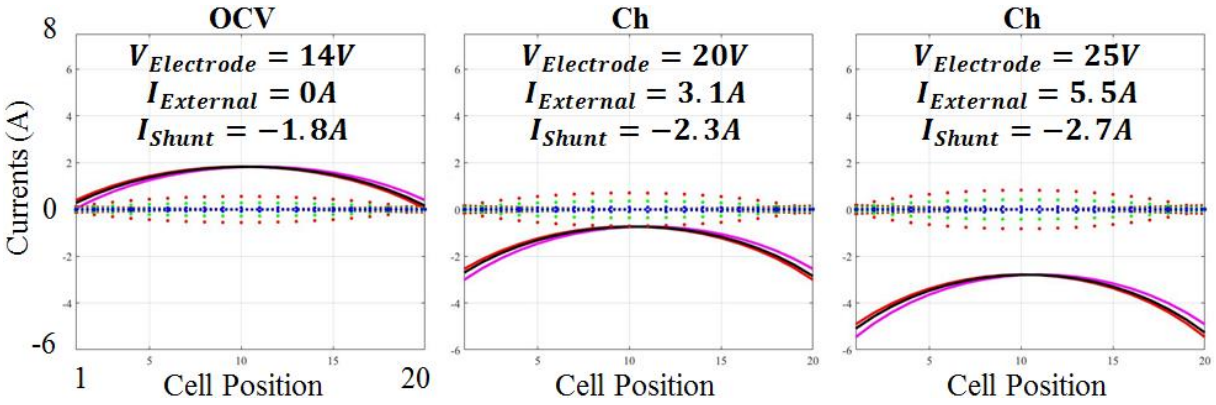

Figure 5.16: Distributions of currents inside of 1M 20 cells stack with active surface of 100cm^2 and discretization number of 50 by charging. $V_{Electrode}$ is the voltage between two electrodes in mathematical model. $I_{External}$ is the electric current in external circuit, and I_{Shunt} is the maximum shunt current inside of stack.

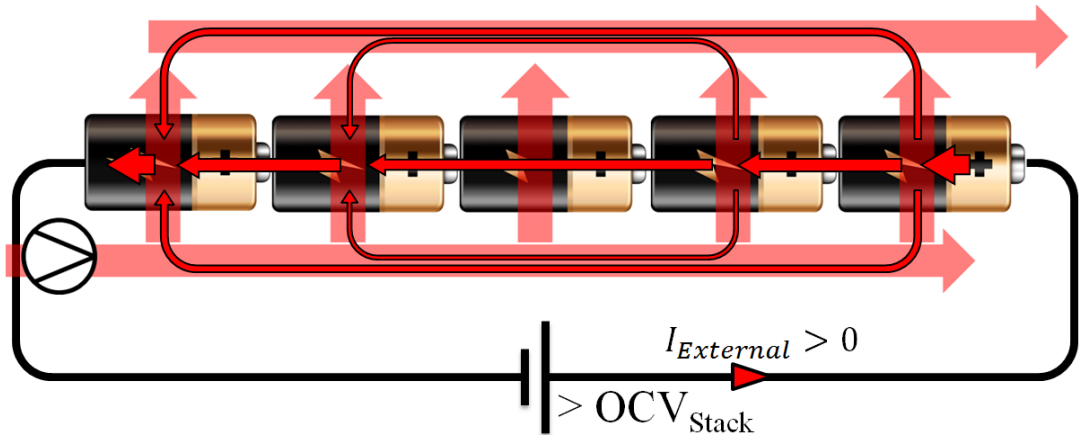

Figure 5.17: Schematic diagram of current distribution inside of REDBP stack by charging.

With increasing charging current $I_{external}$, the shape of I_{cell} does not change much, but its value becomes more negative. The former is due to the existence of shunt current, the latter is due to the definition of charging current being negative value inside of stack. These two phenomena can be explained by figure 5.17. External current will not flow through active surface totally. Some of it will flow through the bypass connections, in which case the shunt current becomes larger with increasing charging current density. This brings two important questions:

(1) What is the charging condition of each BP inside of stack?

(2) Will enlarged shunt current cause safety issue?

The first question is answered by figure 5.18 which is the distribution of voltage difference between BP by charging. $V_{Electrode} = 20V$ which does not include additional 2V for electrode chambers. According to simulation results, except for some area of the first 4 BPs near each electrode, almost all voltage differences between BP are under 0.828V which is regarded as the lowest charging voltage. That means, even by 20V between two electrodes without consideration of electrochemical consumptions in electrode chambers, most of the single cells inside of stack are under discharging condition (more specifically speaking, self-discharging condition). Increasing $V_{Electrode}$ will increase the chance for water-splitting reaction to happen inside of BP interface as shown in figure 5.19 with $V_{Electrode} = 25V$. However, enlarged shunt current will raise the attention on safety issues which will be introduced next.

The second question is answered by figure 5.20 which is the distribution of current densities inside of HCl solution of 1M 20 cells stack by charging. Please note that $V_{Electrode}$ is not including additional consumptions in electrode chambers. The detailed explanations of this figure are in section 5.3.3. Enough attention should be paid on the maximum current density in transition near electrode chamber. The maximum value of $j_{trans.}$ is up to 1.5A/cm^2 by charging process when $V_{Electrode} = 25V$.

It seems like charging process faces a lot of challenges of both efficiency and safety.

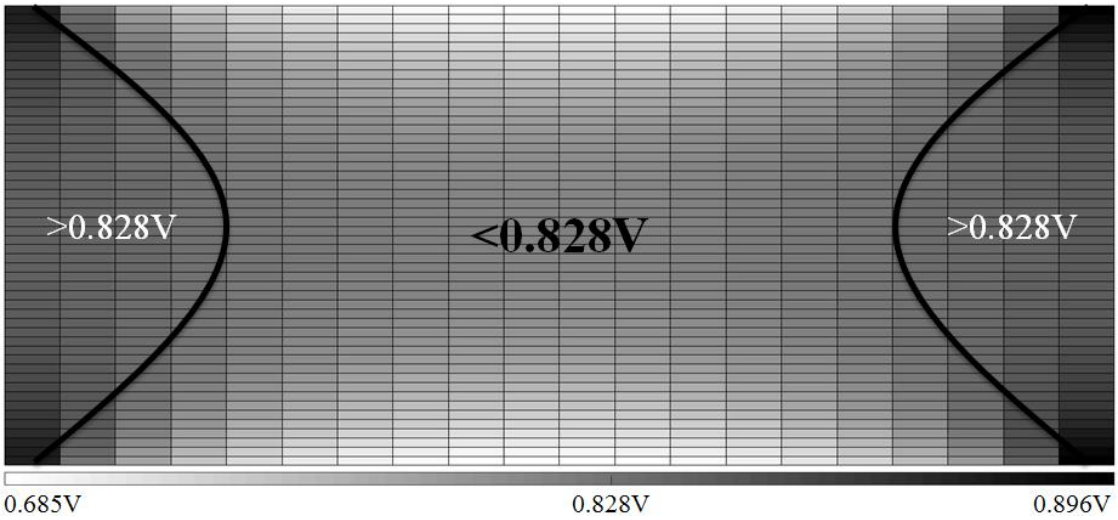

Figure 5.18: Distribution of voltage difference between BP of 1M 20 cells stack by charging. $V_{Electrode} = 20V$ which is not including additional 2V for electrode chambers.

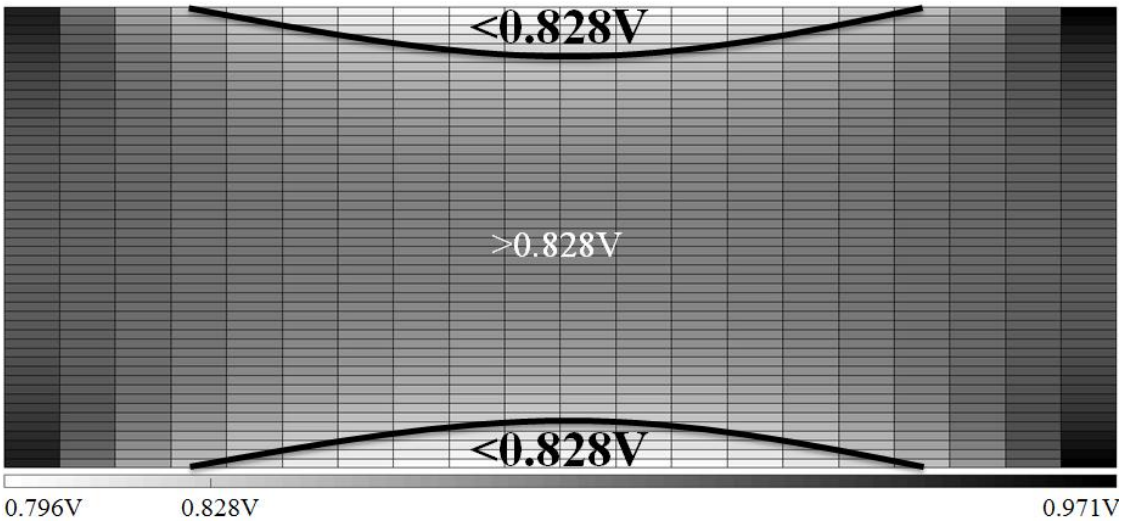

Figure 5.19: Distribution of voltage difference between BP of 1M 20 cells stack by charging. $V_{Electrode} = 25V$ which is not including additional 2V for electrode chambers.

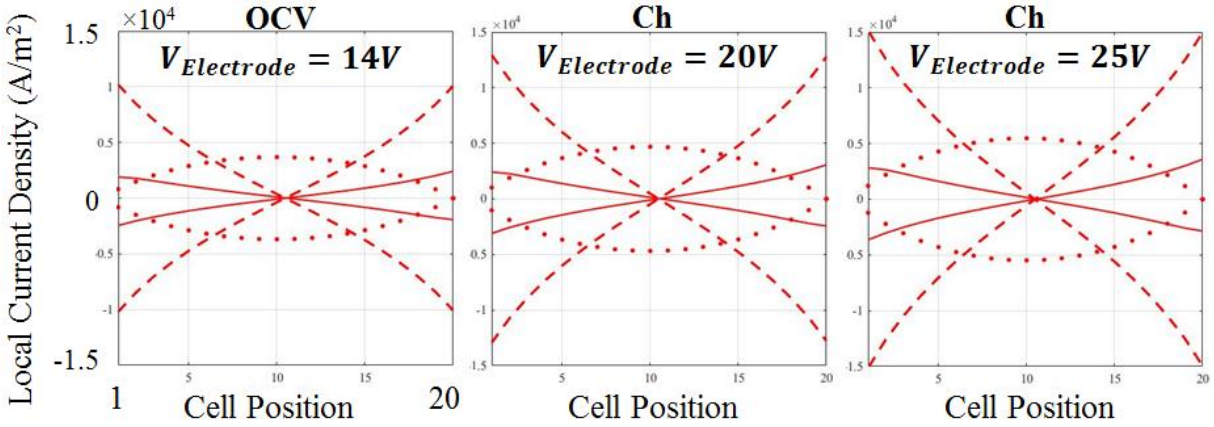

Figure 5.20: Distribution of current densities inside of HCl solution of 1M 20 cells stack by charging. Please note that $V_{Electrode}$ is not including additional consumptions in electrode chambers.

Discharging

Figure 5.21 illustrates the distributions of currents inside of 1M 20 cells stack with active surface of 100cm^2 by discharging. Please note that $V_{Electrode}$ is the voltage between two electrodes in mathematical model. In reality, electrochemical reactions in electrode chambers require another 2V, which is not included in $V_{Electrode}$. With decreasing $V_{Electrode}$ shunt current decreases as illustrated in Figure 5.22.

By consideration of both charging and discharging condition, REDBP is more suitable for discharging process, in which case most of I_{cell} transfer into external electric current. Moreover, charging process will elevate safety issue in transition near electrode chambers.

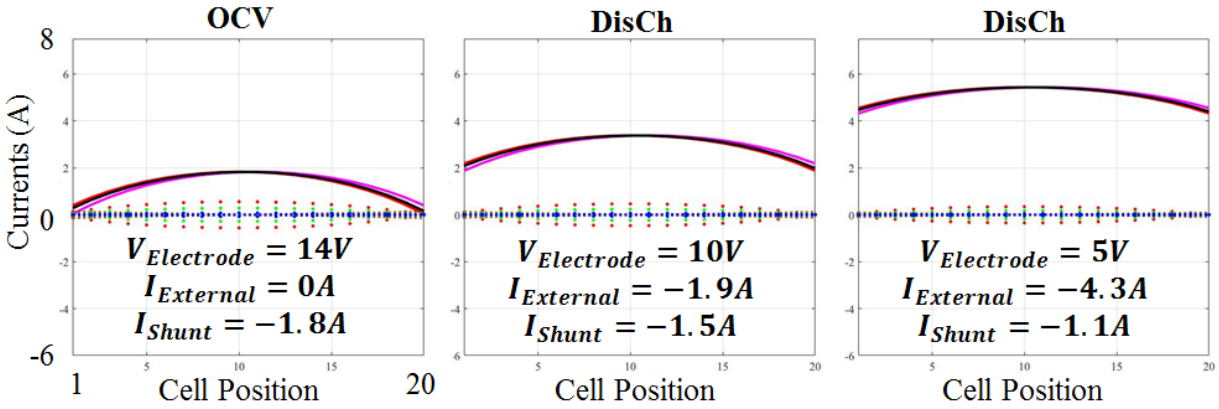

Figure 5.21: Distributions of currents inside of 1M 20 cells stack with active surface of 100cm^2 and discretization number of 50 by discharging. $I_{External}$ is the electric current in external circuit, and I_{Shunt} is the maximum shunt current inside of stack.

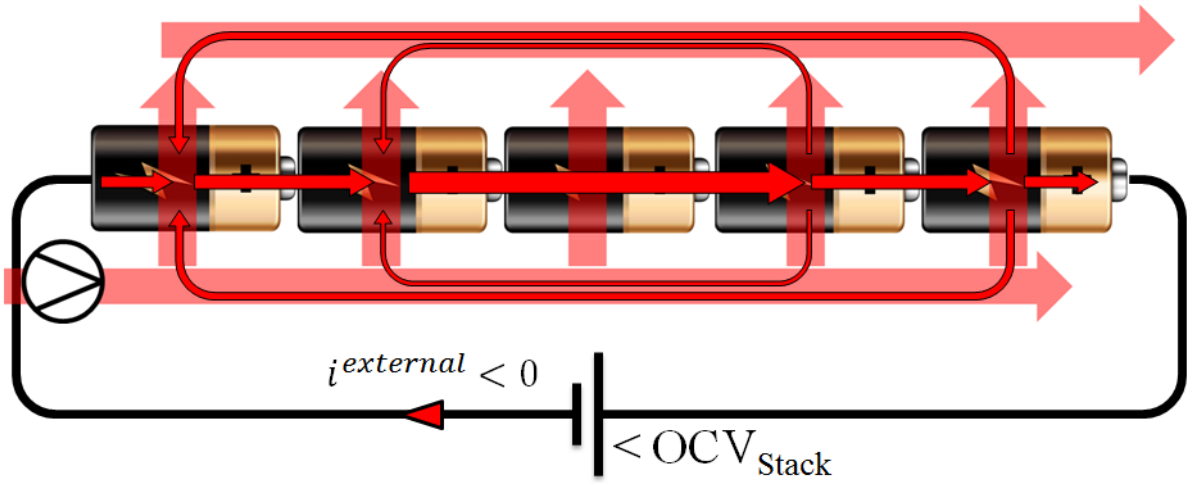

Figure 5.22: Schematic diagram of current distribution inside of REDBP stack by discharging.

5.4.4 Stack Size

Due to the additional necessary energy consumption in both electrode chambers (section 4.1.3), REDBP makes sense only with big stack. However, the stacking up electric potential and increasing number of bypass connections will lead to higher shunt current and its broader affecting area (number of affecting BPs), which elevates the attention on both efficiency and safety.

Figure 5.23 shows the distribution of currents inside of 1M stack with active surface of 100cm^2 by open circuit with increasing stack size. From 5 cells stack to 50 cells stack, the maximum shunt current (the height of the arch bridge in the figures) increases significantly. But from 50 cells stack to 100 cells stack, the affecting number of BPs increases more significantly (the top of the arch bridge becomes flat). Figure 5.24 illustrates the distribution of voltage in electrolyte solution (a) and the distribution of voltage difference between BP (b) of 1M 100 cells stack by open circuit. Due to shunt currents, almost all BPs have been affected. Many voltage differences between BP are around 0.66V, which is 100mV lower than OCV of BP in single membrane experiment. Moreover, shunt current is flowing throughout almost the whole stack, meaning additional voltage drop exists due to the resistance of AEM, CEM, and three solution chambers. That causes additional more than 100mV voltage drop for many each single cells. Therefore, in most cases, the single cell voltage inside of 100 cells stack is around 0.52V. Figure 5.25 shows that the distance between stack size multiplying OCV_{SC} of single membrane experiment (black dashed line) and the voltage of sum of all local single cells inside of stack (black solid line) is getting bigger with increasing stack size. In the figure of 100 cells stack, many single cells have only 0.52V. That causes the voltage of sum of all local single cells V_{sum} only 55V which 22V lower than stack size multiplying OCV_{SC} of single membrane experiment.

Due to the stacking up shunt currents with increasing stack size, REDBP stack may also have safety risks in certain locations such as the channels in the middle of stack and the transitions near electrode chambers. Figure 5.26 illustrates the changing distributions of current densities with increasing stack size. In the figure of 100 cells stack, the maximum $j_{trans.}$ near electrode chamber is higher than 1.2A/cm^2 by open circuit, which requires enough attention for safety concerns. Moreover, unlike in 30 cells or 50 cells stack, in 100 cells stack only half of the single cells contribute significant shunt current J_{cell}, the middle 50 single cells are not adding the shunt current higher but are undergoing discharging process.

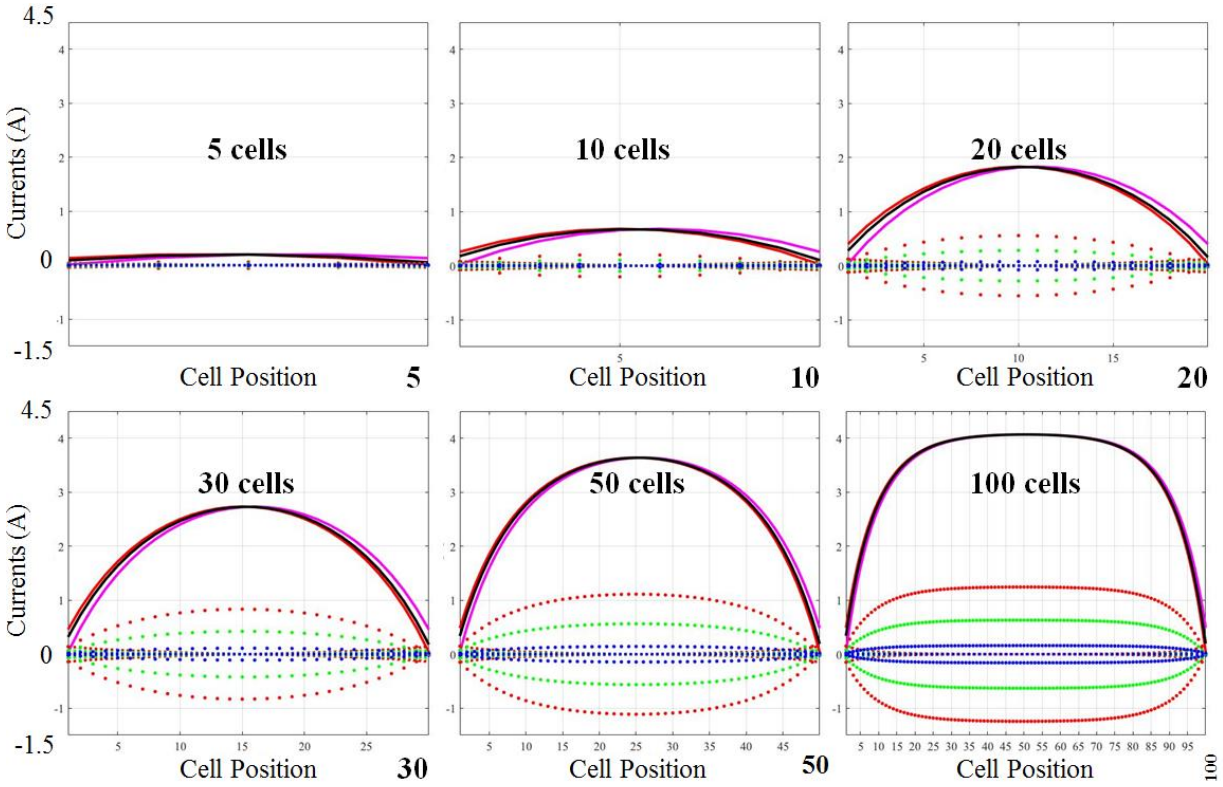

Figure 5.23: Distributions of currents inside of 1M stack with active surface of 100cm^2 and discretization number of 50 by open circuit with increasing stack size.

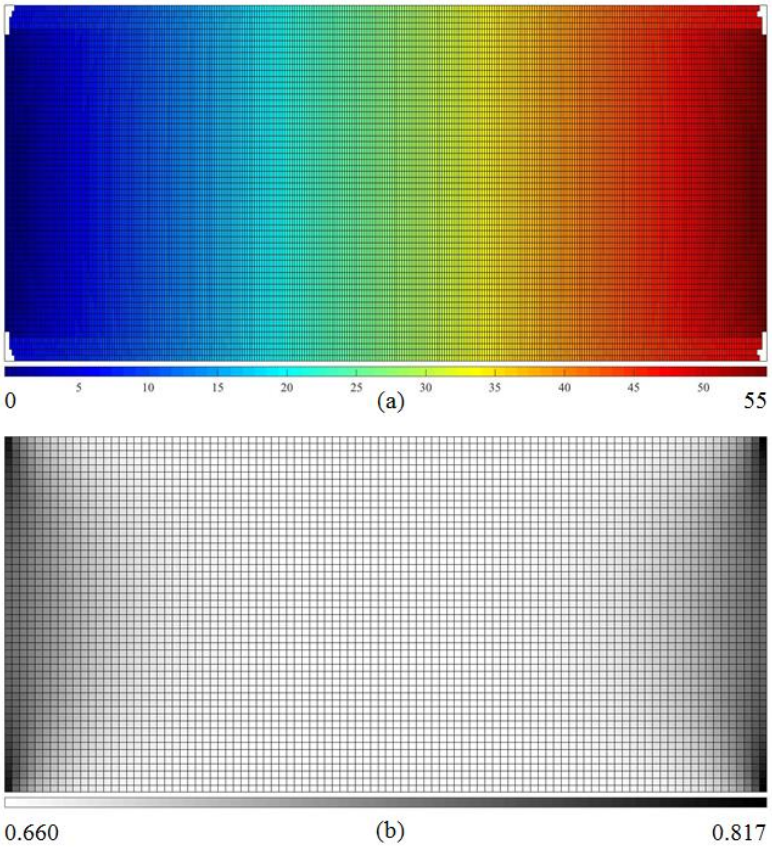

Figure 5.24: Distribution of voltage in electrolyte solution (a) and distribution of voltage difference between BP (b) of 1M 100 cells stack by open circuit.

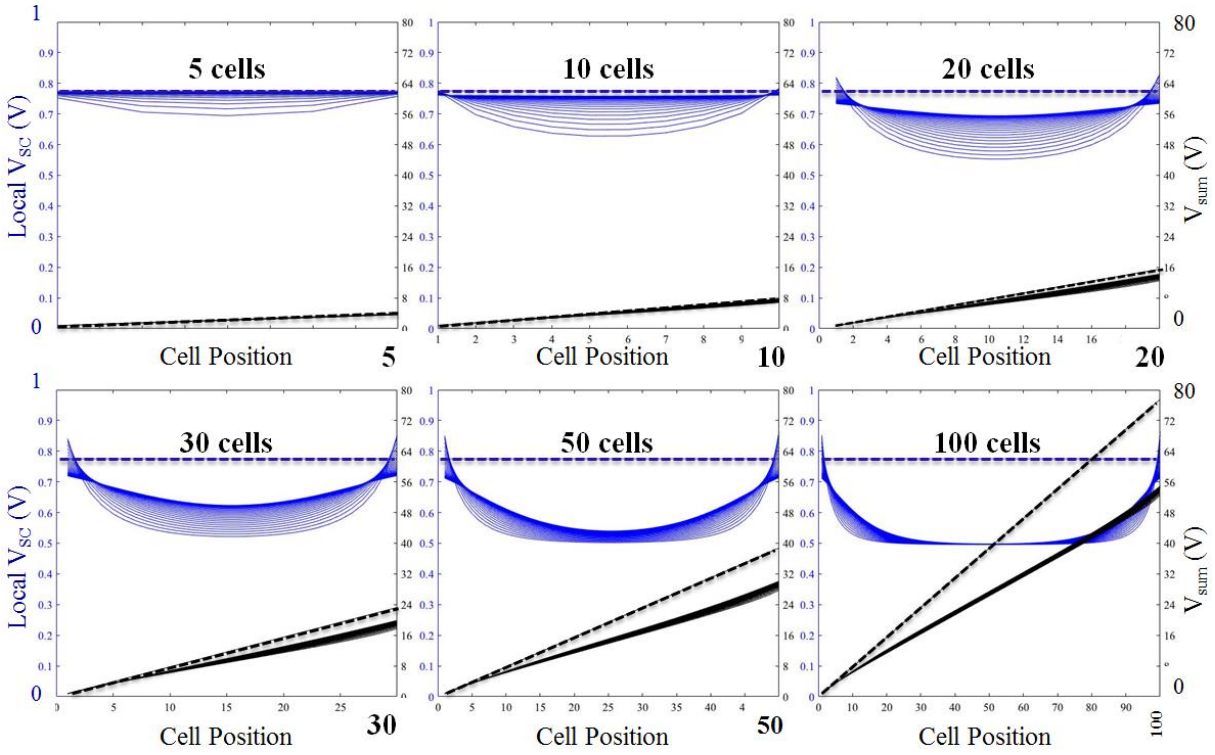

Figure 5.25: Distributions of local single cell voltage and the voltage of sum of all local single cells inside of stack with active surface of 100cm^2 and discretization number of 50 by open circuit with increasing stack size.

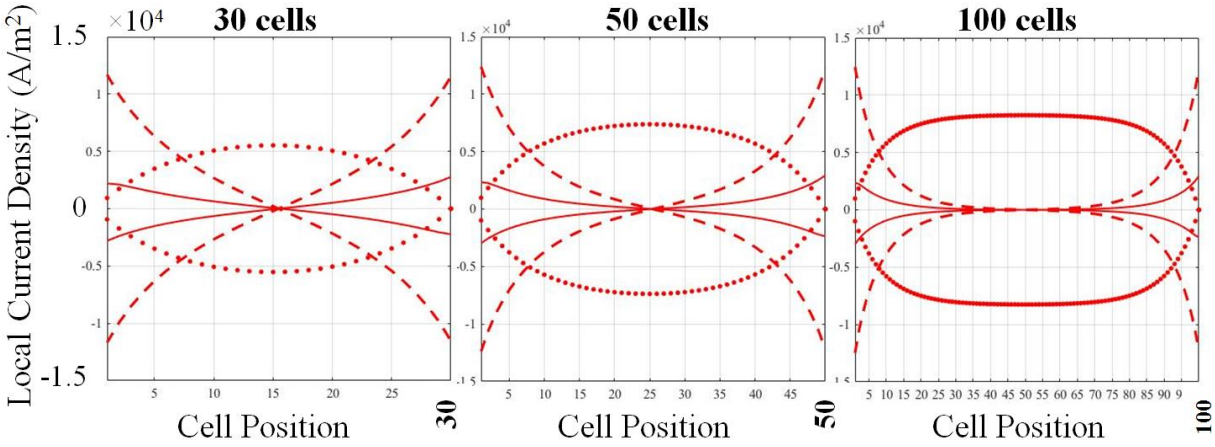

Figure 5.26: Distribution of current density in HCl solution inside of 1M stack with active surface of 100cm^2 by open circuit with increasing stack size.

5.4.5 Active Surface

Stacking up shunt current is due to collecting J_{cell} from each single cell, and most of J_{cell} comes from ΔI_{cell} flowing near inlet/outlet of solution chamber. Therefore, by increasing active surface, especially by increasing the distance between the center of active surface and the inlet/outlet of solution chamber, the overall influence from the shunt current might decrease. Figure 5.27 illustrates distribution of currents (a) and distribution of voltage (b) inside of 1M

20 cells stack with active surface of 2500cm^2 by open circuit. Compared with 100cm^2 stack, the maximum shunt current of 2500cm^2 increases from 1.8A to 2.3A. However, considering the active surface has been increased 25 times, this small increase of maximum shunt current can be neglected. Due to smaller influence of shunt current, most of area of BP in the middle of stack has not been affected, and the stack voltage is almost the same to stack size multiplying single cell voltage, which is required from single cell experiment.

Increasing active surface, especially by increasing the distance between the center of active surface and the inlet/outlet of solution chamber, has a positive influence on the performance of REDBP stack. However, it poses challenge on homogenous transport of electrolyte solution throughout the solution chambers, and homogeneous reaction rate from inlet to outlet.

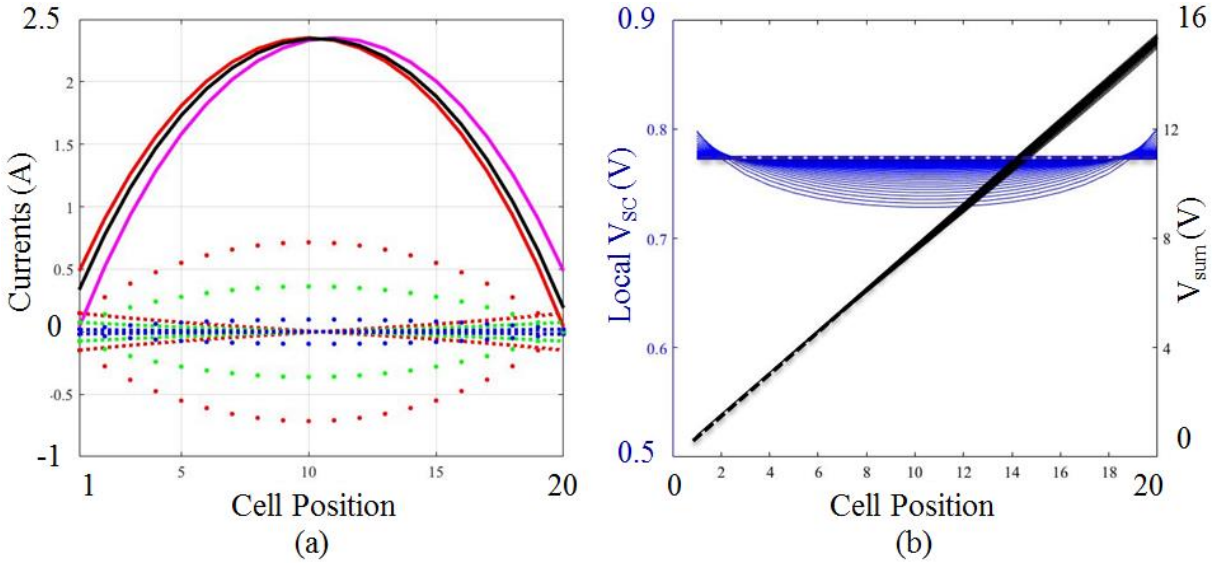

Figure 5.27: Distribution of currents (a) and distribution of voltage (b) inside of 1M 20 cells stack with active surface of 2500cm^2 by open circuit. Discretization number is 250.

5.4.6 Thickness of Chamber

Increasing thickness of solution chamber will simultaneously increase the internal resistance of stack in x direction and decrease the resistance of solution chamber in y direction which enhances the influence of shunt currents. Figure 5.28 illustrates both the distributions of currents (the above four figures) and the distributions of voltage (the lower four figures) with increasing thickness of solution chamber. Thickness of solution chamber in stack experiment is 0.5mm.

In general thicker chamber has a negative influence on the performance of stack. From 0.1mm to 1mm, both of the magnitude of shunt current and the amount of effected BPs become

significant. When thickness is larger than 1mm, the magnitude of shunt current decreases due to low overall voltage of stack and high internal resistance of stack in x direction. However, the amount of affected BPs increases which lowers the overall performance of stack.

Because thickness of chamber has also a direct impact on the overall pressure drop of the stack, a comprehensive assessment is needed to conclude this parameter.

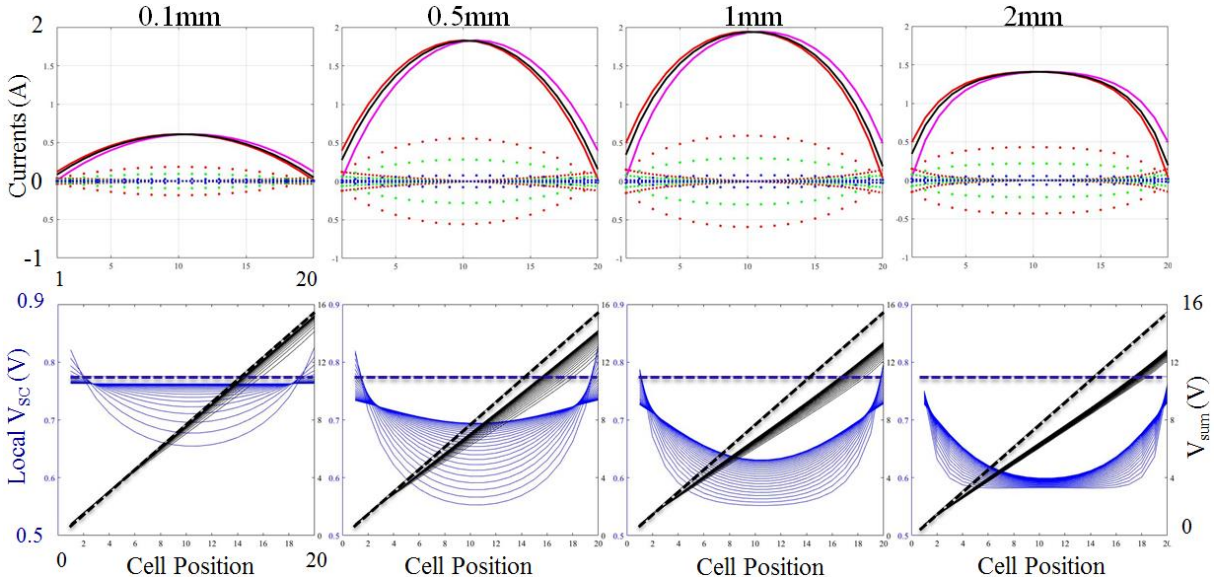

Figure 5.28: Distributions of currents (the above four figures) and distributions of voltage (the lower four figures) inside of 1M 20 cells stack with active surface of 100cm^2 by open circuit with increasing thickness of chamber

5.4.7 Transitions

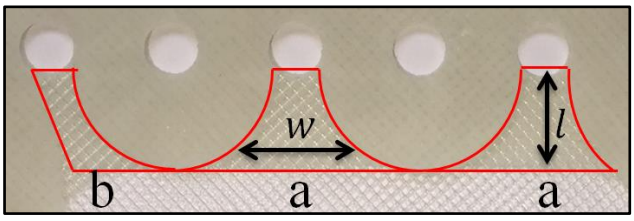

Figure 5.29: Two types of transitions (a and b) connecting solution chamber and solution channel in the stack experiment section of this thesis.

Transitions are connecting solution chamber and solution channel as shown in figure 5.29. The resistance of transition is calculated by:

$$R = \frac{\rho}{f_v}\frac{l}{w \cdot d} \tag{5.10}$$

where ρ is the resistivity of solution; f_v is void factor due to the existence of spacers, in this thesis, f_v=80%; l is the distance between the channel and chamber; w is the width of transition; d is the thickness of transition, normally the same as the thickness of solution chamber.

According to figure 5.29, there are two types of transitions which are labeled as 'a' and 'b'in the stack experiment section of this thesis. Width of transition varies with changing position. Therefore, $\frac{l}{w}$ is defined as pseudo length width ratio $f_{l/w}$, equation 5.10 can be written as:

$$R = \frac{\rho}{f_v} f_{l/w} \frac{1}{d} \tag{5.11}$$

After calculation, $f_{l/w}$ of transition 'a' equals 1.24, while transition 'b' 1.80.

Due to the changing width of transition, the current density inside of transition increases from the chamber to the channel. Therefore, the maximum current density in transition $j_{trans.}$ is near the channel.

Transitions serve as tributaries for bypass connections: By collecting small shunt currents through transitions from each chamber, shunt current in channel reaches its maximum in the middle of the stack. Figure 5.30 is the comparison of the distributions of currents (the above four figures), the distributions of voltage (the middle four figures) and the distributions current densities with increasing pseudo length width ratio $f_{l/w}$. In order to eliminate the influence of resistance of channels, the diameter of solution channel remains constant at 8mm and the minimal width of transition is the diameter of solution channel.

Increasing $f_{l/w}$ from reality (1.24 and 1.8) to 5 decreases shunt currents dramatically due to elevated resistance of transitions. Further increasing $f_{l/w}$ will further decrease shunt currents, but not that significantly. In addition, increasing $f_{l/w}$ will not lead to higher current density in transition, which is very good news by optimization of stack.

Pseudo length width ratio $f_{l/w}$ determines the overall pressure drop of the stack as well, therefore, at moment it is still difficulty to conclude the best $f_{l/w}$.

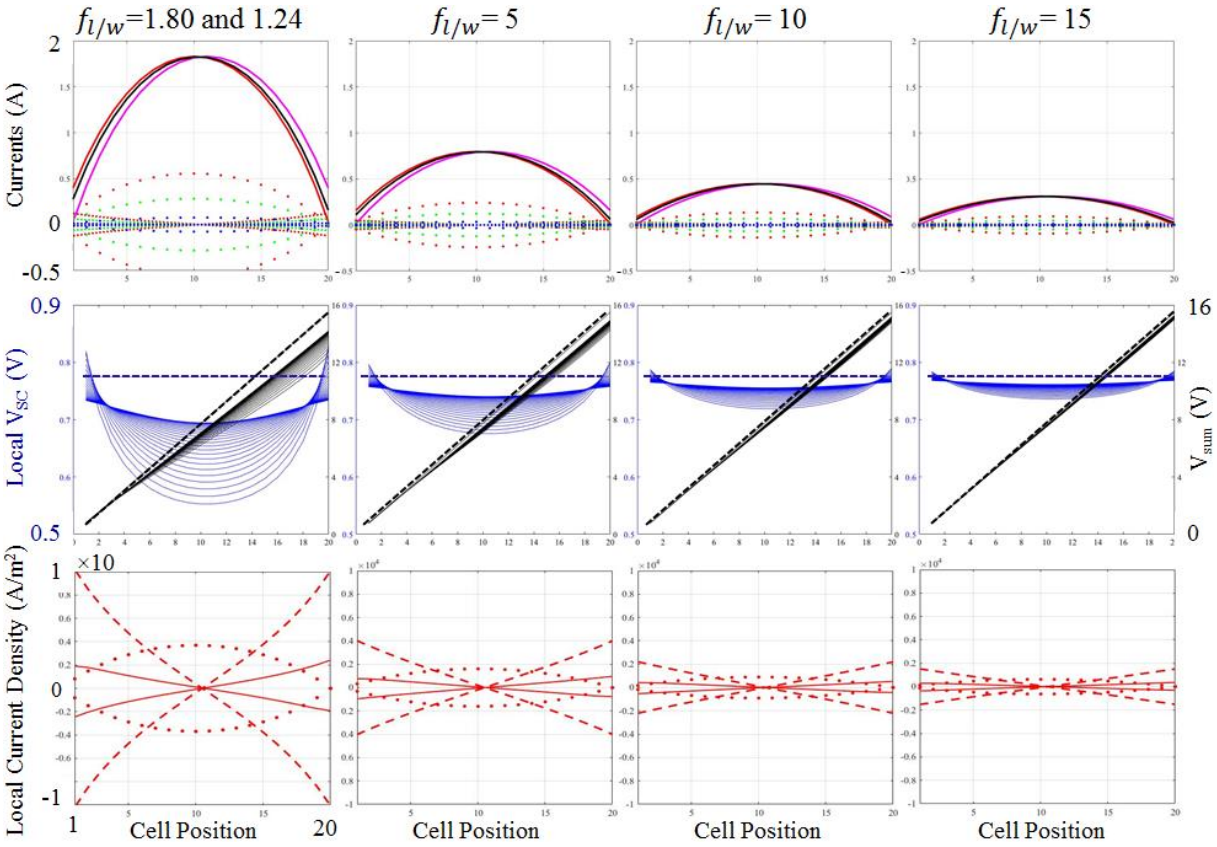

Figure 5.30: Distributions of currents (the above four figures), distributions of voltage (the middle four figures) and distributions current densities (the lower four figures) inside of 1M 20 cells stack with active surface of 100cm^2 by open circuit with increasing pseudo length width ratio $f_{l/w}$. Discretization number is 50. Please note that the diameter of solution channel remains constant at 8mm.

5.4.8 Channels

Solution channel is the main reason of the existence of shunt currents. Decreasing its conductance is one of the main strategies to avoid parasitic currents, for example, by increasing its length, decreasing its diameter and installation of breakpoints.

Figure 5.31 shows the impact of changing diameter of solution channel. 8mm is the diameter in stack experiment of this thesis. Please note that the diameter of solution channel is defined as the minimum width of transitions, and the pseudo length width ratio $f_{l/w}$ is chosen as in figure 5.29.

Decreasing diameter of solution channel is not recommended:

(1) Decreasing diameter of solution channel indeed decreases the magnitude of maximum shunt current, but has little contribution on the amount of affected BPs.

(2) Decreasing diameter of solution channel increases the maximum current density in transitions.

(3) Decreasing diameter of solution channel requires higher energy consumption of pumps.

Therefore, by decreasing the diameter of solution channel, stack cannot be improved. This thesis has only analyzed the impact of diameter of solution channel. The other parameters such as its length and installation of breakpoints are not investigated since these changes will affect the shape and structure of stack too much.

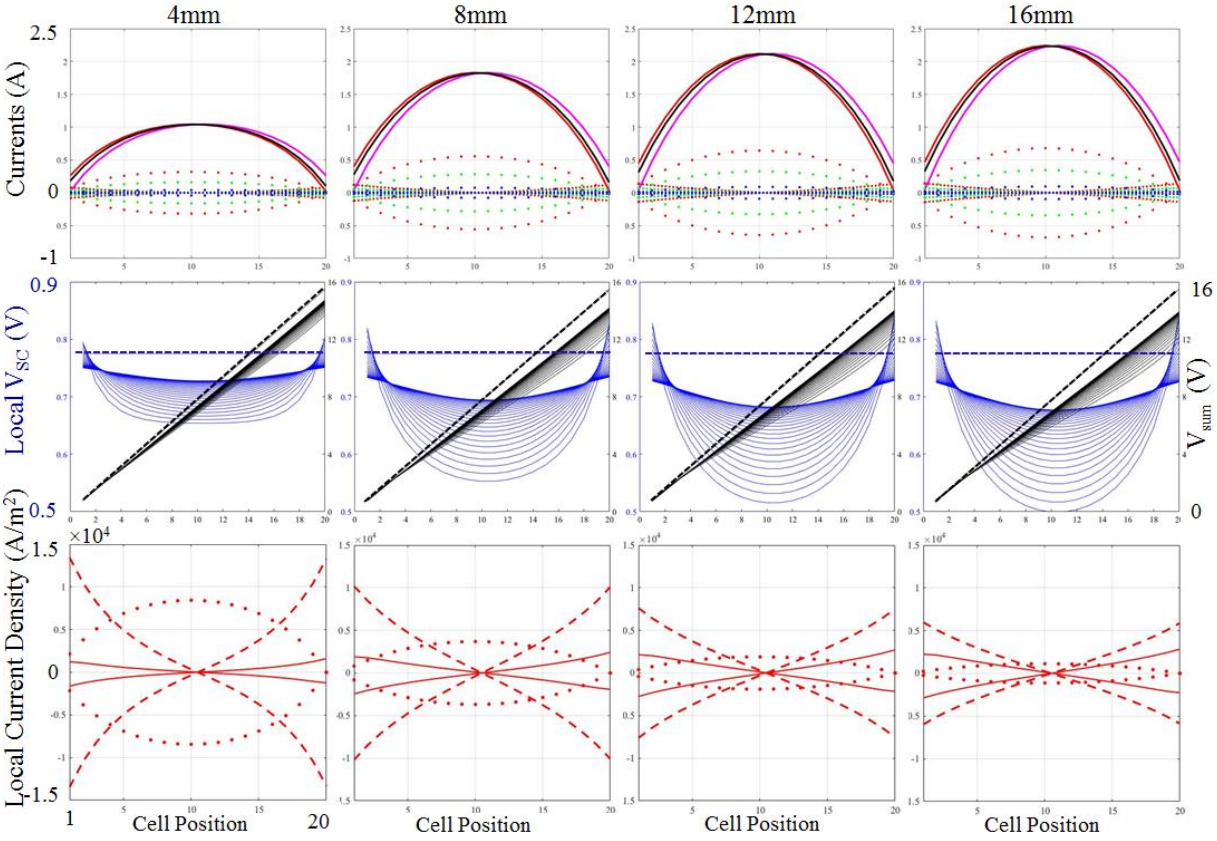

Figure 5.31: Distributions of currents (the above four figures), distributions of voltage (the middle four figures) and distributions current densities (the lower four figures) inside of 1M 20 cells stack with active surface of 100cm^2 by open circuit with increasing diameter of solution channel. Discretization number is 50. Please note that the diameter of solution channel is defined as the minimum width of transitions.

5.4.9 Resistance of IEMs

Besides resistance of electrolyte solution, the main internal resistance[1] of the stack comes from the IEMs. Figure 5.32 illustrated the changing distributions of currents and distributions of voltage with increasing resistance of IEMs. The resistance of IEMs which is measured in single membrane experiment is considered as standard and labelled as 100%. 10% means the resistance of IEMs putting into the mathematical model is 10% of that of standard, for example.

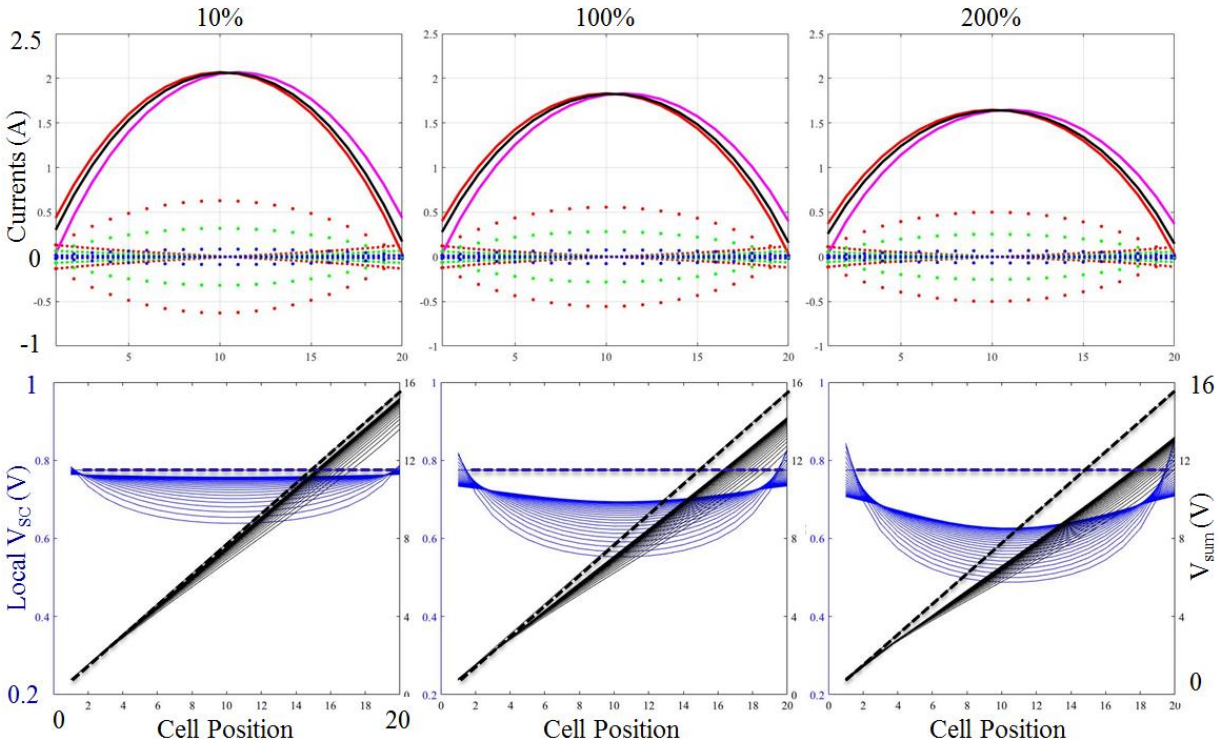

Figure 5.32: Distributions of currents (the above three figures) and distributions of voltage (the below three figures) inside of 1M 20 cells stack with active surface of 100cm^2 by open circuit with increasing resistance of IEMs. Discretization number is 50. Resistance of IEMs which is measured in single membrane experiment is considered as standard and labelled as 100%.

Increasing resistance of IEMs decreases the magnitude of shunt current since shunt current, in essence, is a self-discharging current which is determined by both stack voltage and total resistance (internal resistance, bypass connection resistance and external resistance). Stack voltage decreases with increasing resistance of IEMs due to elevated voltage drop when shunt current is flowing through the stack. Although with higher resistance of IEMs the magnitude of shunt current is smaller, the huge loss of stack voltage makes the overall performance of the stack lower. That means, reducing shunt current is not the ultimate objective of stack

[1] Resistance of electrode, especially due to corrosion and bad connection, contributes the internal resistance of the stack as well.

optimization. The ultimate objective of stack optimization is including achieving overall efficiency considering both voltage and coulomb. Reducing shunt current only improves coulombic efficiency which is not enough for achieving high overall efficiency.

5.5 Comparison with Experiments

Because this mathematical model is constructed based on certain assumptions and simplifications, especially the assumptions of ideal mixing, this model is hardly comparable with real experiment quantitatively. However, this model serves well qualitatively both on design of experiment and analysis of experiment results.

In this section the comparison of simulation and experiment will be shown as well as discussion of the difference between the two.

5.5.1 OCV of Sum of All Single Cells

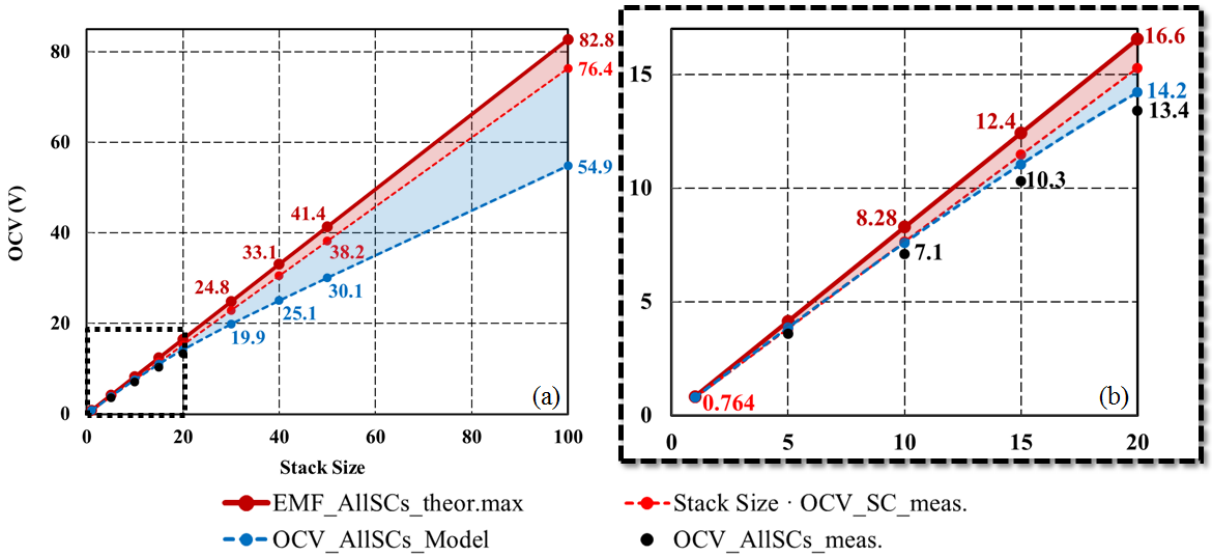

Figure 5.33: Comparison of simulation and experiment of OCV_{AllSCs} with increasing stack size. (b) is detailed diagram of (a). The red solid line is the theoretical maximum OCV_{AllSCs} without any loss. The red dashed line is the stack size multiplying OCV_{SC} obtained from single cell experiment. The blue dashed line is the simulation result of OCV_{AllSCs}. The black points are the experimental OCV_{AllSCs}.

Figure 5.33 illustrates the comparison of simulation and experiment of OCV_{AllSCs} with increasing stack size. The difference between EMF_{AllSCs} and Stack Size·OCV_{SC} of single cell experiment is the loss due to crossover effect. The difference between Stack Size·OCV_{SC} of

experiment and simulated OCV_{AllSCs} is due to simulated stacking up shunt current. The black points are the experimental OCV_{AllSCs}.

Simulation result shows the tendency of separating OCV_{AllSCs} with shunt current from OCV_{AllSCs} without shunt current. The difference between simulated and measured OCV_{AllSCs} is due to non-ideal mixing of electrolyte solution, leakage, side reaction, etc.

5.5.2 Voltage Distribution

In section 4.2.4 the measured voltage distribution inside of stack is introduced. Figure 5.34 is the comparison of simulation and experiment of voltage distribution inside of 1M 20 cells stack. The stack measurements are lower than simulated results. That is because the water production due to accumulated shunt current in the middle of stack in stack experiment lowers the ionic concentration of acid and base near BP. Moreover, non-ideal mixing inside of solution chamber makes this phenomenon more significant in the middle of stack.

By discharging, more water molecules are produced which makes the voltage measurement in the middle of stack even lower. The detailed discussion is in section 4.2.4.

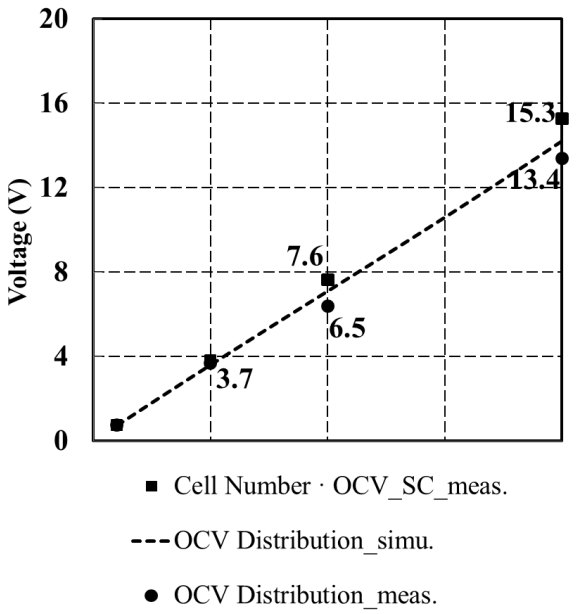

Figure 5.34: Comparison of simulation and experiment of voltage distribution inside of 1M 20 cells stack. Square dots represent Cell Number times measured single cell voltage in Chapter 2. Round dots are stack experimental results while dashed lines are results of stack simulation.

5.6 Conclusion

Originally the purpose of modeling and simulation of REDBP stack is simply for design of experiment and explanation of experimental results using current stack. After several months working on this topic, many phenomena have been found inside of stack which are impossible to measure at moment, and many strategies have been found for improvement of REDBP stack. All the above mentioned points are the main discussions of this chapter.

(1) Due to the bypass connections, three different types of electric currents exit inside of stack. They are the electric current in x direction through active surface I_{cell}, the electric current in y direction flowing through solution chamber and transition J and the electric current in x direction flowing through solution channel outside of active surface $I_{channel}$.

(2) Because of the existence of the above three types of currents, the electric potential in electrolyte solution inside of stack is not homogeneously distributed. Therefore, the unknown measuring positions of Pt wires will cause huge oscillation of experimental results.

(3) Not only the magnitude of shunt current, but also its affecting number of BPs plays very important role.

(4) Voltage between each BP inside of stack is not equal, even between the same piece of BP, the voltage varies at different position.

(5) By charging, part of electric current will flow through bypass connection which elevates the current density at certain position, which ultimately causes safety concerns. By discharging, shunt current decreases with increasing discharging current density.

(6) Stack voltage is not simply stack size multiplying single cell voltage obtained from single cell experiment due to the existence of shunt current. Many influential parameters have been investigated. Some strategies are suggested for improvement of stack, such as increasing active surface (especially increasing the distance between the center of active surface and inlet/outlet of solution chamber), decreasing thickness of solution chambers, increasing pseudo length width ratio $f_{l/w}$ of transition, installation of breakpoints in solution channels and etc.

Of course, all the above findings and suggestions of improvements are based on current model which lacks the hydraulics of the transport of electrolyte solution throughout the stack as well

as neglecting of water transport from BP interface to bulk solution. The above are the suggestions for the future researchers for modeling and simulation of REDBP stack.

Bibliography

[1] A. Mauro, "Space charge regions in fixed charge membranes and the associated property of capacitance," *Biophysical Journal,* vol. 2, pp. 179-198, 1962.

[2] W. Shockley, "The theory of p-n junctions in semiconductors and p-n junction transistors," *The Bell System Technical Journal,* vol. 28, p. 335, 1949.

[3] J. Pretz and E. Staude, "Reverse electrodialysis (RED) with bipolar membranes, an energy storage system," *Physical Chemistry,* vol. 102, pp. 676-685, 1998.

[4] E. K. Zholkovskij, M. C. Müller and E. Staude, "The storage battery with bipolar membranes," *Journal of Membrane Science,* vol. 141, pp. 231-243, 1998.

[5] "DOE Global Energy Storage Database," [Online]. Available: http://www.energystorageexchange.org/projects.

[6] "Battery technology stores clean energy," 2015. [Online]. Available: http://spinoff.nasa.gov/Spinoff2008/er_2.html.

[7] G. Kear, A. A. Shah and F. C. Walsh, "Development of the all-vanadium redox flow battery for energy storage: a review of technological, financial and policy aspects," *International Journal of Energy Research,* vol. 36, pp. 1105-1120, 2012.

[8] "Flow battery," 2016. [Online]. Available: https://en.wikipedia.org/wiki/Flow_battery.

[9] H. Strathmann, H. -J. Rapp, B. Bauer and C. M. Bell, "Theoretical and practical aspects of preparing bipolar membranes," *Desalination,* vol. 90, pp. 303-323, 1993.

[10] H. Strathmann, B. Bauer and H. -J. Rapp, "Better bipolar membranes," *Chemtech,* vol. 23, pp. 17-24, 1993.

[11] H.-J. Rapp, "Die Elektrodialyse mit bipolaren Membranen - Theorie und Anwendung," University of Stuttgart, 1995.

[12] K. Nagasubramanian, F. P. Chlanda and K. Liu, "Use of bipolar membranes for generation of acid and base - an engineering and economic analysis," *Journal of Membrane Science,* vol. 2, pp. 109-124, 1977.

[13] F. G. Wilhelm, "Bipolar Membrane Electrodialysis," Twente University Press, 2001.

[14] R. Simons, "Strong field effects on proton transfer between membrane-bound amines and water," *Nature,* no. 280, p. 824, 1979.

[15] L. Onsager, "Deviations from Ohm´s law in weak electrolytes," *Journal of Chemical Physics ,* no. 2, p. 599, 1934.

[16] A. Alcaraz, P. Ramirez, S. Mafe, H. Holdik and B. Bauer, "Ion selectivity and water dissociation in polymer bipolar membranes studied by membrane potential and current-voltage measurement," *Polymer*, pp. 6627-6634, 2000.

[17] A. Parasuraman, T. Lim, C. Menictas and M. Skyllas-Kazacos, "Review of material research and development for vanadium redox flow battery applications," *Electrochimica Acta,* vol. 101, pp. 27-40, 1 July 2013.

[18] D. W. Green and R. H. Perry, Perry's Chemical Engineers' Handbook, 8 ed., 2008.

[19] L. D. Landau and E. M. Lifshitz, Statistical Physics. Course of Theoretical Physics 5, 3 ed., Oxford: Pergamon Press, 1980.

[20] Wikipeida, "Wikipeida," 22 5 2016. [Online]. Available: https://en.wikipedia.org/wiki/Boltzmann_distribution#cite_note-landau-1.

[21] A. V. Bandura and S. N. Lvov, "The Ionization Constant of Water over Wide Ranges of Temperature and Density," *Journal of Physical and Chemical ,* pp. 15-30, 2006.

[22] W. Garcia-Vasquez, L. Dammak, C. Larchet, V. Nikonenko and D. Grande, "Effects of acid–base cleaning procedure on structure and properties of anion-exchange membranes used in electrodialysis," *Journal of Membrane Science ,* no. 507, p. 12, 2016.

[23] V. Viswanathan, A. Crawford, D. Stephenson, S. Kim, W. Wang, B. Li, G. Coffey, E. Thomsen, G. Graff, P. Balducci, M. Kintner-Meyer and V. Sprenkle, "Cost and performance model for redox flow batteries," *Journal of Power Sources,* vol. 247, pp. 1040-1051, 2014.

[24] D. A. Bograchev, V. M. Volgin and A. D. Davydov, "Mass transfer during metal electrodeposition into the pores of anodic aluminum oxide from a binary electrolyte under the potentiostatic and galvanostatic conditions," *Electronchimica Acta,* vol. 207, pp. 247-256, 20 July 2016.

[25] W. M. Deen, Analysis of Transport Phenomena, Second ed., Oxford University Press, p. 585.

[26] C. Hamann, A. Hamnett and W. Vielstich, Electrochemistry, 2 ed., WILEY-VCH, 2007, p. 115.

[27] P. E. Długołęcki, "Mass Transport in for Sustainable Energy Generation," University of Twente, 2009.

[28] W. J. Hamer and H. J. DeWane, "Electrolytic Conductance and the Conductances of the Hydrohalogen Acids in Water," *Natl. Bur. Standards (U.S.),* no. 33, 1970.

[29] S. Mikhaylin and L. Bazinet, "Fouling on ion-exchange membranes: Classification, characterization and strategies of prevention and control," *Advances in Colloid and Interface Science,* vol. 229, pp. 34-56, March 2016.

[30] N. Gence and N. Ozbay, "pH dependence of electrokinetic behavior of dolomite and magnesite in aqueous electrolyte solution," *Applied Surface Science,* no. 252, pp. 8057-8061, 2006.

[31] C. Casademont, M. Farias, G. Pourcelly and L. Bazinet, "Impact of electrodialytic parameters on cation migration kinetics and fouling nature of ion-exchange membranes during treatment of solutions with different magnesium/calcium ratios," *Journal of Membrane Science,* no. 325, pp. 570-579, 2008.

[32] W. Nernst, "Die elektromotorische Wirksamkeit der Ionen," *Zeitschrift für Physikalische Chemie,* pp. 129-181, 1889.

[33] E. Dickinson, J. Limon-Petersen and R. Compton, "The electroneutrality approximation in electrochemistry," *Journal of Solid State Electrochemistry,* pp. 1335-1345, 2011.

[34] C. Kittel and H. Kroemer, Thermal Physics, 2. ed., p. 124.

[35] F.-F. Kuppinger, Experimentelle Untersuchung und mathematische Moodellierung von Elektrodialyseverfahren, Logos Verlag Berlin, 1997.

[36] F. Sarfert, " Mass transfer limitations in protein separations using ion-exchange membranes," *Journal of Chromatography A,* pp. 3-20, 1997.

[37] M. Gouy, "Sur la constitution de la charge électrique à la surface d'un électrolyte," *Journal de Physique,* vol. 9, pp. 457-468, 1910.

[38] D. L. Chapman, "LI. A contribution to the theory of electrocapillarity," *Philosophical Magazine,* vol. 25, no. 148, pp. 475-481, 1913.

[39] O. Stern, "The theory of the electrolytic doulbe layer," *Z. Elektrochem. Angew. Phys. Chem.,* vol. 30, pp. 508-516, 1924.

[40] C. Yin, S. Guo, H. Fang, J. Liu, Y. Li and H. Tang, "Numerical and experimental studies of stack shunt current for vanadium redox flow battery," *Applied Energy,* vol. 151, pp. 237-248, 1 August 2015.

[41] H. Fink and M. Remy, "Shunt currents in vanadium flow batteries: Measurement, modelling and implications for efficiency," *Journal of Power Sources,* vol. 284, pp. 547-553, 15 June 2015.

[42] Q. Ye, J. Hu, P. Cheng and Z. Ma, "Design trade-offs among shunt current, pumping loss and compactness in the piping system of a multi-stack vanadium flow battery," *Journal of Power Sources,* vol. 296, pp. 352-364, 20 November 2015.

[43] J. Veerman, " Reducing power losses caused by ionic shortcut currents in reverse electrodialysis stacks by a validated model," *Journal of Membrane Science,* vol. 310, pp. 418-430, 2008.

[44] A.H. Galama, D.A. Vermaas, J. Veerman, M. Saakes, H.H.M. Rijnaarts, J.W. Post, K. Nijmeijer, " Membrane resistance: The effect of salinity gradients over a cation exchange membrane, " *Journal of Membrane Science,* vol. 467, pp. 279-291, 2014.

Appendix A

Design of Luggin Capillary

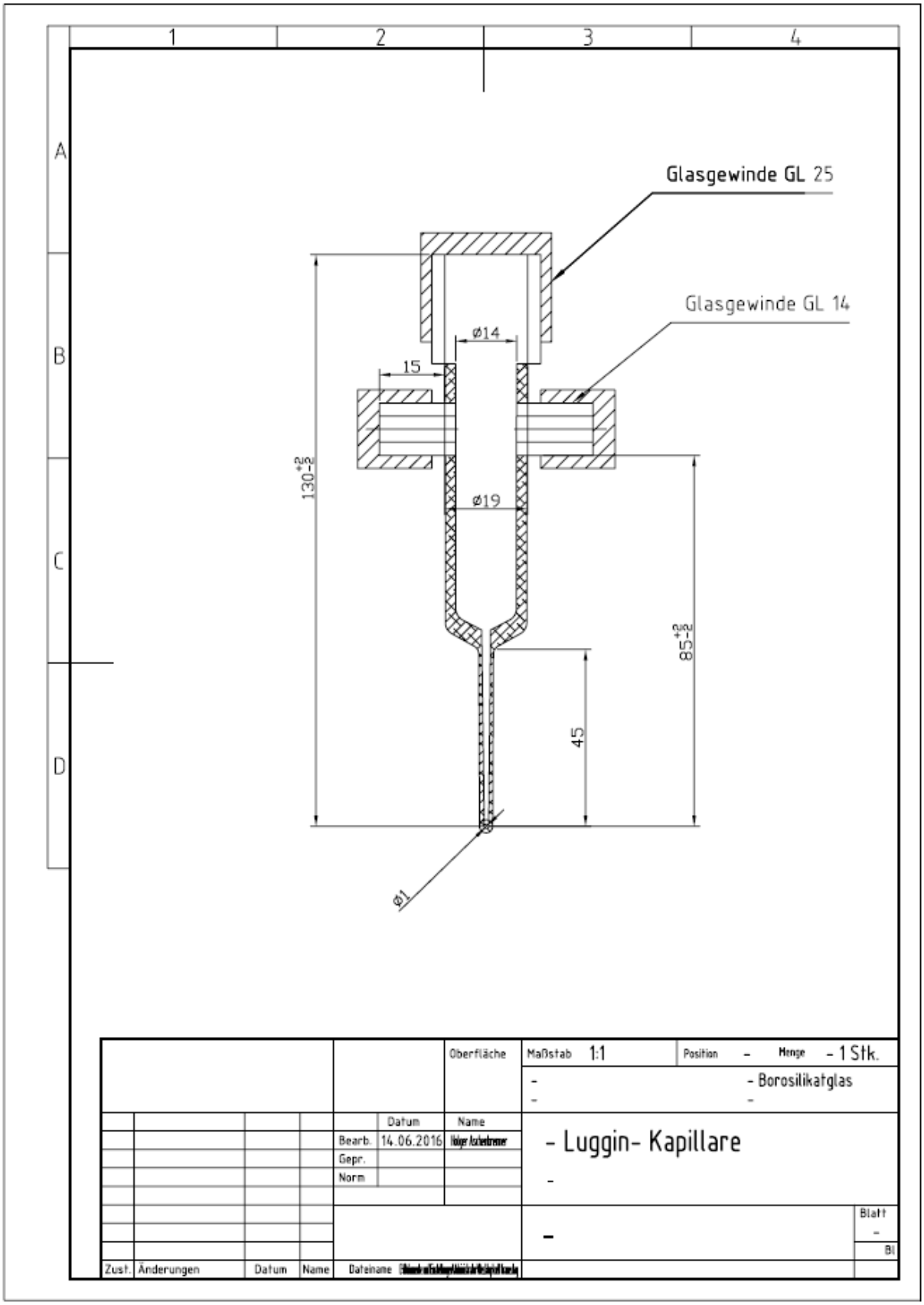

Appendix B

Modeling of BP

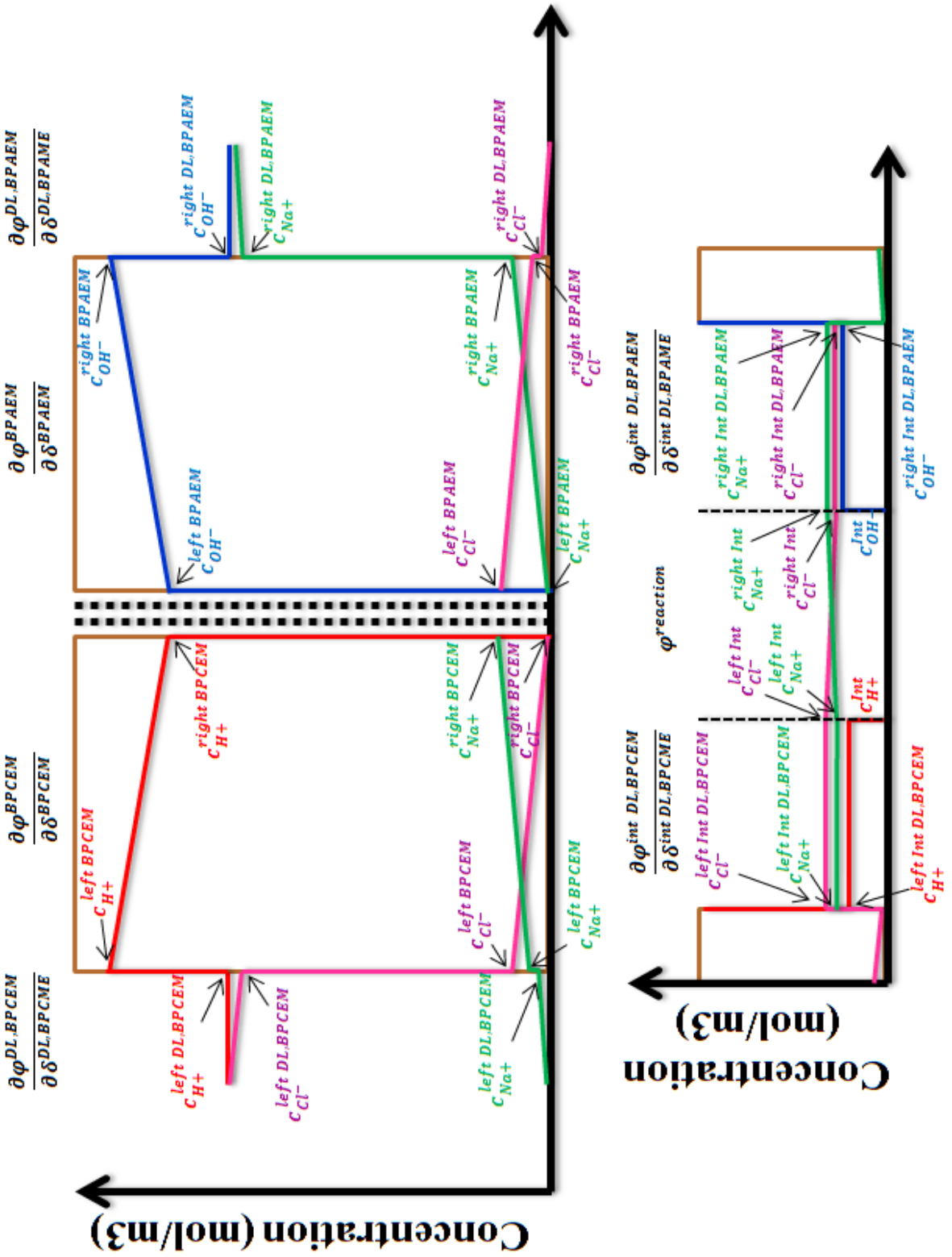

Figure B.1: 37 Unknowns of BP. δ refers to the thickness of certain location.

This section is the detailed explanation of modeling BP. Assuming discretization is 1, BP between acid and base will create 37 unknowns as shown in figure B.1. Please refer figure 3.12 and figure 3.13 of Chapter 3 for better understanding this model.

Table B.1 is the detailed explanation of each unknowns.

Table B.1: Detailed description of each unknown.

Name	Position	Description
$\frac{\partial \varphi^{DL,BPCEM}}{\partial \delta^{DL,\,BPCME}}$	Across diffusional layer between BP and bulk acid solution.	Electric potential gradient across diffusional layer.
$c_{H+}^{left\ DL,\ BPCEM}$	In diffusional layer between BP and bulk acid solution, adjacent to BP.	H^+ concentration at this point.
$c_{Cl^-}^{left\ DL,\ BPCEM}$		Cl^- concentration at this point.
$c_{Na+}^{left\ DL,\ BPCEM}$		Na^{-+} concentration at this point.
$c_{H+}^{left\ BPCEM}$	In BPCEM, adjacent to diffusional layer in acid chamber.	H^+ concentration at this point.
$c_{Cl^-}^{left\ BPCEM}$		Cl^- concentration at this point.
$c_{Na+}^{left\ BPCEM}$		Na^{-+} concentration at this point.
$\frac{\partial \varphi^{BPCEM}}{\partial \delta^{BPCEM}}$	Across BPCEM.	Electric potential gradient across BPCEM.
$c_{H+}^{right\ BPCEM}$	In BPCEM, adjacent to BP interface.	H^+ concentration at this point.
$c_{Na+}^{right\ BPCEM}$		Na^{-+} concentration at this point.
$c_{Cl^-}^{right\ BPCEM}$		Cl^- concentration at this point.
$c_{Cl^-}^{left\ Int\ DL,\ BPCEM}$	In BP interface, adjacent to BPCEM	Cl^- concentration at this point.
$c_{Na+}^{left\ Int\ DL,\ BPCEM}$		Na^{-+} concentration at this point.
$c_{H+}^{left\ Int\ DL,\ BPCEM}$		H^+ concentration at this point.
$\frac{\partial \varphi^{int\ DL,BPCEM}}{\partial \delta^{int\ DL,\ BPCME}}$	Across BP interface diffusional layer, adjacent to BPCEM	Electric potential gradient across diffusional layer.
$c_{Cl^-}^{left\ Int}$	In reaction double layer, acid side.	Cl^- concentration at this point.
$c_{Na+}^{left\ Int}$		Na^{-+} concentration at this point.
c_{H+}^{Int}		H^+ concentration at this point.
$\varphi^{reaction}$	Across reaction double layer.	Electric potential across reaction double layer.

$c_{Na+}^{right\ Int}$	In reaction double layer, base side.	Na^{-+} concentration at this point.
$c_{Cl^-}^{right\ Int}$		Cl^- concentration at this point.
c_{OH-}^{Int}		OH^- concentration at this point.
$\frac{\partial \varphi^{int\ DL,BPAEM}}{\partial \delta^{int\ DL,\ BPAME}}$	Across BP interface diffusional layer, adjacent to BPAEM	Electric potential gradient across diffusional layer.
$c_{Na+}^{right\ Int\ DL,\ BPAEM}$	In BP interface, adjacent to BPAEM	Na^{-+} concentration at this point.
$c_{Cl^-}^{right\ Int\ DL,\ BPAEM}$		Cl^- concentration at this point.
$c_{OH^-}^{right\ Int\ DL,\ BPAEM}$		OH^- concentration at this point.
$c_{OH^-}^{left\ BPAEM}$	In BPAEM, adjacent to BP interface.	OH^- concentration at this point.
$c_{Cl^-}^{left\ BPAEM}$		Cl^- concentration at this point.
$c_{Na+}^{left\ BPAEM}$		Na^{-+} concentration at this point.
$\frac{\partial \varphi^{BPAEM}}{\partial \delta^{BPAEM}}$	Across BPAEM.	Electric potential gradient across diffusional layer.
$c_{OH^-}^{right\ BPAEM}$	In BPAEM, adjacent to diffusional layer in base chamber.	OH^- concentration at this point.
$c_{Na+}^{right\ BPAEM}$		Na^{-+} concentration at this point.
$c_{Cl^-}^{right\ BPAEM}$		Cl^- concentration at this point.
$c_{OH^-}^{right\ DL,\ BPAEM}$	In diffusional layer between BP and bulk base solution, adjacent to BP.	OH^- concentration at this point.
$c_{Na+}^{right\ DL,\ BPAEM}$		Na^{-+} concentration at this point.
$c_{Cl^-}^{right\ DL,\ BPAEM}$		Cl^- concentration at this point.
$\frac{\partial \varphi^{DL,BPAEM}}{\partial \delta^{DL,\ BPAME}}$	Across diffusional layer between BP and bulk base solution.	Electric potential gradient across diffusional layer.

37 unknowns require 37 independent equations to solve, based on electroneutrality, electrochemical equilibrium (Donnan distribution), stationary flow combined with Nernst-Planck equation, Faraday´s law, and Nernst equation.

Table B.2-B.4 show these equations.

Table B.2: 15 independent equations for solving 15 unknowns in BPCEM part.

	In left diffusion layer near BPCEM	In BPCEM near left diffusion layer	In BPCEM near right diffusion layer	In right diffusion layer near BPCEM at BPM interface
Electroneutrality (4 equations)	$c_{Na+}^{left\ DL,BPCEM} + c_{H+}^{left\ DL,BPCEM} = c_{Cl-}^{left\ DL,BPCEM}$	$c_{Na+}^{left\ BPCEM} + c_{H+}^{left\ BPCEM} = X_{bpcem} + c_{Cl-}^{left\ BPCEM}$	$c_{Na+}^{right\ BPCEM} + c_{H+}^{right\ BPCEM} = c_{Cl-}^{right\ BPCEM} + X_{bpcem}$	$c_{Na+}^{left\ Int\ DL,BPCEM} + c_{H+}^{left\ Int\ DL,BPCEM} = c_{Cl-}^{left\ Int\ DL,BPCEM}$
Donnan Distribution (4 equations)	$c_{Na+}^{left\ DL,BPCEM} \cdot c_{Cl-}^{left\ DL,BPCEM} = c_{Na+}^{left\ BPCEM} \cdot c_{Cl-}^{left\ BPCEM}$		$c_{Na+}^{right\ BPCEM} \cdot c_{Cl-}^{right\ BPCEM} = c_{Na+}^{left\ Int\ DL,BPCEM} \cdot c_{Cl-}^{left\ Int\ DL,BPCEM}$	
	$c_{H+}^{left\ DL,BPCEM} \cdot c_{Cl-}^{left\ DL,BPCEM} = c_{H+}^{left\ BPCEM} \cdot c_{Cl-}^{left\ BPCEM}$		$c_{H+}^{right\ BPCEM} \cdot c_{Cl-}^{right\ BPCEM} = c_{H+}^{left\ Int\ DL,BPCEM} \cdot c_{Cl-}^{left\ Int\ DL,BPCEM}$	
Stationary Flow (6 equations)	$\dot{n}_{Na+}^{left\ DL,BPCEM} = \dot{n}_{Na+}^{BPCEM}$		$\dot{n}_{Na+}^{BPCEM} = \dot{n}_{Na+}^{left\ Int\ DL,BPCEM}$	
	$\dot{n}_{Cl-}^{left\ DL,BPCEM} = \dot{n}_{Cl-}^{BPCEM}$		$\dot{n}_{Cl-}^{BPCEM} = \dot{n}_{Cl-}^{left\ Int\ DL,BPCEM}$	
	$\dot{n}_{H+}^{left\ DL,BPCEM} = \dot{n}_{H+}^{BPCEM}$		$\dot{n}_{H+}^{BPCEM} = \dot{n}_{H+}^{left\ Int\ DL,BPCEM}$	
Faraday´s Law (1 equation)	$i = \sum_{j=1}^{J} (F \cdot z_j \cdot \dot{n}_j)$			

Table B.3: 15 independent equations for solving 15 unknowns in BPAEM part.

	In left diffusion layer near BPAEM at BPM interface	In BPAEM near left diffusion layer	In BPAEM near right diffusion layer	In right diffusion layer near BPAEM
Electroneutrality (4 equations)	$c_{Na+}^{right\ Int\ DL,BPAEM} = c_{Cl-}^{right\ Int\ DL,BPAEM} + c_{OH-}^{right\ Int\ DL,BPAEM}$	$c_{Na+}^{left\ BPAEM} + X_{bpaem} = c_{Cl-}^{left\ BPAEM} + c_{OH-}^{left\ BPAEM}$	$c_{Na+}^{right\ BPAEM} + X_{bpaem} = c_{Cl-}^{right\ BPAEM} + c_{OH-}^{right\ BPAEM}$	$c_{Na+}^{right\ DL,BPAEM} = c_{Cl-}^{right\ DL,BPAEM} + c_{OH-}^{right\ DL,BPAEM}$
Donnan Distribution (4 equations)	$c_{Na+}^{right\ Int\ DL,BPAEM} \cdot c_{Cl-}^{right\ Int\ DL,BPAEM} = c_{Na+}^{left\ BPAEM} \cdot c_{Cl-}^{left\ BPAEM}$		$c_{Na+}^{right\ BPAEM} \cdot c_{Cl-}^{right\ BPAEM} = c_{Na+}^{right\ DL,BPAEM} \cdot c_{Cl-}^{right\ DL,BPAEM}$	
	$c_{Na+}^{right\ Int\ DL,BPAEM} \cdot c_{OH-}^{right\ Int\ DL,BPAEM} = c_{Na+}^{left\ BPAEM} \cdot c_{OH-}^{left\ BPAEM}$		$c_{Na+}^{right\ BPAEM} \cdot c_{OH-}^{right\ BPAEM} = c_{Na+}^{right\ DL,BPAEM} \cdot c_{OH-}^{right\ DL,BPAEM}$	
Stationary Flow (6 equations)	$\dot{n}_{Na+}^{right\ Int\ DL,BPAEM} = \dot{n}_{Na+}^{BPAEM}$		$\dot{n}_{Na+}^{BPAEM} = \dot{n}_{Na+}^{right\ DL,BPAEM}$	
	$\dot{n}_{Cl-}^{right\ Int\ DL,BPAEM} = \dot{n}_{Cl-}^{BPAEM}$		$\dot{n}_{Cl-}^{BPAEM} = \dot{n}_{Cl-}^{right\ DL,BPAEM}$	
	$\dot{n}_{OH-}^{right\ Int\ DL,BPAEM} = \dot{n}_{OH-}^{BPAEM}$		$\dot{n}_{OH-}^{BPAEM} = \dot{n}_{OH-}^{right\ DL,BPAEM}$	
Faraday´s Law (1 equation)	$i = \sum_{j=1}^{J} (F \cdot z_j \cdot \dot{n}_j)$			

Table B.4: 7 independent equations for solving 7 unknowns in reaction zone.

	Left layer of reaction zone	Reaction zone	Right layer of reaction zone
Electroneutrality (3 equations)	$c_{Na+}^{left\ Int} + c_{H+}^{Int} = c_{Cl^-}^{left\ Int}$	$c_{H+}^{Int} = c_{OH-}^{Int}$	$c_{Na+}^{right\ Int} = c_{Cl^-}^{right\ Int} + c_{OH-}^{Int}$
Stationary Flow (3 equations)	$\dot{n}_{Na+}^{BPCEM} = \dot{n}_{Na+}^{BPAEM}$		
	$\dot{n}_{H+}^{BPCEM} + \dot{n}_{OH-}^{BPAEM} = 0$		
	$\frac{\dot{n}_{H+}^{BPCEM}}{\delta_{reaction\ zone}} = r_{neutralisation\ reation} = k \cdot c_{H+}^{Int} \cdot c_{OH-}^{Int}$ Where $k = 1.1 \times 10^8\ m^3/(mol \cdot s)$		
Nernst Equation (1 equation)	$\varphi^{reaction} = 90\% \cdot EMF$ Where $EMF = EMF^0 - \frac{R \cdot T}{F} \ln(\frac{c_{H_3^+O}^0 \cdot c_{OH^-}^0}{c_{H+}^{Int} \cdot c_{OH-}^{Int}})$		

Boundary condition is the ionic concentration of bulk acid and base solution. Using MatLab standard solver for nonlinear problems, the simulated results can be obtained.

Please note, that when ionic concentrations at IEM interface are unknown, Donnan potential can be easily calculated.

In order to simplify this model, in this section discretization is set to 1. In Chapter 3, discretization of all diffusional layers is 5, inside of membrane is 15, reaction zone is 1.

Appendix C

Detailed Description of Modeling and Simulation of REDBP Stack

Modeling of RED will first be referenced as an introductory example, since a concentration cell has similarities but is a much simpler process compared with REDBP.

3D to 2D Model of RED

RED, an abbreviation for reverse electro dialysis, is a process for generating electric energy from the salt gradient between two solutions as shown in figure C.1.

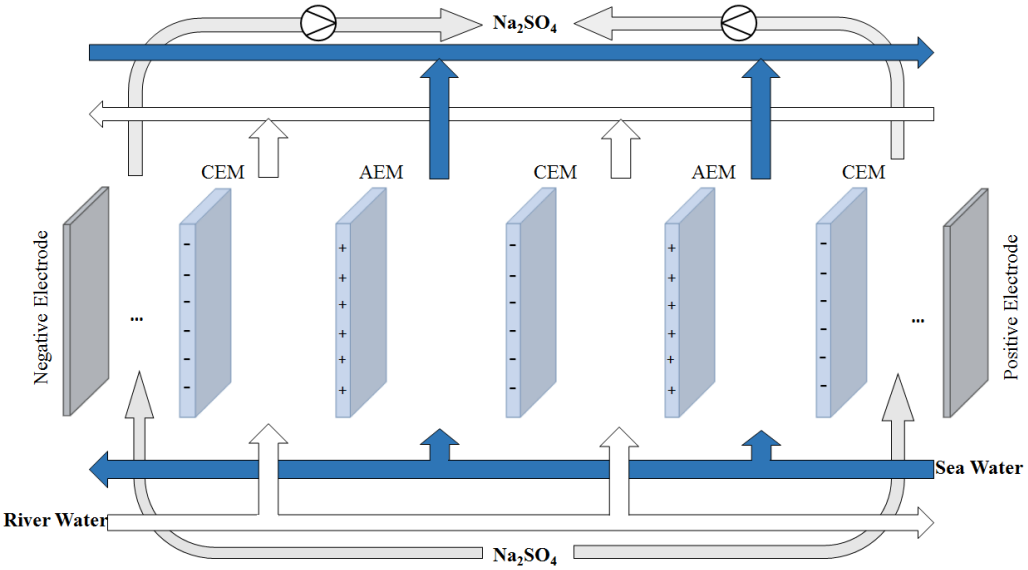

Figure C.1: Schematic diagram of RED process.

The detailed investigations can be found in (but not limited to) the following outstanding dissertations [27] [43] [44]. In general, each single cell of RED has only two IEMs (CEM and AEM) and two solution chambers (salt solutions with different ionic concentration, for example sea water and river water). RED can be viewed as a simplified process of REDBP: Both require additional electrode chambers with Na_2SO_4 solution for transforming ionic transport to electron transport, and both have their single cells interconnected with each other through salt bridges (or bypass connections). If conductivity of river water is neglected, the three dimensional (3D) equivalent circuit of RED stack can be constructed as in figure C.2.

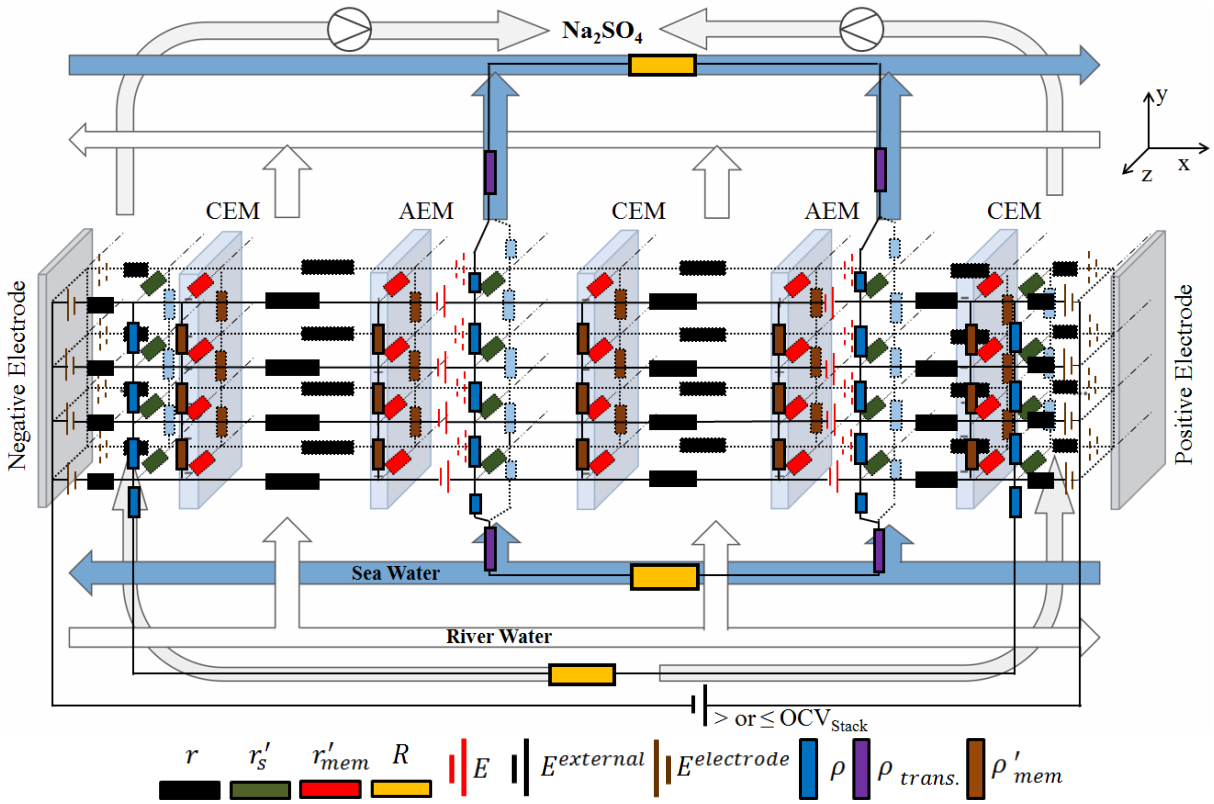

Figure C.2: 3D equivalent circuit of RED process.

Comments:

(8) r: represents the resistance of electrolyte solution and IEM when electric current is flowing in x direction[1]. The value is calculated by multiplying area of finite element and area resistance of electrolytes, which are taken from the single cell experiment (see Chapter 2). Electric current flowing through it is called ΔI_{cell} with the unit of [A]. Its physical meaning is local electric current in x direction through finite active surface. Sum of all ΔI_{cell} is the electric current flowing throughout the entire active surface. ΔI_{cell} dividing area of finite element is local current density i_{cell} with the unit of [A/m^2].

(9) r_s': represents the resistance of electrolyte solution when electric current is flowing in z direction in electrolyte solution.

(10) r_{mem}': represents the resistance of IEM when electric current is flowing in z direction in IEM.

(11) ρ: represents the resistance of electrolyte solution when electric current is flowing in y direction. Figure C.3 shows 2D discretization of resistance of solution chamber when

[1] Sometimes r represents only the resistance of electrolyte solution when electric current is flowing in x direction in electrode chambers.

electric current flows in y direction, arrows are electric currents and blocks are finite elements of electrolyte solution. Discretization number in x direction is 5 while in y direction 1. The reason why discretization number in y direction is always 1 is the ratio of the thickness of solution chamber and the length of active surface is very small. Please note that this figure illustrates electric current flowing in y direction only. The resistance of solution chamber in x and z direction is included in r and r_s', respectively. Electric current flowing through it is called J_{cell} with the unit of [A]. Its physical meaning is local electric current in y direction. J_{cell} tends to accumulate itself from the center of active surface to the both ends (the inlet and outlet of electrolyte solution) and reaches its maximum at both ends. J_{cell} dividing the area it flows through is local current density in y direction j_{cell}. At the entrance and exit of electrolyte solution j_{cell} reaches its maximum.

(12) ρ_{mem}': represents the resistance of IEM when electric current is flowing in y direction in IEM.

(13) $\rho_{trans.}$: represents the resistance as transition between solution chamber and solution channel as shown in figure C.4. This area is out of active surface, meaning electric current flows only in y direction. Electric current flowing through it is the maximum J_{cell} flowing its nearby solution chamber. $j_{trans.}$ represents the local current density flowing through $\rho_{trans.}$.

(14) R: represents the resistance of solution channel. In RED there are 3 different solutions: sea water, river water and Na_2SO_4. The resistance of river water is so big that the bypass connections of river water can be neglected. The resistance of Na_2SO_4 depends primarily[1] on the length and diameter of its pipe, therefore, the usage of a long and small tube can also eliminate the influence of Na_2SO_4 solution. Electric current flowing through it is $I_{channel}$. With increasing stack size, the number of bypass connections increase. Therefore, $I_{channel}$ tends to accumulated itself by collecting more J_{cell} from electrode chamber to the middle of stack and reaches its maximum at the middle of stack. Please note that the pumps serve as breakpoints. Thus, there is no parasitic current flowing through them.

[1] Concentration of Na_2SO_4 is always 0.25M.

(15) E: represents the EMF of single cell. In this thesis, $OCV_{SC\_meas.}$ (Chapter 2) is used as E in order to fulfil the simplifications requirement of equivalent circuit.

(16) $E^{electrode}$: represents the voltage drop in electrode chambers.

(17) $E^{external}$: represents the external constant voltage source for calculating charging or discharging process. By charging process $E^{external}$ is larger than OCV_{Stack}, while by discharging $E^{external}$ is smaller than OCV_{Stack}.

If stack is symmetric[1] in z dimension, 3D model can be simplified into 2D as shown in figure C.5.

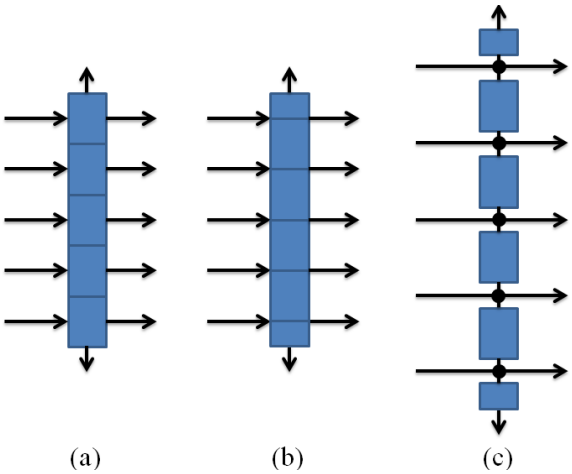

Figure C.3: Discretization of resistance of solution chamber when electric current flows in y direction, arrows are electric currents and blocks are finite elements of electrolyte solution. Discretization number in x direction is 5 while in y direction 1. (a): Solution chamber is divided into 5 parts. (b): Discretization equivalent to (a) but with two smaller parts at the both ends. (c): Transforming (b) into electrical circuit in each point KCL easily applies. Please note that this figure illustrates electric current flowing in y direction only. The resistance of solution chamber in x and z direction is included in r and r_s', respectively.

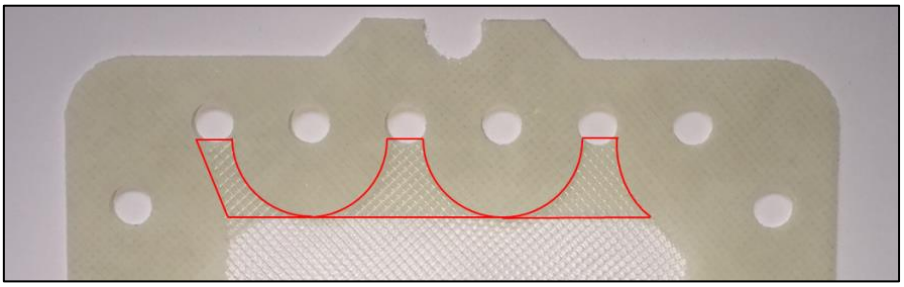

Figure C.4: Transitions between solution chamber and solution channel.

[1] As in figure C.4, stack is not symmetric in z dimension mainly due to the non-symmetric shape of transitions in z dimension which causes nonhomogeneous distribution of electrolyte solution in solution chamber.

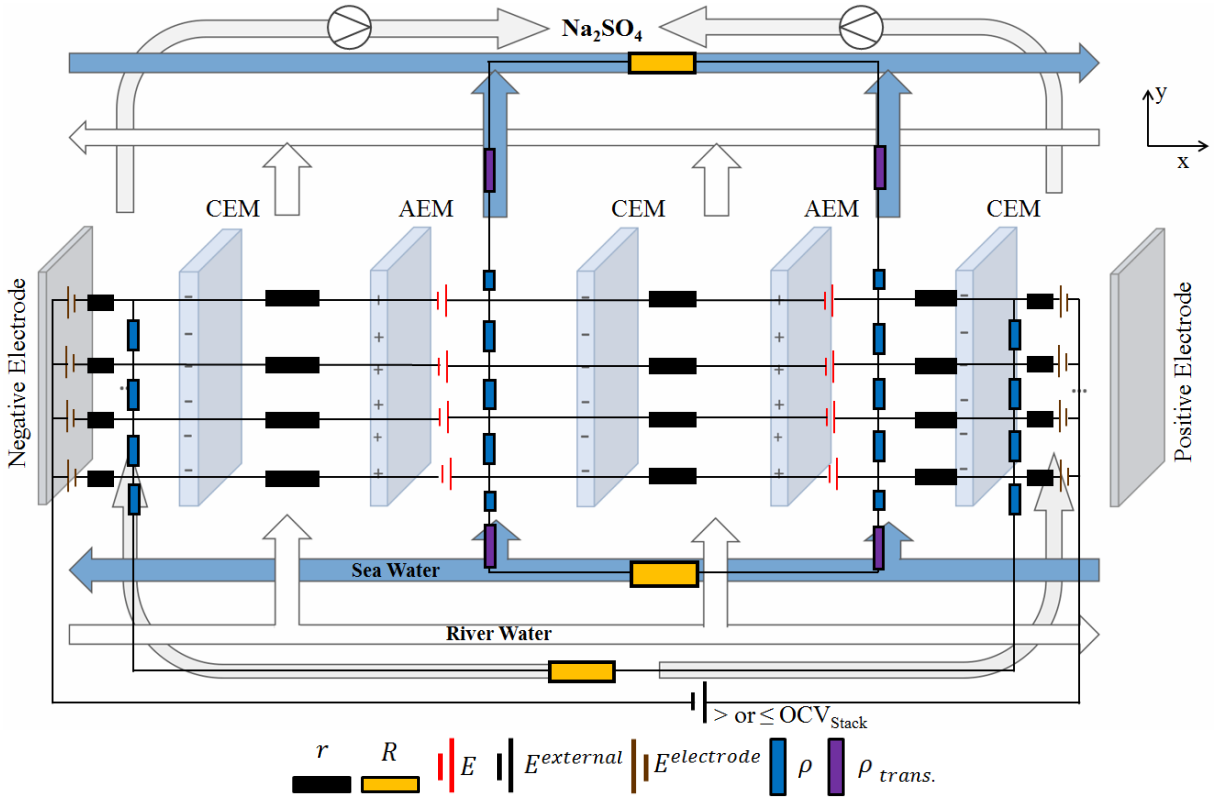

Figure C.5: 2D equivalent circuit of RED process with discretization of 6 in x direction and 1 in y direction.

Simulation Using KVL

Kirchhoff's Voltage Law (KVL) implies that the directed sum of the electrical potential differences (voltage) around any closed network is zero. The law is based on conservation of energy.

$$\sum_{k=1}^{n} V_k = 0$$

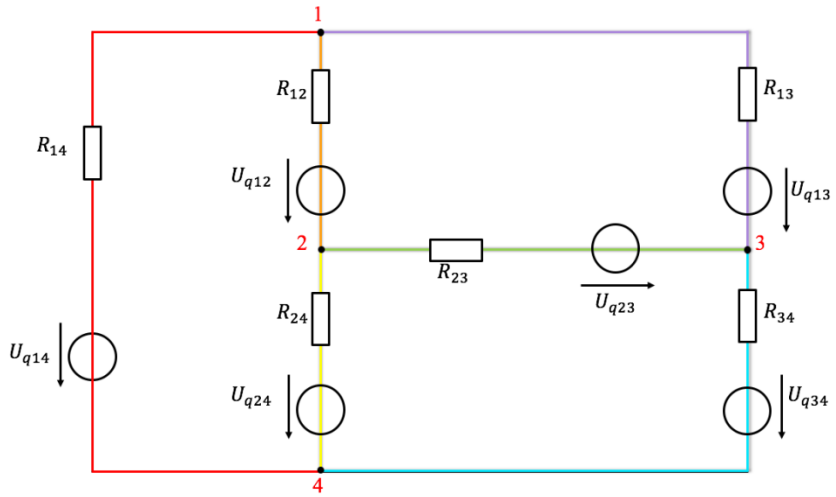

Figure C.6: Electric circuit which consists of 6 paths and 4 knots.

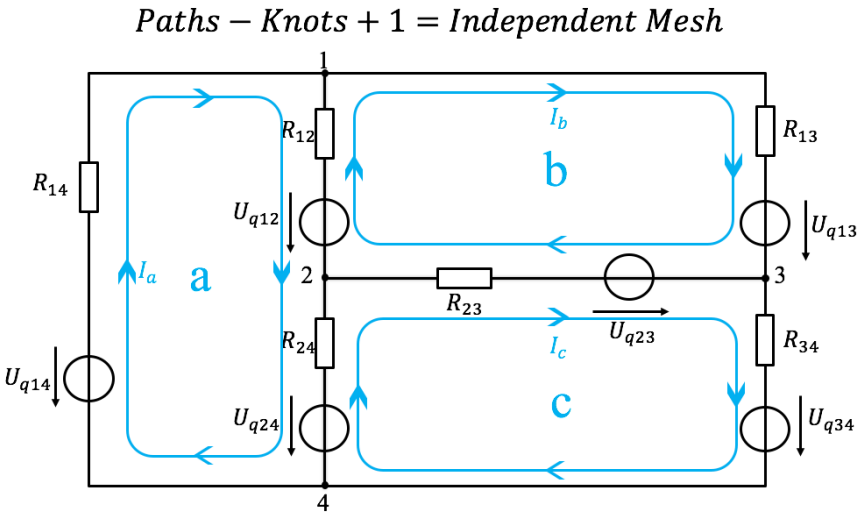

Figure C.7: Electric circuit which consists of 3 independent mesh equations.

Steps to calculate the current, according to KVL:

1) The number of independent mesh equations need to be determined at first. As the picture shows in figure B.1, there are z=6 paths and k=4 knots. So m=z-k+1=3, there are three mesh equations as shown in figure B.2. The left big circle is defined as circle 'a', the right upside circle as circle 'b', the right downside circle as circle 'c'. I_a, I_b and I_c are difined as imaginary currents in each independent mesh.

2) To write the matrix of resistance, the resistances on diagonal (R_{ii}) need to be calculated at first which are the sum of one circle. For example, as for circle 'a', the resistance R_{aa} equals R_{14}+ R_{12} + R_{24}.

Independent Meshes	I_a	I_b	I_c	Voltage Source
a:	R_{aa}	R_{ab}	R_{ac}	U_{qa}
b:	R_{ba}	R_{bb}	R_{bc}	U_{qb}
c:	R_{ca}	R_{cb}	R_{cc}	U_{qc}
	Resistance Matrix			Voltage Source Matrix

3) Clockwise is dictated as direction of positive. The resistance on the other places (R_{ij}) are determined by the relation between circles. For example, to write R_{ab}, there is one path belonging to both circle 'a' and circle 'b'. For circle 'a', current flows through R_{12} downwards. For circle 'b', current flows through R_{12} upwards. There is a conflict

between circle 'a' and 'b', so $R_{ab}= R_{ba}= -R_{12}$. In this way the matrix of resistances is obtained.

4) Q is an m × 1 matrix and the elements of the matrix are the voltage sum of each circle times -1. For example, $Q_{21}= U_{q12} + U_{q23} - U_{q13}$.

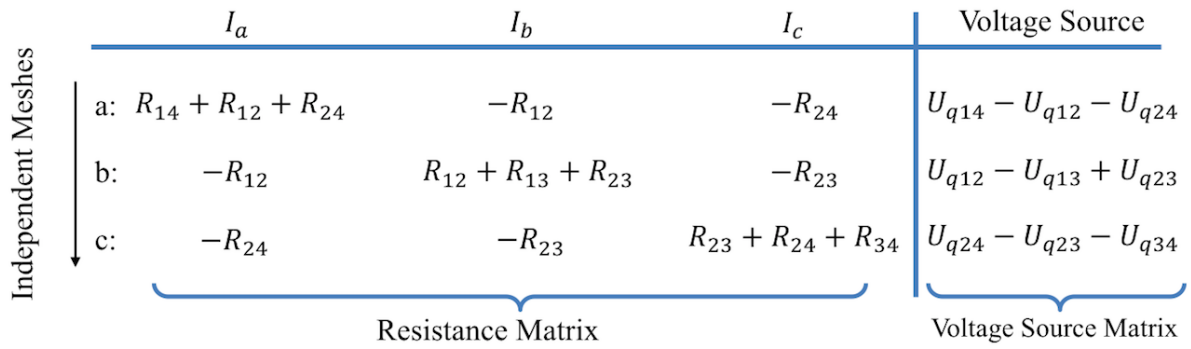

5) Matrix R times $(I_a, I_b, I_c)^T$ equals to matrix Q, therefore, $(I_a, I_b, I_c)^T$ equals to matrix Q divided by matrix R. When a current is negative, the direction of the current is opposite to the definition in this thesis, which means, counter clockwise.

6) The real current of each path is the sum of all imaginary currents flowing through it. For example, the current through knot 1 and 2 is the sum of current I_a and I_b.

7) In the case of REDBP network, each circle is given with a number. The voltage of the very left side, which is the electrode metal, is defined as zero. With all the real currents in network, multiplied by resistances, the voltage of all the important points can be obtained. Important points are defined as the positions between two resistances and the nodes.

In order to program with MatLAB more conveniently, some imaginary circles are necessary, for example, by adding an additional circle to make a matrix a regular quadrilateral.

By providing all the parameter of the system, a matrix of resistance can be written. Then, the matrix of voltage source will be written. Thus the result of currents flowing through each path can be obtained, and ΔI_{cell}, J, $I_{channel}$ and the voltage differences between every two knots can be calculated and compared. Simulink has been used to verify the simulated results from MatLAB.